



UNIVERSITÀ DEGLI STUDI DI TORINO

Department of Molecular Biotechnology and Health Sciences

PhD Programme in Biomedical Sciences and Oncology

Cycle 32

The adaptor protein p130Cas controls pancreatic acinar cell plasticity and cancer initiation through regulation of PI3K-AKT pathway

Candidate: Andrea Costamagna

Supervisor: Prof. Miriam Martini

Academic years of enrolment: 2016/2020

Index

1. Pancreatic cancer: 21 st century big challenge.....	3
a. Definition and molecular genetics	3
b. Pancreatic cancer cell of origin and experimental models	4
2. p130Cas adaptor protein: not only a figurant in cancer history	5
a. Protein structure and function	5
b. Role of p130Cas in cancer	6
3. References	8
4. Introduction and aim of the work	11
a. The adaptor protein p130Cas controls pancreatic acinar cell plasticity and cancer initiation through regulation of PI3K-AKT pathway	
5. Previous works on p130Cas	46
a. Modeling ErbB2-p130Cas interaction to design new potential anticancer agents. (2019)	
b. Conditional ablation of p130Cas/BCAR1 adaptor protein impairs epidermal homeostasis by altering cell adhesion and differentiation. (2018)	
c. Dysregulation of Blimp1 transcriptional repressor unleashes p130Cas/ErbB2 breast cancer invasion. (2017)	
d. p130Cas scaffold protein regulates ErbB2 stability by altering breast cancer cell sensitivity to autophagy. (2015)	

Pancreatic cancer: 21st century big challenge

Definition and molecular genetics

Pancreatic cancer, and its most frequent subtype Pancreatic Ductal Adenocarcinoma (PDAC), is one of the 21st century biggest challenges in the fight against cancer. With a 5-year survival rate of only 3% and a median survival of less than 6 months, a diagnosis of pancreatic cancer carries one of the most dismal prognoses in all of medicine. Due to a lack of specific symptoms and limitations in diagnostic methods, the disease often eludes detection during its formative stages. Surgery has offered the only possibility of cure, although surgical intervention alone rarely achieves a curative end point. For the 15–20% of patients who undergo potentially curative resection, the 5-year survival is only 20%. Some improvements in surgical outcome occur in patients who also receive chemotherapy and/or radiotherapy, although the impact on long-term survival has been minimal owing to the intense resistance of pancreatic adenocarcinoma to all extant treatments. So, management of most patients focuses on palliation ^{1–3}. Pancreatic cancer is generally thought to arise from pancreatic ductal cells; however, this remains an area of ongoing study (see paragraph 1b).

The etiology of pancreatic cancer remains poorly defined, although important clues of disease pathogenesis have emerged from epidemiological and genetic studies. This cancer is associated with advancing age with a characteristic pattern of genetic lesions. The field is now faced with the challenge of understanding how these signature genetic lesions — mutations of KRAS, CDKN2A, TP53, BRCA2 and SMAD4/DPC4— contribute to the biological characteristics and evolution of this disease. KRAS mutations are identified in more than 8 out of 10 patients and tend to be associated with reduced overall survival, regardless of the stage of PDAC ^{4,5}. An activating point mutation of the KRAS oncogene on codon 12 (exon 2) is the initiating event in the majority of PDAC cases (70–95%). This single- nucleotide mutation triggers replacement of the GGT sequence (which encodes glycine) by the GAT sequence (aspartic acid; G12D), GTT (valine; G12V), CGT (arginine; G12R) or GCT (alanine; G12A). The point mutation of KRAS impairs the intrinsic GTPase activity of RAS and prevents GAPs from promoting the conversion of GTP (active) to GDP (inactive). The KRAS protein is thus permanently bound to GTP and constitutively activates downstream signalling pathways, consequently maintaining the cellular processes of proliferation and survival.

Pancreatic cancer cell of origin and experimental models

PDAC was initially characterized by its ductal, glandular morphology, and so it was conventionally conjectured that PDAC originated from ductal cells⁶. Earlier genetically engineered mouse models (GEMM) of PDAC did not pay attention to cell lineage. The KC (Kras/Cre) model, which utilized Pdx1^{Cre} or p48/Ptf1a^{Cre} to activate a conditional knocked-in KrasG12D allele (LSL-KrasG12D) in pancreatic progenitor cells, was the first genetically engineered mouse model (GEMM) to faithfully recapitulate the human PDAC tumorigenesis process in mice⁷. These mice develop pre-cancerous lesions, PanINs (pancreatic intraepithelial neoplasia), that eventually evolve into PDAC tumors. Pdx1 and p48/Ptf1a are expressed in early progenitor cells during pancreatic development. Lineage tracing experiments have shown that both Pdx1 and p48/pft1a expressing cells contribute to all the cell lineages in the pancreas, including both acinar and ductal cells. Unexpectedly, several GEMMs have suggested that, without additional mutations, ductal cells are relatively resistance to oncogenic Kras-induced formation of PDAC precursor lesions. Kopp et al. used transgenic Sox9^{CreER} to activate the expression of a knocked-in KrasG12D allele (LSL- KrasG12D) in ductal cells at postnatal day 10⁸. Although the mutant allele was efficiently recombined in a subset of ductal cells, these mice rarely develop PanINs. Similar results were obtained by Ray et al. using CK19^{CreER} to activate mutant Kras in ductal cells⁹.

Several different studies demonstrated that oncogenic Kras could initiate tumorigenesis in ductal cells in the presence of additional mutations, such as Pten deletion, Fbw7 deletion or Trp53 inactivation¹⁰⁻¹². These data imply that either the acquisition of additional mutations in the presence of oncogenic Kras results in ductal cells bypassing the PanIN stage or, more likely, that ductal cells might be responsible for PDAC initiated from a low-grade PanIN- independent route.

In the past decade, the potential role of the pancreatic acinar cell lineage as the cell of origin of PDAC has been extensively studied. Of the adult cell lineages of the pancreas, acinar cells show the highest plasticity. Pancreatic acinar cells can dedifferentiate or transdifferentiate to an embryonic progenitor phenotype that expresses ductal markers, in a process termed acinar-to-ductal metaplasia (ADM). Multiple factors have been implicated in mediating ADM, including KRAS hyperactivity and increased inflammatory signalling^{13,14}.

Guerra et al. crossed double transgenic Elastase-tTA/Tet-O-Cre mice, which express Cre recombinase under the control of the Elastase promoter in a tet-off system, with a line carrying a knockin conditional KrasG12V allele (LSL-KrasG12V)¹⁵. In this model, oncogenic KrasG12V expression was

turned on in 20% to 30% of acinar cells as well as a low number of centroacinar cells during late embryonic development. These mice readily developed full spectrum PanIN lesions, and some progressed to PDACs with about 1-year latency. The similarity of the phenotype of this model and that of KC mice suggests that acinar cells might be the origin of PDACs developed in those models.

Taking advantage of the fact that Ptf1a expression is limited to the acinar cell lineage in the pancreas after birth, Kopp et al. activate expression of oncogenic KrasG12D and YFP reporter in acinar cells. This lineage tracing model displayed abundant YFP+ PanIN lesions in mice between the ages of 8 and 17 months, clearly demonstrating that these PDAC precursor lesions were derived from acinar cells.

These and other data support the notion that at least embryonic or young acinar cells are susceptible to oncogenic Kras-induced PDAC initiation via a PanIN-dependent route.

p130Cas adaptor protein: not only a figurant in cancer history

Protein structure and function

Proteins of the CAS (CRK-associated substrate) family (BCAR1/p130Cas, NEDD9/HEF1/CAS-L, EFS/SIN and CASS4/HEPL) are integral players in normal and pathological cell biology. CAS proteins by acting as scaffolds can regulate the formation of protein complexes that in turn control cell migration and chemotaxis, apoptosis, cell cycle and differentiation. Reflecting these complex functions, overexpression of CAS proteins is now emerging to correlate with poor prognosis, increased metastatization, as well as resistance to first-line chemotherapeutics in multiple tumor types. These proteins share structure similarity characterized by the presence of multiple protein interaction domains and several tyrosine and serine phosphorylation motifs¹⁶.

p130Cas/BCAR1 protein is characterized by an N-terminal Src-homology 3 (SH3) domain, an adjacent large substrate domain containing 15 repetition of the YxxP motif, a main site of tyrosine phosphorylation upon mechanical stimuli or growth factor receptors/integrins signaling, a proline and serine rich region, a highly conserved four-helix bundle and a well conserved carboxy-terminal domain, containing a YDYVHL motif that acts as docking site for Src family kinases (Src, Fyn, Lyn, Lck)

¹⁷.

Although p130Cas/BCAR1 is devoid of any enzymatic or transcriptional activity, the presence of multiple tyrosine residues in the substrate domain, as well as its modular structure with various binding motifs, allows the formation of multi-protein signaling complexes. This results in the induction and/or maintenance of signaling pathways with pleiotropic effects on cell motility, cell adhesion, cytoskeleton remodelling, invasion, survival and proliferation.

Role of p130Cas in cancer

The relevance of p130Cas/BCAR1 adaptor protein in cancer has been extensively supported by demonstrating the contribution of deregulated expression levels of p130Cas/BCAR1 to cellular transformation and malignancy. Indeed, overexpression of p130Cas/BCAR1 has been detected in human breast, prostate, ovarian, lung, colorectal, pancreatic and hepatocellular carcinoma, as well as in glioma, melanoma, anaplastic large cell lymphoma and chronic myelogenous leukemia, although the exact mechanisms have not been identified yet ^{17,18}.

Specifically, in ErbB2-positive breast cancer, p130Cas/BCAR1 is necessary to induce invasion in three-dimensional culture cells by supporting and amplifying ErbB2 downstream signaling ¹⁹⁻²³. In these cells, p130Cas is a crucial component of a functional molecular complex consisting in ErbB2, c-Src, and FAK. Several experiments demonstrated that ErbB2 oncogene requires p130Cas/BCAR1 as an essential transducer to drive foci formation and anchorage-independent growth. The relevance of p130Cas in tumor growth is also strengthened by in vivo studies, showing that p130Cas silencing is sufficient to inhibit in vivo ErbB2-dependent tumor formation. Using MCF10A.B2 cells expressing the ErbB2 chimera, which is activated by treatment with the synthetic ligand AP1510, Cabodi et al. ²⁴, demonstrated that p130Cas overexpression induces ErbB2 tyrosine phosphorylation in absence of AP1510 and strengthened activation of downstream signaling pathways. This suggests that high levels of p130Cas function as a priming event for partial activation of the receptor. Moreover, they demonstrated that, upon ErbB2 activation by AP1510, p130Cas phosphorylation occurs prior to ErbB2-mediated c-Src activation and is not reduced by pharmacological inhibition of c-Src catalytic activity, suggesting that c-Src is not involved in early p130Cas phosphorylation.

Recent data from the same group indicate that p130Cas by binding to ErbB2, stabilizes the receptor preventing its ubiquitination and subsequent degradation by autophagy ²². Indeed, p130Cas by binding to ErbB2 does not allow the association with CHIP and Cbl E3 Ubiquitin ligases, possibly

through steric hindrance. Their data also indicate that high levels of p130Cas expression inversely correlate with ErbB2 sensitivity to Trastuzumab. The mechanism through which p130Cas mediates resistance to Trastuzumab might rely on the increased ErbB2 stability to the cell membrane. This increased stabilization of ErbB2 by p130Cas might be the crucial event driving breast cancer progression and resistance, strengthening the relevance of p130Cas as putative therapeutic target to overcome resistance to Trastuzumab.

These findings could have important therapeutic and translational implications but until now p130Cas can be targeted only by RNA-interference, limiting its applicability. Due to the absence of enzymatic activity, and by acting only as scaffold protein, no p130Cas catalytic inhibitors or modulators could be developed.

References

1. Bardeesy N, DePinho RA. Pancreatic cancer biology and genetics. *Nat Rev Cancer* 2002;2:897–909. Available at: <http://www.nature.com/doi/10.1038/nrc949>.
2. GÜNGÖR C, Hofmann BT, Wolters-Eisfeld G, et al. Pancreatic cancer. *Br J Pharmacol* 2014;171:849–58. Available at: <http://www.ncbi.nlm.nih.gov/pubmed/24024905> [Accessed February 26, 2019].
3. Bailey P, Chang DK, Nones K, et al. Genomic analyses identify molecular subtypes of pancreatic cancer. *Nature* 2016;531:47–52.
4. Waters AM, Der CJ. KRAS: The Critical Driver and Therapeutic Target for Pancreatic Cancer. *Cold Spring Harb Perspect Med* 2018;8. Available at: <http://www.ncbi.nlm.nih.gov/pubmed/29229669> [Accessed June 23, 2019].
5. Buscail L, Bournet B, Cordelier P. Role of oncogenic KRAS in the diagnosis, prognosis and treatment of pancreatic cancer. *Nat Rev Gastroenterol Hepatol* 2020;17:153–168. Available at: <http://dx.doi.org/10.1038/s41575-019-0245-4>.
6. Xu Y, Liu J, Nipper M, et al. Ductal vs. acinar? Recent insights into identifying cell lineage of pancreatic ductal adenocarcinoma. *Ann Pancreat Cancer* 2019;2:11–11. Available at: <http://apc.amegroups.com/article/view/4880/html> [Accessed January 8, 2020].
7. Hingorani SR, Petricoin EF, Maitra A, et al. Preinvasive and invasive ductal pancreatic cancer and its early detection in the mouse. *Cancer Cell* 2003.
8. Kopp JL, Figura G von, Mayes E, et al. Identification of Sox9-Dependent Acinar-to-Ductal Reprogramming as the Principal Mechanism for Initiation of Pancreatic Ductal Adenocarcinoma. *Cancer Cell* 2012.
9. Ray KC, Bell KM, Yan J, et al. Epithelial Tissues Have Varying Degrees of Susceptibility to KrasG12D-Initiated Tumorigenesis in a Mouse Model Oshima R, ed. *PLoS One* 2011;6:e16786. Available at: <https://dx.plos.org/10.1371/journal.pone.0016786>.
10. Ferreira RMM, Sancho R, Messal HA, et al. Duct- and Acinar-Derived Pancreatic Ductal Adenocarcinomas Show Distinct Tumor Progression and Marker Expression. *Cell Rep* 2017.
11. Lee AYL, Dubois CL, Sarai K, et al. Cell of origin affects tumour development and phenotype

in pancreatic ductal adenocarcinoma. *Gut* 2019;68:487–498.

12. Kopp JL, Dubois CL, Schaeffer DF, et al. Loss of Pten and Activation of Kras Synergistically Induce Formation of Intraductal Papillary Mucinous Neoplasia From Pancreatic Ductal Cells in Mice. *Gastroenterology* 2018.
13. Storz P. Acinar cell plasticity and development of pancreatic ductal adenocarcinoma. *Nat Rev Gastroenterol Hepatol* 2017;14:296–304. Available at: <http://www.nature.com/articles/nrgastro.2017.12> [Accessed April 28, 2019].
14. Storz P, Crawford HC. Carcinogenesis of Pancreatic Ductal Adenocarcinoma. *Gastroenterology* 2020;158:2072–2081.
15. Guerra C, Schuhmacher AJ, Cañamero M, et al. Chronic Pancreatitis Is Essential for Induction of Pancreatic Ductal Adenocarcinoma by K-Ras Oncogenes in Adult Mice. *Cancer Cell* 2007.
16. Cabodi S, Camacho-Leal MDP, Stefano P Di, et al. Integrin signalling adaptors: not only figurants in the cancer story. *Nat Rev Cancer* 2010;10:858–870. Available at: <http://dx.doi.org/10.1038/nrc2967>.
17. Tikhmyanova N, Little JL, Golemis EA. CAS proteins in normal and pathological cell growth control. *Cell Mol Life Sci* 2010;67:1025–1048.
18. Tornillo G, Defilippi P, Cabodi S. Cas proteins: dodgy scaffolding in breast cancer. *Breast Cancer Res* 2014;16:443. Available at: <http://www.pubmedcentral.nih.gov/articlerender.fcgi?artid=4384296&tool=pmcentrez&rendertype=abstract>.
19. Pincini A, Tornillo G, Orso F, et al. Identification of p130Cas/ErbB2-dependent invasive signatures in transformed mammary epithelial cells. *Cell Cycle* 2013;12:2409–2422.
20. Tornillo G, Bisarò B, Camacho-Leal MDP, et al. P130Cas promotes invasiveness of three-dimensional ErbB2-transformed mammary acinar structures by enhanced activation of mTOR/p70S6K and Rac1. *Eur J Cell Biol* 2011;90:237–248. Available at: <http://dx.doi.org/10.1016/j.ejcb.2010.09.002>.
21. Sciortino M, Camacho-Leal M del P, Orso F, et al. Dysregulation of Blimp1 transcriptional repressor unleashes p130Cas/ErbB2 breast cancer invasion. *Sci Rep* 2017;7:1145. Available at: <http://www.nature.com/articles/s41598-017-01332-z> [Accessed May 2, 2017].

22. Bisaro B, Sciortino M, Colombo SM, et al. p130Cas scaffold protein regulates ErbB2 stability by altering breast cancer cell sensitivity to autophagy. *Oncotarget* 2015;132:3–4. Available at: <http://www.oncotarget.com/abstract/6710> [Accessed January 30, 2017].
23. Costamagna A, Rossi Sebastiano M, Natalini D, et al. Modeling ErbB2-p130Cas interaction to design new potential anticancer agents. *Sci Rep* 2019;9:3089. Available at: <http://www.nature.com/articles/s41598-019-39510-w> [Accessed March 11, 2019].
24. Cabodi S, Tinnirello A, Bisaro B, et al. p130Cas is an essential transducer element in ErbB2 transformation. *FASEB J* 2010;24:3796–3808.

Introduction and aim of the work

The adaptor protein p130Cas controls pancreatic acinar cell plasticity and cancer initiation through regulation of PI3K-AKT pathway

1. Abstract

p130Cas adaptor protein is frequently overexpressed in human cancers, including pancreatic ductal adenocarcinoma (PDAC). Its genetic locus repeatedly emerged as interesting candidate to predict PDAC susceptibility, but its contribution remains largely unknown. Public databases, PDAC tissue array and preclinical cancer mouse models were used to investigate the clinical relevance of p130Cas in PDAC. Conditional p130Cas knockout mice ($Pdx^{Cre}; p130Cas^{fl/fl}$) were generated to examine the role of p130Cas during PDAC carcinogenesis. p130Cas was upregulated in human PDAC samples and its expression was correlated with worst OS and PFS. Mechanistically p130Cas deletion in mouse models repressed metaplastic transformation of the pancreatic acinar compartment but did not prevent ductal cells from acquiring tumorigenic ability, resulting in a delayed insurgence of duct-derived tumors. In acinar cells carrying $Kras^{G12D}$, phosphorylated p130Cas was associated with p85 α PI3K-regulatory subunit, promoting PI3K activity, AKT activation and acinar metaplasia. Conversely, p130Cas loss prevented acinar cell from $Kras^{G12D}$ -induced metaplasia through downregulation of PI3K-AKT pathway activation. Of note, pancreatic cancer patients with high p130Cas levels also displayed increased levels of AKT phosphorylation. Together, our findings highlight the function of p130Cas during pancreatic carcinogenesis, and specifically uncover its key role during acinar metaplasia, which would advance our understanding of acinar to ductal metaplasia contribution to PDAC.

1. Introduction

Pancreatic adenocarcinoma (PDAC) is the most common type of pancreatic cancer and one of the biggest challenges in the fight against cancer in the 21st century. This tumor remains one of the most lethal cancers worldwide, regardless of more effective combination treatments and new diagnostic possibilities^{1,2}. Since PDAC is often diagnosed at a metastatic stage, understanding the processes that lead to its initiation is crucial both for the identification of markers for early detection, and to set up new early intervention modalities.

In this context, extensive genome studies have been applied to uncover new potential regulators of malignant transformation in the pancreas. More specifically, genome-wide association studies (GWAS) provide novel insights to identify genomic regions containing potential common risk alleles for human diseases. The actual single-nucleotide polymorphisms identified by GWAS rarely have obvious effects on protein-coding regions, nor are they linked to clear causal variants in adjacent genes³. As a result, GWAS often identify candidate genes of uncertain functional importance, whose actual implication in the disease of interest is unclear. However, in 2014 two studies provided the first functional validation of a GWAS-identified risk factor for PDAC, uncovering the role of Nr5a2 orphan hormone receptor as inhibitor of Kras-driven ADM and subsequent tumorigenesis^{4,5}. An increasing number of similar candidates wait for a functional validation. Among the PDAC risk-associated SNPs and genomic regions from GWAS, *BCAR1* gene has repeatedly emerged as an interesting candidate, even when stringent Bonferroni correction was applied⁶⁻⁸. *BCAR1* gene codes for an adaptor protein called p130Cas that represents a nodal platform on which integrin and growth factor receptor signaling conveys and its aberrant expression is linked with the transformation and progression of multiple cancer types⁹⁻¹¹. It has been demonstrated that p130Cas plays a key role in the control of migration and invasion of ErbB2 positive breast cancer¹², where it can also prevent the autophagic degradation of the receptor¹³. Indeed p130cas overexpression, in combination with ErbB2 amplification, correlates with higher proliferation rate, increased number of distant metastasis and poor prognosis of human breast cancer^{14,15}. Moreover, its overexpression has been indicated as an independent significant prognostic factor for NSCLC¹⁶.

Despite the ductal characteristics of PDAC, recent studies demonstrated that also acinar cells are quite sensitive to oncogenic mutation and can transdifferentiate to an embryonic progenitor phenotype that express ductal markers and represent a precursor stage for the formation of premalignant PanINs¹⁷⁻²³. This trans-differentiation process is known as Acinar to Ductal Metaplasia (ADM). Remarkably, lineage tracing experiments in animal models show that ADM also occurs *in vivo* and can progress to PanINs²⁴⁻²⁸ which can further evolve to PDAC²⁹.

Here, we reported for the first time the involvement of p130Cas adaptor protein in pancreatic tumorigenesis. In particular, we demonstrated that p130Cas expression is upregulated in human PDAC and significantly associates with poor patient survival in multivariate analysis. In mice, p130Cas deletion impaired Kras^{G12D}-dependent acinar cells trans-differentiation through regulation of PI3K-AKT activity.

2. Results

P130Cas is upregulated in human pancreatic cancer and is associated with worst OS and PFS.

The expression levels of p130Cas during pancreatic carcinogenesis is unknown. Analysis of publicly available datasets (GSE16515, GSE62452, GSE28735) ^{30–32} revealed that the p130Cas mRNA is significantly elevated in pancreatic tumors relative to normal tissue (Suppl. Fig. 1A), strengthening the value of the association highlighted by GWAS.

The association between elevated p130Cas expression and pancreatic cancer observed at mRNA level was further validated with a tissue microarray containing specimens of 96 cases of pancreatic cancer and 4 normal pancreatic tissue samples that was immunohistochemically stained with a specific p130Cas antibody. High p130Cas expression was detected in 58 out of 96 of the analyzed samples (60%) (Fig. 1B). Analysis of clinical parameters revealed highlighted the relevance of p130Cas expression as significant predictor of progression-free survival and overall survival in this cohort of PDAC patients. Moreover, p130Cas expression remained a significant predictor of survival and PFS, even after stratifying for tumor grading and vascular infiltration in a multivariate analysis (Fig. 1C and Suppl. Table 1).

P130Cas deletion increases survival of *Kras*^{G12D}; *p53*^{R172H} mice by delaying PDAC onset.

The first genetic event on the road to invasive pancreatic cancer is mutational activation of *Kras*, which occurs in the earliest precancerous PanIN-1 lesions ^{33,34}. Additionally, human PDAC tumors harbor mutations in classical tumor suppressor genes such as TP53, SMAD4 or BRCA1. Point mutation of the TP53 tumor suppressor have been described in approximately 27% of pancreatic cancers ³⁵. Likewise, mice expressing *Kras*^{G12D} in absence of functional p53 protein develop aggressive PanINs and PDAC tumors that result in the death of 50% the animals within their first 4 to 5 months of life ³⁶.

To establish whether p130Cas expression was functionally relevant for PDAC evolution and not only a bystander player, we crossed the aggressive $\text{Pdx}^{\text{Cre}}; \text{Kras}^{\text{G12D}}; \text{Trp53}^{\text{R172H}}$ model of PDAC tumorigenesis (referred to hereinafter as $\text{Kras}^{\text{G12D}}; \text{p53}^{\text{R172H}}$)³⁶ with mice with conditional p130Cas alleles ($\text{p130Cas}^{\text{fl/fl}}$)³⁷ to generate $\text{Kras}^{\text{G12D}}; \text{p53}^{\text{R172H}}$ mice that specifically lack p130Cas expression in pancreatic epithelium (referred to hereinafter as $\text{Kras}^{\text{G12D}}; \text{p53}^{\text{R172H}}; \text{p130Cas}^{\text{KO}}$).

The germ-line knockout p130Cas mouse model generated by and Honda and co-workers³⁸, highlighted the embryonic lethality of p130Cas deficiency, but our previous work suggested that this phenotype could be circumvented by conditional knock-out approach³⁷. To exclude gross pancreatic abnormalities in mice lacking p130Cas, pancreata from $\text{Pdx}^{\text{Cre}}; \text{p130Cas}^{\text{KO}}$ mice were histologically examined. Both at birth and adulthood (6 weeks), these pancreata appeared normal suggesting that p130Cas was dispensable for pancreas development (Suppl. Fig. 1A). Suppression of p130Cas protein expression in pancreatic epithelium was confirmed by Western blot (Suppl. Fig. 1B). $\text{Pdx}^{\text{Cre}}; \text{p130Cas}^{\text{KO}}$ mice were born at expected Mendelian ratio and were viable and fertile (Suppl. Fig. 1C).

As shown in Fig. 2A, $\text{Kras}^{\text{G12D}}; \text{p53}^{\text{R172H}}$ animals carrying wild type p130Cas alleles displayed abundant PanINs and PDAC lesions at 4 months of age. Interestingly, mice carrying conditional p130Cas alleles also displayed neoplastic lesions, but with reduced incidence (Fig. 2B).

To investigate if this phenotype was determined by a delayed onset or by a slower progression of $\text{p130Cas}^{\text{KO}}$ tumors, a cohort of $\text{Kras}^{\text{G12D}}; \text{p53}^{\text{R172H}}$ and $\text{Kras}^{\text{G12D}}; \text{p53}^{\text{R172H}}; \text{p130Cas}^{\text{KO}}$ animals were sacrificed at 2 months of age, an age at which PanIN lesions start to develop in this tumor model. Counting of lesions revealed substantial delayed tumor onset for $\text{Kras}^{\text{G12D}}; \text{p53}^{\text{R172H}}; \text{p130Cas}^{\text{KO}}$ mice (Fig. 2A). When allowed to age, all $\text{Kras}^{\text{G12D}}; \text{p53}^{\text{R172H}}$ animals succumbed to pancreatic tumors around 200 days of age (6.5 months), with a median survival of 144 days. By contrast, $\text{Kras}^{\text{G12D}}; \text{p53}^{\text{R172H}}; \text{p130Cas}^{\text{KO}}$ mice died around 330 days of age (11 months) with a median survival of 235 days (Fig. 2B). Thus, ablation of p130Cas resulted in a 63% increase in survival time. Tumor development in $\text{Kras}^{\text{G12D}}; \text{p53}^{\text{R172H}}; \text{p130Cas}^{\text{KO}}$ mice was not due to incomplete recombination because the large majority of the PanIN lesions and PDAC tumors did not express p130Cas when analyzed by IHC (Suppl. Fig. 1D).

Moreover, IHC staining of end-point tumors from $\text{Kras}^{\text{G12D}}; \text{p53}^{\text{R172H}}; \text{p130Cas}^{\text{KO}}$ mice did not reveal significant differences in proliferation compared to those present in control $\text{Kras}^{\text{G12D}}; \text{p53}^{\text{R172H}}$ animals (Suppl. Fig. 1D), as observed by PCNA staining. These observations indicate that loss of p53

activates oncogenic pathways that bypass the requirement of p130Cas for tumor development. However, although all animals developed terminal PDAC regardless of p130Cas expression, these cumulative evidences strongly support p130Cas as main regulator of tumor onset in murine pancreas, thus reducing tumor burden and improving overall survival.

P130Cas deletion affects PDAC onset by altering the balance between acinar and duct-derived tumors.

To understand the delayed tumor onset observed in $Kras^{G12D}; p53^{R172H}; p130Cas^{KO}$ mice, we focused our attention on the initial phases of PDAC tumorigenesis. Studies with GEM PDAC models have revealed that the different pancreas compartment have different responses to given oncogenic lesions, especially in the earlier steps. Although ductal cells are relatively more resistant to $Kras^{G12D}$ transformation than acinar cells, this scenario changes when additional genetic alterations are incorporated in the same cells^{17,23,24,39–41}. Recent studies highlighted the contribution of both acinar and duct-derived tumor cells in pan-pancreatic mouse models, such as the $Pdx^{Cre}; Kras^{G12D}; Trp53^{R172H}$ adopted in this work, where low or high expression of AGR2 protein was proposed as valuable marker to distinguish acinar and ductal tumors, respectively⁴². In the attempt to clarify how the absence of p130Cas could impact on PDAC onset, $Kras^{G12D}; p53^{R172H}$ and $Kras^{G12D}; p53^{R172H}; p130Cas^{KO}$ pancreata were examined at terminal stages for AGR2 expression to highlight their lineage of origin. As previously reported, tumors from $Kras^{G12D}; p53^{R172H}$ mice exhibit mixed positive and negative AGR2 staining accordingly to the dual contribution of acinar and ductal cells to PDAC onset. Conversely, the absence of p130Cas dramatically shifted the proportion of duct-originated tumors that uniformly stain positive for AGR2 (Fig. 2C). Likewise, strong AGR2 expression could also be detected in human PDAC tissue sections with low p130Cas staining (Fig. 2D).

These data highlighted the different requirements of acinar and ductal cells to promote their conversion into PDAC progenitors and that p130Cas expression is crucial to allow the transformation of the acinar compartment in preclinical PDAC model.

P130Cas overexpression in transforming acinar cells.

To specifically investigate the role of p130Cas during acinar transformation, we took advantage of the $Pdx^{Cre}; Kras^{G12D}$ mouse model (referred to hereinafter as $Kras^{G12D}$)⁴³.

In these transgenic mice, pancreas-specific expression of $Kras^{G12D}$ mutant results in the development of acinar metaplasia at around 8 weeks of age (while ductal cells can tolerate this single hit^{24,41}) that further progress to preneoplastic lesions (mostly PanIN), with PDAC resulting after a long latency in 20% to 30% of mice.

Of note, p130Cas expression was found to be very low/undetectable in untransformed pancreatic acini and normal ducts (Suppl. Fig. 1E). However, we observed that specifically in the areas where acinar cells undergo ADM, p130Cas expression pattern was altered and, by 4- to 6-months of age, p130Cas overexpression can be detected in ADM and PanIN lesions, as well as in PDAC areas, but remains low/undetectable in the adjacent untransformed compartments (Fig. 3A).

Pancreatitis is an inflammatory condition strongly linked to PDAC in humans⁴⁴, but also a critical player in $Kras$ -dependent tumorigenesis²⁹. In animal models, induction of pancreatic injury and inflammation similar to what observed in patients could be achieved by administration of the cholecystokinin analogue caerulein. In $Kras$ wild-type pancreas, this results in the formation of ADM lesions that, in the absence of further injuries, spontaneously resolve within 2 weeks. Conversely, caerulein treatment dramatically exacerbates and accelerates the formation of ADM lesions by mutated $Kras$ and increases their outcome as PanINs^{24,45,46}. To assess whether p130Cas expression levels were regulated during the formation of these precursor lesions, control ($Pdx^{Cre}; Kras^{wt/wt}$) and $Kras^{G12D}$ mice were treated with caerulein to induce ADM. As shown in Fig. 3B, in untreated 6-week-old $Kras^{G12D}$ mice, p130Cas expression was low and indistinguishable from control mice of the same age. After 1 day of caerulein treatment, the upregulation of p130Cas expression was highly detectable in acinar cells undergoing ADM in both genotypes. In absence of oncogenic $Kras$ redifferentiation into functional acinar cells occurs rapidly within 1 week of caerulein treatment, together with the reduction of p130Cas expression levels, suggesting that p130Cas upregulation occurs during pancreatic regeneration but is quiescent in undamaged pancreas. However, mutated $Kras$ blocks acinar regeneration in favor of ductal reprogramming and PanIN formation⁴⁷. In contrast to control mice, $Kras^{G12D}$ mice displayed persistent p130Cas upregulation in metaplastic duct and PanIN lesions at 5- and 14-days post caerulein injection, suggesting a specific role for p130Cas upregulation in the $Kras$ -induced reprogramming of acinar cells into PanIN precursors. These observations paralleled with the significantly upregulated p130Cas mRNA levels detected in publicly available dataset (GSE41418, GSE109227, GSE77983)⁴⁸⁻⁵⁰ of caerulein-induced pancreatitis in wild type and $Kras^{G12D}$ mice (Suppl. Fig. 1 F).

Cell autonomous p130Cas overexpression in response to EGF and oncogenic Kras in pancreatic acinar explant

To verify whether the potential role of p130Cas in ADM was strictly dependent by Kras activation and to exclude potential microenvironmental influences, we next adopted an established explant model in which mouse primary pancreatic acinar cells were isolated, reseeded *ex vivo* in collagen I 3D culture and transdifferentiation was then induced either by EGF or by the presence of Kras^{G12D}, as described previously^{18,51,52}. These primary acinar cells undergo ADM within 5 days (Fig. 3C-D). p130Cas upregulation was observed during acinar transdifferentiation either in primary acinar cells treated with EGF or expressing Kras^{G12D} (Fig. 3E). Interestingly, p130Cas expression was increased in Kras mutant acini in unstimulated conditions at day 1, compared to wild type counterparts; and correlates with the acquisition of the ductal phenotype. This result showed that p130Cas upregulation is a conserved cell-autonomous characteristic of acini that undergo ADM in response to transdifferentiation stimuli or oncogenic Kras.

Pancreatic epithelial p130cas deletion inhibits both spontaneous and pancreatitis-induced PanINs formation

To assess whether the absence of p130Cas interfered with Kras-induced ADM and tumorigenesis, we generated Pdx^{Cre}; Kras^{G12D}; p130Cas^{KO} mice (referred to hereinafter as Kras^{G12D}; p130Cas^{KO}). Kras-dependent ADM and PanIN formation was evaluated in 6 months-old Kras^{G12D} and Kras^{G12D}; p130Cas^{KO} mice. Results indicate that, although we detected some rare and occasional PanINs in Kras^{G12D}; p130Cas^{KO} mice, the pancreatic area occupied by oncogenic lesions was significantly smaller compared to Kras^{G12D} mice, as evaluated by both mucin accumulation and loss of amylase staining (Fig. 4A-B). The sporadic PanINs detected in Kras^{G12D}; p130Cas^{KO} mice were not due to incomplete recombination because the large majority of the PanIN lesions did not express p130Cas when analyzed by IHC (Suppl. Fig. 2A). These data suggest that p130Cas loss interferes with Kras-induced formation of ADM and precursor lesions during cancer progression. Interestingly, Kras^{G12D}; p130Cas^{KO} mice did not develop PDAC even after 12 months, further strengthening the idea that p130Cas loss completely blocked Kras oncogenic potential and prevented acinar transdifferentiation, thus impairing tumor onset in this model.

As reported above, the cholecystinin analogue caerulein induces acute pancreatitis in mice, accompanied by widespread ADM. Whereas normal acini regenerate upon resolution of the inflammatory stimulus, in the context of Kras mutation, ADM is not resolved but instead progresses to PanIN. Therefore, we examined if p130Cas loss was able to block Kras-driven PanIN formation even in the setting of acute pancreatitis (Fig. 4C-D). By 5 days after caerulein injection, the exocrine compartment of Kras^{G12D} mice was nearly completely replaced by fibrosis and ductal structures, as evident by rare expression of the acinar marker amylase. These ductal structures often acquire strong expression of CK19 ductal marker 14 days after caerulein injection indicating their progression towards PanIN lesions. In stark contrast, pancreata of Kras^{G12D}; p130Cas^{KO} mice did not display gross fibrosis and ADM after caerulein treatment and retained dramatically more amylase-positive parenchyma. Interestingly, this protection could not be detected in p130Cas^{KO} mice carrying wild type Kras allele when treated with caerulein (Suppl. Fig. 2B), supporting the hypothesis that p130Cas loss-mediated protection is strictly connected to Kras^{G12D} expression in the pancreatic epithelium.

P130Cas deletion prevents Kras^{G12D}-induced PI3K-AKT activation

To further test the cell-autonomous mechanism underlying this p130Cas^{KO}-mediated protection, we explanted acini from Kras^{G12D} and Kras^{G12D}; p130Cas^{KO} mice and cultured them as 3D culture (Fig. 5A-B). After 5 days in culture, we observed significantly less ductal structures in Kras^{G12D}; p130Cas^{KO} acini compared to Kras^{G12D} acinar explants, suggesting that p130Cas contributes to Kras-induced acinar to ductal transdifferentiation through cell-autonomous mechanisms.

Mutant Kras signaling in PDAC is highly complex and dynamic engaging various downstream effectors such as RAF/MEK/ERK and PI3K/Pdk/AKT pathways^{53,54}. Experiments in mice demonstrated that PI3K-AKT signaling plays a pivotal role in pancreatic cancer initiation^{55,56}.

To test if p130Cas deletion could impact on Kras downstream pathways, isolated acini derived from Kras^{G12D} and Kras^{G12D}; p130Cas^{KO} mice were analyzed for the phosphorylation of downstream effectors AKT and ERK1/2. Interestingly, following EGF stimuli, isolated Kras^{G12D} acini lacking p130Cas revealed a reduction in AKT phosphorylation compared to wild type counterpart with less evident effects on ERK1/2 phosphorylation (Fig. 5C). GTP-Kras has been shown to essentially engage and activate PI3K by direct binding to p110 catalytic subunit⁵⁷. However, even in the presence of constitutively active Kras^{G12D} oncoprotein, the release of p110 from p85-inhibition is still required

to achieve full activation of PI3K-AKT pathway⁵⁸. Inactivation of p85 depends on its binding to tyrosine phosphorylated proteins^{59,60}. Of note, the formation of a transient molecular complex including p130Cas, the PI3K p85 subunit and Src was observed in breast cancer cells upon estrogen treatment or adenovirus cell entry^{61,62}. Moreover, phosphorylated-p130Cas has been shown to co-immunoprecipitate with p85 in v-Crk transformed cells, where it correlates with PI3K activity. In absence of p130Cas, v-Crk expression failed to mediate growth in low serum condition and this phenotype was rescued by wild type p130Cas but not by expression of a p130Cas mutant unable to bind p85⁶³. On these bases, we hypothesized that p130Cas could release PI3K from p85 inhibitory function also in transforming acinar cells and its deletion could reduce Kras-mediated PI3K activation by maintaining intact p85-mediated inhibition. To this end, we first tested p130Cas-p85 α association in isolated Kras^{G12D} acini. In low-serum condition, p85 α was barely detectable in p130Cas immunoprecipitates but p85-p130Cas interaction increased upon 10 minutes of EGF stimulation (Fig. 5D). Moreover, we observed that p85 α efficiently co-immunoprecipitated with tyrosine-phosphorylated p130Cas upon EGF stimuli and this was correlated with increased PI3K activity, measured by PI(3,4,5)P3 ELISA (Fig. 5D-E). Accordingly, the absence of p130Cas decreased PI3K activity in Kras^{G12D}, consistent with the maintenance of p85 α -mediated PI3K inhibition in Kras^{G12D}; p130Cas^{KO} acini (Fig. 5E).

P130Cas expression in human PDAC correlates with AKT activation.

Elevated activation of PI3K-AKT pathway is a classical and uniform feature of human PDAC with strong pAKT staining in ADM, PanIN and PDAC specimens⁵⁵. To highlight the connection between p130Cas and PI3K activation in human PDAC, frozen tissues from 8 PDAC patients with high and 8 PDAC patients with low p130Cas expression were selected and tested for the phosphorylation of AKT and ERK1/2 by ELISA. Tumors with higher p130Cas levels also displayed increased phosphorylation of AKT but not phosphorylated ERK1/2 (Fig. 5F), in line with data obtained from animal models. MAPK dysregulation and ERK1 activation are also a well characterized events in pancreatic cancer that frequently match PI3K-AKT pathway upregulation downstream oncogenic Kras³⁴. ERK phosphorylation uniformly distributed between p130Cas^{high} and p130Cas^{low} tumors reinforcing the influence of p130Cas expression on PI3K-AKT pathway.

These data support the relevance of p130Cas expression in the modulation of PI3K-AKT signaling in response to oncogenic Kras through the regulation of PI3K/AKT pathway in human pancreatic cancer.

3. Discussion

In this study, we found that p130Cas deletion affected pancreatic acinar plasticity and malignant transformation induced by oncogenic Kras mutation. To our knowledge, this is the first animal model that interprets the function of p130Cas in PDAC, shedding light on the connection between p130Cas and pancreatic cancer suggested by GWAS.

Despite the clear role of Kras mutations as oncogenic drivers of PDAC, several evidences highlight the fact that Kras signaling must reach a certain threshold in order to transform the pancreatic cells and that this process mainly depends on the regulation of downstream activation of PI3K-AKT pathway^{26,54,64}. In this context, both EGFR and Kras signaling are necessary to elevate PI3K activity to induce acinar metaplasia locking them in a persistently dedifferentiated, ductal state that is susceptible to mutant Kras oncogenic transformation^{65,66}. Accordingly, targeting of EGFR-mediated Kras activation or the direct inhibition of PI3K downstream pathway are able to prevent Kras-induced transformation^{56,65–67}, but other important regulators of acinar plasticity are still unknown. It has been recently demonstrated by Li and colleagues that oncogenic Kras is able to stabilize a key transcriptional program in acinar cells, locking them into a progenitor-like state to initiate tumorigenesis. More efforts are still necessary to identify determinants that allow acinar cells to respond to oncogenic Kras injury and to adopt this progenitor state.

In this context, our studies provide insights into how p130Cas coopts with oncogenic Kras to activate PI3K-AKT effector pathway to initiate ADM program allowing the transition of acinar cells into ductal intermediates susceptible to malignant transformation.

Initial analysis of human samples revealed that a large proportion of PDAC cases display high p130Cas levels, similarly to what observed in other tumor types⁶⁸, that correlate with OS and PFS in multivariate analysis. However, these data did not elucidate the precise role of p130Cas in the complex scenario of PDAC origin and evolution.

As recently demonstrated in mouse models^{23,39,42}, both acinar and ductal cells have the potential to behave as PDAC cell of origin, that, through various steps, acquires tumorigenic characteristics. The final composition of PDAC, in terms of acinar and ductal-derived cancer cells, mainly depends on the different genetic lesions introduced into the cells. Acinar and ductal cells have different degree of susceptibility to Kras^{G12D}-induced transformation, where acinar cells are the most sensitive and quickly undergo ADM while ductal cells are more refractory to this injury²⁴. It has been demonstrated that the introduction of inactivating TP53 mutations, like in the Pdx^{Cre}; Kras^{G12D};

Trp53^{R172H} model adopted in this study, generates both acinar and duct-derived tumors that could be distinguished by AGR2 protein expression.

This knowledge helped us to understand why p130Cas deletion in Kras^{G12D}; p53^{R172H} animals did not prevent tumor development, although tumors appear with considerable delay, extending mice survival. In p53-null mice, neoplastic lesions lacking p130Cas take longer to develop than the p130Cas-positive ones resulting in a shifted survival curve with the same progression profile. This kinetic could be potentially by the different contribution of p130Cas to tumor onset in acinar or ductal cells. Indeed, p130Cas-null PDAC displayed uniform AGR2 staining and exclusive ductal origin. These data suggest that in Kras^{G12D}; p53^{R172H} animals p130Cas absence delayed tumor onset by limiting early acinar transformation, whereas ductal cells bypass p130Cas requirement and form tumors at later time points.

Accordingly, we predicted that p130Cas should mostly influence acinar-dependent tumorigenesis.

In Kras wild-type mice subjected to caerulein administration, p130Cas expression increased in acini undergoing ADM but readily dropped during acinar recovery. In Kras^{G12D} mice treated with caerulein, p130Cas levels increased similarly but were maintained over time, along with the stabilization of ADM lesions.

Strikingly, loss of p130Cas prevented acinar transdifferentiation and malignant transformation induced by Kras^{G12D}, even in the setting of experimental pancreatitis. In animal models, it has been demonstrated that both PI3K-AKT and EGFR signaling pathways are crucial regulators of cancer onset induced by Kras oncogene^{55,56,65,69}. In p130Cas-deficient acinar cells we found an impaired activation of PI3K-AKT pathway following EGF stimulation or Kras^{G12D} oncogenic signaling without evident effect on ERK1/2 activation. In addition, we validated the already reported p130Cas-p85 α interaction also in pancreatic acinar cells. We demonstrated that p85 regulatory subunit interacts with tyrosine-phosphorylated p130Cas and this association correlates with increased PI3K activity. This led us to hypothesize a specific role for p130Cas in the release of p85 α -mediated inhibition of PI3K catalytic subunit, allowing the production of PI(3,4,5)P3 lipid moiety required for AKT activation. This work provided another proof that Kras mutation, of itself, could not be sufficient to drive tumorigenesis in particular cellular contexts and that converging signaling pathways or

environmental factors are necessary to elevate Kras signaling above a certain threshold and unleash its oncogenic potential. To this end, high p130Cas expression is required to overcome this limitation, similar to what has been already demonstrated for EGFR signaling and inflammation.

High p130Cas protein levels, that occurred in about 60% of human PDAC samples, were correlated with increased phosphorylation of AKT compared to samples with low p130Cas expression. In this context we could not detect statistical differences in ERK1/2 phosphorylation in regard to p130Cas expression, supporting the specific influence of p130Cas on PI3K-AKT pathway activation in PDAC.

This scenario opens the possibility to explore the potential vulnerability of p130Cas-overexpressing tumors to PI3K-AKT inhibitors. The use of these drugs, despite the large numbers of clinical trials, still remains very limited in part due to the amendable patients selection^{70,71} and we speculate that p130Cas expression might be used to select the most responsive ones.

Ongoing efforts to establish how the different mutational spectra impact on PDAC cell-of-origin might help us to identify those additional pathways affected by p130Cas, shedding light on this complex scenario together with the increasing availability of acinar and duct-specific conditional mouse models. In summary, our findings highlight supportive role of p130Cas in acinar- to- ductal reprogramming during pancreatic carcinogenesis, in the context of oncogenic Kras activation, via regulation of PI3K-AKT pathway. Thus, our studies on the molecular mechanism of p130Cas will advance our understanding of Kras-dependent carcinogenesis in the pancreas and might highlight new vulnerabilities to be exploited for therapeutic intervention.

4. References

1. Neoptolemos JP, Kleeff J, Michl P, et al. Therapeutic developments in pancreatic cancer: current and future perspectives. *Nat Rev Gastroenterol Hepatol* 2018;15:333–348. Available at: <http://dx.doi.org/10.1038/s41575-018-0005-x>.
2. Siegel RL, Miller KD, Jemal A. Cancer statistics, 2019. *CA Cancer J Clin* 2019.
3. Visscher PM, Brown MA, McCarthy MI, et al. Five years of GWAS discovery. *Am J Hum Genet* 2012.
4. Figura G Von, Morris IV JP, Wright CVE, et al. Nr5a2 maintains acinar cell differentiation and constrains oncogenic Kras-mediated pancreatic neoplastic initiation. *Gut* 2014.
5. Flandez M, Cendrowski J, Cañamero M, et al. Nr5a2 heterozygosity sensitises to, and cooperates with, inflammation in KRasG12V-driven pancreatic tumourigenesis. *Gut* 2014.
6. Childs EJ, Mocci E, Campa D, et al. Common variation at 2p13.3, 3q29, 7p13 and 17q25.1 associated with susceptibility to pancreatic cancer. *Nat Genet* 2015;47. Available at: <https://www.nature.com/ng/journal/v47/n8/pdf/ng.3341.pdf> [Accessed May 24, 2017].
7. Zhong J, Jermusyk A, Wu L, et al. A Transcriptome-Wide Association Study (TWAS) Identifies Novel Candidate Susceptibility Genes for Pancreatic Cancer. *JNCI J Natl Cancer Inst* 2020. Available at: <https://academic.oup.com/jnci/advance-article/doi/10.1093/jnci/djz246/5698709>.
8. Wolpin BM, Rizzato C, Kraft P, et al. Genome-wide association study identifies multiple susceptibility loci for pancreatic cancer. *Nat Genet* 2014;46:994–1000. Available at: <https://www.nature.com/ng/journal/v46/n9/pdf/ng.3052.pdf> [Accessed May 24, 2017].
9. Tikhmyanova N, Little JL, Golemis EA. CAS proteins in normal and pathological cell growth control. *Cell Mol Life Sci* 2010;67:1025–1048.
10. Tornillo G, Defilippi P, Cabodi S. Cas proteins: dodgy scaffolding in breast cancer. *Breast Cancer Res* 2014;16:443. Available at: <http://www.pubmedcentral.nih.gov/articlerender.fcgi?artid=4384296&tool=pmcentrez&rendertype=abstract>.
11. Defilippi P, Stefano P Di, Cabodi S. p130Cas: a versatile scaffold in signaling networks.

Trends Cell Biol 2006;16:257–263.

12. Tornillo G, Bisarò B, Camacho-Leal MDP, et al. P130Cas promotes invasiveness of three-dimensional ErbB2-transformed mammary acinar structures by enhanced activation of mTOR/p70S6K and Rac1. *Eur J Cell Biol* 2011;90:237–248. Available at: <http://dx.doi.org/10.1016/j.ejcb.2010.09.002>.
13. Bisaro B, Sciortino M, Colombo SM, et al. p130Cas scaffold protein regulates ErbB2 stability by altering breast cancer cell sensitivity to autophagy. *Oncotarget* 2015;132:3–4. Available at: <http://www.oncotarget.com/abstract/6710> [Accessed January 30, 2017].
14. Cabodi S, Tinnirello A, Bisaro B, et al. p130Cas is an essential transducer element in ErbB2 transformation. *FASEB J* 2010;24:3796–3808.
15. Cabodi S, Tinnirello A, Stefano P Di, et al. p130Cas as a new regulator of mammary epithelial cell proliferation, survival, and HER2-Neu oncogene- dependent breast tumorigenesis. *Cancer Res* 2006;66:4672–4680.
16. Miao Y, Li AL, Wang L, et al. Expression of p130cas, E-cadherin and β -Catenin and their correlation with clinicopathological parameters in non-small cell lung cancer: P130cas over-expression predicts poor prognosis. *Folia Histochem Cytobiol* 2012;50:392–397.
17. Storz P. Acinar cell plasticity and development of pancreatic ductal adenocarcinoma. *Nat Rev Gastroenterol Hepatol* 2017;14:296–304. Available at: <http://www.nature.com/articles/nrgastro.2017.12> [Accessed April 28, 2019].
18. Means AL, Meszoely IM, Suzuki K, et al. Pancreatic epithelial plasticity mediated by acinar cell transdifferentiation and generation of nestin-positive intermediates. *Development* 2005;132:3767–3776.
19. Xu Y, Liu J, Nipper M, et al. Ductal vs. acinar? Recent insights into identifying cell lineage of pancreatic ductal adenocarcinoma. *Ann Pancreat Cancer* 2019;2:11–11. Available at: <http://apc.amegroups.com/article/view/4880/html> [Accessed January 8, 2020].
20. Giroux V, Rustgi AK. Metaplasia: Tissue injury adaptation and a precursor to the dysplasia-cancer sequence. *Nat Rev Cancer* 2017;17:594–604.
21. Bailey JM, DelGiorno KE, Crawford HC. The secret origins and surprising fates of pancreas tumors. *Carcinogenesis* 2014;35:1436–1440. Available at:

<https://academic.oup.com/carcin/article-lookup/doi/10.1093/carcin/bgu056> [Accessed July 3, 2019].

22. Carrière C, Seeley ES, Goetze T, et al. The Nestin progenitor lineage is the compartment of origin for pancreatic intraepithelial neoplasia. *Proc Natl Acad Sci U S A* 2007;104:4437–42. Available at: <http://www.ncbi.nlm.nih.gov/pubmed/17360542> [Accessed July 3, 2019].
23. Storz P, Crawford HC. Carcinogenesis of Pancreatic Ductal Adenocarcinoma. *Gastroenterology* 2020;158:2072–2081.
24. Kopp JL, Figura G von, Mayes E, et al. Identification of Sox9-Dependent Acinar-to-Ductal Reprogramming as the Principal Mechanism for Initiation of Pancreatic Ductal Adenocarcinoma. *Cancer Cell* 2012.
25. La O J-P De, Emerson LL, Goodman JL, et al. Notch and Kras reprogram pancreatic acinar cells to ductal intraepithelial neoplasia. *Proc Natl Acad Sci* 2008;105:18907–18912. Available at: <http://www.pnas.org/cgi/doi/10.1073/pnas.0810111105>.
26. Friedlander SYG, Chu GC, Snyder EL, et al. Context-Dependent Transformation of Adult Pancreatic Cells by Oncogenic K-Ras. *Cancer Cell* 2009.
27. Liu J, Akanuma N, Liu C, et al. TGF- β 1 promotes acinar to ductal metaplasia of human pancreatic acinar cells. *Sci Rep* 2016.
28. Akanuma N, Liu J, Liou GY, et al. Paracrine Secretion of Transforming Growth Factor β by Ductal Cells Promotes Acinar-to-Ductal Metaplasia in Cultured Human Exocrine Pancreas Tissues. *Pancreas* 2017.
29. Guerra C, Schuhmacher AJ, Cañamero M, et al. Chronic Pancreatitis Is Essential for Induction of Pancreatic Ductal Adenocarcinoma by K-Ras Oncogenes in Adult Mice. *Cancer Cell* 2007.
30. Pei H, Li L, Fridley BL, et al. FKBP51 Affects Cancer Cell Response to Chemotherapy by Negatively Regulating Akt. *Cancer Cell* 2009.
31. Yang S, He P, Wang J, et al. A novel MIF signaling pathway drives the malignant character of pancreatic cancer by targeting NR3C2. *Cancer Res* 2016.
32. Zhang G, He P, Tan H, et al. Integration of metabolomics and transcriptomics revealed a fatty acid network exerting growth inhibitory effects in human pancreatic cancer. *Clin*

Cancer Res 2013.

33. Habbe N, Shi G, Meguid RA, et al. Spontaneous induction of murine pancreatic intraepithelial neoplasia (mPanIN) by acinar cell targeting of oncogenic Kras in adult mice. *Proc Natl Acad Sci* 2008;105:18913–18918. Available at: <http://www.pnas.org/cgi/doi/10.1073/pnas.0810097105>.
34. Buscail L, Bournet B, Cordelier P. Role of oncogenic KRAS in the diagnosis, prognosis and treatment of pancreatic cancer. *Nat Rev Gastroenterol Hepatol* 2020;17:153–168. Available at: <http://dx.doi.org/10.1038/s41575-019-0245-4>.
35. Bailey P, Chang DK, Nones K, et al. Genomic analyses identify molecular subtypes of pancreatic cancer. *Nature* 2016;531:47–52.
36. Hingorani SR, Wang L, Multani AS, et al. Trp53R172H and KrasG12D cooperate to promote chromosomal instability and widely metastatic pancreatic ductal adenocarcinoma in mice. *Cancer Cell* 2005;7:469–483. Available at: <http://www.ncbi.nlm.nih.gov/pubmed/15894267> [Accessed October 27, 2017].
37. Camacho Leal M del P, Costamagna A, Tassone B, et al. Conditional ablation of p130Cas/BCAR1 adaptor protein impairs epidermal homeostasis by altering cell adhesion and differentiation. *Cell Commun Signal* 2018;16:73. Available at: <https://biosignaling.biomedcentral.com/articles/10.1186/s12964-018-0289-z> [Accessed December 11, 2018].
38. Honda H, Oda H, Nakamoto T, et al. Cardiovascular anomaly, impaired actin bundling and resistance to Src- induced transformation in mice lacking p130(Cas). *Nat Genet* 1998;19:361–365. Available at: <https://pubmed.ncbi.nlm.nih.gov/9697697/> [Accessed December 21, 2020].
39. Lee AYL, Dubois CL, Sarai K, et al. Cell of origin affects tumour development and phenotype in pancreatic ductal adenocarcinoma. *Gut* 2019;68:487–498.
40. Bailey JM, Hendley AM, Lafaro KJ, et al. p53 mutations cooperate with oncogenic Kras to promote adenocarcinoma from pancreatic ductal cells. *Oncogene* 2016;35:4282–4288. Available at: <http://www.nature.com/articles/onc2015441> [Accessed January 29, 2020].
41. Ray KC, Bell KM, Yan J, et al. Epithelial Tissues Have Varying Degrees of Susceptibility to

KrasG12D-Initiated Tumorigenesis in a Mouse Model Oshima R, ed. PLoS One

2011;6:e16786. Available at: <https://dx.plos.org/10.1371/journal.pone.0016786>.

42. Ferreira RMM, Sancho R, Messal HA, et al. Duct- and Acinar-Derived Pancreatic Ductal Adenocarcinomas Show Distinct Tumor Progression and Marker Expression. *Cell Rep* 2017.
43. Hingorani SR, Petricoin EF, Maitra A, et al. Preinvasive and invasive ductal pancreatic cancer and its early detection in the mouse. *Cancer Cell* 2003.
44. Kirkegård J, Mortensen FV, Cronin-Fenton D. Chronic Pancreatitis and Pancreatic Cancer Risk: A Systematic Review and Meta-analysis. *Am J Gastroenterol* 2017;112:1366–1372.
45. Morris IV JP, Cano DA, Sekine S, et al. β -catenin blocks Kras-dependent reprogramming of acini into pancreatic cancer precursor lesions in mice. *J Clin Invest* 2010.
46. Guerra C, Schuhmacher AJ, Cañamero M, et al. Chronic Pancreatitis Is Essential for Induction of Pancreatic Ductal Adenocarcinoma by K-Ras Oncogenes in Adult Mice. *Cancer Cell* 2007;11:291–302. Available at: <https://linkinghub.elsevier.com/retrieve/pii/S153561080700027X> [Accessed January 8, 2020].
47. Fukuda A, Wang SC, Morris JP, et al. Stat3 and MMP7 Contribute to Pancreatic Ductal Adenocarcinoma Initiation and Progression. *Cancer Cell* 2011.
48. Ulmasov B, Oshima K, Rodriguez MG, et al. Differences in the degree of cerulein-induced chronic pancreatitis in C57BL/6 mouse substrains lead to new insights in identification of potential risk factors in the development of chronic pancreatitis. *Am J Pathol* 2013.
49. Norberg KJ, Nania S, Li X, et al. RCAN1 is a marker of oxidative stress, induced in acute pancreatitis. *Pancreatology* 2018.
50. Hong X, Zhang J, Wu Q, et al. Challenges in detecting pre-malignant pancreatic lesions during acute pancreatitis using a serum microRNA assay: A study based on KrasG12D transgenic mice. *Oncotarget* 2016.
51. Lisle RC De, Logsdon CD. Pancreatic acinar cells in culture: Expression of acinar and ductal antigens in a growth-related manner. *Eur J Cell Biol* 1990.
52. Wang L, Xie D, Wei D. Pancreatic Acinar-to-Ductal Metaplasia and Pancreatic Cancer. In:

Methods in Molecular Biology. Vol 1882.; 2019:299–308. Available at:
http://link.springer.com/10.1007/978-1-4939-8879-2_26.

53. Jonckheere N, Vasseur R, Seuningen I Van. The cornerstone K-RAS mutation in pancreatic adenocarcinoma: From cell signaling network, target genes, biological processes to therapeutic targeting. *Crit Rev Oncol Hematol* 2017.
54. Eser S, Schnieke A, Schneider G, et al. Oncogenic KRAS signalling in pancreatic cancer. *Br J Cancer* 2014;111:817–822. Available at: <http://www.nature.com/articles/bjc2014215> [Accessed February 26, 2019].
55. Eser S, Reiff N, Messer M, et al. Selective requirement of PI3K/PDK1 signaling for kras oncogene-driven pancreatic cell plasticity and cancer. *Cancer Cell* 2013.
56. Baer R, Cintas C, Dufresne M, et al. Pancreatic cell plasticity and cancer initiation induced by oncogenic Kras is completely dependent on wild-type PI 3-kinase p110 α . *Genes Dev* 2014;28:2621–35. Available at: <http://www.ncbi.nlm.nih.gov/pubmed/25452273> [Accessed March 19, 2019].
57. Rodriguez-Viciano P, Warne PH, Vanhaesebroeck B, et al. Activation of phosphoinositide 3-kinase by interaction with Ras and by point mutation. *EMBO J* 1996.
58. Jiménez C, Hernández C, Pimentel B, et al. The p85 Regulatory Subunit Controls Sequential Activation of Phosphoinositide 3-Kinase by Tyr Kinases and Ras. *J Biol Chem* 2002;277:41556–41562. Available at: <http://www.jbc.org/lookup/doi/10.1074/jbc.M205893200> [Accessed January 20, 2020].
59. Cuevas BD, Lu Y, Mao M, et al. Tyrosine Phosphorylation of p85 Relieves Its Inhibitory Activity on Phosphatidylinositol 3-Kinase. *J Biol Chem* 2001;276:27455–27461.
60. Pleiman CM, Hertz WM, Cambier JC. Activation of phosphatidylinositol-3' kinase by Src-family kinase SH3 binding to the p85 subunit. *Science* 1994;263:1609–12. Available at: <http://www.ncbi.nlm.nih.gov/pubmed/8128248> [Accessed November 15, 2019].
61. Cabodi S, Moro L, Bergatto E, et al. Integrin regulation of epidermal growth factor (EGF) receptor and of EGF-dependent responses. *Biochem Soc Trans* 2004;32:438–442.
62. Li E, Stupack DG, Brown SL, et al. Association of p130CAS with phosphatidylinositol-3-OH kinase mediates adenovirus cell entry. *J Biol Chem* 2000;275:14729–35. Available at:

<http://www.ncbi.nlm.nih.gov/pubmed/10799562> [Accessed June 23, 2019].

63. Riggins RB, DeBerry RM, Toosarvandani MD, et al. Src-dependent association of Cas and p85 phosphatidylinositol 3'-kinase in v-crk-transformed cells. *Mol Cancer Res* 2003;1:428–37. Available at: <http://www.ncbi.nlm.nih.gov/pubmed/12692262> [Accessed June 23, 2019].
64. Ji B, Tsou L, Wang H, et al. Ras Activity Levels Control the Development of Pancreatic Diseases. *Gastroenterology* 2009.
65. Ardito CM, Grüner BM, Takeuchi KK, et al. EGF Receptor Is Required for KRAS-Induced Pancreatic Tumorigenesis. *Cancer Cell* 2012;22:304–317. Available at: <https://www.sciencedirect.com/science/article/pii/S1535610812003376?via%3Dihub> [Accessed February 26, 2019].
66. Navas C, Hernández-Porras I, Schuhmacher AJ, et al. EGF Receptor Signaling Is Essential for K-Ras Oncogene-Driven Pancreatic Ductal Adenocarcinoma. *Cancer Cell* 2012;22:318–330. Available at: <https://www.sciencedirect.com/science/article/pii/S1535610812003388?via%3Dihub> [Accessed March 19, 2019].
67. Carrer A, Trefely S, Zhao S, et al. Acetyl-CoA Metabolism Supports Multistep Pancreatic Tumorigenesis. *Cancer Discov* 2019;9:416–435. Available at: <http://www.ncbi.nlm.nih.gov/pubmed/30626590> [Accessed July 15, 2019].
68. Cabodi S, Camacho-Leal MDP, Stefano P Di, et al. Integrin signalling adaptors: not only figurants in the cancer story. *Nat Rev Cancer* 2010;10:858–870. Available at: <http://dx.doi.org/10.1038/nrc2967>.
69. Navas C, Hernández-Porras I, Schuhmacher AJ, et al. EGF Receptor Signaling Is Essential for K-Ras Oncogene-Driven Pancreatic Ductal Adenocarcinoma. *Cancer Cell* 2012;22:318–330. Available at: <https://linkinghub.elsevier.com/retrieve/pii/S1535610812003388>.
70. Santis MC De, Gulluni F, Campa CC, et al. Targeting PI3K signaling in cancer: Challenges and advances. *Biochim Biophys Acta - Rev Cancer* 2019.
71. Hanker AB, Kaklamani V, Arteaga CL. Challenges for the Clinical Development of PI3K Inhibitors: Strategies to Improve Their Impact in Solid Tumors. *Cancer Discov* 2019;9:482–491. Available at: <http://cancerdiscovery.aacrjournals.org/lookup/doi/10.1158/2159->

8290.CD-18-1175.

5. Methods

Mice

The LSL-Kras^{G12D} and LSL-p53^{R172H} knock-in (from D. Tuveson, Mouse Models of Human Cancers Consortium repository, National Cancer Institute-Frederick), Pdx1^{Cre} (from D.A. Melton, Harvard University, Cambridge, MA) and p130Cas^{fl/fl} (from S. Cabodi, University of Torino) strains were interbred on a mixed background (SV129/C57Bl6) to obtain compound mutant Pdx^{Cre}; Kras^{G12D} (named Kras^{G12D}), Pdx^{Cre}; Kras^{G12D}; Trp53^{R172H} (named Kras^{G12D}; p53^{R172H}), Pdx^{Cre}; Kras^{G12D}; p130Cas^{KO} (named Kras^{G12D}; p130Cas^{KO}), Pdx^{Cre} Kras^{G12D}; p53^{R172H}; p130Cas^{KO} (Kras^{G12D}; p53^{R172H}; p130Cas^{KO}). Pdx1^{Cre} mice of the same age were used as controls. All procedures and animal housing conformed to the regulatory standards and were approved by the ethical committee according the Guide for the Care and Use of Laboratory Animals published by the U.S. National Institutes of Health and approved by the Italian Health Minister (authorization n° 64-2016PR). Pancreatic injury was induced in young mice (8–12 weeks) by a series of six hourly intraperitoneal injections of caerulein (75 mg per kilogram of body weight) that was repeated after 48 hours. Animals were euthanized 1, 5, or 14 days later.

Histology and immunohistochemistry

Normal tissues, pancreata, and cancer tissues of mice at specific age timepoints were fixed with 10% buffered formalin solution overnight and embedded into paraffin by the institutional pathology core laboratory. Sections cut from each paraffin block were stained with hematoxylin/eosin and Alcian Blue following standard protocols. For immunolabeling, unstained 5-mm sections were cut from paraffin blocks and the slides deparaffinized by routine techniques followed by incubation in 1X sodium citrate antigen retrieval buffer (ThermoFisher) before steaming for 20 minutes in pressure cooker. Slides were cooled 2 hours, blocked and incubated overnight with primary antibodies. Immunolabeling was detected using Novolink Polymer Detection System (Leica Biosystems), and sections were counterstained with hematoxylin.

Protein analysis

Cells were homogenized in lysis buffer (120 mM NaCl, 50 mM Tris-HCl pH=8, 1% Triton X-100) supplemented with 25x protease inhibitor cocktail (Roche), 50 mM sodium fluoride and 1 mM sodium orthovanadate. Lysates were cleared by centrifugation at 13,000 rpm for 15 min at 4°C. Protein concentration was determined by Bradford method and supernatants were analyzed for

immunoblotting or for immunoprecipitation (IP) with the indicated antibodies. Membranes probed with the indicated antibodies were then incubated with HRP conjugated secondary antibodies (anti-mouse used 1:10000, anti-rabbit 1:5000, Sigma) and developed with enhanced chemiluminescence (ECL, Biorad). For IP assays, cells were lysed in IP lysis buffer (150 mM NaCl, 50 mM Tris (pH 7.5), 1% Igepal CA-630, 0.5% deoxycholate) and 1 mg of pre-cleared extracts were incubated with 1 µg of the indicated antibody at 4°C on a rotating rack overnight. Then 15 µl of protein G-Dynabeads (ThermoFisher) were added for 2 hours. Samples were collected by centrifugation (13000 rpm 1 min) and washed six-times with IP lysis buffer. Bound protein complexes were then eluted by adding 30 µl Laemmli sample buffer.

Antibodies

Mouse monoclonal antibodies to human/murine p130Cas were produced in our department. Additional p130Cas antibodies were purchased from BD Transduction Laboratory (Material number 610272) and Cell Signaling Technology (cloneE1L9H, #13846). Antibodies against ERK1/2 (4696), P-ERK1/2 (4370), AKT (2920), P-AKT (9271 and 9277), GAPDH (2118), were from Cell Signaling Technology. Antibodies against Amylase (A8273), AGR2 (HPA007912), CK19 (MABT913) were from Sigma Aldrich.

PI(3,4,5)P3 quantification

Levels of PI(3,4,5)P3 were measured by ELISA kit (Echelon Bioscience, K2500) following manufacturer protocol.

Preparation of Pancreatic Epithelial Explants Culture

The procedure to isolate primary pancreatic acinar cells was described in detail previously (Means et al, 2005). In brief, the pancreas was removed, washed twice with ice-cold Hank's balanced salt solution (HBSS) media, minced into 1–5mm pieces and digested with collagenase I (37 °C, shaker). Collagen digestion was stopped by adding an equal volume of ice- cold HBSS media containing 5% fetal bovine serum (FBS). The digested pancreatic pieces were washed twice with HBSS media containing 5% FBS and then pipetted through 500 µm and then 105 µm meshes. The supernatant of the cell suspension containing acinar cells was added dropwise to 20ml HBSS containing 30% FBS. Acinar cells were then pelleted (1,000 r.p.m., 2min at 4 °C), re-suspended in 10 ml RPMI complete media (1% FBS, 0.1 mg/ml trypsin inhibitor, 1 mg/ml dexamethasone) and plated into low-adhesion

dishes for standard culture. For the 3D explant culture, cell culture plates were coated with collagen I. Isolated primary pancreatic acinar cells were added as a mixture with collagen I/medium media on the top of this layer. Further, complete media was added on top of the cell/gel mixture, replaced the following day and then every other day.

Tissue microarrays (TMAs), Immunohistochemistry (IHC) and correlation with clinical outcome

To evaluate novel proteins as potential prognostic biomarker we selected a cohort of early stage patients (stage I–IIb, n = 95) treated with gemcitabine in the adjuvant setting. Representative cores of individual primary PDAC FFPE tissues prior to treatment were selected and combined in TMAs, as described previously (Giovannetti et al., 2014). IHC staining of p130Cas was performed according to manufacturer's protocol. As negative control, slides stained with no primary antibody were used. Visualization was obtained with BenchMark Special Stain Automation system (Ventana Medical Systems, Export, USA). Staining was evaluated by a molecular pathologist, assessing the amount of tumor and tissue loss, background, and overall interpretability. Immunostaining intensity was classified into two grades: low and high 130Cas expression using a scoring system based on staining intensity and on the number of stained cells, as follows: immunostaining intensity was classified into four grades: 0 (absent), 1 (weak), 2 (moderate), 3 (strong). We attributed one, two, or three additional points if the percentage of positive cells was less than 25%, 25% to 50%, or greater than 50%, respectively. Neoplastic cells were always uniformly stained and positivity assessment was made by counting all the tumor cells present in three tumor cores. All patients provided written informed consent for the storage, analysis of their tumor material and survival data. This study was approved by the Local Ethics Committee of the University of Pisa (Ethics approval #3909, 3 July 2013). Correlation with clinicopathological characteristics, including progression-free survival (PFS) and overall survival (OS), was tested with Kaplan–Meier curves and the log-rank test. Univariate analysis was performed and factors with a p value below 0.1 were evaluated in the multivariate analysis according to the Wald model, using SPSS software version 26 (IBM Corp, Armonk, NY). Statistical significance was set at p values below 0.05.

Tissue extracts and phospho-AKT and phospho-ERK enzyme-linked immunosorbent assays (ELISA)

Pancreatic levels of phospho-AKT and phospho-ERK were determined in stored supernatants from homogenized pancreatic cancer tissues by use of ELISA kits. In particular, the dual phosphorylation of ERK2 at threonine-185 and tyrosine-187 (ERK2 [pTpY185/187]) and ERK1 at threonine-202 and tyrosine-204 (ERK1 [pTpY202/204]) and the AKT phosphorylation at serine-473 (AKT [pS473]) were

evaluated with specific ELISA assays (Invitrogen), as described previously (Giovannetti et al, 2011). Selected frozen tissues from 8 PDAC patients with high and 8 PDAC patients with low p130Cas expression were collected and weighed in the same manner during preparation. Extract preparation was performed as recommended by the manufacturer. Briefly, each tissue sample was prepared with PBS and homogenized in cell lysis buffer (Cell Signaling Technology) containing Protease Inhibitor Cocktail. After incubation on ice for 30 minutes, the homogenate was centrifuged at 14,000 x g for 10 min at 4°C, and the supernatant was transferred to microtiter plates coated with monoclonal antibodies specific for phospho-AKT and phospho-ERK. Standard curves were run with each assay using 100, 50, 25, 12.5, 6.25, 3.12, and 1.6 U/ml phosphorylated full-length human recombinant phospho-AKT and phospho-ERK. After overnight incubation at 4°C, the solution was aspirated from wells, and 100 µl of rabbit anti-phospho-AKT or anti-phospho-ERK was added into each well. Plates were incubated at room temperature for 1 hour, washed four times, and 100 µl of a working solution of horseradish peroxidase-labeled anti-rabbit IgG was added into each well. After 30 minutes, a chromogen solution was added; 20 minutes later, the reactions were stopped with 100 µl of a stop solution, and the absorbance was read at 450 nm at 20 minutes intervals for 120 minutes to construct a plot of absorbance increase as a function of time. To calculate phospho-AKT and phospho-ERK concentrations, a standard curve method was used.

Statistical analysis

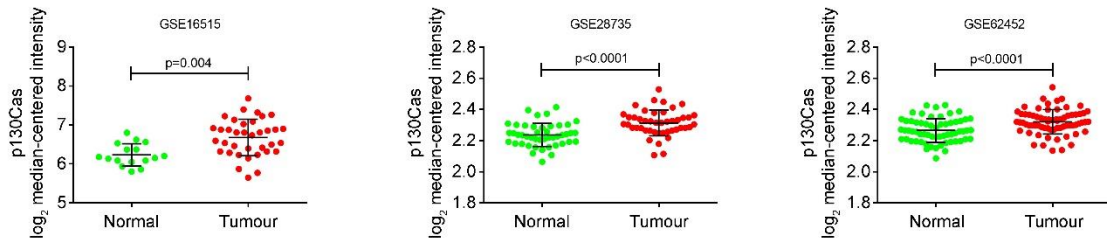
Prism software (GraphPad) was used for statistical analysis. Significance was calculated with Student t test and one- or two-way analysis of variance tests (ANOVA) followed by Bonferroni's post hoc analysis, or Mantel Cox log-rank test where appropriate. Values are reported as the mean ± standard deviation (SD).

Table 1

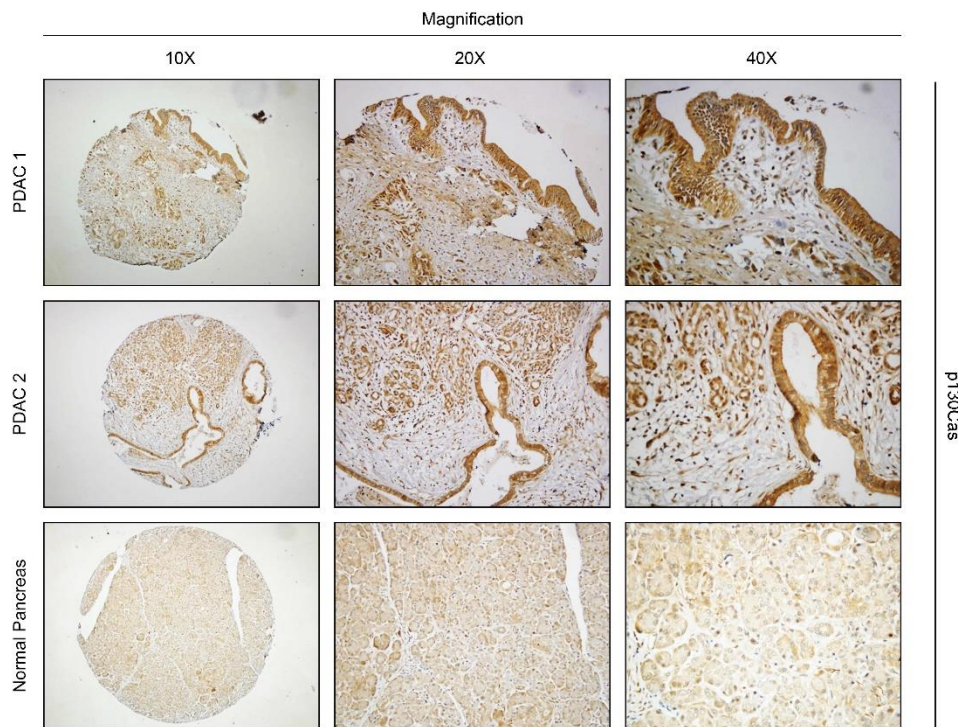
Table X. Patients' clinicopathological characteristics and outcome						
Univariate analysis	Overall Survival (OS)			Progression-Free Survival (OS)		
	N (%)	months mean (95% CI)	p-value	N (%)	months mean (95% CI)	p-value
No. patients	98 (100)	20.5 (18.2-22.8)		98 (100)	17.3 (15.5-19.1)	
Age (years at time of diagnosis)						
<= 65	60 (61.2)	21.28 (16.4-22.1)		60 (61.2)	18.9 (15.6-20.5)	0.224
> 65	38 (38.8)	19.26 (17.9-24.6)	0.352	38 (38.8)	16.2 (13.7-18.6)	
Gender						
Female	41 (41.8)	23.0 (19.0-27.1)	0.081	41 (41.8)	17.9 (15.2-20.7)	0.686
Male	57 (58.2)	18.7 (15.9-21.4)		57 (58.2)	16.9 (14.5-19.2)	
Performance Status						
0-1	77 (78.6)	21.2 (18.5-24.0)	0.200	77 (78.6)	17.9 (15.8-20.0)	0.154
2	21 (21.4)	17.8 (13.8-21.9)		21 (21.4)	15.4 (12.2-18.5)	
Vascular Infiltration						
no	36 (36.7)	24.6 (20.2-29.0)	0.011	36 (36.7)	20.1 (16.9-23.5)	0.019
yes	62 (63.3)	18.1 (15.6-20.6)		62 (63.3)	15.7 (13.7-17.6)	
Tumor grade						
Grade 1-2	49 (50.0)	22.9 (19.2-26.7)	0.035	49 (50.0)	19.7 (16.9-22.4)	0.027
Grade 3	49 (50.5)	18.1 (15.4-20.7)		49 (50.5)	15.0 (12.8-17.1)	
Resection Margin						
no	52 (53.1)	18.8 (15.3-22.4)	0.220	52 (53.1)	18.5 (15.9-20.9)	0.198
yes	46 (46.9)	21.9 (18.6-24.7)		46 (46.9)	16.1 (13.5-18.6)	
p130Cas/BCAR1						
low	41 (41.8)	23.9 (19.8-28.2)	0.017	41 (41.8)	20.3 (17.1-23.3)	0.005
high	57 (58.2)	18.0 (15.5-20.6)		57 (58.2)	15.2 (13.2-17.2)	
Multivariate analysis		Risk of death, HR (95% CI)	p-value		Risk of progression, HR (95% CI)	p-value
Vascular Infiltration (no vs. yes)		0.47 (0.22-0.81)	0.033		0.58 (0.28-0.79)	0.038
Grading (3 vs. 1-2)		0.62 (0.29-0.95)	0.047		0.61 (0.30-0.87)	0.042
p130Cas/BCAR1 (low vs. high)		0.51 (0.25-0.87)	0.044		0.34 (0.21-0.72)	0.031

Figures

A



B



C

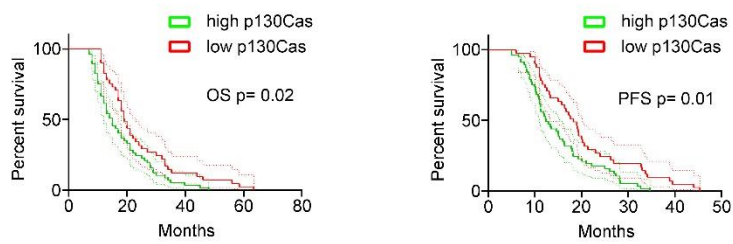
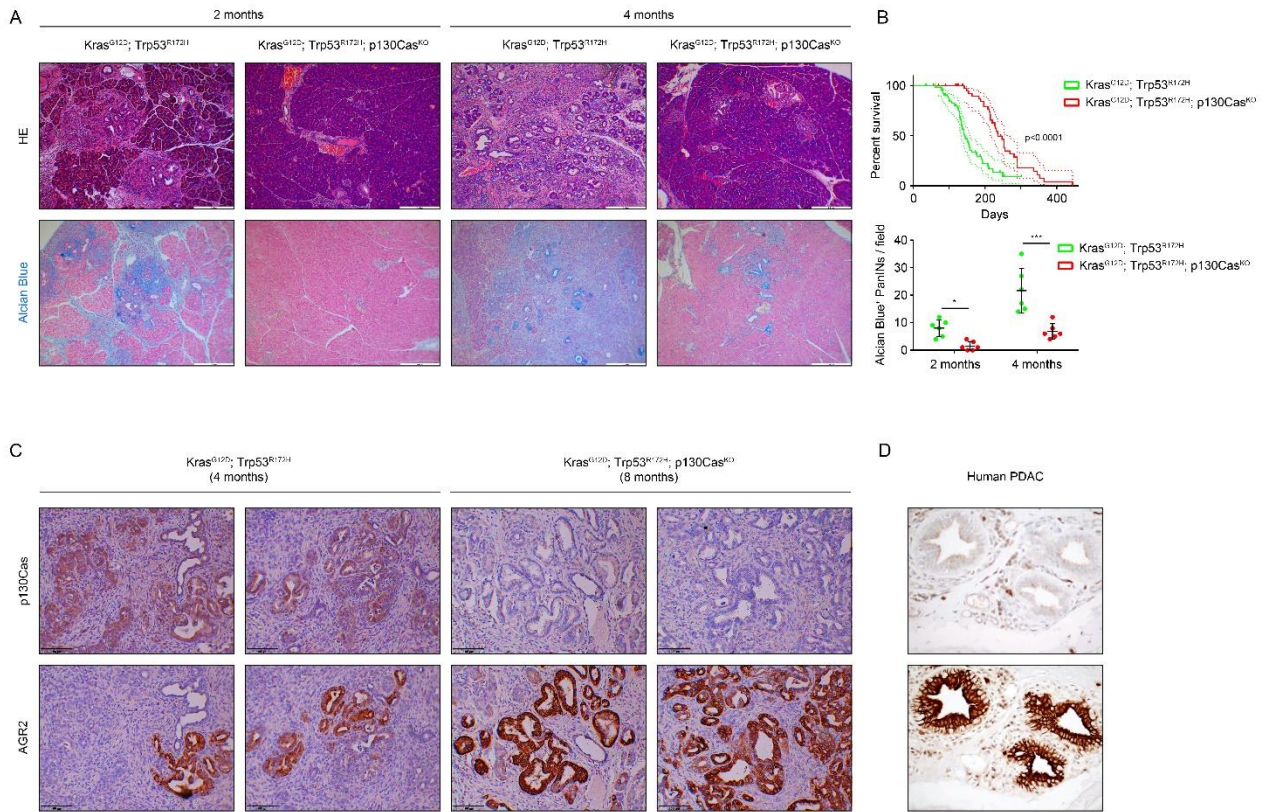


Fig. 1



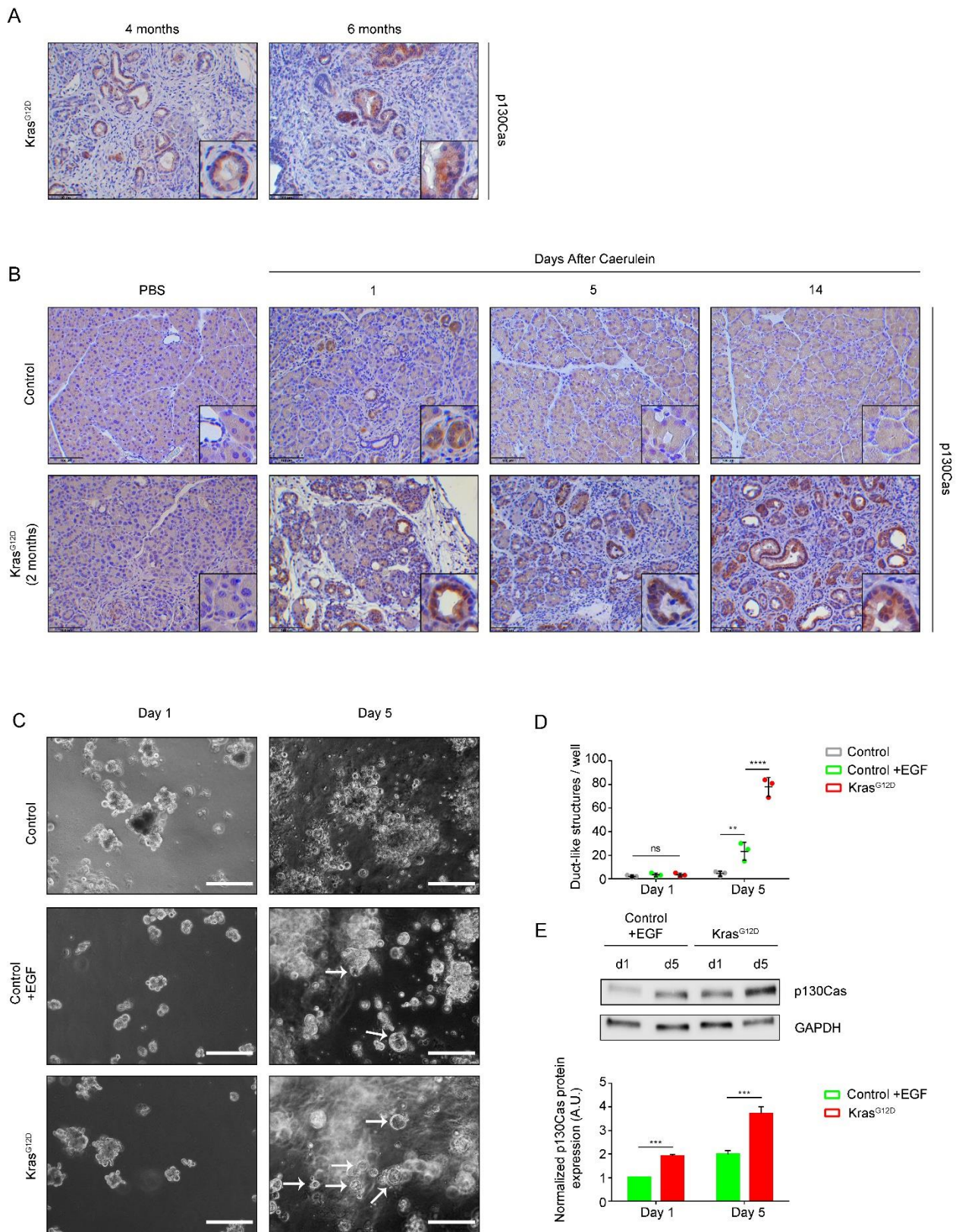


Fig. 3

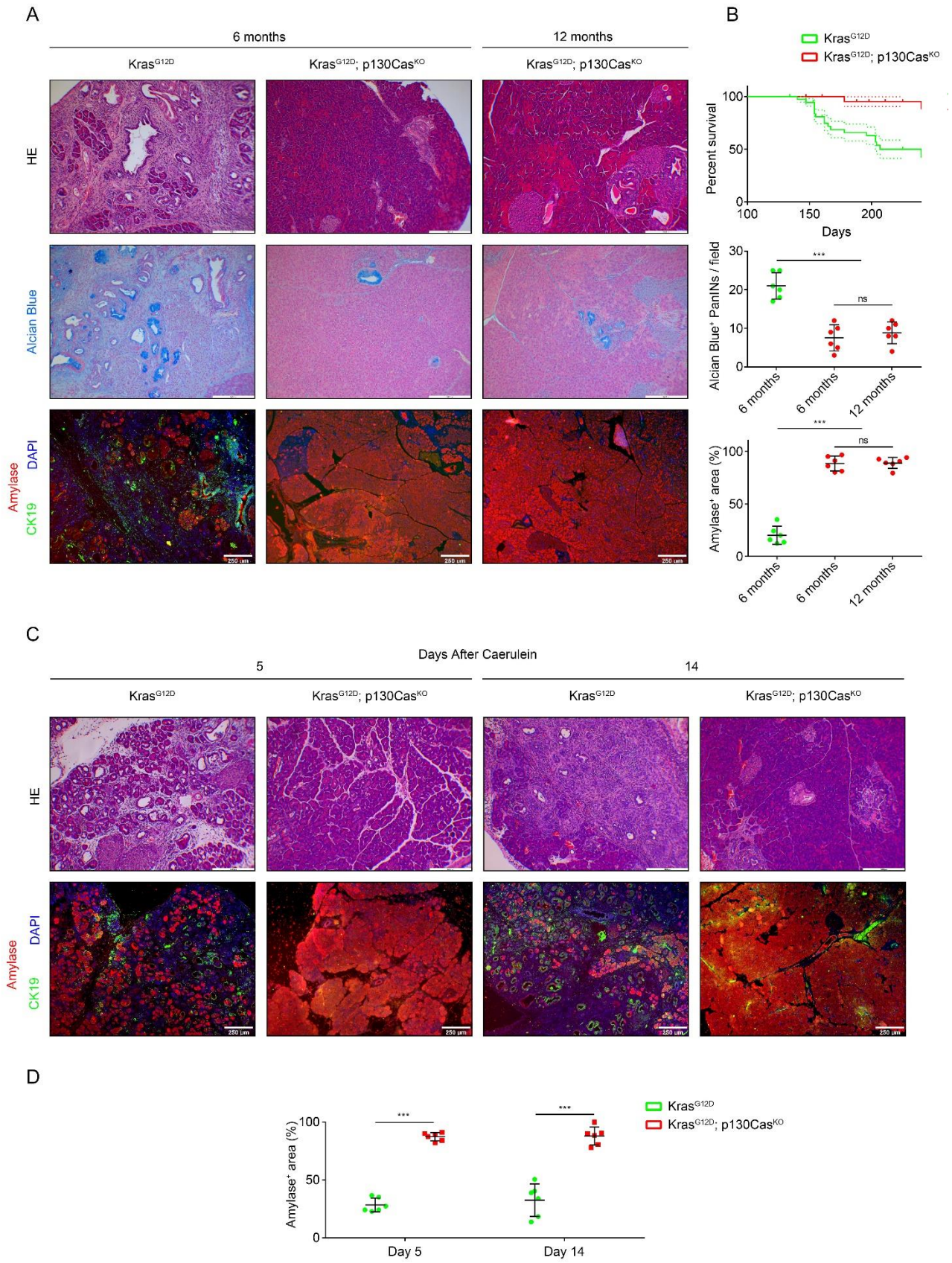


Fig. 4

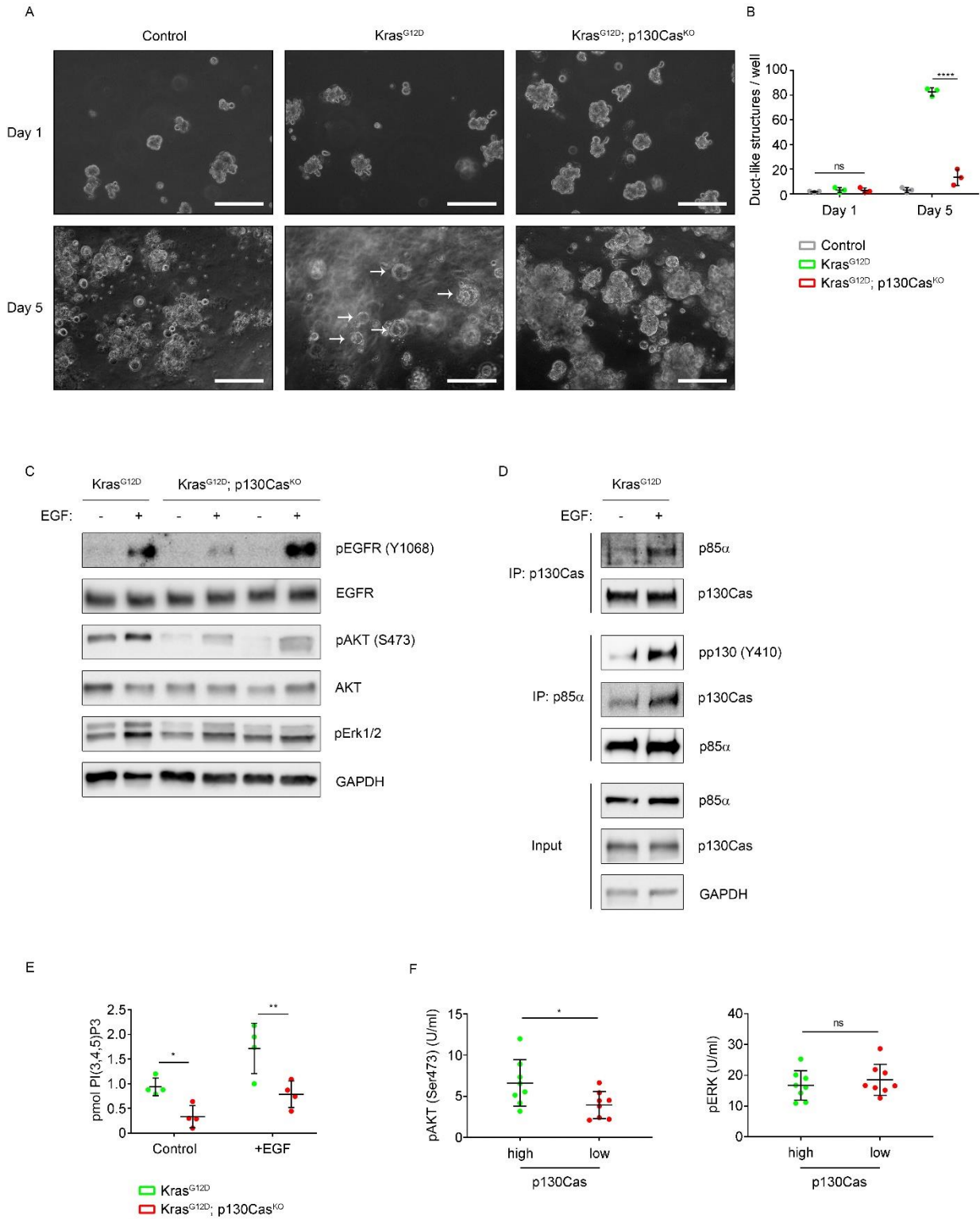
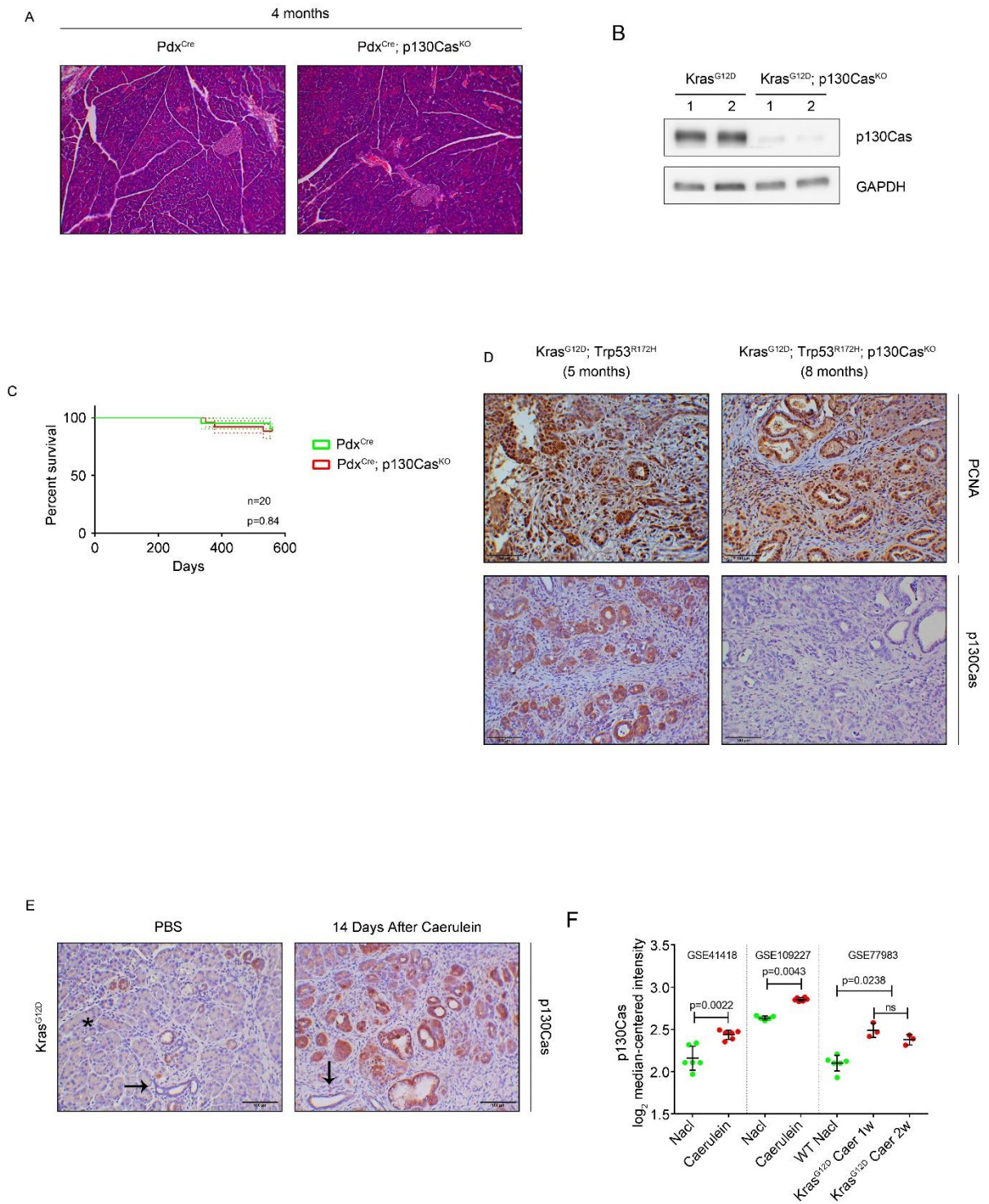
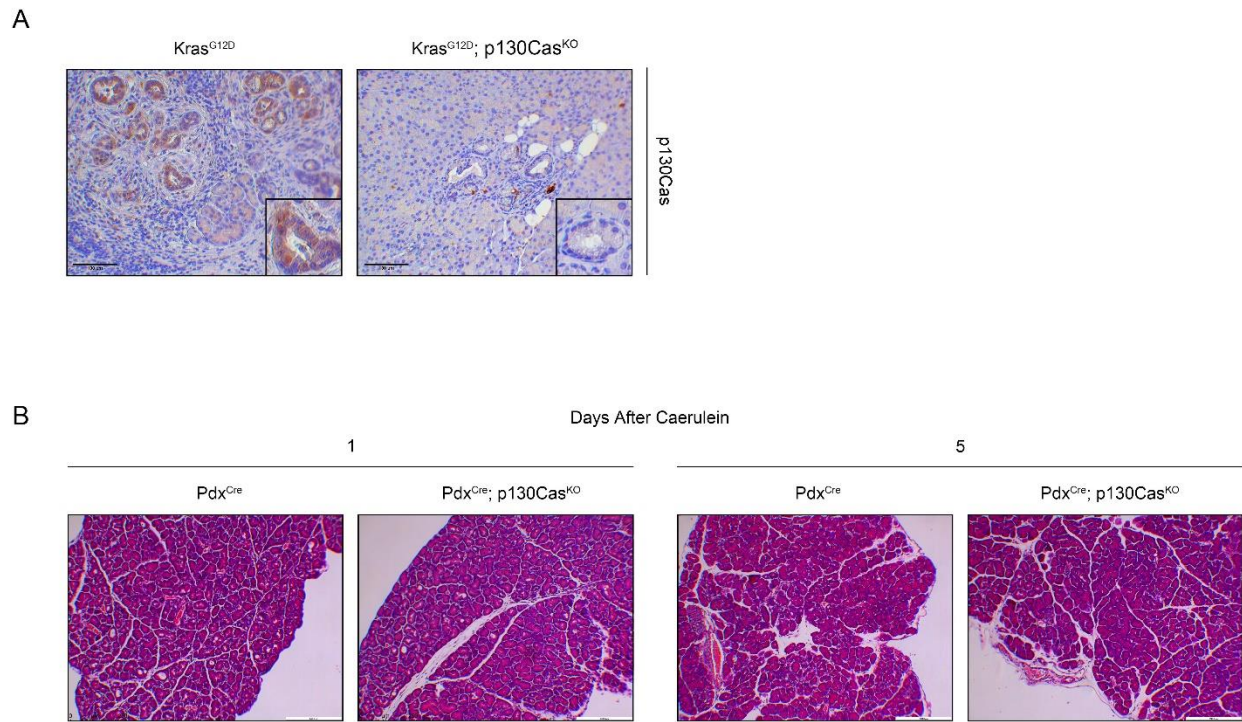


Fig. 5



Suppl. Fig. 1



Suppl. Fig. 2

6. Figure legends

Figure 1. (A) Log₂ median-centered p130Cas RNA expression in normal vs. PDAC samples from indicated studies. Exact P-values determined by Mann–Whitney test. (B) Representative results from IHC staining for p130Cas in human PDAC (n = 96) and normal pancreas (n = 4) samples. (C) Kaplan-Meier curves showing significantly lower OS and PFS in patients with elevated p130Cas staining (green) than with low p130Cas staining (red). Statistical analysis was performed with Mantel-Cox log rank test.

Figure 2. (A) Pancreatic tissue (normal acinar area and regions with ADM and PanINs) from *Kras*^{G12D}; *Trp53*^{R172H} and *Kras*^{G12D}; *Trp53*^{R172H}; *p130Cas*^{KO} mice was stained with haematoxylin and eosin (H&E) and Alcian Blue, as indicated. (B upper panel) Statistical analysis of Alcian Blue-positive lesions of pancreata from *Kras*^{G12D}; *Trp53*^{R172H} (n = 6) and *Kras*^{G12D}; *Trp53*^{R172H}; *p130Cas*^{KO} (n = 6) mice. (B lower panel) Kaplan- Meier survival curve between *Kras*^{G12D}; *Trp53*^{R172H} (n = 70) and *Kras*^{G12D}; *Trp53*^{R172H}; *p130Cas*^{KO} (n = 51) mice. Statistical analysis was performed with Mantel-Cox log rank test. (C) IHC for p130Cas and AGR2 in *Kras*^{G12D}; *Trp53*^{R172H} and *Kras*^{G12D}; *Trp53*^{R172H}; *p130Cas*^{KO} mice. (D) IHC for p130Cas and AGR2 in a p130Cas-low PDAC human sample. Statistical analysis was performed with 2way ANOVA and presented as mean±SD. *p<0.05; ***p<0.001.

Figure 3. (A) IHC for p130Cas in 4- and 6- months old *Kras*^{G12D} pancreata. (B) IHC for p130Cas in control (upper panel) or 2-months old *Kras*^{G12D} pancreata (lower panel) after PBS and caerulein treatments. (C) Primary acinar cells were isolated from mouse pancreas, seeded in 3D culture in collagen and transdifferentiation was induced with EGF as indicated. (D) Ducts formed were photographed, counted, and isolated from the collagen and (E) analysed by western blotting for expression of p130Cas, as indicated (scale bar, 100 μm). Statistical analysis of p130Cas expression and ADM formation were performed with 2way ANOVA from at least three independent experiments. ** p<0.01; ***p<0.001; ****p<0.0001. Data are presented as mean±SD.

Figure 4. (A) Pancreatic tissue (normal acinar area and regions with ADM and PanINs) from *Kras*^{G12D} and *Kras*^{G12D}; *p130Cas*^{KO} mice was stained with haematoxylin and eosin (H&E), Alcian Blue, or analysed by IF for expression of Amylase (red), CK19 (green) and DAPI (blue), as indicated. (B upper

panels) Statistical analysis of Alcian Blue-positive lesions and amylase area of pancreata from $Kras^{G12D}$ (n = 6) and $Kras^{G12D}; p130Cas^{KO}$ (n = 6) mice. (B lower panel) Kaplan- Meier survival curve between $Kras^{G12D}$ (n = 39) and $Kras^{G12D}; p130Cas^{KO}$ (n = 24) mice. Statistical analysis was performed with Mantel-Cox log rank test. (C) Pancreatic tissue (normal acinar area and regions with ADM and PanINs) from $Kras^{G12D}$ and $Kras^{G12D}; p130Cas^{KO}$ mice after caerulein treatment was stained with haematoxylin and eosin (H&E) or analysed by IF for expression of Amylase (red), CK19 (green) and DAPI (blue), as indicated. (D) Statistical analysis of Alcian Blue-positive lesions and amylase area of pancreata from $Kras^{G12D}$ (n = 6) and $Kras^{G12D}; p130Cas^{KO}$ (n = 6) mice. Statistical analysis was performed with 2way ANOVA and presented as mean \pm SD. ***p<0.001.

Figure 5. (A) Primary acinar cells were isolated from mouse pancreas, seeded in 3D culture in collagen and followed for spontaneous transdifferentiation (scale bar, 100 μ m). Ducts formed were photographed and counted. (B) Statistical analysis of ADM formation was performed with 2way ANOVA from at least three independent experiments. (C) WB of primary acinar cells isolated from mouse pancreas and treated with PBS or EGF for 10 minutes, as indicated. (D) Primary acinar cells isolated from mouse pancreas were treated with PBS or EGF for 10 minutes and subjected to immunoprecipitation with anti-p130Cas antibodies. p130Cas/p85 interaction was revealed by WB with anti-p85 antibodies. (E) Primary acinar cells isolated from mouse pancreas were treated with PBS or EGF for 10 minutes and subjected to lipid extraction and PI(3,4,5)P3 ELISA. Statistical analysis was performed with 2way ANOVA and presented as mean \pm SD. *p<0.05; **p<0.01; ****p<0.0001. (F) Quantification of pAKT (Ser473) and pERK1/2 from high-p130cas (n = 8) and low-p130Cas (n = 8) human PDAC samples. Statistical analysis was performed with 2way ANOVA and presented as mean \pm SD. *p<0.05

Supplementary Figure 1. (A) Pancreatic tissue from Pdx^{Cre} and $Pdx^{Cre}; p130Cas^{KO}$ mice was stained with haematoxylin and eosin (H&E). (B) Western blot analysis of pancreatic lysates from Pdx^{Cre} and $Pdx^{Cre}; p130Cas^{KO}$ mice. (C) Kaplan- Meier survival curve between Pdx^{Cre} (n=21) and $Pdx^{Cre}; p130Cas^{KO}$ (n=24) mice. Statistical analysis was performed with Mantel-Cox log rank test. (D) IHC for PCNA and p130Cas in $Kras^{G12D}; Trp53^{R172H}$ and $Kras^{G12D}; Trp53^{R172H}; p130Cas^{KO}$ mice. (E) IHC for p130Cas in 2-months old $Kras^{G12D}$ pancreata treated with saline or caerulein (14 days). Asterisks indicate healthy acini, arrowheads indicate normal pancreatic ducts. (F) Log2 median-centered p130Cas RNA expression in saline-treated (n = 6) vs. caerulein-treated mice (n = 6) (GSE41418),

saline-treated (n = 5) vs. caerulein-treated mice (n = 6) (GSE109227), or saline-treated (n = 6) vs. caerulein-treated *Kras*^{G12D} mice after 1 week (n = 3) or 2 weeks (n = 3) (GSE77983) samples from indicated studies. Exact P-values determined by Mann–Whitney test or one-way ANOVA.


Supplementary Figure 2. (A) IHC for p130Cas in 4-old from *Kras*^{G12D} and *Kras*^{G12D}; p130Cas^{KO} pancreata showing absence of p130Cas expression in rare lesions present in KO animals. (B) Pancreatic tissue from *Pdx*^{Cre} and *Pdx*^{Cre}; p130Cas^{KO} mice after caerulein treatment was stained with haematoxylin and eosin (H&E)

SCIENTIFIC REPORTS



OPEN

Modeling ErbB2-p130Cas interaction to design new potential anticancer agents

Andrea Costamagna¹, Matteo Rossi Sebastiano², Dora Natalini¹, Matilde Simoni¹, Giorgio Valabrega³, Paola Defilippi¹, Sonja Visentin¹, Giuseppe Ermondi¹, Emilia Turco¹, Giulia Caron¹ & Sara Cabodi¹ 

The ErbB2 receptor tyrosine kinase is overexpressed in approximately 15–20% of breast tumors and associated with aggressive disease and poor clinical outcome. p130Cas represents a nodal scaffold protein regulating cell survival, migration and proliferation in normal and pathological contexts. p130Cas overexpression in ErbB2 human breast cancer correlates with poor prognosis and metastasis formation. Recent data indicate that p130Cas association to ErbB2 protects ErbB2 from degradation, thus enhancing tumorigenesis. Therefore, inhibiting p130Cas/ErbB2 interaction might represent a new therapeutic strategy to target breast cancer. Here we demonstrate by performing Molecular Modeling, Molecular Dynamics, dot blot, ELISA and fluorescence quenching experiments, that p130Cas binds directly to ErbB2. Then, by structure-based virtual screening, we identified two potential inhibitors of p130Cas/ErbB2 interaction. Their experimental validation was performed *in vitro* and in ErbB2-positive breast cancer cellular models. The results highlight that both compounds interfere with p130Cas/ErbB2 binding and significantly affect cell proliferation and sensitivity to Trastuzumab. Overall, this study identifies p130Cas/ErbB2 complex as a potential breast cancer target revealing new therapeutic perspectives for protein-protein interaction (PPI).

Breast cancer is the second most common cancer worldwide after lung cancer, the fifth most common cause of cancer death, and the leading cause of cancer death in women¹.

In the last decades breast cancer treatment has greatly improved due to the development of targeted therapies against Receptor Tyrosine Kinases (RTKs) whose hyperactivation or overexpression leads to increased cell proliferation, survival and transformation². In particular, there is a huge interest among medicinal chemists for inhibitors of the epidermal growth factor receptor (EGFR) family which includes four structurally related receptor tyrosine kinases (ErbB1–4). The ErbB proteins function as homo- and hetero- dimerizer upon ligand binding, but ErbB2 is an orphan receptor and its activation upon homo- and hetero- dimerization is ligand-independent. Notably, over-expression or amplification of ErbB2 tyrosine kinase occurs in up to 20% of human breast cancers, where it is predictive of aggressive disease and poor clinical outcome³. Several anti-ErbB2 therapies have been recently proposed including receptor tyrosine kinase inhibitors and humanized monoclonal antibodies. Among them, Trastuzumab was approved for the treatment of breast cancers overexpressing ErbB2, alone or in combination with standard chemotherapy. The mechanism of action of Trastuzumab is complex and not well understood, resulting in modest downregulation of the ErbB2 receptor^{4,5}.

p130Cas is an adaptor protein devoid of any enzymatic or transcriptional activity and its modular structure with various binding motifs allows the formation of multi-protein signaling complexes. This results in the induction and/or maintenance of signaling pathways with pleiotropic effects on cell motility, cell adhesion, cytoskeleton remodeling, invasion, survival and proliferation. The relevance of p130Cas adaptor protein in cancer has been extensively supported. p130Cas overexpression has been detected in human breast, prostate, ovarian, lung, colorectal, pancreatic and hepatocellular carcinoma, as well as in glioma, melanoma, anaplastic large cell

¹Department of Molecular Biotechnology and Health Sciences, University of Torino, Via Nizza 52, 10126, Torino, Italy.

²Institut für Pharmacologie, Universität Bern, Inelspital INO-F, CH-3010, Bern, Switzerland. ³Department of Medical Sciences, University of Torino, Torino, Italy. Andrea Costamagna and Matteo Rossi Sebastiano contributed equally. Giulia Caron and Sara Cabodi jointly supervised this work. Correspondence and requests for materials should be addressed to S.C. (email: sara.cabodi@unito.it)

lymphoma and chronic myelogenous leukemia, although the exact mechanisms that drive p130Cas overexpression in cancer have not yet been identified^{6–8}.

Specifically, in ErbB2-positive breast cancer, p130Cas overexpression correlates with poor prognosis and increase metastatization⁹. From a molecular point of view, it has been demonstrated that p130Cas is a crucial component of a functional molecular complex consisting in ErbB2, c-Src, and FAK supporting cell proliferation and invasion¹⁰. Recently, it was reported that p130Cas is able to stabilize ErbB2, by binding and protecting it from autophagic degradation. Indeed, p130Cas binding to ErbB2 does not allow the association of CHIP and Cbl, the major E3 ubiquitin ligases binding ErbB2, possibly through steric hindrance⁵.

These data also indicate that high levels of p130Cas expression inversely correlate with ErbB2 sensitivity to Trastuzumab. The mechanism through which p130Cas mediates resistance to Trastuzumab might rely on the increased ErbB2 stability to the cell membrane. This increased stabilization of ErbB2 by p130Cas might be the crucial event driving breast cancer progression and resistance, strengthening the relevance of p130Cas as putative therapeutic target to overcome resistance to Trastuzumab⁵.

In addition, alternative ErbB2 targeted therapies, such as Pertuzumab or Trastuzumab-Emtansine (T-DM1) were developed. Combination of Trastuzumab and Pertuzumab treatment have shown a statistically significant increase in overall survival of ErbB2 positive metastatic breast cancer patients^{11,12}, while T-DM1 improved overall survival of ErbB2-positive metastatic patients that failed other ErbB2-targeted drugs¹³.

Even though these therapies extend overall survival in responders, a high percentage of patients develop resistance. Indeed, Trastuzumab/Pertuzumab/Docetaxel versus Trastuzumab/Docetaxel combination treatment increased the patients' responsiveness from 29% to 45.8%¹⁴, while T-DM1 failed to induce response in 57% of patients¹⁵.

Therefore, alternative strategies are needed. Tyrosine kinase inhibitors (TKI) have been proposed as alternative treatments to counteract Trastuzumab resistance, but they have some limitations. The most critical drawback is the development of drug resistance due to secondary mutations of the targeted receptors or to compensatory activation of other RTKs that renders the therapies ineffective.

Consequently, key protein-protein interactions involved in RTKs signaling could represent a major source of novel pharmacological targets. In contrast to enzyme inhibitors (es. TKI), protein-protein interaction inhibitors target larger contact surface often involving more than two contact pockets composed of multiple amino acids located in different region of the protein^{16,17}. This in turn, should limit or delay development of drug resistance due to secondary mutation of the targeted receptor.

Taken together this evidence suggests important therapeutic and translational applications of p130Cas in ErbB2 breast cancer and supports the hypothesis that p130Cas/ErbB2 interaction can serve as a potential target for the discovery and development of new anticancer agents, that can be used in combination with standard therapy to manage and control Trastuzumab resistance.

To verify this hypothesis, we have initially used computer strategies, *in vitro* proteomic approach and cellular models and showed that the SH3 domain of p130Cas binds a specific sequence of ErbB2 intracellular domain. Then, a structure-based virtual screening (SBVS) procedure identified molecules with potential inhibitory activity vs p130Cas/ErbB2 interaction. Two *ad hoc* selected hits resulting from the computational screening were experimentally tested both *in vitro* and in breast cancer cell lines. Finally, the physico-chemical and ADME-Tox profiles of the two molecules were predicted to exploit their full potential as drugs.

Overall this study supports p130Cas/ErbB2 complex as a potential breast cancer target and shows the drugability of this protein-protein interaction (PPI) that might benefit of a more advanced optimization effort for therapeutic applications.

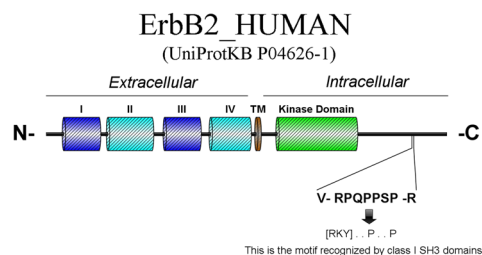
Results

Modeling the interaction of p130Cas and ErbB2. Literature analysis suggests that p130Cas scaffold might independently associate with ErbB2 in a direct way. Due to the structural complexity of the partners, the study focused only on the interaction region between the two proteins. Therefore, we searched for protein-protein binding sequences on ErbB2 cytosolic portion by the online algorithm Eukaryotic Linear Motif (ELM) (www.elm.eu). ELM is a bioinformatic resource combining experimental evidences with a predictive algorithm that returns the biological function (experimentally determined if possible or predicted) of recognized short sequences in eukaryotic proteins¹⁸.

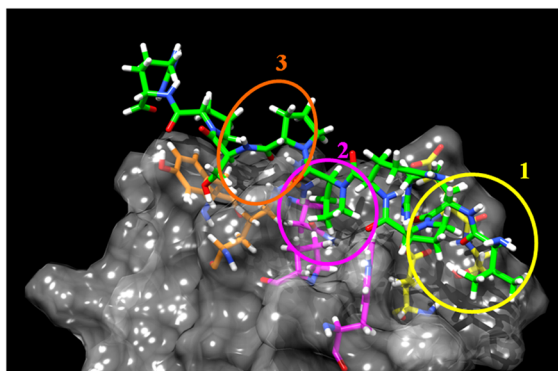
The ELM sequence analysis of C-terminal cytosolic domain of ErbB2 predicts the presence in position 1145–1153 of a -V[RPQPPSP]R- nine amino acid sequence (PPII_ErbB2). The motif is a polyproline type II domain, i.e. a left hand, trans proline coil whose 1–4–7 residue-side chains have the same spatial orientation (RxxPxxP) and could act as a binding site for the SH3 domain of p130Cas (Fig. 1A)^{19–21}. On the basis of these evidences, an *in-silico* interaction model of the PPII_ErbB2 peptide and p130Cas SH3 domain (SH3_p130Cas) was thus built using a template-based modeling strategy²². The structure of the SH3 domain of p130Cas was downloaded from the PDB (PDB code 1WYX, resolution = 1.1 Å)²³. PPII_ErbB2 was modeled using the crystallographic structure of the complex between PD1R, a synthetic peptide with polyproline type II conformation, and the SH3 domain of p85 subunit of PI3K (highly homologous to SH3_p130Cas) (PDB code 3I5R, resolution 1.7 Å). The interaction model (see Experimental Section) shows three contact regions (named 1, 2 and 3 in Fig. 1B): the first concerns PPII_ErbB2 Arg2 that interacts with SH3_p130Cas Glu15 and Glu19 and forms a network of reinforced hydrogen bonds, the second and the third are hydrophobic interactions involving Pro5 and Pro8 (PPII_ErbB2) and apolar pockets of SH3_p130Cas.

Molecular Dynamics (MD) simulations. MD simulations were performed to check the stability over the time of the interaction described above. Results are resumed in Fig. 1C which shows the energy variation with the time (t). No dissociation of the SH3_p130Cas/PPII_ErbB2 complex is observed. As a negative control we

A



B



C

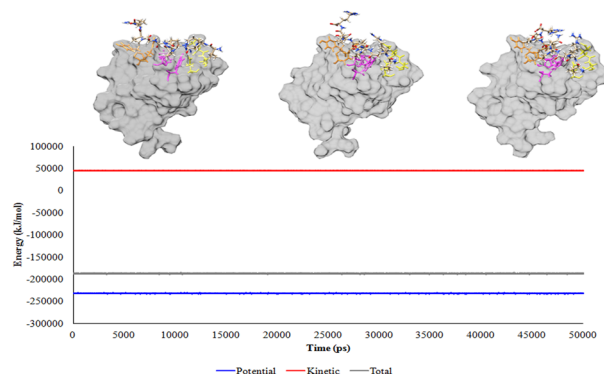


Figure 1. Modeling of SH3_p130Cas/PPII_ErbB2 interaction. (A) Schematic representation of the ErbB2 receptor. The class I SH3 ligand in position 1146–1152 shown in the inset is located in the unstructured carboxy-terminal portion of ErbB2 receptor. (B) PPII_ErbB2 peptide is shown in green, hydrophobic and positive charge interaction surfaces are in grey, negative charge interaction surfaces in cyan. The three interaction sites (1, 2 and 3) are circled in white. The PPII_ErbB2 Arg2, Pro5 and Pro8 side-chains are highlighted in green. Interacting residues for SH3_p130Cas are described in the text. (C) Not standard conditions stages (black dots), standard condition stages (light blue dots), U_{ab} trend line (green), SH3_p130Cas (blue chain), PPII_ErbB2 (red chain). This is shown by the four snapshots in Fig. 2 that represent four dynamics stages distributed along the simulation (standard conditions P [90;110] kPa and T [230;310] K). Stage 2 represents a “peak” in the trend of U_{ab} values; it has been chosen to demonstrate that this U_{ab} variation does not lead to the dissociation of the complex. Apart from stage 2 (and stage 0, the starting point from SH3_p130Cas/PPII_ErbB2 interaction model) no substantial variation in the U_{ab} general trend values were observed, suggesting that there is no difference in complex stability between each couple of stages.

mutated the three PPII residues mainly involved in the interaction into amino acids less prone to stabilize the binding (positive charged Arg2 into negative charged Glu, small Pro5 and Pro8 into the larger Asn) and applied the same MD protocol. Results show a weaker interaction between the mutated peptide and SH3_p130Cas (see Fig. S1 in Supporting Information).

Furthermore, MD simulations were also successfully used to support the binding orientation, –VRPQPPSPR– of the SH3 domain to the polyproline domain (see Fig. S2 in Supporting Information).

***In vitro* validation of the direct interaction between SH3 domain of p130Cas and ErbB2.** We expressed and purified recombinant proteins for p130Cas and ErbB2 as described in the Experimental Section

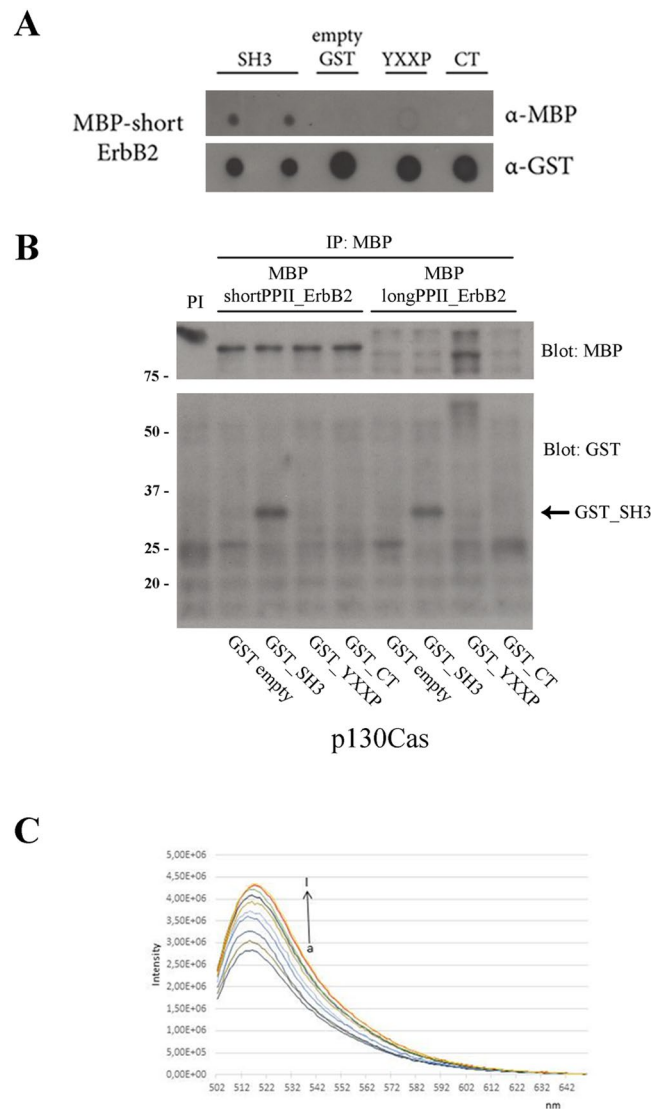


Figure 2. SH3_p130Cas directly interacts with shortPPII_ErbB2 and longPPII_ErbB2 *in vitro*. (A) Dot blot experiment revealed a direct interaction between GST_SH3_p130Cas and MBP_shortPPII_ErbB2 (lane 1–2), using anti-MBP antibody. No interactions were detected with control GST_ctrl, GST_YXXP_p130Cas and GST_CT_p130Cas recombinant proteins (lane 3–5). Normalization was performed with anti-GST antibody. (B) GST_SH3_p130Cas was able to interact with MBP_shortPPII_ErbB2 and MBP_longPPII_ErbB2 in solution (lane 2 and 6). After standard immunoprecipitation with anti-MBP antibody, the interaction was revealed with anti-GST antibody. No interaction or little aspecific interaction were detected with control GST_ctrl (lane 1 and 5), GST_YXXP_p130Cas (lane 3 and 7) and GST_CT_p130Cas (lane 4 and 8) recombinant proteins. (C) Enhancement fluorescence of Fl-GST_SH3_p130Cas (3.0 μM) in presence of increasing concentrations of MBP_shortPPII_ErbB2 (0, 0.05, 0.1, 0.3, 0.75, 1, 2, 3 μM).

and Table 1 (see Fig. S3 in Supporting Information). Three domains of p130Cas, i.e. the SH3 domain (SH3), the substrate domain (YXXP) and the carboxy-terminal domain (CT), were tested for their ability to bind two recombinant proteins for the C-terminal tail of ErbB2 (MBP_shortPPII_ErbB2 and MBP_longPPII_ErbB2, see Table 1), containing the putative polyproline type II sequence, in two different *in vitro* assays.

As shown in Fig. 2A, dot blot assays were performed by spotting the GST-tagged p130Cas domains on nitrocellulose membrane and probing them with MBP_shortPPII_ErbB2. Western blot analysis clearly revealed that the interaction between SH3_p130Cas and shortPPII_ErbB2 was specific as no binding was observed with other p130Cas domains (Fig. 2A).

As a further validation of the SH3_p130Cas/PPII_ErbB2 interaction, *in vitro* binding assays were performed. GST- and MBP- tagged recombinant proteins were kept in solution overnight at 4 °C and then immunoprecipitated with anti-MBP antibody. Western blot analysis indicates that the interaction between p130Cas and ErbB2 indeed occurred through the SH3 domain of p130Cas (Fig. 2B).

To quantify the entity of the interaction, we performed a fluorescence assay. As shown in Fig. 2C an increasing concentration of MBP_shortPPII_ErbB2 causes an enhancement in fluorescence intensity emission of

ErbB2	
PPII_ErbB2	Polyproline domain type II identified in ErbB2 protein sequence by ELM algorithm. Sequence: V[RPQPPSP]R Position: 1145–1153 in the ErbB2 protein sequence (Isoform 1, identifier: P04626-1).
MBP_longPPII_ErbB2	Recombinant protein containing an N-terminal MBP tag followed by a fragment of ErbB2 cytosolic portion (aminoacids 1103–1255). This fragment starts 30 aminoacids before the putative polyproline domain (PPII_ErbB2) and ends 30aa after.
MBP_shortPPII_ErbB2	Recombinant protein containing an N-terminal MBP tag followed by a fragment of ErbB2 cytosolic portion (aminoacids 1103–1194). This fragment starts 30 aminoacids before the putative polyproline domain (PPII_ErbB2) and ends with the endogenous C-terminal of the protein.
MBP_ctrl	MBP tag (Maltose Binding Protein from E. Coli) used as affinity purification tag for ErbB2 recombinant constructs. MBP protein alone was used as control.
MBP_R → D_shortPPII_ErbB2	This recombinant protein was generated from MBP_shortPPII_ErbB2 by site-directed mutagenesis. It carries an Arginine to Aspartate (R to D) substitution at position 44 (position 1146 in the original ErbB2 sequence). This substitution alters the putative polyproline domain identified in ErbB2 protein sequence from V[RPQPPSP]R to V[DPQPPSP]R.
MBP_PP → AA_shortPPII_ErbB2	This recombinant protein was generated from MBP_shortPPII_ErbB2 by site-directed mutagenesis. It carries two Proline to Alanine (P to A) substitutions at position 47 and 50 (position 1149 and 1152 in the original ErbB2 sequence). These substitutions alter the putative polyproline domain identified in ErbB2 protein sequence from V[RPQPPSP]R to V[RPQAPSA]R.
MBP_RPP → DAA_shortPPII_ErbB2	This recombinant protein was generated from MBP_shortPPII_ErbB2 by site-directed mutagenesis. It carries an Arginine to Aspartate (R to D) substitution at position 44 (position 1146 in the original ErbB2 sequence) and two Proline to Alanine (P to A) substitutions at position 47 and 50 (position 1149 and 1152 in the original ErbB2 sequence). These substitutions alter the putative polyproline domain identified in ErbB2 protein sequence from V[RPQPPSP]R to V[DPQAPSA]R.
MBP_deleter_shortPPII_ErbB2	This recombinant protein was generated from MBP_shortPPII_ErbB2 by site-directed mutagenesis. This protein carries a 7-aminoacid deletion from position 44 to 50 (position 1146–1152 in the original ErbB2 sequence). This deletion abrogates the putative polyproline domain identified in ErbB2 protein sequence.
p130Cas	
GST_SH3_p130Cas	Recombinant protein containing an N-terminal GST tag followed by a fragment of p130Cas protein (aminoacids 3–71). This fragment represents the SH3 domain of p130Cas as described in ²³ .
GST_YXXP_p130Cas	Recombinant protein containing an N-terminal GST tag followed by a fragment of p130Cas protein (aminoacids 80–400). This fragment represents a large central substrate domain composed of 15 repeats of a four amino acid sequence (YXXP) ²³ .
GST_CT_p130Cas	Recombinant protein containing an N-terminal GST tag followed by a fragment of p130Cas protein (aminoacids 654–874). This fragment represents the carboxy-terminal (CT) domain of p130Cas which possess consensus binding sites for the SH2 and SH3 domains of Src ²³ .
GST_ctrl	GST tag (Glutathione S-Transferase from Schistosoma japonicum) used as affinity purification tag for p130Cas recombinant constructs. GST protein alone was used as control.

Table 1. List of constructs used.

Fl-GST_SH3_p130Cas. Fluorescence data were analyzed with a nonlinear least-squares fit (Fig. S4a) and produced a $K_d = 4.07 \times 10^{-8}$ M, a value that could be ascribed to a moderate-strength interaction.

Overall *in vitro* assays demonstrated that p130Cas can effectively bind ErbB2 receptor in a direct way, and that this association is mediated by the SH3 domain of p130Cas.

Validation of key aminoacids involved in p130Cas/ErbB2 interaction. To avoid false positive results due to the incorrect folding of proteins expressed in bacteria, we validated the p130Cas/ErbB2 interaction in 293T mammalian cell line that express normal levels of p130Cas but no detectable expression levels of ErbB2. We cloned and transfected plasmids containing GFP-tagged version of ErbB2 recombinant proteins (GFP_shortPPII_ErbB2 and GFP_longPPII_ErbB2) as described in the Experimental Section. Five days after transfection, standard co-immunoprecipitation was performed using anti-p130Cas mouse antibody. GFP-tagged ErbB2 constructs co-immunoprecipitated with endogenous p130Cas in 293T cell line and thus false positive results due to the misfolding of recombinant proteins were excluded (Fig. 3A).

To verify in a cellular model that the interaction between p130Cas and ErbB2 occurs between p130Cas SH3 domain and the PPII domain of ErbB2, mutagenesis experiments were performed by modifying key residues of the polyproline type II motif of ErbB2. Specifically, cationic Arg2 was mutated to the anionic residue Asp; Pro5 and Pro8 were mutated to Ala. Proline is unique among the 20 common amino acids in having its side chain cyclized onto the backbone nitrogen atom, conferring it special chemical and physical characteristics that cannot be mimic by other amino acids²⁴. Pro-Ala substitution was chosen to at least partially maintain the little size and the hydrophobic interactions of proline residue. We also generated a mutant in which the PPII domain of ErbB2 was completely deleted (named “deleter”) to assess if this motif was essential to drive p130Cas/ErbB2 interaction. Four different mutants for GFP_shortPPII_ErbB2 were generated as described in the Experimental Section to perform co-immunoprecipitation in 293T cell line (Fig. 3B). The same mutants were also produced as MBP-tagged recombinant proteins to perform an *in vitro* ELISA direct binding assay (Fig. 3C).

Both experiments show that mutagenesis of key residues in PPII_ErbB2 sequence alters its binding to SH3 domain of p130Cas. Interestingly, the substitution of Pro5 and Pro8 to Ala strongly affects the amount of binding, while the substitution of Arg to Asp does not impair the binding suggesting that the reinforced hydrogen bond plays a minor role in the interaction. On the contrary, mutation and/or deletion of the core PxxP motif (either by Proline substitution or by complete deletion of the PPII motif) strongly reduced SH3_p130Cas/shortPPII_ErbB2

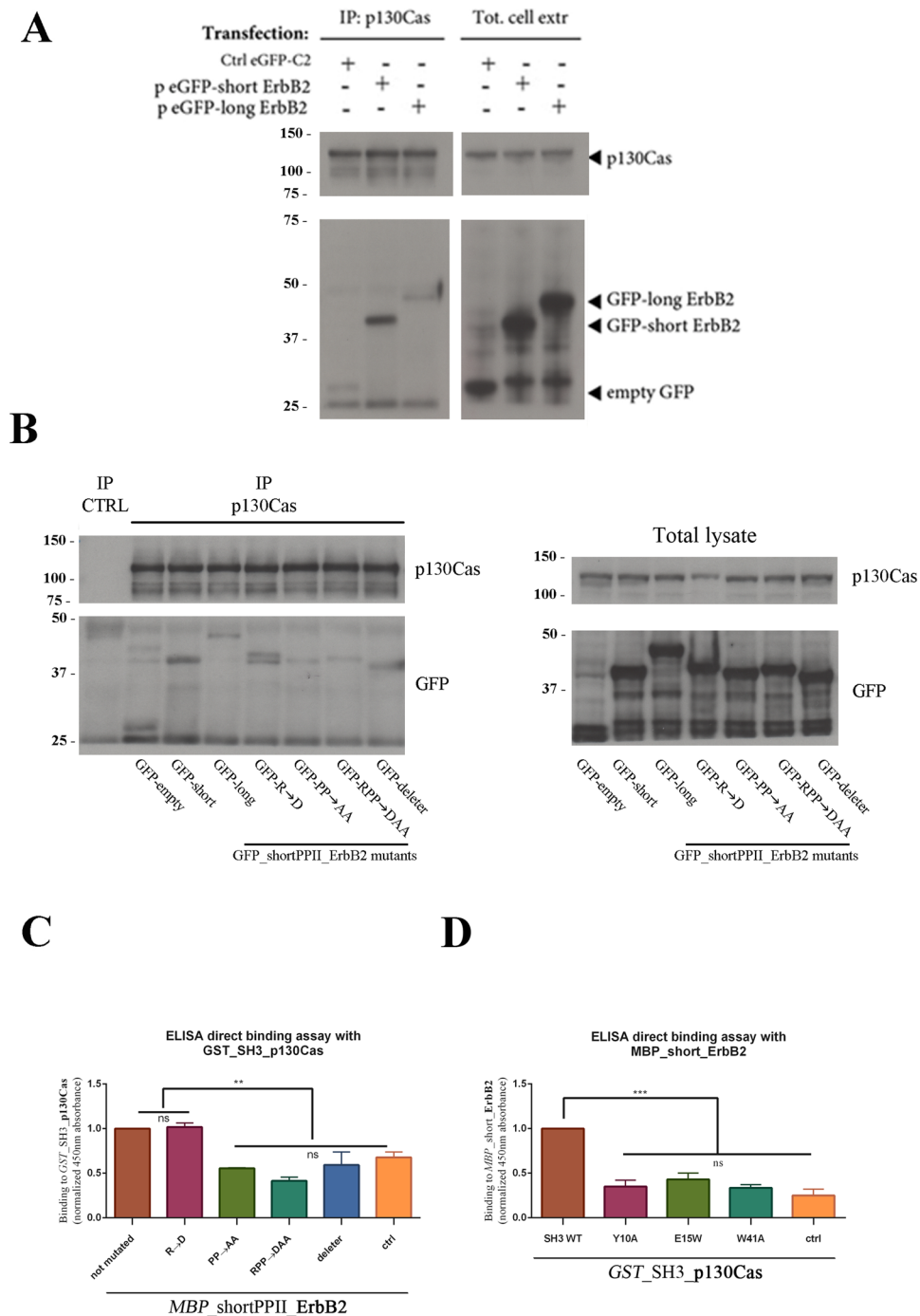


Figure 3. Validation of p130Cas/ErbB2 direct interaction in 293T cell line. **(A)** 293T cells were transfected with GFP-tagged constructs for shortPPII_ErbB2 and longPPII_ErbB2. Five days after transfection, endogenous p130Cas was immunoprecipitated with anti-p130Cas antibody. Interacting proteins were detected with anti-GFP antibody. Endogenous p130Cas interacts with both *GFP_shortPPII_ErbB2* and *GFP_longPPII_ErbB2*, although little aspecific interaction was detected with control *GFP_ctrl* (left). Total cell extracts were blotted with anti-p130Cas and anti-GFP antibodies to assess transfection efficiency (right). **(B)** 293T cells were transfected with mutant forms of *GFP_shortPPII_ErbB2*. Five days after transfection, endogenous p130Cas was immunoprecipitated with anti-p130Cas antibody. Interactions were revealed using anti-GFP antibody (left). Mutation of the cationic residue Arg2 slightly reduced *GFP_shortPPII_ErbB2* binding to endogenous p130Cas; conversely, mutations affecting Pro5 and Pro8 markedly decreased their association, as well as deletion of the PPII motif. Total cell extracts were blotted with anti-p130Cas and anti-GFP antibodies to assess mutants expression (right). **(C)** ELISA direct binding assay recapitulated results obtained using Co-Immunoprecipitation experiments in 293T cell line. Mutation of the cationic residue Arg2 does not affect the binding of *MBP_shortPPII_ErbB2* to *GST_SH3_p130Cas*; conversely, mutations affecting Pro5 and Pro8 markedly decreased their association, as well as deletion of the PPII motif. Data are represented as mean \pm SD.

p < 0.01. (D) ELISA direct binding assay was performed with *GST_SH3_p130Cas* mutants to assess their binding to *MBP_shortPPII_ErbB2*. Recombinant SH3 domains carrying mutations in the three main interaction sites show impaired binding with PPII-containing recombinant protein, validating the importance of these residues for the interaction between SH3 domain and polyproline peptides. Data are represented as mean \pm SD. *p < 0.001.

association, *in vitro* and in cellular model, demonstrating the importance of PPII located residues as suggested by the *in-silico* molecular model.

The same strategy was used to validate the PPII-binding pockets in the SH3 domain of p130Cas. Three SH3-mutants carrying mutations in the three main sites of the interaction were generated and subjected to an *in vitro* ELISA direct binding assay to evaluate their ability to bind ErbB2 recombinant proteins (Fig. 3D). Aromatic residues were changed to alanine to replace bulky hydrophobic residues with small apolar residues (Y10A and W41A). In addition, a conserved hydrophilic residue was substituted with a large hydrophobic residue (E15W). These mutations involved aminoacids exposed to the solvent on the surface of the SH3 domain and are not implicated in any contacts to main-chain atoms that maintain the structural stability of the SH3 domain²⁵. Notably, all SH3 mutants failed to associate with the PPII domain of ErbB2 (Fig. 3D).

Structure-based virtual screening (SBVS). Once validated, the molecular model for p130Cas/ErbB2 interaction was used to run a SBVS of the ZINC database using FLAP software (see Experimental Section). The rationale was to find candidates that bind the SH3 domain of p130Cas (SH3_p130Cas) using the same interaction pockets used by polyproline ErbB2 sequence (PPII_ErbB2) (see above) thereby inhibiting the binding of ErbB2 to p130Cas.

Screening results are in Table S2 (Pocket Point Radius = 2 Å), which shows the ten molecules expected to have the best capacity to inhibit the SH3_p130Cas/PPII_ErbB2 interaction ranked by their Glob-Prod index (see Experimental Section). Potential hits from this SBVS were screened for PAINS using the tool implemented in ZINC15 (<http://zinc15.docking.org/patterns/home/>) to exclude the presence of known classes of assay interference groups in 1 and 2.

ZINC84136897 (1) and ZINC39121740 (2) (chemical structures in Fig. 4A) were selected to submit to experimental validation. Compound 1 is larger than 2 (MW = 375) and could be described as a urea derivative. Compound 2 is a relatively small compound (MW = 226) bearing a sulfonamide group. The choice of these two compounds also allows to explore the impact on the inhibitory activity of different binding modes since 1 exploits its action by interacting with p130Cas in three regions, whereas the interaction of 2 with p130Cas is driven by hydrogen bonding (HB) interactions (Fig. 4B).

***In vitro* validation of the compounds identified by virtual screening.** To experimentally validate the binding of compound 1 and 2 on *GST_SH3_p130Cas* recombinant protein, fluorescence quenching experiments were performed.

The fluorescence spectra of Fl-*GST_SH3_p130Cas* in the absence and in the presence of 1 and 2 at different concentrations are shown in Fig. 4C. Fl-*GST_SH3_p130Cas* shows a strong fluorescence emission at 518 nm and its fluorescence intensity decreases gradually with the increase of compound's concentration. The analysis of equilibrium dissociation constants showed values with different order of magnitude, $K_D = 2.0 \times 10^{-7}$ M for compound 1 and $K_D = 5.0 \times 10^{-6}$ M for compound 2 (Fig. 4C left and right panel, respectively) (see also Fig. S4b,c).

The two compounds were then tested *in vitro* using a competitive ELISA binding assay, which demonstrated their inhibitory activity against the interaction between *GST_SH3_p130Cas* and *MBP_shortPPII_ErbB2* recombinant proteins (Fig. 5A). The assay nicely showed reduced interaction between p130Cas and ErbB2 recombinant proteins with increasing concentration of tested compounds, while no modulation was revealed with increasing concentration of DPN (non-specific control). This experimental evidence validates the SH3 domain of p130Cas as possible pharmacological target since its binding to the polyproline domain of ErbB2 is amenable for modulation by inhibitory compounds 1 and 2.

As a further confirmation of the 1 and 2 efficacies of inhibiting *GST_SH3_p130Cas/MBP_shortPPII_ErbB2* interaction, fluorescence quenching experiments were performed. As shown in Fig. 5B, compound 1 is more efficient in preventing the binding between Fl-*GST_SH3_p130Cas* and *MBP_shortPPII_ErbB2*, compared to compound 2 (Fig. 5B left and right panel, respectively).

To assess whether these compounds could interfere with p130Cas/ErbB2 association in a cellular context, ErbB2-positive BT474 breast cancer cells were pre-treated for 24 hours with 1 or 2 and subjected to co-immunoprecipitation experiments. As shown in Fig. 5C, treatment with selected inhibitory compounds reduced the association of p130Cas to ErbB2 also in BT474 breast cancer cells.

Validation in cellular models of the identified inhibitors. *In vitro* data indicate that compounds 1 and 2 can interfere with p130Cas/ErbB2 interaction, although with different binding modalities and different affinities. To test which are the consequences of such interference in a cellular context we performed cell proliferation and cytotoxicity assays. To this end, BT474 and SKBR3 breast cancer cells were chosen as a suitable experimental model as they express high endogenous levels of both ErbB2 and p130Cas⁵. As shown in Fig. 6A, treatment of BT474 cells with serial dilutions of the compounds indicates that compound 1 exhibits toxic effects starting from 75 μ M, while for compound 2 we did not detect cytotoxic effects even at 250 μ M. In addition, since we already demonstrated that p130Cas/ErbB2 association triggers proliferation of breast cancer cells (as demonstrated by soft agar assay in¹⁰), a cell proliferation assay was employed to determine EC₅₀ values of 1 and 2 compounds

in BT474 (1 $EC_{50} = 52.3 \pm 6.38 \mu\text{M}$, 2 $EC_{50} = 239.5 \pm 25.98 \mu\text{M}$) and in SKBR3 (1 $EC_{50} = 69.8 \pm 4.44 \mu\text{M}$, 2 $EC_{50} = 273.9 \pm 27.18 \mu\text{M}$) cells as shown in Fig. 6B,C. It should be noted that both compounds achieved 50% inhibition of proliferation at concentrations below their cytotoxic threshold.

Notably, compound **1** seems to be more effective on the inhibition of cell proliferation in these specific cellular models (Fig. 6B,C). Interestingly, these compounds have no significant effect on the proliferation of ErbB2-negative HEK 293T cells (Fig. S5), suggesting that the anti-proliferative effect of **1** and **2** in BT474 and SKBR3 cells is mainly linked to the inhibition of p130Cas/ErbB2 association, rather than a broad, non-specific inhibition of p130Cas-related pathways.

Moreover, results shown in Fig. 6E indicate that compound **1** significantly enhances the efficacy of Trastuzumab treatment in SKBR3 cell line, thus suggesting that inhibition of p130Cas-ErbB2 interaction could improve Trastuzumab efficacy by decreasing the stability of ErbB2. Consistently, the treatment of SKBR3 Trastuzumab-resistant cells with compound **1** partially restores the sensitivity of resistant cells to Trastuzumab (Fig. 6F). Our data suggest that the inhibition of ErbB2-p130Cas interaction might impact on both breast cancer cell proliferation and resistance to Trastuzumab, opening up new therapeutic perspectives.

ADME-Tox prediction. To explore the future as a drug of **1** and **2** we used free online tools to predict both physico-chemical (pK_a and $\log D^{7.4}$) and ADME-Tox properties. Data are shown in Table 2. According to pK_a prediction, both compounds are expected to be in their neutral state at physiological pH and have a similar lipophilicity. Although the ADME-Tox profile is globally acceptable, both molecules have defaults. In particular, **2** is predicted to be poorly permeable (using pkCSM predictor the threshold to distinguish highly from poorly permeable compounds is 0.90), whereas **1** is expected to be a substrate of P-glycoprotein which could adversely affect the drug candidate effectiveness.

Discussion

Despite the enormous interest in targeting Protein-Protein Interactions (PPIs), the discovery of drugs capable to interfere with these interactions has been proven to be very challenging. The transient nature of these interactions, moderate affinity, and promiscuity of recognition are among the many factors that have contributed to difficulty in discovering effective modulators^{26–28}. Target validation is an essential step in the drug discovery process and one of the major causes of attrition. Therefore, the first aim of this study consisted in providing strong support for using p130Cas/ErbB2 as a target for the discovery of anticancer drugs.

We reported here, for the first time, that p130Cas association to ErbB2 receptor is indeed direct. *In silico* simulations, *in vitro* data and experiments in 293T cell line support that the direct binding is mediated by the SH3 domain of p130Cas that recognizes a polyproline type II motif located within the unstructured carboxy-terminal tail of the receptor. MD simulations suggest that this polyproline sequence is energetically favored in the interaction acting as a ligand for class I SH3 domain. This evidence partially contrasts with data reported in 1995 by Polte and Hanks²⁹ showing that the direct binding of SH3 domain of p130Cas with Focal Adhesion Kinase occurs through the Pro-rich sequence –APPKPSR– that represents a class II SH3 domain ligand. However, several data reported that some SH3 domains (i. e. Src SH3 domain) can bind both class I and class II polyproline peptides³⁰.

In accordance with our results, mutagenesis experiments of key amino acids in the PPI motifs allowed us to establish that among the three important residues, the cationic Arg2 residue plays a minor role in the specificity of the interaction with the SH3 domain of p130Cas. This led us to hypothesize that the essential “core” for the association of polyproline type II peptides with the SH3 domain of p130Cas is the PxxP motif, regardless of the position of the charged residue. This in turn might explain why p130Cas can associate through its SH3 domain with class I and class II peptides.

The experimental evidence of the direct interaction between p130Cas and ErbB2 is however not sufficient to establish whether this protein-protein interaction (PPI) is druggable (i.e. if it could be disrupted by a third molecule) or not.

To investigate the druggability of p130Cas/ErbB2 interaction, we firstly performed structure based virtual screening using a dataset of small molecules (SMs). This choice is in line with a recent PDB-wide analysis which shows that nearly half of all PPIs may be susceptible to SM inhibition³¹.

Among chemicals predicted to be valuable inhibitors of the investigated interaction we submitted to experimental validation two compounds exhibiting a different binding mode: **1** exploits its action by interacting with p130Cas in three regions, whereas the interaction of **2** with p130Cas is driven by hydrogen bonding (HB) interactions.

In vitro experiments showed that the two compounds similarly inhibit PPI and suggest that molecules with different binding modes could share similar inhibition properties. Conversely, cell line experiments showed that **1** may stronger slow down cell proliferation in BT474 and SKBR3 cell line (models of ErbB2-overexpressing breast tumor) than **2**. Permeability prediction could explain this behavior since **1** is expected to be significantly more permeable than **2**.

We previously demonstrated that high levels of p130Cas expression inversely correlate with ErbB2 sensitivity to Trastuzumab probably by binding to ErbB2 and increasing its stability to the cell membrane⁵.

Interestingly, a small molecule inhibitor (compound **1**) able to interfere with p130Cas/ErbB2 association synergized with Trastuzumab treatment in Trastuzumab-sensitive SKBR3 cells, thus suggesting that inhibition of p130Cas-ErbB2 interaction might be used to improve Trastuzumab efficacy. Notably, this beneficial effect was also observed in Trastuzumab-resistant cells, in which compound **1** partially restores their sensitivity to Trastuzumab. These effects might rely on the ability of compound **1** to interfere with p130Cas/ErbB2 association, thus reducing p130Cas-mediated ErbB2 stabilization at the cell membrane⁵. These results strongly enforce the hypothesis that the increased stabilization of ErbB2 by p130Cas might be a crucial event driving breast cancer progression and resistance to antibody-based anti-ErbB2 therapies, opening new therapeutic alternatives.

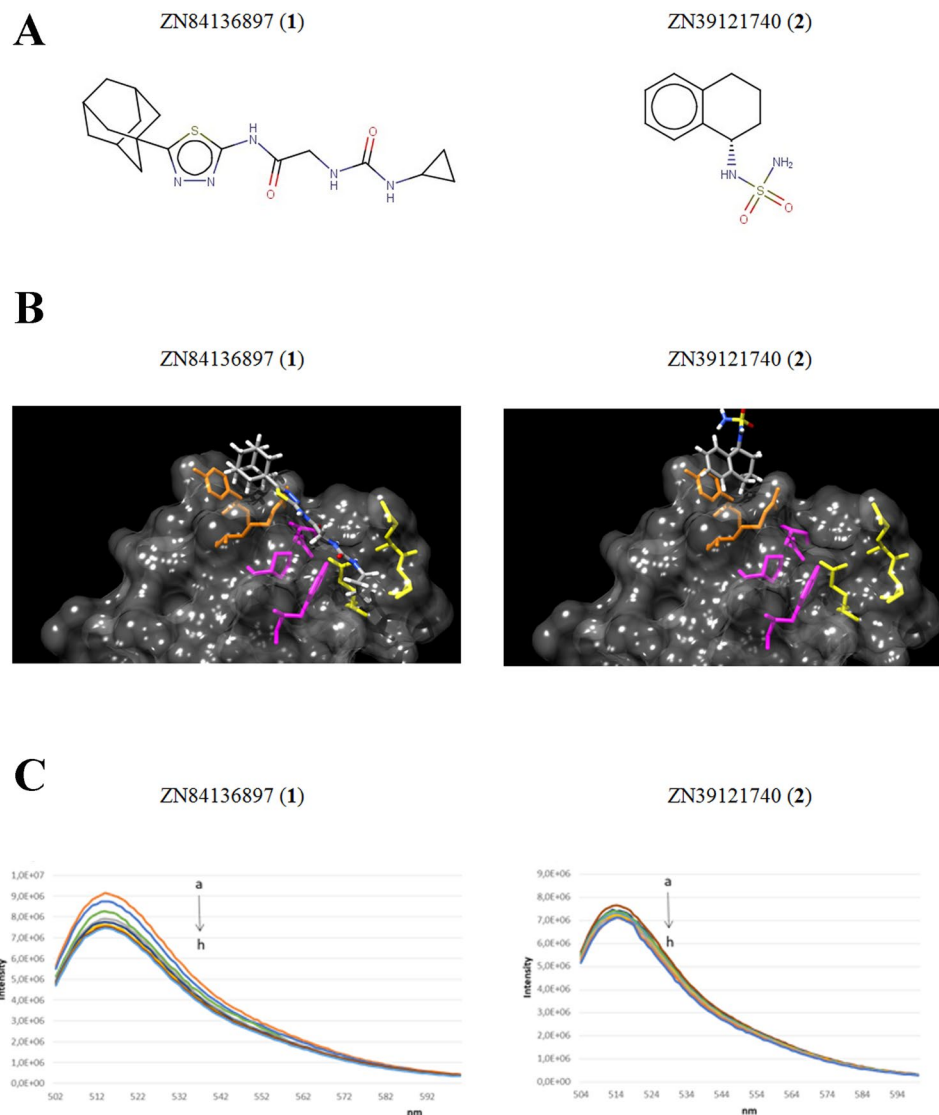


Figure 4. Structure-based virtual screening identifies compounds with potential inhibitory properties. **(A)** Chemical structures of two high ranked compounds from the SBVS: ZINC84136897 (**1**) and ZINC39121740 (**2**). **(B)** Binding mode of **1** (left panel) and **2** (right panel) with SH3_p130Cas. The selected compounds showed different binding modalities since **1** exploits its action by interacting with SH3_p130Cas in three regions, whereas the interaction of **2** with SH3_p130Cas is driven by hydrogen bonding (HB) interactions. **(C)** Fluorescence quenching spectra of the complex Fl-GST_SH3_p130Cas (0.07 μ M) in the absence and presence of **1** (0, 0.07, 0.21, 0.7, 3.5, 7.0, 14, 21 μ M) (left panel) and in the absence and presence of **2** (0, 2.1, 3.5, 5.5, 7.0, 10, 15, 21 μ M) (right panel) demonstrating the binding between the selected compounds and the target protein.

In this regard, a medicinal chemistry effort is required to optimize compounds' potency. To this end, virtual libraries of analogues of **1** and **2** will be obtained, screened for their activity using structure-based virtual screening (SBVS) as above, and then filtered based on synthetic accessibility and physicochemical properties. These procedures allow to test the most promising candidates in order to find an optimized lead compound.

Overall, this study provides a potential hit compound that through a number of optimization steps could gain relevance as an anticancer drug candidate and proposes a strategy to discover small molecules which may target protein-protein interactions. It is worth noting that the results reported in this study represent the first attempt to translate the current large knowledge on p130Cas, and its contribution to breast cancer progression, into something that may be employed as therapeutic agent in the future.

Experimental Section

Cloning of p130Cas. Coding sequence for p130Cas SH3 domain (3–71) (named SH3_p130Cas) was amplified from cDNA with PCR using 5'-GGATCCACCTGAACGTGCTGGC-3' forward primer and 5'-GCGGCCGCTATTATGGCTTCTTATCATAACA-3' reverse primer and cloned in-frame into pGEX-4T3 vector using BamHI and NotI restriction sites.

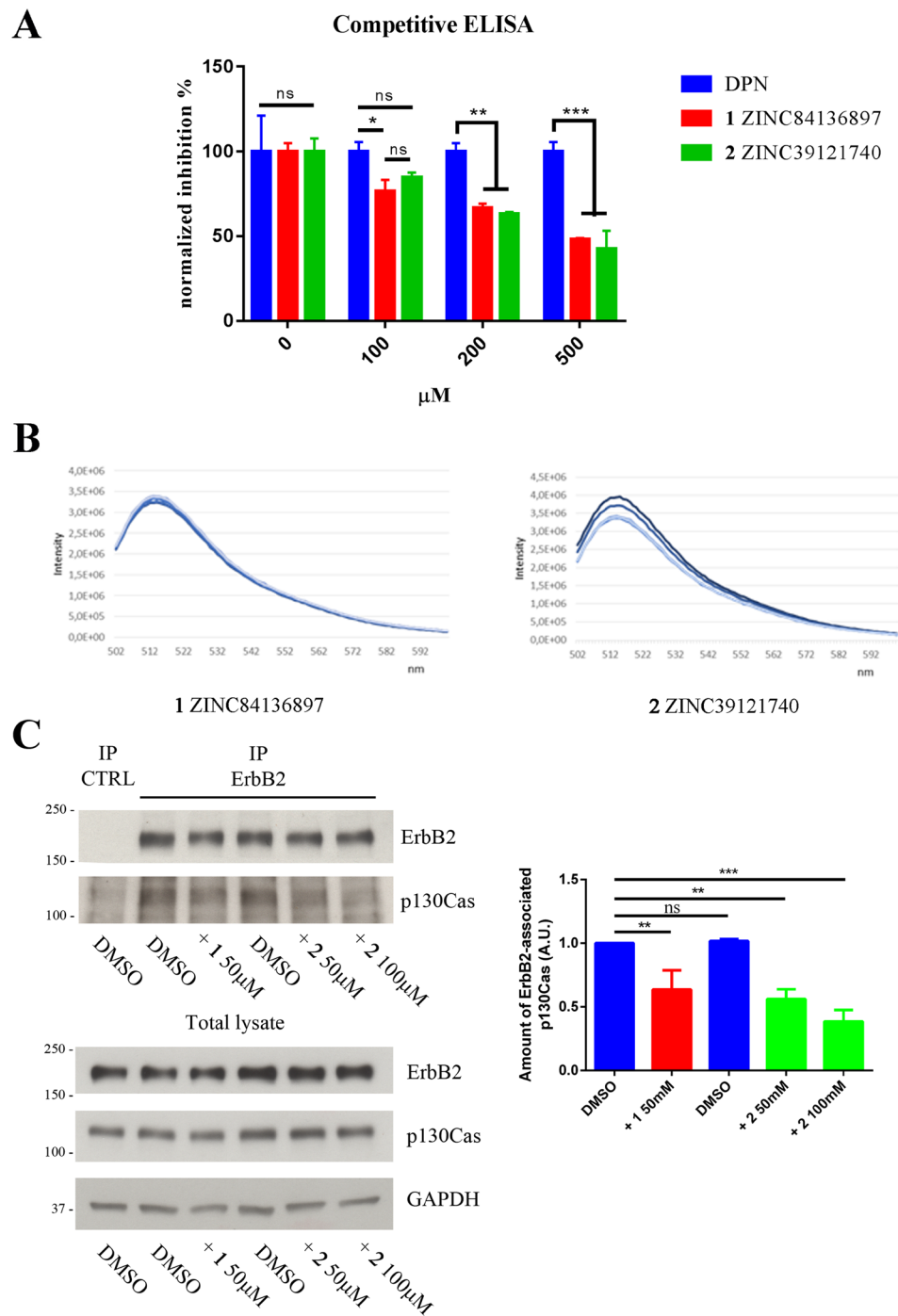


Figure 5. Screened compounds inhibit *GST_SH3_p130Cas/MBP_shortPPII_ErbB2* association *in vitro*. **(A)** Competitive ELISA binding assay was performed to validate two high ranked selected compounds (**1** and **2**) as inhibitor of p130Cas/ErbB2 interaction. Both compounds demonstrated dose-dependent inhibition of the association between *GST_SH3_p130Cas/MBP_shortPPII_ErbB2* purified recombinant proteins *in vitro*. DPN (Diarylpropionitrile) was low-ranked by virtual screening and therefore used as control for non-specific inhibition (see Experimental Section). **(B)** Fluorescence spectra of the complex FI-*GST_SH3_p130Cas/1* (0.01 μM and 3 μM respectively) in presence of increasing concentrations of *MBP_shortPPII_ErbB2* (0.1, 0.3, 0.5, 0.75 μM (left panel)); the complex FI-*GST_SH3_p130Cas/2* (0.01 μM and 1 μM respectively) in presence of increasing concentrations of *MBP_shortPPII_ErbB2* (0.1, 0.3, 0.5, 0.75 μM (right panel)). **(C)** Co-immunoprecipitation experiment in BT474 cell line. Cells were pre-treated with selected inhibitory compounds for 24 hours and subjected to immunoprecipitation with anti-ErbB2 antibodies. Western blot with anti-p130Cas antibodies revealed that both compounds were able to reduce the amount of endogenous p130Cas/ErbB2 complex in BT474 cells (upper left panel) and quantified by densitometric analysis (right panel). Total cell extracts blotted with anti-ErbB2 and anti-p130Cas revealed no changes in ErbB2 or p130Cas expression during the treatment (lower left panel). GAPDH expression was used as loading control. Data are represented as mean ± SD. ***p* < 0.01, ****p* < 0.001.

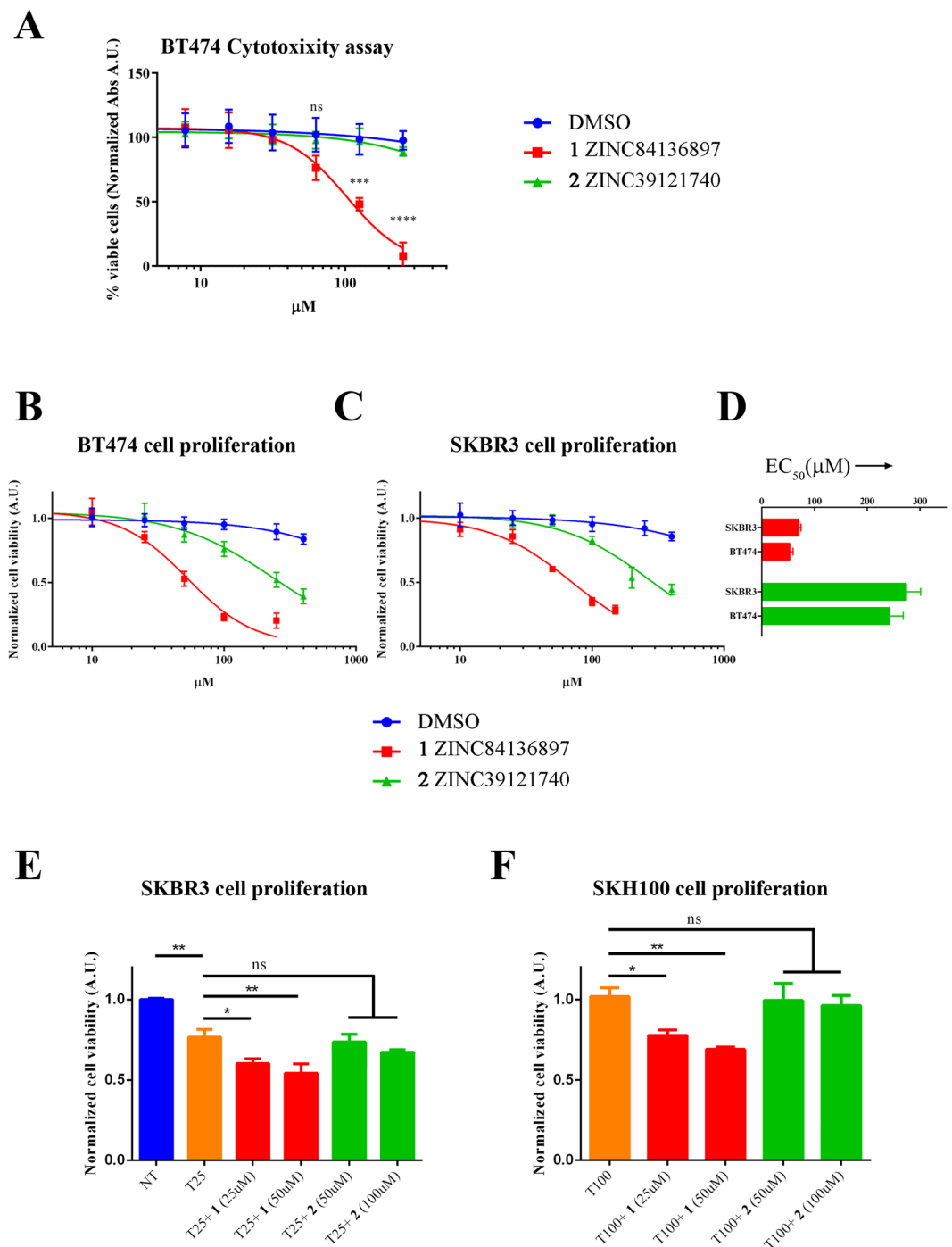


Figure 6. Impact of **1** and **2** compounds on BT474 breast cancer cells. **(A)** To assess whether **1** and **2** could trigger cytotoxic effects on living cells, BT474 cells were treated with serial dilutions of **1** and **2** (or sterile DMSO). After three days, live cells were detected by standard MTT assay, highlighting the appearance of cytotoxic effects above 75 μM for compound **1**. Compound **2** did not show cytotoxic effects even at 250 μM. ****p* < 0.001; *****p* < 0.0001. **(B)** **1** and **2** compounds inhibit cell proliferation of BT474 and **(C)** SKBR3 breast cancer cell lines. Cells were treated with different concentration of the **1** and **2** and proliferation was assayed three days later by performing MTT assay. Results were fitted with four-parameter dose-response curve using GraphPad Prism7 software. **(D)** EC₅₀ values for **1** and **2** in BT474 and SKBR3 breast cancer cell lines are represented as histogram with 95% confidence intervals. **(E)** SKBR3 cells were treated with Trastuzumab (25 μg/ml) either alone or in combination with compound **1** or **2** at the indicated doses. After three days, live cells were detected by standard MTT assay. Data are represented as mean ± SD. **p* < 0.05, ***p* < 0.01. **(F)** SKH100 Trastuzumab-resistant cells were treated with Trastuzumab (100 μg/ml) either alone or in combination with compound **1** or **2** at the indicated doses. After three days, live cells were detected by standard MTT assay. Data are represented as mean ± SD. **p* < 0.05, ***p* < 0.01.

	Source	1	2
pK _a	MoKa	3.44 (b); 9.97 (a)	9.45 (a)
log D ^{7.4}	MoKa	1.5	2.0
TPSA	ZINC	96	72
permeability	pkCSM	1.07 × 10 ⁻⁶ cm/s	0.69 × 10 ⁻⁶ cm/s
P-glycoprotein substrate	pkCSM	Yes (inhibitor)	No
Cyp3A4 substrate	pkCSM	Yes	No
hERG toxicity	pkCSM	No	No
AMES toxicity	pkCSM	No	No

Table 2. Predicted physico-chemical and ADME-Tox properties of the two investigated compounds.

pGEX vectors containing p130Cas substrate domain (named YXXP_p130Cas) and p130Cas carboxy-terminal domain (named CT_p130Cas) were engineered by Prof. Emilia Turco, MBC, University of Torino. All PCR amplifications and cloning procedures were verified by Sanger sequencing.

Cloning of ErbB2. Two different ErbB2 constructs containing the putative polyproline domain (named shortPPII_ErbB2 and longPPII_ErbB2) were amplified from ErbB2 cDNA and cloned in-frame in pMAL-C2 vector for recombinant protein production and in pEGFP-C2 vector for 293T transfection, using SacI and SalI restriction sites.

Expression and purification of recombinant proteins. pGEX-4T3 and pMAL-C2 engineered vectors were purified using commercial silica column and transformed into competent BL21 bacteria for expression of recombinant fusion proteins. MBP and GST fusion proteins were produced in *Escherichia coli* BL21 bacteria strain together with GST and MBP proteins alone (GST_ctrl and MBP_ctrl, respectively) as controls and then purified on a Sepharose amylose (New England Biolabs) or Sepharose glutathione column (GE Healthcare) according to the manufacturer's instructions. After elution step all recombinant proteins were dialyzed two times against PBS at 4 °C, aliquoted and stored at -80 °C. See Table 1 for recombinant proteins details.

Site directed mutagenesis. Site directed mutagenesis of shortPPII_ErbB2 sequence (in pMAL-C2 and pEGFP-C2 vectors) was performed with QuickChange Site-Directed Mutagenesis Kit (Agilent) following manufacturer instructions. Mutagenic primers were the same for both plasmids (Table S1).

Mutants of shortPPII_ErbB2 protein in pMAL-C2 vector were expressed, purified and quantified as reported above. See Table 1 for recombinant protein details.

Site directed mutagenesis of SH3_p130Cas sequence (in pGEX-4T3 vector) was performed with QuickChange Site-Directed Mutagenesis Kit (Agilent) following manufacturer instructions. Mutagenic primers were reported (Table S1). Mutants of SH3_p130Cas protein in pGEX-4T3 vector were expressed, purified and quantified as reported above.

Antibodies. Mouse monoclonal antibodies to human p130Cas were produced in our department (see⁵) Additional mouse monoclonal p130Cas antibodies were purchased from BD Transduction Laboratory (Franklin Lakes, NJ, USA) (Material number 610272). Antibodies to GST (mouse monoclonal), MBP (rabbit polyclonal) and GFP (mouse monoclonal and rabbit polyclonal) tags were produced at the MBC, University of Torino. Additional rabbit polyclonal antibodies to GST, MBP and GFP tags were obtained from Thermo Scientific (catalog # A-5800) and Sigma Aldrich (catalog #M1321 and # G1544).

Dot blot binding assay. For dot blot experiments, 1 μl of GST-tagged p130Cas purified recombinant proteins was manually spotted onto nitrocellulose and let air-dry for 30 minutes at room temperature. Saturation was performed using 5% BSA in TBS-0.3% Tween20 at room temperature for 3 hours. After 3 washing steps with TBS-0.3% Tween20, nitrocellulose filters were incubated with MBP-tagged ErbB2 purified recombinant proteins (1 μg/ml) in Interaction Buffer (50 mM Tris-HCl pH7.4, 150 mM NaCl, 1% Triton-X100) at 4 °C overnight. The day after, nitrocellulose filters were washed twice with Interaction Buffer and twice with TBS-0.3% Tween20. The interacting proteins were detected using rabbit polyclonal anti-MBP antibody and peroxidase conjugated anti-rabbit secondary antibody with chemoluminescent ECL reagent.

Nitrocellulose filters were then extensively washed with TBS-0.3% Tween20 and incubated overnight at 4 °C with mouse monoclonal anti-GST antibody and detected by peroxidase conjugated anti-mouse secondary antibody. This process revealed the amount of GST-tagged p130Cas purified recombinant proteins that were directly spotted onto nitrocellulose.

In vitro binding assay. For the *in vitro* binding assay, GST-tagged p130Cas and MBP-tagged ErbB2 purified recombinant proteins were mixed together in solution (Interaction Buffer with 1% BSA) overnight at 4 °C. The day after, standard immunoprecipitation with anti-MBP rabbit polyclonal antibody and proteinA Sepharose (GE Healthcare) was performed. After 3 washing steps, proteins were eluted with 2X Laemmli loading buffer. Proteins were run on SDS-PAGE under reducing condition, transferred to nitrocellulose and probed with specific antibodies. Interacting partners were revealed using anti-GST mouse monoclonal antibody.

ELISA. For ELISA binding assay, 100 nM/well of *GST_SH3_p130Cas* and *GST_ctrl* purified recombinant proteins were coated to a 96-well microtiter plate in 100 μ l of PBS buffer overnight at 4 °C. The day after, washing steps and saturation were performed using PBS and 3% BSA in PBS at room temperature. *MBP*-tagged ErbB2 purified recombinant proteins and *MBP_ctrl* (100 nM/well) were added in 100 μ l/well of PBS for 2 h. After washing, anti-*MBP* mouse monoclonal antibody (0.25 μ g/ml) was added for 2 h followed by peroxidase conjugated anti-mouse secondary antibody for 1 h. Detection of the protein-protein interaction was revealed by standard colorimetric reaction adding 90 μ l of chromogenic TMB substrate (3,3',5,5'-tetramethylbenzidine). The reaction was stopped with 90 μ l of 0.5 M HCl and absorbance at 450 nm was measured using ELISA plate reader. *GST_ctrl* and *MBP_ctrl* proteins served as control for non-specific binding between recombinant proteins.

For validation of inhibitory activity of selected compounds, ELISA binding assay was setup as reported above. Briefly, **1** and **2** compounds were mixed at various concentration with *MBP_shortPPII_ErbB2* purified recombinant protein and allowed to interact with pre-absorbed *GST_SH3_p130Cas* 2 h at room temperature. Detection of the protein-protein interaction was revealed as reported above. DPN (Diarylpropionitrile, from Sigma Aldrich, catalog number H5915, CAS Number 1428-67-7) was used as control for non-specific inhibition of protein-protein interaction³².

Inhibitory compounds. ZINC84136897 (**1**) and ZINC39121740 (**2**) were purchased from Enamine Ltd. (Kiev, UA) as lyophilized powder and dissolved at 25 mM concentration in 75% DMSO/water. Solubilized chemicals were aliquoted and stored at -20 °C protected from light.

Standard MS and H¹NMR were performed to validate structure and quality.

Cell cultures. HEK 293T cells (from ATCC, CRL3216) were maintained in DMEM (Thermo Fisher Scientific), 10% FBS at 37 °C, 5% CO₂ in humidified incubator.

BT474 cells (from ATCC, HTB20) were cultured in DMEM-F12 (Thermo Fisher Scientific), 10% FBS at 37 °C, 5% CO₂ in humidified incubator.

SKBR3 cells were cultured in McCoy's 5 A (Thermo Fisher Scientific), 15% FBS at 37 °C, 5% CO₂ in humidified incubator.

SKBR3 resistant cells (SKH100) made resistant to Trastuzumab were generated by Dr. Valabrega and maintained as described in³³.

All used cell lines were authenticated in the last 6 months by BMR Genomics (Padova, Italy), using the CELL ID System (Promega, Madison, WI).

All cells were regularly checked for mycoplasma contamination by specific PCR.

293T transfection. For transfection of pEGFP-C2 vectors containing *GFP*-tagged ErbB2 constructs, 293T cells were seeded in 10-cm dishes at 5 × 10⁶ cells/dish. After cells reached 90–95% confluence, plasmid vectors (8 μ g/dish) with Lipofectamine 2000 (Invitrogen Inc.) were transfected into 293T cells following manufacturer instructions.

Cytotoxicity assay. For cytotoxicity assay BT474 cells were seeded at 5000 cells/well concentration (100% confluency) in a 96-well cell culture plate and incubated with serial dilutions of **1** and **2** compounds (from 250 μ M to 0.12 μ M). Cytotoxicity was evaluated after 3 days by MTT assay (11465007001 Roche, Cell Proliferation Kit I) following manufacturer instruction.

Cell proliferation assay. For proliferation assay BT474, SKBR3 and SKH100 cells were seeded in 8 replicates at 1000 cells/well concentration (25% confluency) in four different 96-well cell culture plates and then incubated with increasing concentration of **1** and **2** for 3 days. Changes in proliferation rate were detected by MTT assay (11465007001 Roche, Cell Proliferation Kit I) following manufacturer instruction. Sterile DMSO was used as control for non-specific solvent effect on proliferation.

Statistical analysis. All the results are representative of at least three independent experiments performed in triplicate.

All data obtained on protein-protein interaction were normalized using *GST_ctrl* and *MBP_ctrl* as non-specific control. Data obtained from ELISA and MTT assays using **1** and **2** were normalized using either DPN or DMSO as non-specific control.

Statistical analysis of data obtained from ELISA and MTT assays was performed using 2-way ANOVA corrected for multiple comparison by Tukey test. p-value < 0.05 (95% confidence interval) were considered significant.

Fluorescence quenching experiments. All fluorescence spectra were recorded with a Horiba Jobin Yvon Fluorolog3 TCSPC spectrofluorophotometer with 1.0 cm quartz cells

For fluorescence experiments, *GST_SH3_p130Cas* was firstly tagged with fluorescein (Fl-*GST_SH3_p130Cas*) using a methodology described in the literature³⁴ (see Supporting Information). The fluorescence spectra of Fl-*GST_SH3_p130Cas* were obtained using a fixed concentration of 3.0 μ M in the absence and in the presence of *MBP_shortPPII_ErbB2* (concentration range: 0.05–3.0 μ M). Fluorescence emission spectra of Fl-*GST_SH3_p130Cas* in the presence of **1** and **2** were obtained using the following concentrations: Fl-*GST_SH3_p130Cas* = 0.7 μ M; **1** and **2** = 0–21 μ M. Finally, *MBP_shortPPII_ErbB2* (concentration range: 0–75 μ M) was added to the complexes between Fl-*GST_SH3_p130Cas* and the two compounds.

The variation in fluorescence emission at 518 nm of Fl-*GST_SH3_p130Cas* was monitored in all experiments.

Computational section. In this study, we used two crystallographic structures: the SH3 domain of p130Cas (PDB code 1WYX) and the SH3 domain of p85 in complex with the peptide PD1R (PDB code 3I5R). Both structures were downloaded from the Protein Data Bank (www.rcsb.org). The ErbB2 sequence was submitted to Eukaryotic Linear Motif (ELM) (www.elm.org)¹⁸ by using the FASTA format as an input.

The interaction complex SH3_p130Cas/PPII_ErbB2 was built with MOE version 2010.10 (www.chemcomp.com).

The virtual screening for inhibitors of the SH3_p130Cas/PPII_ErbB2 interaction has been performed by FLAP version 2.0.2 (www.moldiscovery.com). The screening has been made over the 15 million compound subset “drug-like clean” of the ZINC database v.13 (www.zinc.docking.com).

Preparation of the complex SH3_p130Cas/PPII_ErbB2. Two starting structures were downloaded from the Protein Data Bank (www.rcsb.org): the SH3 domain of p130Cas (PDB code 1WYX) and the SH3 domain of p85 in complex with the peptide PD1R (PDB code 3I5R). 1WYX and 3I5R were imported in MOE (ver. 2016.08, www.chemcomp.com).

Firstly, PD1R 3D structure was extracted from 3I5R. Four amino acids, i.e. K, L, L and S, present in the PD1R sequence (KRPLPLPS) were mutated into V, Q, S and R, respectively, to obtain PPII_ErbB2 model (VRQPSPR).

The structure of the SH3 domain of p130Cas was prepared starting from 1WYX: one monomer was retained, and water molecules and ions were removed. The structure was then protonated using MOE Protonate3D (T = 310,15 K, pH = 6,8, I.F. = 0,2 mM). The same procedure was applied to the SH3 domain of p85 present in the pdb file 3I5R.

Finally, the structure of the complex SH3_p130Cas/PPII_ErbB2 was obtained through alignment and superposition of SH3_p130Cas and PPII_ErbB2 with the SH3 domain of p85 and PD1R, respectively.

The complex was minimized using the CHARMM22 force field (RMS gradient less than 0.001 kcal mol⁻¹ Å⁻²).

Molecular Dynamics simulations. All steps of MD simulations were set up using the BiKi Life Science software (default settings for plain MD simulations, ver. 1.3.5, <http://www.bikitech.com/>) which provides an intuitive GUI interface to GROMACS and Amber tools. In particular, the setup of the simulations is based on Antechamber software (ver. 14, <http://ambermd.org/antechamber/ac.html>) whereas MD simulations were performed with GROMACS (ver.4.6.1, <http://www.gromacs.org/>) package using the Amber ff14 force field³⁵. Water molecules were described using the TIP3P model³⁶ and periodic boundary conditions were applied. The system was neutralized by adding a sodium ion.

The solvated system was minimized using a steepest descent minimization (the maximum number of minimization cycles was set to 5000). Equilibration was carried out in four steps: firstly, three 100 ps NVT simulations were performed to gradually increase the temperature up to the final 300 K, then one 1 ns NPT step was carried out to allow the system to stably reach the pressure condition of 1 atm. Finally, one 50 ns MD production run was performed with a time step for integration equal to 0.002 ps and a number of steps equal to 25000000. Coordinates were saved every 10 ps; in total 5000 snapshots were obtained. The temperature coupling was done using a velocity rescaling with a stochastic term that ensures that a proper canonical ensemble is generated³⁷.

Dataset preparation. The subset of compounds named “Clean Drug-Like” was downloaded from the ZINC database (ver. 13, www.zinc.docking.org). This subset contains about 15 million of molecules which were filtered by applying the following criteria: (a) Lipinski’s rules of five (i.e. no more than 5 hydrogen bond donors and 10 hydrogen bond acceptors, a molecular mass less than 500 Daltons, ClogP less than 5), (b) molecular mass greater than 150 Daltons, (c) number of rotatable bonds lower than 7, (d) formal charge in the range [−2; +2].

Structure based virtual screening (SBVS). The SH3_p130Cas/PPII_ErbB2 structure was imported in FLAP (v. 2.2.1, www.moldiscovery.com) and the interface between the protein and the peptide was used to define the pocket for the SBVS (Pocket Point Radius = 2 Å). MIFs with the default probes DRY, O, N1, and H were calculated for the residues in the pocket and FLAP fingerprints for SH3_p130Cas were generated³⁸.

The compounds resulting from the previous step were submitted to FLAP in their ionization state at pH = 7. FLAP generates 25 low energy conformers for each compound. For each of these conformations, the molecular interaction fields (MIFs) for H, O, N1, and DRY GRID probes were calculated at a 0.75 Å grid resolution, and FLAP fingerprints were generated. To reduce the number of molecules in the dataset, a quick pre-filtering run was performed using the implemented procedure in the bit-string mode. The Glob-Sum similarity score was used to rank the compounds in the dataset and the 10000 compounds with the higher score were retained.

Finally, the reduced dataset was screened against the SH3_p130Cas model scoring the complementarity between the candidate and the protein pocket. The Glob-Prod similarity was used to rank the molecules in the dataset.

Physico-chemical and ADME-Tox prediction. For calculating pK_a and log D^{7.4} we used MoKa v. 2.6.5 (www.moldiscovery.com). To predict the pharmacokinetic profile of **1** and **2** we used pkCSM (<http://biosig.unimelb.edu.au/pkcsml/>), a free Web tool, properly documented in the literature³⁹.

All calculations were run on an Aethia EXA-W 4 core Xeon workstation.

References

1. Ferlay, J. *et al.* Cancer incidence and mortality worldwide: sources, methods and major patterns in GLOBOCAN 2012. *Int J Cancer* **136**, E359–386 (2015).
2. Lemmon, M. A. & Schlessinger, J. Cell signaling by receptor tyrosine kinases. *Cell* **141**, 1117–1134 (2010).
3. Harari, D. & Yarden, Y. Molecular mechanisms underlying ErbB2/HER2 action in breast cancer. *Oncogene* **19**, 6102–6114 (2000).

4. Appert-Collin, A., Hubert, P., Cremel, G. & Bennisroune, A. Role of ErbB Receptors in Cancer Cell Migration and Invasion. *Front Pharmacol* **6**, 283 (2015).
5. Bisaro, B. *et al.* p130Cas scaffold protein regulates ErbB2 stability by altering breast cancer cell sensitivity to autophagy. *Oncotarget* **7**, 4442–4453 (2016).
6. Cabodi, S., del Pilar Camacho-Leal, M., Di Stefano, P. & Defilippi, P. Integrin signalling adaptors: not only figurants in the cancer story. *Nat Rev Cancer* **10**, 858–870 (2010).
7. Defilippi, P., Di Stefano, P. & Cabodi, S. p130Cas: a versatile scaffold in signaling networks. *Trends Cell Biol* **16**, 257–263 (2006).
8. Tornillo, G., Defilippi, P. & Cabodi, S. Cas proteins: dodgy scaffolding in breast cancer. *Breast Cancer Res* **16**, 443 (2014).
9. Tornillo, G. *et al.* p130Cas promotes invasiveness of three-dimensional ErbB2-transformed mammary acinar structures by enhanced activation of mTOR/p70S6K and Rac1. *Eur J Cell Biol* **90**, 237–248 (2011).
10. Cabodi, S. *et al.* p130Cas is an essential transducer element in ErbB2 transformation. *FASEB J* **24**, 3796–3808 (2010).
11. Baselga, J. *et al.* Pertuzumab plus trastuzumab plus docetaxel for metastatic breast cancer. *N Engl J Med* **366**, 109–119 (2012).
12. Zanardi, E., Bregni, G., de Braud, F. & Di Cosimo, S. Better Together: Targeted Combination Therapies in Breast Cancer. *Semin Oncol* **42**, 887–895 (2015).
13. Montemurro, F. Trastuzumab emtansine in HER2-positive metastatic breast cancer. *Lancet Oncol* **18**, 696–697 (2017).
14. Gianni, L. *et al.* Efficacy and safety of neoadjuvant pertuzumab and trastuzumab in women with locally advanced, inflammatory, or early HER2-positive breast cancer (NeoSphere): a randomised multicentre, open-label, phase 2 trial. *Lancet Oncol* **13**, 25–32 (2012).
15. Verma, S. *et al.* Trastuzumab emtansine for HER2-positive advanced breast cancer. *N Engl J Med* **367**, 1783–1791 (2012).
16. Arkin, M. R. & Whitty, A. The road less traveled: modulating signal transduction enzymes by inhibiting their protein-protein interactions. *Curr Opin Chem Biol* **13**, 284–290 (2009).
17. Cierpicki, T. & Grembecka, J. Targeting protein-protein interactions in hematologic malignancies: still a challenge or a great opportunity for future therapies? *Immunol Rev* **263**, 279–301 (2015).
18. Dinkel, H. *et al.* ELM 2016—data update and new functionality of the eukaryotic linear motif resource. *Nucleic Acids Res* **44**, D294–300 (2016).
19. Dalgarno, D. C., Botfield, M. C. & Rickles, R. J. SH3 domains and drug design: ligands, structure, and biological function. *Biopolymers* **43**, 383–400 (1997).
20. Saksela, K. & Permi, P. SH3 domain ligand binding: What's the consensus and where's the specificity? *FEBS Lett* **586**, 2609–2614 (2012).
21. Bornet, O. *et al.* Identification of a Src kinase SH3 binding site in the C-terminal domain of the human ErbB2 receptor tyrosine kinase. *FEBS Lett* **588**, 2031–2036 (2014).
22. Szilagyi, A. & Zhang, Y. Template-based structure modeling of protein-protein interactions. *Curr Opin Struct Biol* **24**, 10–23 (2014).
23. Wisniewska, M. *et al.* The 1.1 Å resolution crystal structure of the p130cas SH3 domain and ramifications for ligand selectivity. *J Mol Biol* **347**, 1005–1014 (2005).
24. Kay, B. K., Williamson, M. P. & Sudol, M. The importance of being proline: the interaction of proline-rich motifs in signaling proteins with their cognate domains. *FASEB J* **14**, 231–241 (2000).
25. Erpel, T., Superti-Furga, G. & Courtneidge, S. A. Mutational analysis of the Src SH3 domain: the same residues of the ligand binding surface are important for intra- and intermolecular interactions. *EMBO J* **14**, 963–975 (1995).
26. Aloy, P. & Russell, R. B. Structural systems biology: modelling protein interactions. *Nat Rev Mol Cell Biol* **7**, 188–197 (2006).
27. Corbi-Verge, C. & Kim, P. M. Motif mediated protein-protein interactions as drug targets. *Cell Commun Signal* **14**, 8 (2016).
28. Villoutreix, B. O. *et al.* Drug-Like Protein-Protein Interaction Modulators: Challenges and Opportunities for Drug Discovery and Chemical Biology. *Mol Inform* **33**, 414–437 (2014).
29. Polte, T. R. & Hanks, S. K. Interaction between focal adhesion kinase and Crk-associated tyrosine kinase substrate p130Cas. *Proc Natl Acad Sci USA* **92**, 10678–10682 (1995).
30. Feng, S., Chen, J. K., Yu, H., Simon, J. A. & Schreiber, S. L. Two binding orientations for peptides to the Src SH3 domain: development of a general model for SH3-ligand interactions. *Science* **266**, 1241–1247 (1994).
31. Koes, D. R. & Camacho, C. J. Small-molecule inhibitor starting points learned from protein-protein interaction inhibitor structure. *Bioinformatics* **28**, 784–791 (2012).
32. Hamilton, N. *et al.* Biologic roles of estrogen receptor-beta and insulin-like growth factor-2 in triple-negative breast cancer. *Biomed Res Int* **2015**, 925703 (2015).
33. Valabrega, G. *et al.* HER2-positive breast cancer cells resistant to trastuzumab and lapatinib lose reliance upon HER2 and are sensitive to the multitargeted kinase inhibitor sorafenib. *Breast Cancer Res Treat* **130**, 29–40 (2011).
34. Barbero, N. *et al.* A study of the interaction between fluorescein sodium salt and bovine serum albumin by steady-state fluorescence. *Dyes and Pigments* **80**, 307–313 (2009).
35. Maier, J. A. *et al.* ff14SB: Improving the Accuracy of Protein Side Chain and Backbone Parameters from ff99SB. *J Chem Theory Comput* **11**, 3696–3713 (2015).
36. Jorgensen, W. L., Chandrasekhar, J., Madura, J. D., Impey, R. W. & Klein, M. L. Comparison of simple potential functions for simulating liquid water. *Comparison of simple potential functions for simulating liquid water* **2**, 9 (1983).
37. Bussi, G., Donadio, D. & Parrinello, M. Canonical sampling through velocity rescaling. *J Chem Phys* **126**, 014101 (2007).
38. Cross, S., Baroni, M., Goracci, L. & Cruciani, G. GRID-based three-dimensional pharmacophores I: FLAPPharm, a novel approach for pharmacophore elucidation. *J Chem Inf Model* **52**, 2587–2598 (2012).
39. Pires, D. E., Blundell, T. L. & Ascher, D. B. pkCSM: Predicting Small-Molecule Pharmacokinetic and Toxicity Properties Using Graph-Based Signatures. *J Med Chem* **58**, 4066–4072 (2015).

Acknowledgements

We would like to thank Prof. Valetti F. for providing us BL21 *Escherichia coli* bacterial strain for production of recombinant proteins. G.E. thanks NVIDIA for donating Titan Xp graphic card. S.V., G.E., G.C. and S.C. were supported by ex-60% funding from the University of Torino.

Author Contributions

A.C. and M.R.S. performed the experiments, analyzed the data and wrote the manuscript. D.N. and M.S. performed the proliferation experiments. G.V. generated SKH100 Trastuzumab-resistant cells. S.V. and G.E. contributed to validation experiments. P.D. and E.T. took part in discussions of the experiments, G.C. and S.C. designed and supervised the experiments and wrote the manuscript. All authors read and approved the final manuscript.

Additional Information

Supplementary information accompanies this paper at <https://doi.org/10.1038/s41598-019-39510-w>.

Competing Interests: The authors declare no competing interests.

Publisher's note: Springer Nature remains neutral with regard to jurisdictional claims in published maps and institutional affiliations.



Open Access This article is licensed under a Creative Commons Attribution 4.0 International License, which permits use, sharing, adaptation, distribution and reproduction in any medium or format, as long as you give appropriate credit to the original author(s) and the source, provide a link to the Creative Commons license, and indicate if changes were made. The images or other third party material in this article are included in the article's Creative Commons license, unless indicated otherwise in a credit line to the material. If material is not included in the article's Creative Commons license and your intended use is not permitted by statutory regulation or exceeds the permitted use, you will need to obtain permission directly from the copyright holder. To view a copy of this license, visit <http://creativecommons.org/licenses/by/4.0/>.


© The Author(s) 2019

RESEARCH

Open Access



Conditional ablation of p130Cas/BCAR1 adaptor protein impairs epidermal homeostasis by altering cell adhesion and differentiation

Maria del Pilar Camacho Leal[†], Andrea Costamagna[†], Beatrice Tassone, Stefania Saoncella, Matilde Simoni, Dora Natalini, Aurora Dadone, Marianna Sciortino, Emilia Turco, Paola Defilippi, Enzo Calautti[‡] and Sara Cabodi^{*‡} 

Abstract

Background: p130 Crk-associated substrate (p130CAS; also known as BCAR1) is a scaffold protein that modulates many essential cellular processes such as cell adhesion, proliferation, survival, cell migration, and intracellular signaling. p130Cas has been shown to be highly expressed in a variety of human cancers of epithelial origin. However, few data are available regarding the role of p130Cas during normal epithelial development and homeostasis.

Methods: To this end, we have generated a genetically modified mouse in which p130Cas protein was specifically ablated in the epidermal tissue.

Results: By using this murine model, we show that p130Cas loss results in increased cell proliferation and reduction of cell adhesion to extracellular matrix. In addition, epidermal deletion of p130Cas protein leads to premature expression of “late” epidermal differentiation markers, altered membrane E-cadherin/catenin proteins localization and aberrant tyrosine phosphorylation of E-cadherin/catenin complexes. Interestingly, these alterations in adhesive properties in absence of p130Cas correlate with abnormalities in progenitor cells balance resulting in the amplification of a more committed cell population.

Conclusion: Altogether, these results provide evidence that p130Cas is an important regulator of epidermal cell fate and homeostasis.

Keywords: Adaptor proteins, Mouse primary keratinocytes, Cell adhesion, Cell signaling and cell differentiation

Background

p130Cas is a multifunctional adaptor protein required for embryonic development and is characterized by structural motifs that enable interactions with a variety of signaling molecules and the modulation of pathways controlling cell proliferation, survival, actin cytoskeleton organization and extracellular matrix degradation [1]. p130Cas/BCAR1 expression has been shown to be fundamental for cell transformation and tumor progression in several cancers but also in other diseases [2, 3].

The early embryonic lethality of the germ-line knock-out (KO) p130Cas/BCAR1 mouse points out its crucial role during mouse development [4]. To circumvent embryonic lethality in order to investigate the role of p130Cas in mammalian developmental process, we have established a p130Cas tissue-specific knockout mouse line, utilizing Cre transgene under control of the human cytokeratin 14 (K14) gene promoter, which is active in dividing cells of several stratified epithelial tissues, including skin and mammary gland [5].

Epidermal stratification is achieved through two distinct mechanisms. The first one involving the basal cells detachment and transition from the basement membrane to the suprabasal layers. The second mechanism accounts for the asymmetrical cell division of stem cells

* Correspondence: sara.cabodi@unito.it

[†]Maria del Pilar Camacho Leal and Andrea Costamagna contributed equally to this work.

[‡]Enzo Calautti and Sara Cabodi contributed equally to this work.

Department of Biotechnology and Health Science, Molecular Biotechnology Center, Università di Torino, Via Nizza 52, Torino, Italy



residing in the basal layer that generate a suprabasal cell that is committed to terminal differentiation but still undergoes a limited number of cell division and a slow cycling cell that remains confined into the basal layers [6–8].

Once detached from the basal membrane, epithelial cells undergo differentiation progressing through a series of stage-specific morphological and biochemical changes leading to the synthesis of the differentiation-specific keratins such as Cytokeratin 1 (K1) and Cytokeratin 10 (K10), as well as involucrin, filaggrin, and loricrin [9, 10]. In *in vitro* cell culture, elevation of calcium concentrations induces keratinocyte differentiation program characterized by differentiation markers expression, rapid redistribution of cadherins to the membrane and consequent adherens junctions and desmosomes formation, reorganization of the cytoskeleton, polarization and stratification [11].

Analysis of mouse skin tissue *in vivo* and mouse keratinocyte cultures showed that the absence of p130Cas expression is sufficient to alter epidermal homeostasis. Indeed, epidermal ablation of p130Cas impairs cell-matrix adhesion, increases cell proliferation and expression of terminal differentiation markers both *in vivo* and *in vitro*. Interestingly, undifferentiated p130CasKO keratinocyte cultures display features of early commitment to differentiation characterized by E-cadherin cell membrane localization along with an increased tyrosine phosphorylation of E-cadherin and beta-catenin. The alterations in cell proliferation, differentiation and adhesion properties observed in p130Cas null keratinocytes correlate with the expansion of cell population, with reduced clonogenic ability, which are consistent with a differentiation committed phenotype.

Materials and methods

Knock-out mice generation

The use of animals was in compliance with the Guide for the Care and Use of Laboratory Animals published by the U.S. National Institutes of Health and approved by the Italian Health Minister (authorization n° 24-2014PR).

C57/BL mice containing loxP sites flanking exon 5 and 6 and the neomycin cassette were generated by first crossing them with flipper (FLPe) and then crossing p130Cas^{fl/fl} mice with K14-Cre transgenic animals. Genotypes were determined by PCR screening of tail biopsies by using the following primers: p130CasloxP FW (5'-GATACCTTC TGGGTCTCCTGTACCCC AAGG-3') and p130CasloxP RW (5'-CCTCTGCTTCCCAAATGCTGGGATCAA AG G-3') to identify loxP sites flanking p130Cas gene, Cre F W (5'-GGACATGTTTCAGGGATCGCCAGGCG-3') and Cre RW (5'-GCATAACCAGTG AACAGCATTGCT G-3') to identify Cre recombinase.

Cell proliferation, differentiation and ECM-cell adhesion assays

For keratinocyte cell differentiation, 2 mM CaCl₂ was added to keratinocyte culture medium. For proliferation assays 5 × 10⁵ cells/ml were plated in triplicate on collagen coated 12-well dishes in low calcium medium (minimal essential medium with 4% Chelex treated fetal calf serum (Hyclone), epidermal growth factor (EGF; 10 ng/ml, Collaborative Research, Inc., Cambridge, MA), and 0.05 mM CaCl₂ (low calcium medium) as described in (Calautti et al.,1998). Cells were counted from the first day after plating for three days in triplicate. For cell adhesion experiments, the number of attached cells to the ECM components was evaluated the day after plating.

Immunoprecipitations

Mouse primary keratinocytes immunoprecipitation experiments were performed as described in (Calautti et al.,1998). Briefly, keratinocytes were lysed and quantified. Same extract amounts were incubated ON at 4 °C with antibodies followed by addition of Protein G-agarose beads for 2 h at 4 °C. Immune-complexes were washed four times, eluted in boiling Laemmli sample buffer and separated by SDS-PAGE.

Western blot analysis

Extracts from different tissues (heart, brain and skin) were prepared from 3-day-old mice. Tissues were lysed with Ultra Turrax in boiling SDS Lysis Buffer (2% SDS, Tris HCl pH 7.5, 0.5 M EDTA), with protease inhibitor cocktail (Roche), and centrifuged at 13000 rpm for 15 min. Primary keratinocytes lysates were prepared by scraping 6-well dishes into 100 µl boiling SDS Lysis Buffer, vortexed and boiled several times. Lysates were subjected to western blotting analysis with the following antibodies: filaggrin, loricrin, keratin 1 and keratin 5 (Covance (Princeton, NJ, USA)); p130Cas, ΔNp63, E-cadherin, beta-catenin and alpha-catenin (BD Transduction Laboratories (San Jose, CA,USA)); tubulin and c-Src (Sigma (St. Louis, MO, USA)); phospho-Erk1/2 MAPKs (Thr202/Tyr204), phospho-Src (Tyr416), phospho-YAP and Yap (Cell Signaling (Danvers, MA, USA)); Erk1/2, CyclinD1, pTyr (Santa Cruz (Palo Alto, CA, USA)). Secondary antibodies were incubated for 1 h at RT, and detection performed with ECL Prime (GE Healthcare, Chicago, IL, USA). Protein band intensities were determined using the Image J software. All comparative images of blots shown are resulting from same exposures of the same membranes.

Immunohistochemistry and immunofluorescence analysis

For histological analysis, frozen sections from 3-days-old mice dorsal skin were stained with hematoxylin/eosin

(H/E). For immunofluorescence staining, sections were fixed in methanol/acetone solution, permeabilized with PBS/0.5% Triton X-100, saturated with blocking buffer for 30' and incubated with primary antibodies at 4 °C ON followed by 1 h incubation at RT with Alexa Fluor 488 or 568 antibodies (Invitrogen). Images were taken at HCX PL APO CS 40X-63X 1.4 OIL Leica TCS-SP5 II confocal microscope and analysed with LASAF software or at Zeiss Observer Z.1 microscope ($\times 20/0.50$ objective) with the ApoTome module. For PCNA and Ki67 staining (Santa Cruz, (Palo Alto, CA, USA); Novocastra, (Leica, UK)), sections were fixed and stained as above. Staining was detected by peroxidase reaction with DAB. ImageJ software (NIH, Bethesda USA) was used for quantification and/or counting analysis.

Primary mouse keratinocyte cell culture and treatments

Primary epidermal keratinocytes were isolated from the skin as previously described (Calautti et al., 1998). Briefly, skin was removed from 3-days-old pups; the epidermis was peeled away from the dermis, minced and filtered to release single cells. Keratinocytes (1×10^6 cells/ml) were plated in culture plates coated with collagen and cultured in low calcium medium at 34 °C and 8% CO₂.

Colony-forming efficiency (CFE) assays

Colony-forming efficiency (CFE) assays were performed as described in [12], with minor modifications. 10^3 cells were plated on lethally irradiated feeder layer 3 T3-J2 cells. After 12 days, colonies were fixed, stained with rhodamine-B and scored under a dissecting microscope. Total colonies were calculated as a percentage of total plated cells (colonies number $\times 100$ /cell plated number). For second progeny experiments, primary cells isolated from WT and p130CasKO mice were maintained in low calcium condition for 7 days. Then CFE assays were performed with an increased number of cells (5×10^4). Colonies were classified based on morphological parameters [12, 13].

Dispase treatment of mouse primary keratinocytes

Dispase treatment was performed as described in [14]. Briefly, duplicate 60-mm dishes of confluent keratinocyte cultures in low or high calcium medium were washed twice in PBS and incubated in 2 ml dispase solution in PBS (2.4 units/ml; Roche) at 34 °C. Cells were analyzed under the microscope at 5-min intervals, for 35 min. After 35 min, cells were scraped, then washed twice in PBS and centrifuged. Cell pellets were resuspended and counted as single cells with an hemocytometer. Results are expressed as percentage of dispase released cells over the total number of cells.

Statistical analysis

Statistical analyses were performed with Student t test or two-way analysis of variance (ANOVA, Bonferroni posttest analysis) for comparison of two or multiple groups, respectively, using Prism 5.0 (GraphPad, San Diego, CA). Mann-Whitney nonparametric test was applied when quantified results do not follow normal distribution. Differences with *P*-values less than 0.05 were considered statistically significant.

Results

Generation of mice with epidermis-restricted deletion of the p130Cas/BCAR1 gene

To conditionally ablate p130Cas expression in the epidermis, we employed the Cre-LoxP system. p130Cas fl/fl mutant mice harbors a construct in which exons 5 and 6 of the p130Cas gene were flanked with Cre-lox recombination (loxP) sites (Fig. 1a). Mice were first mated with flipper (FLPe) mice to remove the neo-cassette and one FLPe recognition target (FRT) site, leaving behind the two loxP sites. p130Cas^{fl/fl} mice were bred with transgenic mice expressing Cre recombinase under the control of the human K14 promoter. This promoter is active in dividing cells of several stratified epithelia, such as skin, mammary gland and thymus (Jonkers et al., 2001). To evaluate the absence of p130Cas in the Knock-Out (KO) mice, western blot analyses were performed on extracts of skin isolated from 3-day-old p130CasKO mice (Fig. 1b) and of different tissues, such as brain, heart and thymus (Additional file 1: Figure S1). This analysis confirmed that Cre recombination occurred in the epidermis and in thymus as reported, but not in other tissues. p130CasKO pups were born at the expected Mendelian ratio, were viable and fertile, and no significant differences were observed at birth in growth or macroscopic defects of the skin relative to control littermates lacking Cre recombinase (Fig. 1b).

p130Cas deficiency alters the balance between epidermal cell proliferation and differentiation

Histological examination of the epidermis of 3-day-old p130CasKO and Wild-Type (WT) pups revealed a significant epidermal thickening in mutant mice, indicating altered skin morphogenesis in the absence of p130Cas (Fig. 1c and d). We also analyzed the expression of K1, an early differentiation marker typical of the spinous suprabasal epidermal layer as well as of K14, whose expression is confined in basal undifferentiated epidermal layer under homeostatic physiological conditions [15]. K1 staining was significantly enhanced in the suprabasal layers of p130CasKO skin as compared to WT counterparts. Moreover, we also observed a higher number of K14 positive cells in the suprabasal layers of p130CasKO mice, suggestive of abnormalities in the balance between

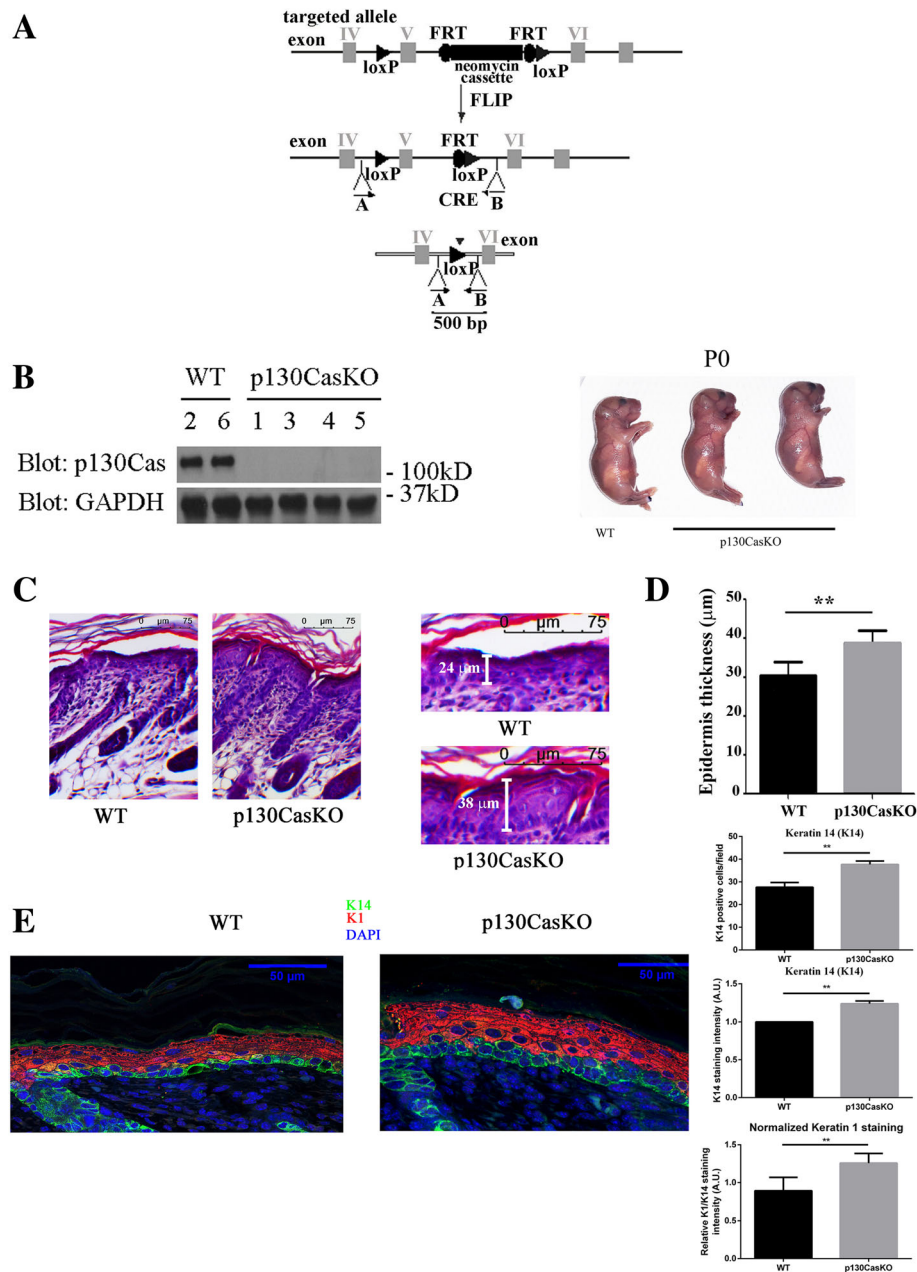


Fig. 1 Conditional deletion of p130Cas in the mouse epidermis. **(a)** Schematic representation of p130Cas/BCAR1 gene targeting strategy. **(b)** Epidermis isolated from WT (mice 2, 6) and p130CasKO (mice 1, 3, 4 and 5) 3 days old pups were lysed and cell extracts were subjected to western blotting protein analysis. Representative images of WT and p130CasKO mice at birth (P0) (right panels). **(c)** Representative haematoxylin/eosin stained sections from WT and p130CasKO skins of 3 days old pups (10X) (left panels). Higher magnification insets of representative haematoxylin/eosin stained section from WT and p130CasKO skins (20X) (right panels). **(d)** Quantification of epidermis thickness in WT and p130CasKO. The data represented the mean \pm S.D. from 10 WT and 10 p130CasKO mice (** $p < 0.01$). **(e)** Representative images of K14 and K1 fluorescence staining of WT and p130CasKO 3-day-old pups skin (40X) (left panel). Quantification of immunofluorescent stainings is shown in the right panels. K1 staining intensity was normalized for K14 staining intensity. The data represented the mean \pm S.D. from 6 WT and 6 p130CasKO mice (** $p < 0.01$) (field equal to 200 μ m)

keratinocyte proliferation and differentiation (Fig. 1e and Additional file 1: Figure S2).

To determine whether the epidermal thickening and suprabasal K14⁺ cells observed in p130Cas-deficient mice correlate with increased keratinocyte proliferation,

we assessed the expression of Ki67 and PCNA proliferative markers. As shown in Fig. 2a-d and in Additional file 1: Figure S3, Ki67 and PCNA were significantly increased in the basal layer of p130CasKO mice compared to WT, indicating an increased tendency of mutant

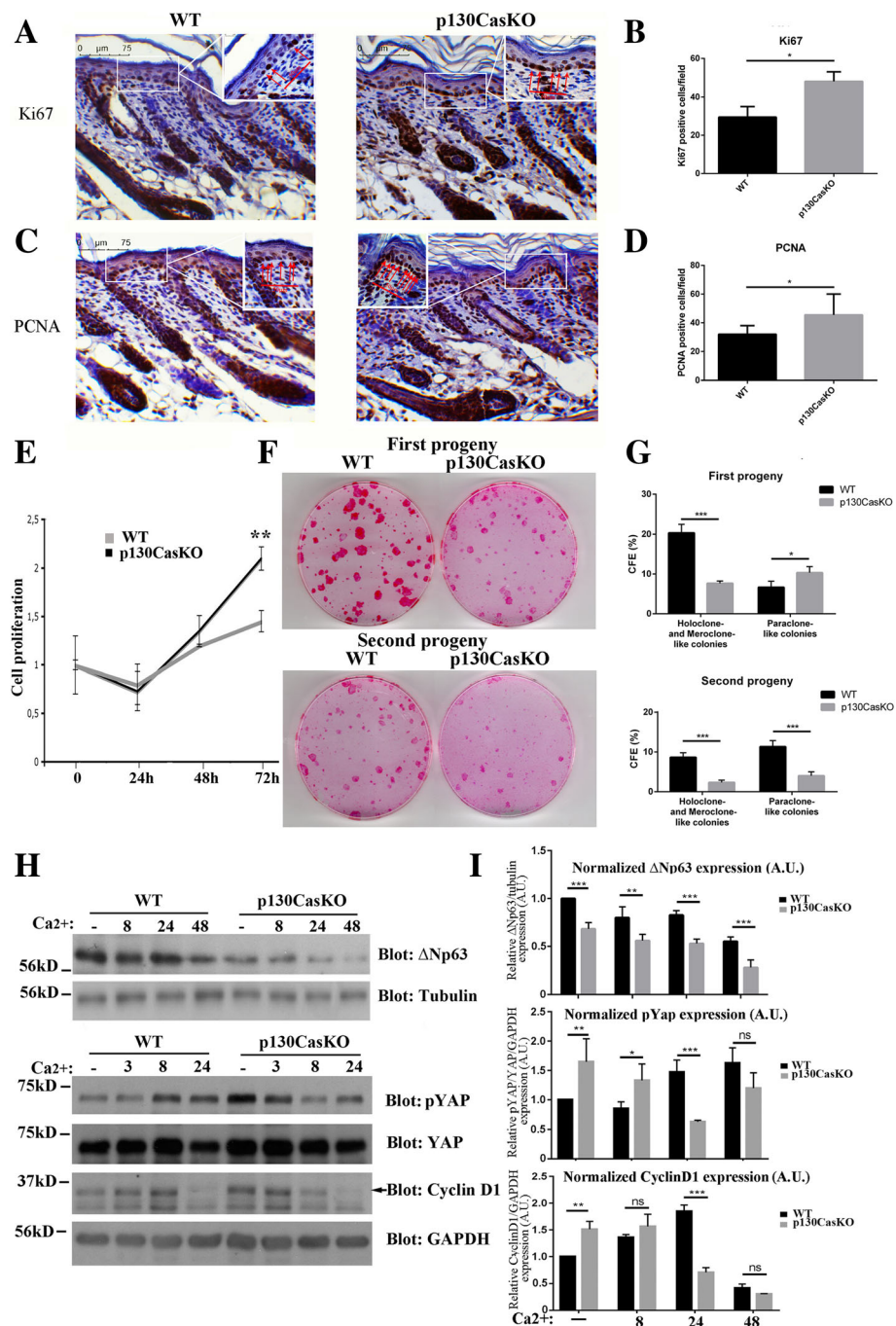


Fig. 2 p130Cas deletion alters the balance between epidermal proliferation and differentiation. **(a, b)** Representative images of Ki67 staining from WT and p130CasKO of 3-day-old pups skin (20X). Quantification was performed by counting Ki67 basal positive cells on the entire images (field equal to 350 μ m). The data represented the mean \pm S.D. from 10 WT and 10 p130CasKO mice (**p* < 0.05). Inset were taken at 100X magnification. **(c, d)** Representative images of PCNA staining from WT and p130CasKO of 3-day-old pups skin (20X). Quantification was performed by counting PCNA basal positive cells on the entire images (field equal to 350 μ m). The data represented the mean \pm S.D. from 10 WT and 10 p130CasKO mice (**p* < 0.05). Inset were taken at 100X magnification. **(e)** WT and p130CasKO keratinocytes were plated in triplicate on collagen coated dishes and counted every day for 72 h. Data are expressed as mean \pm S.D. of results from three independent experiments (***p* < 0.01). **(f)** Representative images of first and second progeny of WT and p130CasKO keratinocytes cultured under clonogenic conditions for 12 days, followed by rhodamine-B staining. **(g)** SEM of colonies of the indicated sizes. 100 colonies were counted from duplicate plates and classified based on morphological parameters. Data represent two independent experiments. **(h)** Untreated and calcium-treated WT and p130CasKO keratinocytes extracts blotted for Δ Np63 (Tubulin as loading control), phospho-YAP, YAP, Cyclin D1 (GAPDH as the loading control). **(i)** Densitometric analysis of protein levels of at least three independent experiments is shown (***p* < 0.05, ****p* < 0.001, ns = not significant)

keratinocytes to proliferate. Interestingly, PCNA staining was detected in a significant amount of suprabasal cells at both embryonic day 18.5 and P3 in p130CasKO epidermis (Additional file 1: Figure S5).

To provide insights into the control of p130Cas-dependent skin homeostatic processes, *in vitro* culture of primary keratinocytes isolated from 3 days-old pups were established [16]. In this *in vitro* model, proliferation assays were performed by counting every day for 72 h WT and p130CasKO keratinocytes plated on collagen coated dishes. The proliferative curve shown in Fig. 2e indicates that p130CasKO keratinocytes possess higher proliferation rates than WT keratinocytes.

Since epidermal stratification involves delamination and asymmetrical cell division of basal cells [7, 8], and we observed a higher percentage of K14 positive cells in the suprabasal layers of the p130CasKO, we hypothesized that p130Cas deletion might impact progenitor cells commitment toward differentiation. Consistently, we found that freshly isolated p130CasKO primary keratinocytes have an overall reduced clonogenic capacity with a strong reduction of colonies displaying holoclone- and meroclone-like morphology, which was also maintained in second-generation clonogenic assays (Fig. 2f and g). Overall, these data are consistent with an anticipated commitment of p130CasKO progenitor cells to differentiation. Accordingly, the levels of $\Delta Np63\alpha$, a transcription factor governing keratinocyte stem cell fate [17], were found reduced in p130CasKO in undifferentiated conditions compared to WT cells, and further diminished upon differentiation induction triggered by elevation of the extracellular calcium concentration (high calcium medium) (Fig. 2h, i and Additional file 1: Figure S4A). Consistently, p63 expression was found decreased in p130CasKO epidermis at both E18.5 (mouse embryonic day 18.5) and P3 (Additional file 1: Figure S5). Moreover, inactivating phosphorylation of YAP, a transcriptional activator implicated in skin homeostasis control [18, 19], was found up-regulated in p130CasKO keratinocytes compared to WT cell under basal conditions. Moreover, although the YAP protein levels did not differ significantly between genotypes in response to calcium (Additional file 1: Figure S4B), the kinetics of YAP phosphorylation indicated an opposite trend between WT and p130CasKO keratinocytes, with an increase in the former and a decrease in the latter cells (Fig. 2h and i). In newborn skin, YAP expression was detected in few basal cells in both WT and mutant mice as previously reported [19, 20]. Notably, p130CasKO epidermis contained a significant amount of nuclear YAP in isolated suprabasal cells compared to WT controls (Additional file 1: Figure S5), and a similar trend was also observed in mutant mice at E18.5 (data not shown). Cyclin D1 expression *in vitro* was more

elevated in proliferating p130CasKO as compared to WT cells (Fig. 2h and i). Overall, these data suggest a role for p130Cas in the maintenance of epidermal homeostasis by promoting keratinocyte quiescence and preventing commitment toward differentiation.

The increased proliferation rates observed in p130CasKO cells coupled with their reduced clonogenic capacity suggest that these cells may be more prone to engage the terminal differentiation program. To verify this hypothesis, we compared keratinocytes isolated from WT and mutant mice under undifferentiated conditions or during calcium-induced differentiation. Upon calcium switch, keratinocytes cultures acquire a squamous morphology, become stratified, form desmosomes and adherens junctions, undergo growth arrest and express markers typical of suprabasal epidermal layers. In undifferentiated conditions p130CasKO keratinocytes display a flat and round-shaped morphology compared to wild-type cells. Upon differentiating conditions, p130CasKO cells appear bigger with less evident cell-cell borders (Fig. 3a). Notably, under low calcium culture conditions, p130CasKO cells display a higher expression of granular layer differentiation markers (filaggrin and loricrin) but not spinous layer marker (K1) (Fig. 3b and c). Upon differentiating stimulus, an expected induction of both early and late differentiation marker expression in WT keratinocytes was observed, whereas p130CasKO cells displayed a robust K1 induction after calcium stimulation which was consistent with the increased K1 expression observed *in vivo* (Fig. 1e). Moreover, although the absolute level of filaggrin and loricrin were overall increased in mutant cells, the levels of these proteins did not further increase upon calcium treatment (Fig. 3b and c). Consistently, filaggrin and loricrin expression was also increased in the intact epidermis of p130CasKO mice (Fig. 3d and e and Additional file 1: Figure S6).

Overall, these data indicate that p130Cas deficiency affects keratinocytes proliferation and differentiation both *in vitro* and *in vivo* and renders the cells more prone to engage differentiation.

p130Cas is required for proper ECM and cell-cell adhesion

A critical step in the differentiation process of all epithelial cells is cell detachment from the basement membrane, mostly dependent on modification in integrin-matrix interactions. Indeed, activation of beta1 integrins in normal keratinocytes abrogates differentiation while inhibition of integrin downstream signaling promotes keratinocytes differentiation [21–23]. Several lines of evidence have placed p130Cas as an important modulator of signals emanating from integrins and ECM [2]. Therefore, to determine whether the altered differentiation process observed in p130CasKO is due to

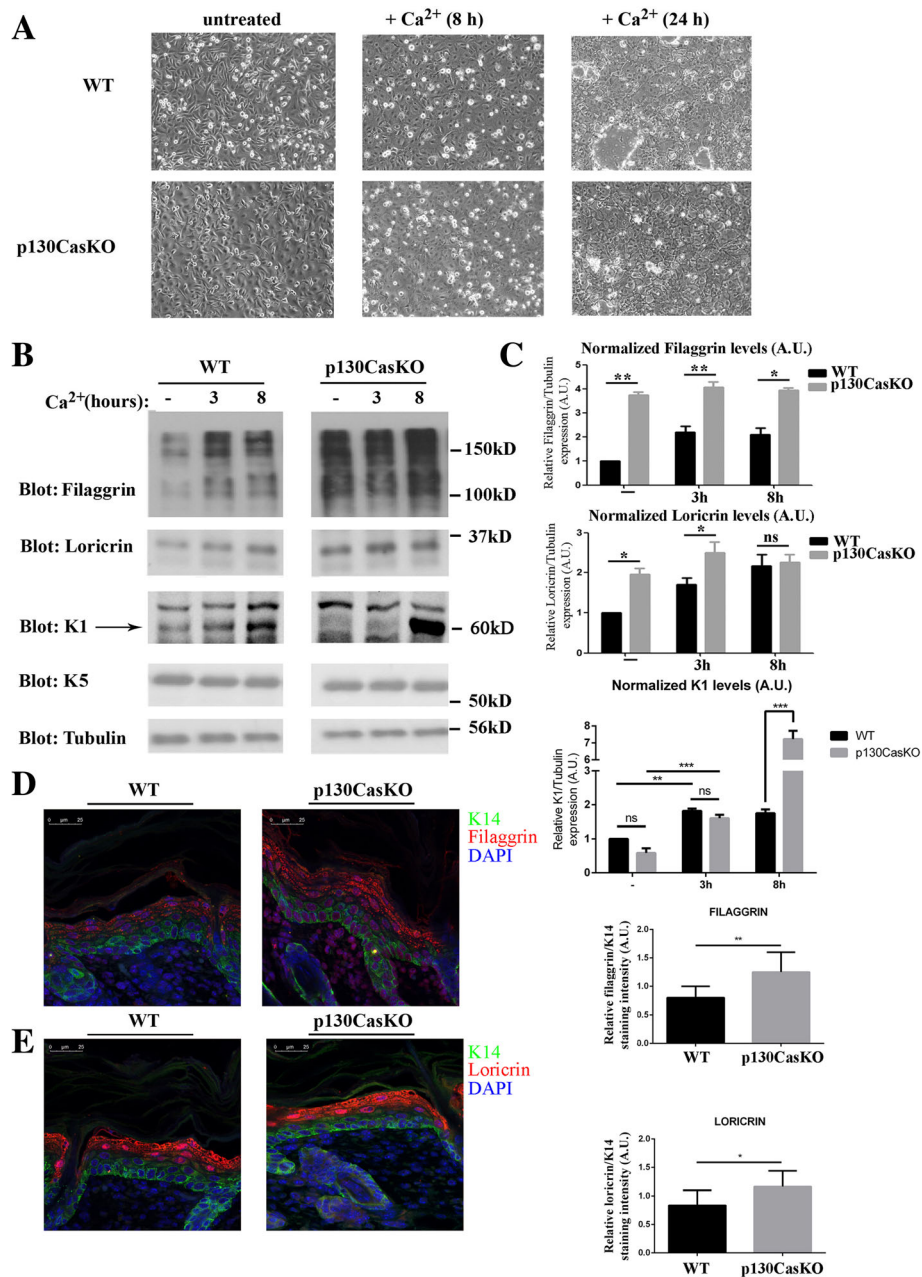


Fig. 3 p130Cas loss affects keratinocytes differentiation. **(a)** Representative images of confluent WT and p130CasKO keratinocytes in low calcium condition and after 8 and 24 h of calcium treatment (20X magnification). **(b)** Western blot analysis of early and late differentiation markers of WT and p130CasKO keratinocytes either untreated or calcium treated. **(c)** Densitometric analysis of protein levels of at least three independent experiments is shown ($p < 0.05$, $**p < 0.01$). **(d)** Representative images and quantification of filaggrin fluorescence staining of WT and p130CasKO 3-day-old pups skin (left and right panel, respectively) (40X). **(e)** Representative images and quantification of lorincrin fluorescence staining of WT and p130CasKO 3-day-old pups skin (left and right panel, respectively) (40X). Data are expressed as mean \pm S.D. of three independent experiments

aberrant ECM-keratinocyte cell adhesion, we performed keratinocyte cell adhesion assays to fibronectin, laminin and collagen ECM components. Specifically, p130CasKO keratinocytes display reduced adhesion to both collagen and laminin as compared to WT cells (Fig. 4a), indicating that p130Cas deficiency in keratinocytes leads to alterations in cell adhesion to basement membrane

components. The ECM-cell adhesion reduction observed in p130KO keratinocytes may reflect an aberrant expression of integrin receptors in the basal layer of the mouse epidermis. To test this possibility, we evaluated integrin receptor beta1 and beta4 protein expression levels in keratinocytes derived from WT and KO mice. However, neither beta1 nor beta4 integrin protein levels were

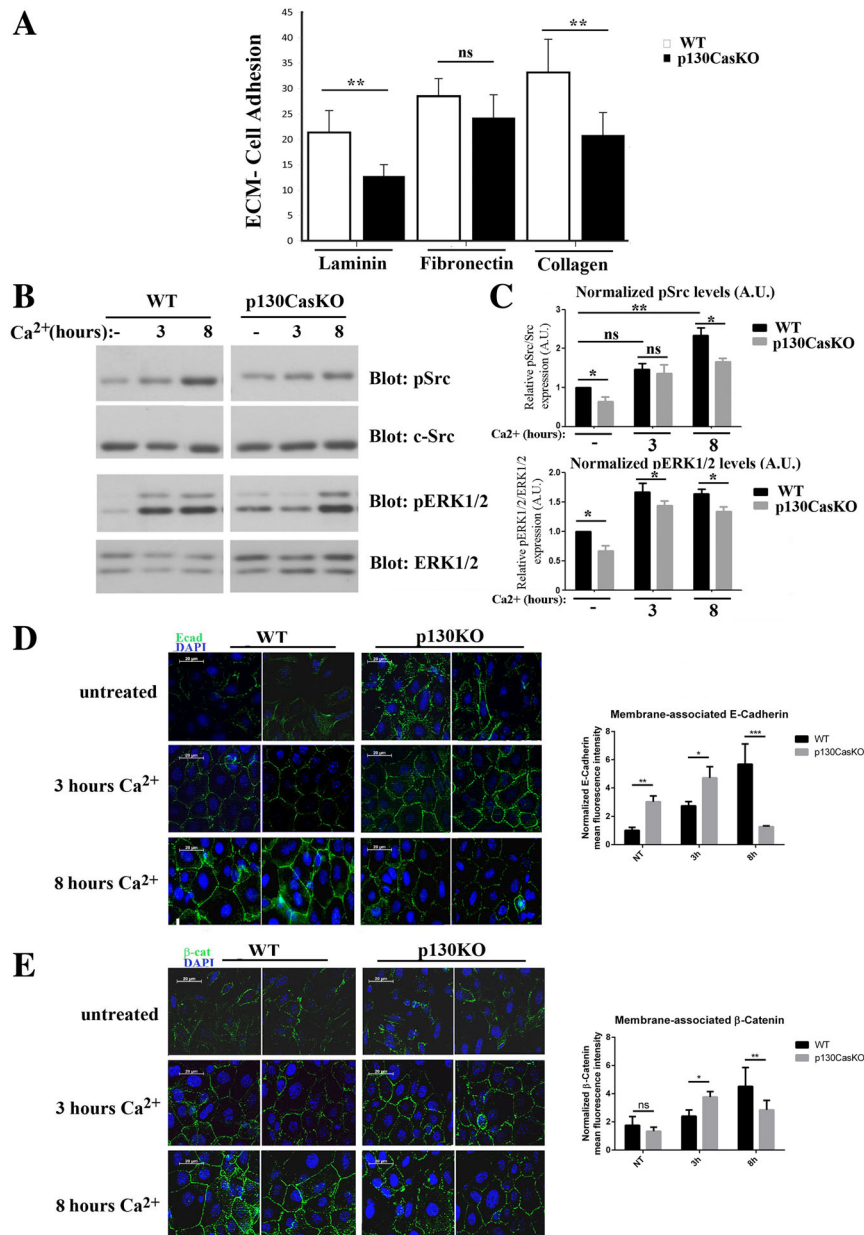


Fig. 4 p130Cas is required for proper ECM and cell-cell adhesion. **(a)** Adhesion quantification of freshly isolated WT and p130CasKO primary keratinocytes on laminin, fibronectin and collagen after 12 h of cell adhesion. Data are expressed as mean \pm S.D. of five independent experiments (** $p < 0.01$). **(b)** Western blotting analysis for phospho-Src (pSrc), c-Src, phospho-ERK1/2 MAPKs (pERK1/2) and ERK1/2 MAPKs from confluent untreated and calcium-treated WT and p130CasKO keratinocytes. **(c)** Densitometric analysis of protein levels of at least three independent experiments is shown ($p^* < 0.05$, ** $p < 0.01$). Activation of Src and ERK1/2 MAPKs was normalized to c-Src and ERK1/2 levels, respectively, as loading control. **(d, e)** Representative images of E-cadherin **(d)** and beta-catenin **(e)** stainings in untreated and calcium-treated WT and p130CasKO keratinocytes. DAPI stained nuclei (63X magnification) (left panels). Quantification of immunofluorescent staining of membrane-associated E-cadherin and beta-catenin is shown in the right panels. The data represented the mean \pm S.D. of 4 independent experiments (* $p < 0.05$, ** $p < 0.01$, *** $p < 0.001$) (field equal to 50 μ m)

affected by p130Cas ablation (Additional file 1: Figure S7). To evaluate whether the observed cell adhesion reduction upon p130Cas deletion may result from defective integrin signaling, we tested whether phosphorylation of Src was altered in p130CasKO keratinocytes compared to WT cells. Src kinase activation is one of the early event

associated with integrin engagement to the ECM and is required for p130Cas phosphorylation [24]. As shown in Fig. 4b and c, phosphorylation of Src was significantly reduced in p130CasKO keratinocytes even in low calcium medium, indicating that integrin downstream signaling is impaired. Moreover, ERK1/2 MAPKs activation upon

integrin clustering has been correlated to cell decision to undergo differentiation. Indeed, in absence of differentiative stimuli, the levels of ERK1/2 MAPKs activity reflect the capacity of keratinocytes to undergo differentiation [21, 25–27]. Consistently, the deletion of p130Cas in the basal layer impairs integrin signaling resulting in lower activation of MAPKs both in undifferentiated and differentiated condition (Fig. 4b and c).

These results suggest that the absence of p130Cas in basal keratinocytes leads to an alteration in integrin signaling, reflected by an aberrant basal membrane adhesion and a commitment to cell differentiation.

In addition to integrin-cell adhesion, E-cadherin cell-cell dependent adhesion has a crucial role during keratinocyte differentiation. To determine whether alterations in E-cadherin localization and/or activation are implicated in the abnormal cell differentiation of p130Cas-null keratinocytes, we performed E-cadherin and beta-catenin immunofluorescence analysis of insoluble-detergent fractions in confluent WT and mutant primary keratinocytes cultures either kept undifferentiated in low calcium medium or at different times following 2 mM calcium switch. Surprisingly, E-cadherin appeared recruited at the cell membrane in p130CasKO keratinocytes already in low calcium medium while in WT cells, it localized at the cell membrane only after the calcium switch, as expected. (Fig. 4d and e). Interestingly, this increased recruitment of E-cadherin and beta-catenin at the cell membrane, was even more pronounced at early times after calcium treatment in p130CasKO cells. In fact, after 3 h of calcium treatment, p130Cas KO keratinocytes show an almost complete sealing of adjacent cell membranes of juxtaposed cells while WT keratinocytes as reported previously [14, 28, 29] were found in the “zipper-like” stage. However, at later times (8 h), E-cadherin and beta-catenin were found decreased at the cell borders of mutant cultures. These data suggest abnormalities in the ordered assembly of E-cadherin-dependent adhesive structures in the absence of p130Cas.

p130Cas is required for cell-cell adhesion dynamics

Tyrosine phosphorylation of adherens junction components is a hallmark of keratinocytes differentiation [14, 28]. Therefore, we investigated whether p130Cas ablation in the epidermis also affects tyrosine phosphorylation dynamics of E-cadherin/beta-catenin complexes. For this reason, we determined the amount of E-cadherin/beta-catenin complexes that could be recovered after immunoprecipitation with anti-phosphotyrosine antibodies (p-Tyr) both in low and high calcium condition (8 h). In undifferentiated conditions, increased E-cadherin and beta-catenin tyrosine phosphorylation was observed in

p130CasKO immunoprecipitates compared to WT. While in WT keratinocytes calcium addition increased the amounts of E-cadherin and beta-catenin precipitated by p-Tyr antibodies, as expected, in p130CasKO cells the levels of E-cadherin/beta-catenin in complex with p-Tyr were similar in both low- and high calcium conditions (Fig. 5a). Interestingly, in p130CasKO cells alpha-catenin failed to associate to E-cadherin/beta-catenin complexes in high calcium conditions, while no differences in E-cadherin/beta-catenin association were observed in the absence of p130Cas (Fig. 5b).

To evaluate the presence of functional defects in cell-cell junctions caused by p130Cas deletion, we performed a dispase treatment as described in [14]. Indeed, a lack of cohesive strength may be revealed under these conditions, when keratinocytes lose attachment to their support and are connected to each other only through direct intercellular contacts. As shown in Fig. 5c, after 1 h of calcium treatment, p130CasKO keratinocytes display a significantly enhanced strength of cell-cell junctions after dispase treatment compared to WT cells. Interestingly, the anticipation of cell-cell adhesion observed in p130CasKO keratinocytes were reverted at later time points where cells display reduced strength of cell-cell adhesion after 8 h of calcium treatment. However, at even later time points (24 h) no significant changes in dispase sensitivity were observed between WT and p130CasKO keratinocytes, indicating a transient alteration of the adherence junction dynamics *in vitro*. Interestingly, a similar transient defect of E-cadherin localization at the cell borders, was observed at E18.5 in mutant embryos and this coincided with partial loss of epidermal barrier function (Additional file 1: Figure S8). However, in mutant newborn mice, these defects were fully recovered as they did not display either defects of E-cadherin localization or alterations of barrier function (data not shown).

Moreover, to verify whether the alterations in cell-cell adhesion associate with alterations in actin cytoskeleton, WT and p130CasKO primary keratinocytes in low calcium and after 1 h of calcium treatment, were stained with phalloidin and vinculin. The results shown in Fig. 5d, indicate that in low calcium condition actin fibers are more densely packed in p130CasKO compared to WT cells. After 1 h of calcium exposure, p130Cas KO keratinocytes show increased cortical actin at cell-cell borders while in WT keratinocytes peripheral actin is mainly found “zipper-like” structures.

Under low calcium conditions, p130CasKO keratinocytes show a diffused, not-polarized vinculin staining that differs from WT cells in which vinculin is concentrated in focal points. To verify whether this changes correlate with a different cell migratory behavior, we performed *in vitro* wound healing experiments and found a

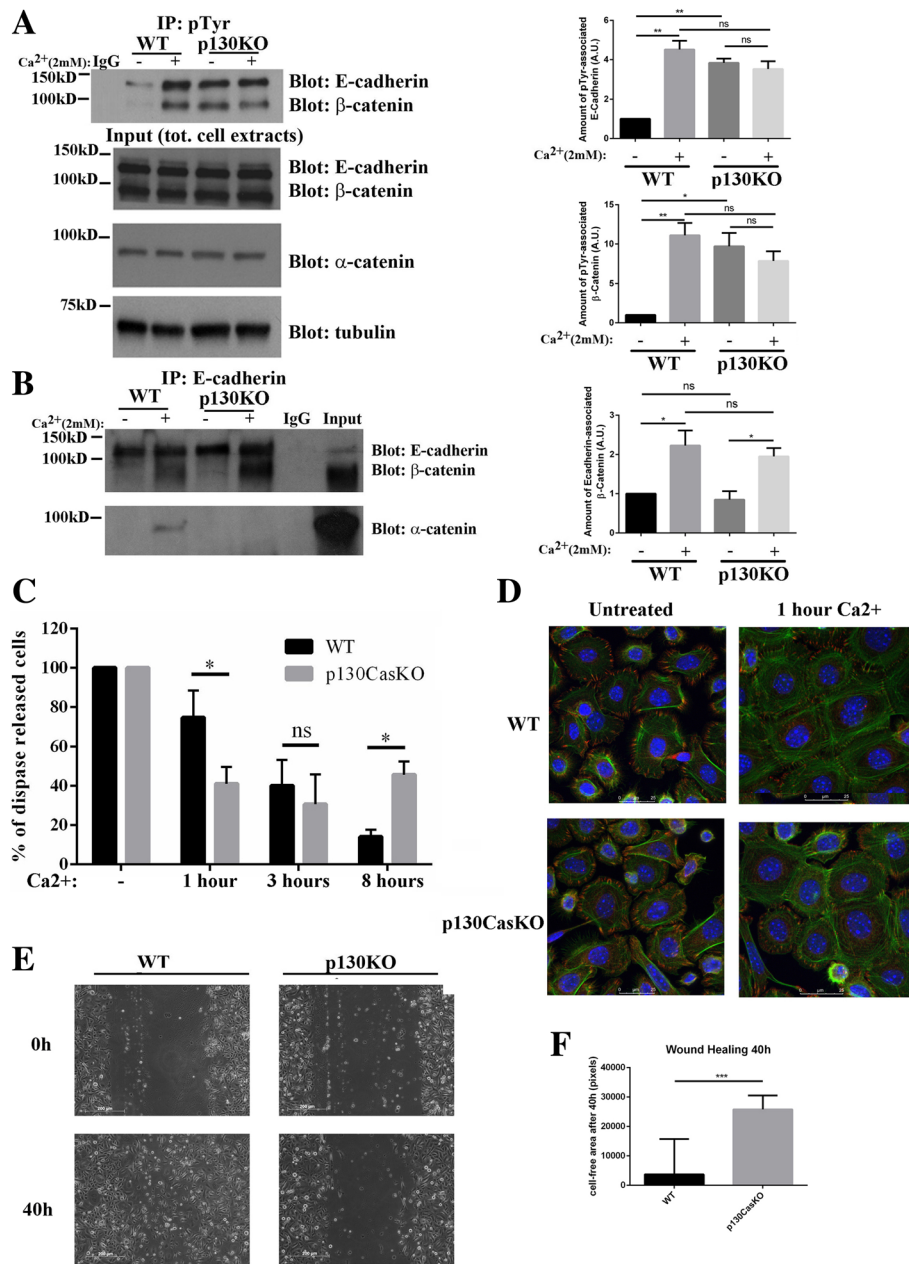


Fig. 5 p130Cas impairs cell-cell adhesion dynamics. **(a)** Phospho-tyrosine immunoprecipitates from confluent untreated and calcium-treated WT and p130CasKO keratinocytes blotted with E-cadherin and beta-catenin antibodies. IgG indicates the immunoprecipitation control. Cell extracts are shown at the bottom (left panels). Densitometric analysis of protein levels of at least three independent experiments is shown in the right panels ($p^* < 0.05$, $p^{**} < 0.01$). **(b)** E-cadherin immunoprecipitates from the same extracts as in **(a)** blotted with alpha-catenin antibodies (left panels). Densitometric analysis of protein levels of at least three independent experiments is shown on the right panel ($p^* < 0.05$). **(c)** Triplicate samples of primary keratinocytes from WT or p130Cas KO mice were kept under low calcium condition or treated with calcium for 1, 3 and 8 h. Data are expressed as percentage of single cells released by mechanical disruption after disperse treatment versus total number of cells recovered after subsequent treatment of the same sample with trypsin. **(d)** Representative images of actin (green) and vinculin (red) staining of WT and p130CasKO keratinocytes in LCM or 1 h after calcium treatment (63X). Experiments in **c** and **d** were performed three times. **(e)** Representative images of wound healing experiments at time 0 and after 48 h (10X) (left panel), and relative quantification (right panel) by using nonparametric Mann-Whitney test ($***p < 0.001$). Data are expressed as median \pm range of three independent experiments

significant reduction of p130CasKO keratinocytes in wound closure (Fig. 5e and f).

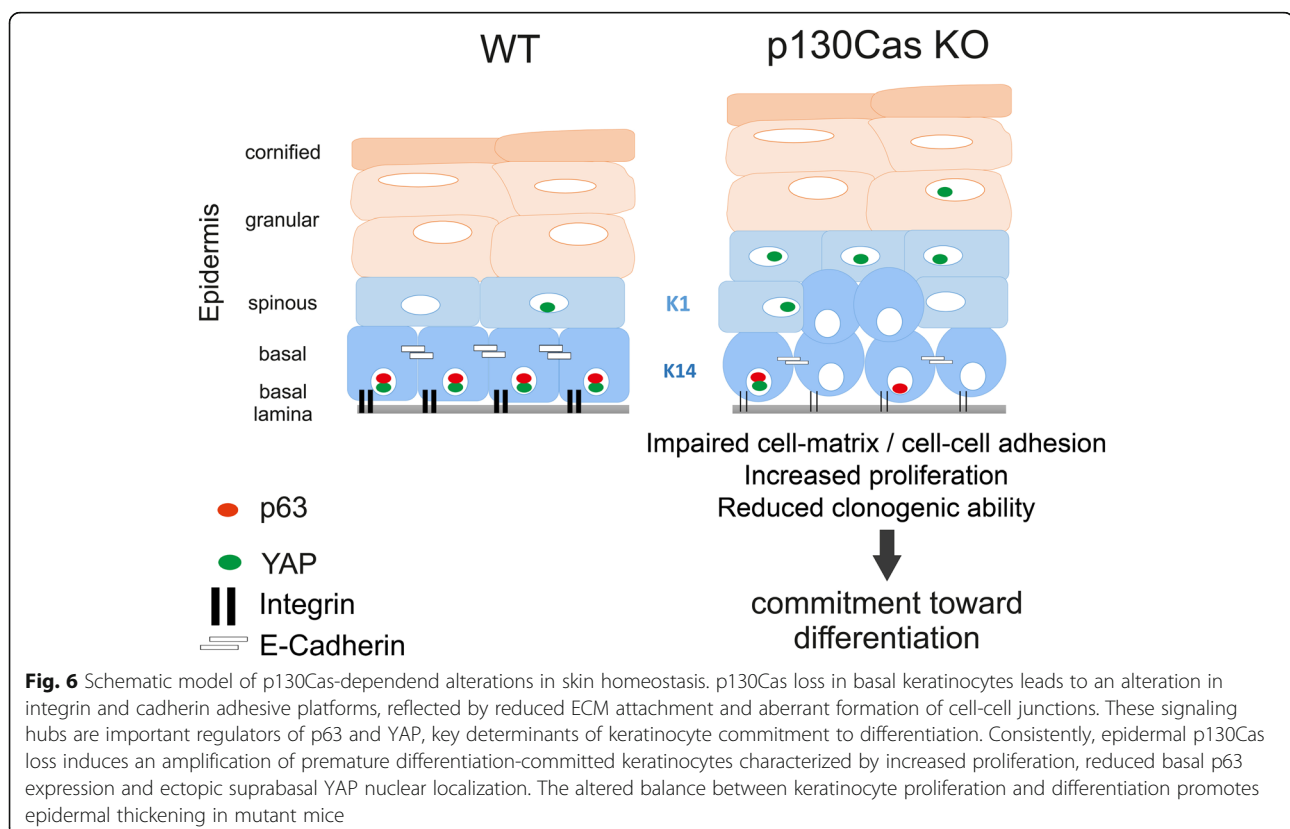
In conclusion, these data indicate that absence of p130Cas alters the correct execution of the keratinocyte differentiation program, by anticipating events connected to adhesion and/or cytoskeleton dynamics that are typical of early stages of differentiation (Fig. 6).

Discussion

In this study we show that the conditional deletion of p130Cas/BCAR1 gene in the epidermis impacts on keratinocyte biology. Newborn mice lacking p130Cas have epidermal tissue characterized by increased thickness coupled with an increased proliferation in the basal layer compartment and increased expression of K1, filaggrin and loricrin differentiation markers in the suprabasal epidermal layers. Primary keratinocytes derived from these mice also show enhanced proliferation and increased expression of filaggrin and loricrin when kept under standard undifferentiated conditions. p130Cas-null primary keratinocytes also display defects in ECM and cell-cell adhesion. The coexistence of enhanced proliferation coupled with premature differentiation is consistent with an amplification of differentiation-committed progenitor cell populations.

In the epidermis, the stem cell compartment undergoes asymmetrical cell division generating committed, differentiating progenitor cells that are further subjected to few rounds of cell division after which they undergo terminal differentiation by moving upward [8, 30]. The prerequisite to generate these progenitor cells is loss of integrin-based adhesion. Several reports have indeed demonstrated that reduced integrin expression or signaling in adherent cells triggers terminal differentiation and that increased activation of beta 1 integrin prevents terminal differentiation [22, 25, 31]. A key downstream signaling through which integrin-mediated adhesion can mediate keratinocytes differentiation is the ERK1/2 MAPK pathway. Specifically, it has been demonstrated that beta 1-induced activation of ERK1/2 MAPK pathway suppresses terminal differentiation [21, 25–27]. Interestingly, we demonstrate that the absence of p130Cas in keratinocytes impairs Src and ERK1/2 MAPK signaling that is known to be a crucial downstream effector of integrin-based cell-matrix adhesion. Thus, our data are consistent with a loser attachment of cells to the ECM and subsequent impairment in integrin-downstream signaling being important determinants of p130CasKO premature differentiation.

Our data also indicate that p130Cas KO keratinocytes have overall reduced clonogenic abilities, consistent with



the possibility that p130Cas plays a role in maintaining stem/progenitor cells in the undifferentiated compartment while its absence promotes the exit of cells toward differentiation.

This possibility is further supported by the observation that Δ Np63 expression, whose downregulation is an important determinant of commitment of keratinocytes toward differentiation [32], is reduced both in p130CasKO cultured cells and epidermis *in vivo*. Additionally, several reports indicate also that YAP1 is an essential regulator of epidermal maintenance and skin homeostasis [20, 33]. It has been shown that dephosphorylation of YAP and its consequent nuclear translocation regulate the balance between stem cell proliferation and differentiation [34]. Notably, our data indicate that YAP phosphorylation is enhanced in p130CasKO keratinocytes under culture conditions known to maintain the undifferentiated state, with a parallel anticipation of differentiation marker expression. Interestingly, p130CasKO epidermis contained significant amounts of nuclear YAP in isolated suprabasal cells, condition reminiscent of suprabasal YAP expression of alpha-catenin KO epidermis, which also displays increased basal and suprabasal cell proliferation [33].

Moreover, both Δ Np63 and YAP functions in skin homeostasis are linked to both cell-matrix and cell-cell based adhesion [20, 32–36]. Consistently, our data indicate also that loss of p130Cas has unexpected effects on keratinocyte cell-cell adhesion during differentiation.

Adherence junctions are constantly remodeled during epidermal cell differentiation and stratification [9, 37]. The epithelial AJ transmembrane core consists of E-cadherin, whose extracellular domain binds calcium ions to mediate homophilic interactions between neighboring cells [29]. The E-cadherin intracellular domain binds directly to beta-, gamma- catenins, which in turn bind to alpha-catenin, tethering adherence junctions with the underlying actin cytoskeleton, thus providing adhesive strength. Our results indicate that in p130CasKO keratinocytes, E-cadherin is prematurely recruited at cell membrane even in the absence of calcium-induced cadherin engagement. Moreover, pTyr-immunoprecipitated E-cadherin/beta-catenin complexes, which are normally found in WT cells in differentiating conditions [14, 16], are robustly detected in p130CasKO cells already under proliferating/undifferentiated conditions, further indicating an anticipation of differentiation-related events occurring in mutant cells. However, our data suggest also that the anticipated engagement of cell-cell adhesion in p130CasKO keratinocytes is not sustained at later times of differentiation, as indicated by dispase-based cell-cell adhesion assay. This may depend, at least in part, to the

impairment of alpha-catenin association with E-cadherin/beta-catenin complexes in p130CasKO cells, with a subsequent weakening of the link between adherens junction components and the actin cytoskeleton. It has been proposed that actin cytoskeleton assembly both in response to integrin-mediated and cell-cell adhesion regulates terminal differentiation [38, 39]. Of note, a relevant, albeit transient, impairment in epidermal barrier function was detected in embryonic mutant epidermis that was paralleled with a decrease of E-cadherin at cell borders and enhancement of cell proliferation, a phenotype reminiscent of the one caused by E-cadherin ablation in the epidermis [40].

Conclusions

We propose that p130Cas by regulating both integrin-dependent and cell-cell adhesion at the cell differentiation switch, finely tunes the balance between epidermal cell proliferation and differentiation by integrating multiple signaling pathways that are essential for epidermal morphogenesis and homeostasis (see Fig. 6), reinforcing the emerging view that in the epidermis cell-cell and cell-ECM adhesion are tightly linked in their regulatory mechanisms.

Additional file

Additional file 1: Figure S1. Skin specific deletion of p130Cas/BCAR1 gene. **Figure S2.** Keratin1 staining. **Figure S3.** Dot plot quantification of Ki67 and PCNA. Fig. S4 Δ Np63 and YAP expression. **Figure S5.** Epidermal PCNA, YAP and Δ Np63 expression in WT and p130CasKO mice. **Figure S6.** Dot plot quantification of loricrin and filaggrin staining. **Figure S7.** Deletion of p130Cas does not alter expression of β 1 and β 4 integrins. **Figure S8.** Epidermal p130Cas loss alters E-cadherin expression and barrier formation. (DOCX 6794 kb)

Abbreviations

E18.5: mouse embryonic day 18.5; K1: Cytokeratin 1; K10: Cytokeratin 10; K14: Cytokeratin 14; K5: Cytokeratin 5; KO: Knock-Out; pTyr: phosphoTyrosine; WT: Wild-type

Acknowledgements

Marta Gai for help and assistance to immunofluorescence experiments. Stefania Rocca for help and assistance to FACS experiments.

Funding

This work has been supported by AIRC (Associazione Italiana Ricerca Cancro) to SC (IG11346) and PD (IG15399); MIUR (Ministero Università Ricerca, PRIN 2010/2011) to PD and Compagnia San Paolo, Turin; Progetto d'Ateneo, University of Turin 2011 to PD.

Availability of data and materials

Data sharing is not applicable to this article as no datasets were generated or analysed during the current study.

Authors' contributions

MPCL and AC contribute to design and to perform the experiments, BT, SS, MS, DN, AD and MS performed the experiments, ET and PD critically revised the experiments, EC and SC designed the experiments, critically revised the data and wrote the manuscript. All authors read and approved the final manuscript.

Ethics approval and consent to participate

The use of animals was in compliance with the Guide for the Care and Use of Laboratory Animals published by the U.S. National Institutes of Health and approved by the Italian Health Minister (authorization n° 24-2014PR).

Consent for publication

Not applicable.

Competing interests

The authors declare that they have no competing interests.

Publisher's Note

Springer Nature remains neutral with regard to jurisdictional claims in published maps and institutional affiliations.


Received: 4 May 2018 Accepted: 25 October 2018

Published online: 03 November 2018

References

- Camacho Leal Mdel P, Sciortino M, Tornillo G, Colombo S, Defilippi P, Cabodi S: p130Cas/BCAR1 scaffold protein in tissue homeostasis and pathogenesis. *Gene*. 2015;562:1–7.
- Cabodi S, del Pilar Camacho-Leal M, Di Stefano P, Defilippi P. Integrin signalling adaptors: not only figurants in the cancer story. *Nat Rev Cancer*. 2010;10:858–70.
- Tikhmyanova N, Little JL, Golemis EA. CAS proteins in normal and pathological cell growth control. *Cell Mol Life Sci*. 2010;67:1025–48.
- Honda H, Oda H, Nakamoto T, Honda Z, Sakai R, Suzuki T, Saito T, Nakamura K, Nakao K, Ishikawa T, et al. Cardiovascular anomaly, impaired actin bundling and resistance to Src-induced transformation in mice lacking p130Cas. *Nat Genet*. 1998;19:361–5.
- Jonkers J, Meuwissen R, van der Gulden H, Peterse H, van der Valk M, Berns A. Synergistic tumor suppressor activity of BRCA2 and p53 in a conditional mouse model for breast cancer. *Nat Genet*. 2001;29:418–25.
- Jones PH, Simons BD, Watt FM. Sic transit gloria: farewell to the epidermal transit amplifying cell? *Cell Stem Cell*. 2007;1:371–81.
- Lechler T, Fuchs E. Asymmetric cell divisions promote stratification and differentiation of mammalian skin. *Nature*. 2005;437:275–80.
- Rangel-Huerta E, Maldonado E. Transit-amplifying cells in the fast lane from stem cells towards differentiation. *Stem Cells Int*. 2017;2017:7602951.
- Simpson CL, Patel DM, Green KJ. Deconstructing the skin: cytoarchitectural determinants of epidermal morphogenesis. *Nat Rev Mol Cell Biol*. 2011;12:565–80.
- Sumigray KD, Lechler T. Cell adhesion in epidermal development and barrier formation. *Curr Top Dev Biol*. 2015;112:383–414.
- Bikle DD, Xie Z, Tu CL. Calcium regulation of keratinocyte differentiation. *Expert Rev Endocrinol Metab*. 2012;7:461–72.
- Saoncella S, Tassone B, Deklic E, Avolio F, Jon C, Tornillo G, De Luca E, Di Iorio E, Piva R, Cabodi S, et al. Nuclear Akt2 opposes limbal keratinocyte stem cell self-renewal by repressing a FOXO-mTORC1 signaling pathway. *Stem Cells*. 2014;32:754–69.
- Orecchia V, Regis G, Tassone B, Valenti C, Avalle L, Saoncella S, Calautti E, Poli V. Constitutive STAT3 activation in epidermal keratinocytes enhances cell clonogenicity and favours spontaneous immortalization by opposing differentiation and senescence checkpoints. *Exp Dermatol*. 2015;24:29–34.
- Calautti E, Cabodi S, Stein PL, Hatzfeld M, Kedersha N, Paolo Dotto G. Tyrosine phosphorylation and src family kinases control keratinocyte cell-cell adhesion. *J Cell Biol*. 1998;141:1449–65.
- Kulukian A, Fuchs E. Spindle orientation and epidermal morphogenesis. *Philos Trans R Soc Lond Ser B Biol Sci*. 2013;368:20130016.
- Cabodi S, Calautti E, Talora C, Kuroki T, Stein PL, Dotto GP. A PKC-eta/Fyn-dependent pathway leading to keratinocyte growth arrest and differentiation. *Mol Cell*. 2000;6:1121–9.
- Yao JY, Chen JK. Roles of p63 in epidermal development and tumorigenesis. *Biom J*. 2012;35:457–63.
- Sambandam SA, Kasetti RB, Xue L, Dean DC, Lu Q, Li Q. 14-3-3sigma regulates keratinocyte proliferation and differentiation by modulating Yap1 cellular localization. *J Invest Dermatol*. 2015;135:1621–8.
- Zhang H, Pasolli HA, Fuchs E. Yes-associated protein (YAP) transcriptional coactivator functions in balancing growth and differentiation in skin. *Proc Natl Acad Sci U S A*. 2011;108:2270–5.
- Elbediwy A, Vincent-Mistiaen ZI, Spencer-Dene B, Stone RK, Boeing S, Wculek SK, Cordero J, Tan EH, Ridgway R, Brunton VG, et al. Integrin signalling regulates YAP and TAZ to control skin homeostasis. *Development*. 2016;143:1674–87.
- Levy L, Broad S, Diekmann D, Evans RD, Watt FM. Beta 1 integrins regulate keratinocyte adhesion and differentiation by distinct mechanisms. *Mol Biol Cell*. 2000;11:453–66.
- Watt FM. Role of integrins in regulating epidermal adhesion, growth and differentiation. *EMBO J*. 2002;21:3919–26.
- Watt FM, Fujiwara H. Cell-extracellular matrix interactions in normal and diseased skin. *Cold Spring Harb Perspect Biol*. 2011;3.
- Playford MP, Schaller MD. The interplay between Src and integrins in normal and tumor biology. *Oncogene*. 2004;23:7928–46.
- Evans RD, Perkins VC, Henry A, Stephens PE, Robinson MK, Watt FM. A tumor-associated beta 1 integrin mutation that abrogates epithelial differentiation control. *J Cell Biol*. 2003;160:589–96.
- Haase I, Hobbs RM, Romero MR, Broad S, Watt FM. A role for mitogen-activated protein kinase activation by integrins in the pathogenesis of psoriasis. *J Clin Invest*. 2001;108:527–36.
- Zhu AJ, Haase I, Watt FM. Signaling via beta1 integrins and mitogen-activated protein kinase determines human epidermal stem cell fate in vitro. *Proc Natl Acad Sci U S A*. 1999;96:6728–33.
- Calautti E, Grossi M, Mammucari C, Aoyama Y, Pirro M, Ono Y, Li J, Dotto GP. Fyn tyrosine kinase is a downstream mediator of rho/PRK2 function in keratinocyte cell-cell adhesion. *J Cell Biol*. 2002;156:137–48.
- Nelson WJ. Regulation of cell-cell adhesion by the cadherin-catenin complex. *Biochem Soc Trans*. 2008;36:149–55.
- Blanpain C, Fuchs E. Epidermal homeostasis: a balancing act of stem cells in the skin. *Nat Rev Mol Cell Biol*. 2009;10:207–17.
- Grose R, Hutter C, Bloch W, Thorey I, Watt FM, Fassler R, Brakebusch C, Werner S. A crucial role of beta 1 integrins for keratinocyte migration in vitro and during cutaneous wound repair. *Development*. 2002;129:2303–15.
- Romano RA, Smalley K, Magraw C, Serna VA, Kurita T, Raghavan S, Sinha S. DeltaNp63 knockout mice reveal its indispensable role as a master regulator of epithelial development and differentiation. *Development*. 2012;139:772–82.
- Schlegelmilch K, Mohseni M, Kirak O, Pruszk J, Rodriguez JR, Zhou D, Kreger BT, Vasioukhin V, Avruch J, Brummelkamp TR, Camargo FD. Yap1 acts downstream of alpha-catenin to control epidermal proliferation. *Cell*. 2011;144:782–95.
- Hu JK, Du W, Shelton SJ, Oldham MC, DiPersio CM, Klein OD. An FAK-YAP-mTOR signaling Axis regulates stem cell-based tissue renewal in mice. *Cell Stem Cell*. 2017;21:91–106 e106.
- Akladios B, Mendoza-Reinoso V, Samuel MS, Hardeman EC, Khosrotehrani K, Key B, Beverdam A. Epidermal YAP2-5SA-DeltaC drives beta-catenin activation to promote keratinocyte proliferation in mouse skin in vivo. *J Invest Dermatol*. 2017;137:716–26.
- Li P, Silvis MR, Honaker Y, Lien WH, Arron ST, Vasioukhin V. alphaE-catenin inhibits a Src-YAP1 oncogenic module that couples tyrosine kinases and the effector of hippo signaling pathway. *Genes Dev*. 2016;30:798–811.
- Tinkle CL, Pasolli HA, Stokes N, Fuchs E. New insights into cadherin function in epidermal sheet formation and maintenance of tissue integrity. *Proc Natl Acad Sci U S A*. 2008;105:15405–10.
- Connelly JT, Gautrot JE, Trappmann B, Tan DW, Donati G, Huck WT, Watt FM. Actin and serum response factor transduce physical cues from the microenvironment to regulate epidermal stem cell fate decisions. *Nat Cell Biol*. 2010;12:711–8.
- Livshits G, Kobiela A, Fuchs E. Governing epidermal homeostasis by coupling cell-cell adhesion to integrin and growth factor signaling, proliferation, and apoptosis. *Proc Natl Acad Sci U S A*. 2012;109:4886–91.
- Tinkle CL, Lechler T, Pasolini HA, Fuchs E. Conditional targeting of E-cadherin in skin: insights into hyperproliferative and degenerative responses. *Proc Natl Acad Sci U S A*. 2004;101:552–7.

SCIENTIFIC REPORTS



OPEN

Dysregulation of Blimp1 transcriptional repressor unleashes p130Cas/ErbB2 breast cancer invasion

Marianna Sciortino¹, Maria del Pilar Camacho-Leal¹, Francesca Orso¹, Elena Grassi¹, Andrea Costamagna¹, Paolo Provero¹, Wayne Tam², Emilia Turco¹, Paola Defilippi¹, Daniela Taverna¹ & Sara Cabodi¹

ErbB2 overexpression is detected in approximately 20% of breast cancers and is correlated with poor survival. It was previously shown that the adaptor protein p130Cas/BCAR1 is a crucial mediator of ErbB2 transformation and that its overexpression confers invasive properties to ErbB2-positive human mammary epithelial cells. We herein prove, for the first time, that the transcriptional repressor Blimp1 is a novel mediator of p130Cas/ErbB2-mediated invasiveness. Indeed, high Blimp1 expression levels are detected in invasive p130Cas/ErbB2 cells and correlate with metastatic status in human breast cancer patients. The present study, by using 2D and 3D breast cancer models, shows that the increased Blimp1 expression depends on both MAPK activation and miR-23b downmodulation. Moreover, we demonstrate that Blimp1 triggers cell invasion and metastasis formation via its effects on focal adhesion and survival signaling. These findings unravel the previously unidentified role that transcriptional repressor Blimp1 plays in the control of breast cancer invasiveness.

The amplification or overexpression of the tyrosine kinase receptor ErbB2 accounts for approximately 20% of all breast cancers¹, and ErbB2 amplification is detected in about 50% of ductal carcinomas *in situ* (DCIS) of the mammary gland². This implies that the aggressive invasive phenotype that is associated with ErbB2 is not solely due to its overexpression, but that additional factors are required before the transition towards invasive carcinoma occurs³. However, the mechanisms that underlie the progression towards invasive tumor formation are still unclear.

We have already demonstrated that the adaptor protein p130Cas/BCAR1 (Crk associated substrate/Breast Cancer Anti-estrogen Resistance protein 1) plays a key role in the control of migration and invasion in ErbB2 positive breast cancer^{4,5}. It is also well known that 3D cultures of MCF10A.B2 mammary epithelial cells, which contain a chimeric and activatable ErbB2 receptor, can form spheroid structures called acini⁶, meaning that these structures recapitulate the architecture of the ductal lobular unit in the human mammary gland and can therefore be considered a faithful model with which to study mammary gland biology *in vitro*. We have previously shown that MCF10A.B2 cells are able to develop invasive protrusions upon the concomitant activation of ErbB2 and overexpression of the p130Cas protein⁵. Moreover, *in vivo* analyses of human breast cancer have confirmed that the amplification of ErbB2 in combination with the overexpression of p130Cas induces a higher proliferation rate and an increased number of distant metastases as well as correlating with poor prognosis^{5,7}. At the molecular level, the invasive behavior resulting from the p130Cas/ErbB2 interaction relies on the activation of AKT/PI3K and Erk1/2 MAPKs signaling pathways⁸.

An analysis of the transcriptional changes that occur during p130Cas/ErbB2 invasion in MCF10A.B2 spheroids⁴, has highlighted the upregulation of PRDM1 (PR domain containing 1) mRNA in p130Cas/ErbB2 invasive acini. The PRDM1 gene encodes for the human Blimp1 protein (B-lymphocyte-induced maturation protein-1) and its role as a transcriptional repressor in the immune system has been widely studied⁹. Indeed, Blimp1 is able to recruit chromatin modifiers, such as methyltransferases and deacetylases, that can, in turn, regulate B and T

¹Department of Biotechnology and Health Sciences, University of Turin, Via Nizza 52, 10126, Turin, Italy.

²Department of Pathology and Laboratory Medicine, Weill Cornell Medicine, New York, NY, USA. Correspondence and requests for materials should be addressed to S.C. (email: sara.cabodi@unito.it)

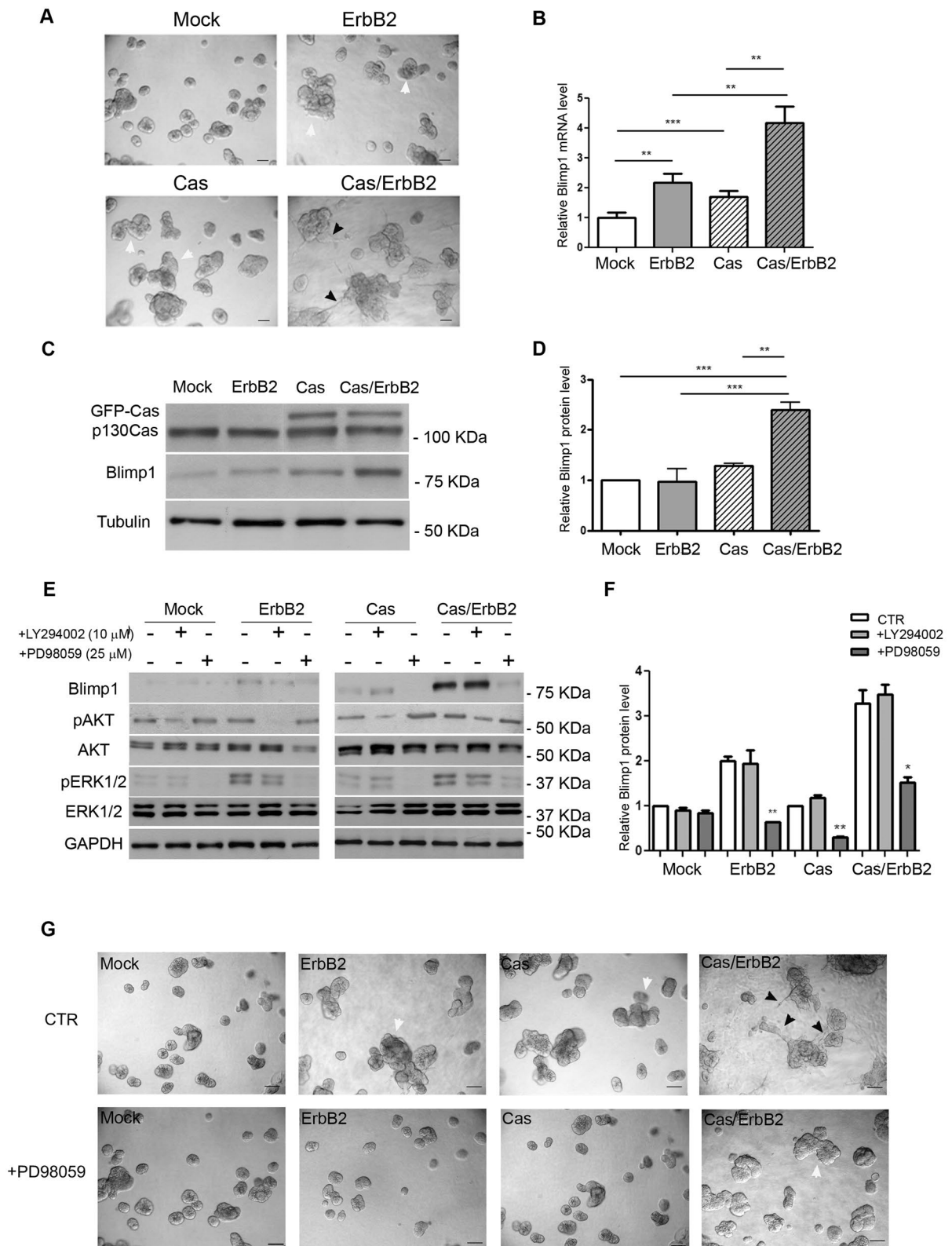


Figure 1. High expression of Blimp1 protein in p130Cas/ErbB2 invasive acini is sustained by Erk1/2 activation. **(A)** Day 14 culture of control (Mock) and p130Cas overexpressing MCF10A.B2 (Cas) plated on a matrigel:collagen matrix and treated with either 1 μ M ethanol (vehicle) or AP1510 on day 10 to activate ErbB2 (ErbB2; Cas/ErbB2). Scale bars, 50 μ m. Magnification 20X. White arrowheads indicate multiacinar structures. Black arrowheads indicate invasive acini. **(B)** On day 14 acinar structures were recovered and lysed and Blimp1 mRNA expression levels were evaluated by RT-PCR. Statistical analysis was performed using the Student's t-test (* $p < 0.05$, ** $p < 0.01$, *** $p < 0.001$). **(C)** Day 14 protein extracts were probed for Blimp1 in a western blot analysis. Tubulin was used as the loading control. **(D)** Densitometric analysis of protein levels of at least

three independent experiments is shown (mean \pm s.e.m). Blimp1 protein modulation was calculated relative to Mock level and normalized on tubulin as the loading control. Statistical analyses were performed using the Student's t-test (** $p < 0.01$, *** $p < 0.001$). (E) Acini derived from Mock and Cas cells were treated on day 10 with either DMSO (vehicle), 10 μ M LY294002 (PI3K inhibitor) or 25 μ M PD98059 (MAPK pathway inhibitor) in both in the presence and absence of 1 μ M of AP1510. After 4 days of treatment, acini were recovered and lysed. Total cell extracts were probed for Blimp1 in a western blot analysis. GAPDH was used as loading control. (F) Densitometric analysis of protein levels of at least three independent experiments is shown (mean \pm s.e.m). Protein modulation was calculated relative to Mock level and normalized to GAPDH as the loading control. Statistical analyses were performed using the Student's t-test (* $p < 0.05$, ** $p < 0.01$). (G) Representative phase images of day 14-acinar structures showing invasive protrusion impairment upon AKT/PI3K and MAPK pathway inhibition. Scale bars, 50 μ m. Magnification 20X. White arrowheads indicate multiacinar structures. Black arrowheads indicate invasive acini.

cell differentiation¹⁰. The function of Blimp1 in cell migration during the developmental and physiological processes has been described in a number of animal models and tissues^{11–13}. In pathological conditions, Blimp1 acts as a tumor suppressor in different types of lymphomas from B, T and NK cells^{14,15}, however, only a small number of reports have discussed its function in non-hematopoietic tumors^{16–18}. In fact, Blimp1 has been reported to mediate EMT upon TGF- β 1 stimulation in ER-negative breast cancer cells by repressing BMP-5 and, in turn, activating the transcription factor Snail¹⁶. Moreover, Blimp1 has been found to act as a mediator of Ras/Raf/AP-1 signaling in lung cancer cell lines¹⁸.

Importantly, the non-coding signature that characterizes p130Cas/ErbB2 invasive behavior has highlighted miR-23b role as a putative regulator of Blimp1 expression. Indeed, miR-23b has been found to be downmodulated in invasive p130Cas/ErbB2 acini and bioinformatics analyses have proposed Blimp1 as a putative miR-23b target gene⁴. miR-23b belongs to the miR-23b~27b~24-1 cluster which is intronically present on chromosome 9 of the aminopeptidase O gene¹⁹. The function of miR-23b in breast cancer pathogenesis is still debated, as some reports attribute miR-23b with a tumor suppressor role, while others suggest that its oncogenic function depends on cellular model²⁰.

Our results provide evidence of a new-found, pro-invasive function for Blimp1 in p130Cas/ErbB2 invasive breast cancer and describes its regulation, mechanism of action and *in vivo* functions. Moreover, it is demonstrated, for the first time in a non-hematopoietic system, that miR-23b is a direct Blimp1 regulator, a discovery that provides insights into miR-23b target genes in breast cancer.

Results

p130Cas and ErbB2 induce Blimp1 overexpression in human invasive breast cancer via Erk1/2 MAPKs pathway activation. We have previously shown that MCF10A.B2 human mammary acini grown in 3D form polarised, quiescent single acini, that upon activation of ErbB2 with the synthetic ligand AP1510, undergo proliferation and disruption of apical polarity, forming multiacinar structures. The overexpression of p130Cas in MCF10A.B2 cells is sufficient to give rise to multiacinar structures that upon stimulation with AP1510 acquire invasive protrusions⁸. The gene signature underlying the transition from multiacinar structures, characterized by p130Cas overexpression or ErbB2 activation, to invasive p130Cas/ErbB2 acini has also been identified⁴. The transcriptional repressor Blimp1/PRDM1 mRNA was found to be upregulated in invasive acini. We therefore decided to explore its involvement in p130Cas/ErbB2 mediated breast cancer invasion.

Blimp1 mRNA and protein expression levels were thus evaluated in control MCF10.B2 cells grown in 3D (Mock, Fig. 1A), in ErbB2 that was activated by treatment with the AP1510 homodimerizer (ErbB2, Fig. 1A), in Cas overexpressing (Cas; Fig. 1A) and in invasive Cas overexpressing and ErbB2 activated acini (Cas/ErbB2; Fig. 1A). As shown in Fig. 1B, the mRNA levels of PRDM1, as measured by qRT-PCR, are significantly upregulated, relative to controls, in multiacinar structures that result from ErbB2 activation or p130Cas overexpression. Moreover, even higher PRDM1 mRNA level induction was observed in Cas/ErbB2 invasive acini, indicating the existence of a synergistic effect between ErbB2 activation and p130Cas overexpression. In fact, Blimp1 protein levels were found to be significantly enhanced in p130Cas/ErbB2 invasive acini (Fig. 1C and D). Interestingly, we did not observe a perfect match between RNA and protein levels in p130Cas overexpressing and ErbB2 activated multiacini, suggesting the existence of additional post-transcriptional regulation mechanisms.

Our previous work has demonstrated that high levels of p130Cas expression, in the presence of ErbB2 activation, in 3D acini trigger the activation of both the PI3K/Akt and MAPK signaling pathways⁸. It was therefore decided to investigate the possible involvement of these two pathways in Blimp1 expression modulation. To this end, Mock and Cas acini, stimulated or not with AP1510 to trigger ErbB2 activation, shown in Supplementary Figure 1, were treated with either LY294002 (10 μ M) or PD98059 (25 μ M) to inhibit the PI3K and MAPK pathways, respectively. As shown in Fig. 1E,F and in Supplementary Figure 2, Blimp1 expression in Cas/ErbB2 multiacinar and invasive structures is preferentially modulated upon MAPK pathway activation. Indeed, while treatment with the PI3K inhibitor LY294002 gave no significant changes in Blimp1 expression levels, the addition of MAPK inhibitor PD98059 led to a reduction in these levels in all conditions, thus suggesting that MAPKs are a major regulator of Blimp1 expression. Interestingly, the reduction in Blimp1 expression upon MAPK inhibitor treatment resulted in a reduced formation of ErbB2 and p130Cas multiacinar structures and in the abrogation of invasive protrusions in Cas/ErbB2 acini (Fig. 1G and Supplementary Figure 3 for quantification). These data indicate that the activation of MAPK signaling induces Blimp1 expression in both multiacinar and invasive structures. Consequently, the pharmacological inhibition of MAPK signaling results in the impairment of multiacinar and invasive structure formation.

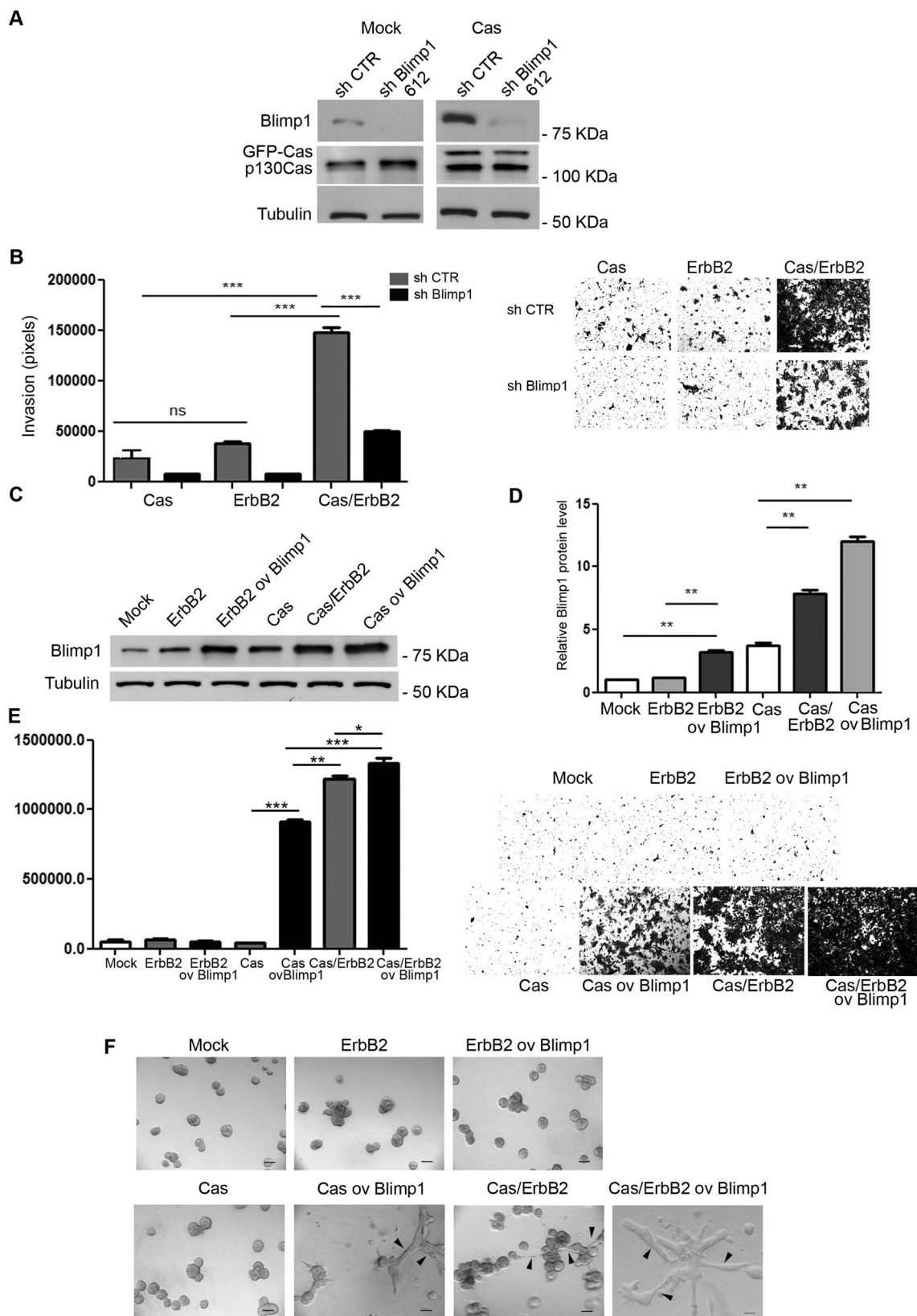


Figure 2. Blimp1 expression modulation influences migratory capacity in 2D and 3D cultured cells. **(A)** Mock and Cas cells were transduced with the sh Blimp1 clone 612 vector and the Blimp1 and p130Cas protein levels were evaluated using western blot analysis. Tubulin was used as the loading control. **(B)** Mock and Cas cells, that had either been transduced with human sh Blimp1 clone 612 vector or scrambled ctr vector, were subjected to transwell invasion assays for 48 hours both in the presence and absence of 1 μ M AP1510. Cell invasion quantification was performed over three different experiments. Results are presented as mean \pm s.e.m.

of the area covered by invaded cells. Representative images of invaded cells after 48 hours, fixed and stained with Crystal violet are shown (** $p < 0.001$). Magnification 5X. (C) Mock and Cas cells were transduced with Blimp1 overexpressing vector and treated or not with 1 μM AP1510 for 48 hours. Total cell extracts were probed for Blimp1 in a western blot analysis. Tubulin was used as the loading control. (D) Densitometric analyses of protein levels of at least three independent experiments are shown (mean \pm s.e.m). Blimp1 protein modulation was calculated relative to Mock level and normalized to tubulin as the loading control. Statistical analyses were performed using the Student's t-test (** $p < 0.01$). (E) Invasion of Blimp1 overexpressing ErbB2, Cas and Cas/ErbB2 cells was evaluated by transwell invasion assays in the presence or absence of 1 μM AP1510. Results are presented as mean \pm s.e.m. of the area covered by invaded cells. Representative images of invaded cells after 48 hours, fixed and stained with Crystal violet are shown (* $p < 0.05$, ** $p < 0.01$, *** $p < 0.001$). Magnification 5X. (F) Representative phase contrast images of acinar structures taken at day 14 are presented. Magnification 20X, scale bars 50 μm . Black arrowheads indicate invasive acini.

Modulation of Blimp1 expression affects p130Cas/ErbB2 dependent invasion *in vitro*. In order to investigate whether Blimp1 is required for p130Cas/ErbB2 mediated invasion, Mock and Cas overexpressing MCF10.B2 cells were infected with lentiviruses that expressed either Blimp1 or scrambled control shRNA sequences (Fig. 2A) and assessed for their invasive behavior by performing Transwell invasion assays in transwell-coated with matrigel/collagen (Fig. 2B). These experiments indicate that the lowering of Blimp1 levels is sufficient to impair the invasive phenotype driven by p130Cas overexpression and ErbB2 activation (Fig. 2B).

To exclude the off-target effects of the shBlimp1 sequence, another sh sequence was tested and it was confirmed that lowering Blimp1 expression does causes severe alterations in cell invasion and does not alter p130Cas expression (Supplementary Figure 4A,B). To test whether Blimp1 overexpression alone is able to trigger invasion in non-invasive Cas and ErbB2 multiacinar structures, we generated lentiviruses that overexpressed Blimp1 and infected Mock and Cas cells, that were either subsequently treated with the ErbB2 homodimerizer or left untreated (Fig. 2C and D). Transwell invasion assays and 3D cell cultures revealed that Blimp1 overexpression is sufficient to induce invasion in Cas overexpressing cells that usually give rise to non-invasive multiacinar structures (see Fig. 1A). Conversely, Blimp1 overexpression is not able to induce either multiacinar structures or invasion in Mock (Supplementary Figure 5) and in ErbB2 transformed cells in itself, suggesting that p130Cas overexpression is required for cell invasion (Fig. 2E,F). Notably, the activation of ErbB2 in Cas cells that overexpress Blimp1 further increases their invasive capability, indicating a synergistic effect of p130Cas and ErbB2 in Blimp1-dependent cell invasion. These data indicate that high levels of Blimp1 in p130Cas overexpressing cells trigger the transition of breast epithelial cells from a non-invasive to a migratory and invasive cell phenotype and that the activation of ErbB2 in this context amplifies the invasiveness.

Silencing Blimp1 expression impairs focal adhesion formation. p130Cas has been described as playing an active role in cell migration and invasion by regulating FAK (Focal Adhesion Kinase) and focal adhesion dynamics^{21–24}, and it has also been shown that the recruitment of p130Cas and FAK at focal adhesions is required for proper extracellular matrix degradation and, consequently, efficient cancer cell invasion^{25–28}. It was therefore decided to investigate whether FAK is implicated in the mechanism that underlies Blimp1-dependent cell invasion in p130Cas overexpressing and ErbB2 transformed mammary epithelial cells.

As shown in Fig. 3A and B, FAK expression levels and activation were significantly reduced in Cas overexpressing cells silenced for Blimp1 but not in ErbB2 cells. Noteworthy, the downregulation of FAK expression and activity levels was even stronger in Cas/ErbB2 cells, thereby further indicating that p130Cas per se is sufficient to exert a regulatory mechanism on FAK by Blimp1 while ErbB2 can contribute to FAK regulation by Blimp1 only in presence of p130Cas. Consistently, Blimp1 overexpression in Cas cells strongly enhanced FAK activation and expression levels (Fig. 3C,D and Supplementary Figure 6). The fact that Blimp1 overexpression significantly induces FAK expression and activation also in Mock and ErbB2 cells supports a more general role for Blimp1 in FAK expression regulation (Fig. 3C,D). Interestingly, *in silico* analysis searching for Blimp1 binding sites on FAK promoter identified 1133 base pairs upstream of the FAK transcription start site, a ChIP-seq peak for PRDM1 by the Encode project (Fig. 3E), this peak also contains a DNA sequence that has a high log-likelihood (13.79) for the PRDM1 PWM, further supporting the experimental evidence of PRDM1 binding (Fig. 3E)^{29,30}. Notably, Blimp1 silenced Cas/ErbB2 cells that do not show invasive properties display impaired focal adhesion distribution and FAK localization compared to invasive Cas/ErbB2 cells (Fig. 3F and Supplementary Figure 7). Consistently, the overexpression of Blimp1 in Cas/ErbB2 cells further enhances focal adhesion structures (Supplementary Figure 8). These data indicate that Blimp1 favors cell invasion by altering focal adhesion dynamics and that FAK activation and expression regulation may depend on Blimp1 expression levels.

Blimp1 expression is required for tumor growth and lung metastases formation *in vivo*. No data on the role of Blimp1 in *in vivo* solid tumors are currently available. As MCF10A.B2 cells do not support *in vivo* growth, we chose N202-1A cells as experimental model to investigate this aspect. N202-1A cells derive from HER2/neu transgenic mice, express high levels of p130Cas and require p130Cas expression for *in vivo* tumor formation and dissemination⁵. To examine the relevance of Blimp1 in *in vivo* tumorigenesis, N202-1A cells were infected with control or lentiviral vectors carrying Blimp1 shRNA. As shown in Fig. 4A, an efficient knock-down of Blimp1 was observed along with a significant reduction of FAK protein activation and expression levels (Fig. 4A and B). Moreover, silencing of Blimp1 in N202-1A cells was sufficient to reduce cell invasion *in vitro* (Fig. 4C), further confirming that Blimp1 is critical for p130Cas/ErbB2-driven invasion in another cell model of breast cancer. In addition, silencing of Blimp1 is sufficient to reduce significantly N202-1A cell viability

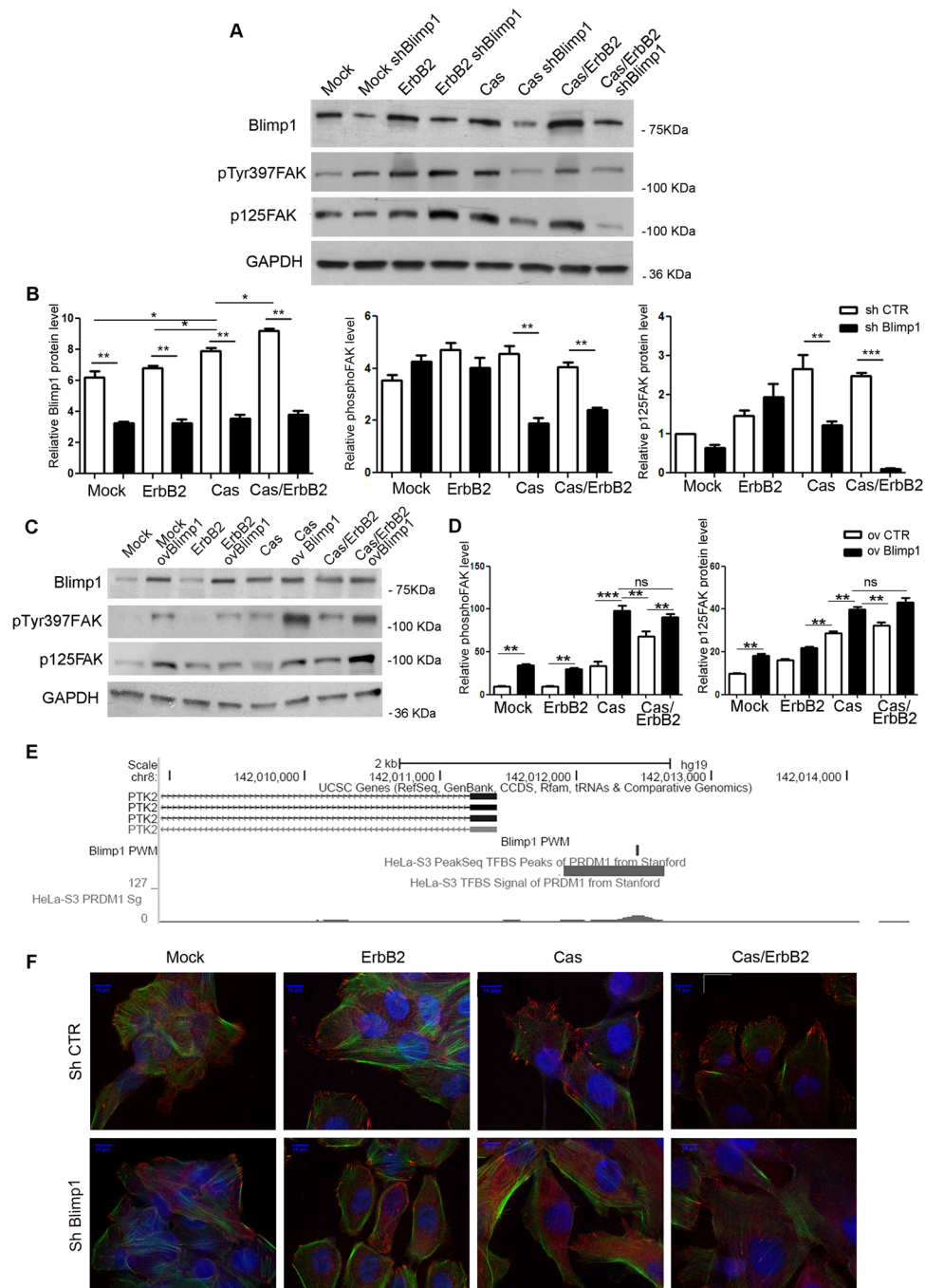


Figure 3. Focal adhesion protein expression is altered upon Blimp1 silencing. **(A)** Mock and Cas cells were transfected with the sh Blimp1 vector and treated with 1 μ M AP1510 for 48 hours. Total cell extracts were probed for Blimp1, phospho-p125Fak(Tyr397), p125FAK, in a western blot analysis. GAPDH was used as the loading control. **(B)** Densitometric analysis of protein levels in at least three independent experiments is shown (mean \pm s.e.m). Protein modulation was calculated relative to Mock level and normalized to GAPDH as the loading control. Statistical analyses were performed using the Student's t-test (* $p < 0.05$, ** $p < 0.01$, *** $p < 0.001$). **(C)** Mock and Cas cells were transfected with Blimp1 overexpressing vectors and treated or not with 1 μ M AP1510 for 48 hours. Total cell extracts were probed for Blimp1, phospho-p125Fak(Tyr397) and p125FAK in a western blot analysis. GAPDH was used as the loading control. **(D)** Densitometric analyses of protein levels in at least three independent experiments are shown (mean \pm s.e.m). Phospho-p125Fak(Tyr397) and p125FAK modulation was calculated relative to Mock level and normalized to GAPDH as the loading control. Statistical analyses were performed using the Student's t-test (** $p < 0.01$). **(E)** The core promoter of PTK2 (FAK) harbors a Blimp1 PWM match (rectangle) with a log-likelihood of 13.79, in correspondence with a ChIP-seq peak identified in the HeLa cells. **(F)** Immunofluorescence staining for vinculin (red) and phalloidin (green) of Mock and Cas MCF10A.B2 treated or not with 1 μ M AP1510 for 48 hours. Scale bars: 10 μ m. Magnification 63X.

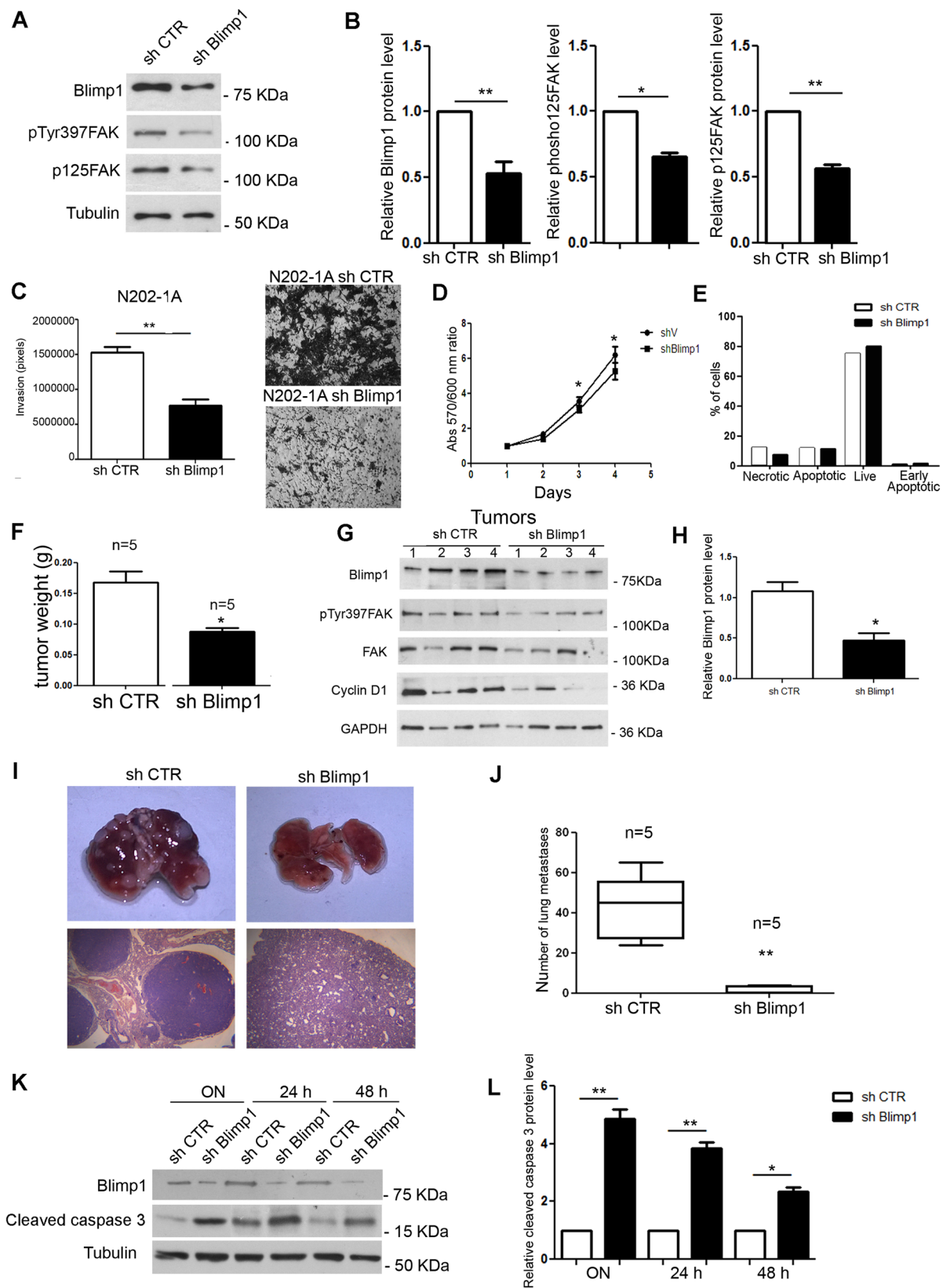


Figure 4. Blimp1 silencing impairs cell motility and *in vivo* metastasization of N202-1A cells. (A) N202-1A cells were transduced with a mouse shRNA sequence for Blimp1 and total cell extracts were probed for Blimp1, phospho-FAK(Tyr397) and p125FAK in a western blot analysis. Tubulin was used as the loading control. (B) Densitometric analyses of Blimp1, phospho-FAK(Tyr397) and FAK protein levels in at least three independent experiments are shown (mean \pm s.e.m). Protein modulation was calculated relative to control cells and normalized on tubulin as loading control. Statistical analyses were performed using the Student's t-test

(* $p < 0.05$, ** $p < 0.01$). (C) N202-1A control and sh Blimp1 cells were subjected to transwell invasion assays for 72 hours both in the presence and the absence of 20% FBS. Cell invasion quantification was performed over three different experiments. Results are presented as mean \pm s.e.m. of the area covered by invaded cells (left panel). Representative images of invaded cells after 72 hours, fixed and stained with Crystal violet are reported (** $p < 0.01$) (right panel). Magnification 5X. (D) Cell viability of N202-1A control and sh Blimp1 cells in 2D adherent conditions (* $p < 0.02$). (E) Cell survival of N202-1A control and sh Blimp1 cells in 2D adherent conditions. (F) Weight quantification of tumors derived from NSG mice injected into the mammary fat pad with control or sh Blimp1 N202-1A cells (** $p < 0.05$). (G) Total cell extracts of tumors from control and sh Blimp1 N202-1A cells were probed for Blimp1, phosphoFAK(Tyr397), p125FAK, cyclinD1 in a western blot analysis. GAPDH was used as loading control. (H) Densitometric analyses of Blimp1 protein level modulation was calculated relative to control and normalized to GAPDH is shown (mean \pm s.e.m) (** $p < 0.01$). (I) Pictures of representative whole lung and H&E staining of lung metastasis from NSG mice 5 weeks after the tail vein injection of either the N202-1A control or sh Blimp1 cells are shown. (J) Total number of metastases per lung is shown as box and whisker plots with median and minimum/maximum ($n = 5$ mice per group). Statistical analyses were performed using the Student's t-test (** $p < 0.01$). (K) Total cell extracts from control and sh Blimp1 N202-1A cells grown in a suspension overnight, for 24 or 48 hours were probed for Blimp1 in a western blot analysis. Tubulin was used as the loading control. (L) Densitometric analysis of cleaved caspase 3 levels in at least three independent experiments is shown (mean \pm s.e.m). Cleaved caspase 3 protein modulation was calculated relative to control cell level and normalized to tubulin as the loading control. Statistical analyses were performed using the Student's t-test (* $p < 0.05$, ** $p < 0.01$).

in adherent conditions (Fig. 4D) but does not alter cell survival (Fig. 4E), indicating that cells silenced for Blimp1 proliferate less than control cells.

To investigate the possible contribution of Blimp1 to mammary tumor growth, Blimp1-silenced and relative control N202-1A cells were orthotopically injected into the mammary fat pad of NSG immune-compromised mice. After three weeks, tumors were excised and measured. Notably, in Blimp1-depleted tumors the weight was significantly reduced compared to controls (Fig. 4F). Western blot analysis of tumor protein extracts revealed that Blimp1 was effectively knocked down *in vivo*, and its down-regulation correlated with decreased FAK activation and expression and decreased expression of Cyclin D1 (Fig. 4G,H). Thus, these experiments demonstrate that Blimp1 expression impairs ErbB2/p130Cas-dependent tumor growth *in vivo*, by affecting cell proliferation.

Next, to explore the involvement of Blimp1 in tumor progression, experimental metastasis formation assays were performed by injecting N202-1A control and Blimp1 silenced cells into the tail veins of NSG mice. The mice were sacrificed and their lungs recovered to assess metastasis formation after 5 weeks. As displayed in Fig. 4I and J, stronger lung nodule reduction was detected in lungs derived from shBlimp1 cell injected mice than in controls. In a further experiment, N202-1A control and Blimp1 silenced cells were seeded on low adhesion plates and apoptosis was evaluated in order to assess whether the impaired lung colonization of Blimp1 silenced cells was due to increased cell death. Indeed, cleaved Caspase-3 expression levels increased only in Blimp1 silenced cells, indicating that these cells are more susceptible to apoptosis induced by cell detachment and thereby less efficient in driving lung colonization (Fig. 4K,L). These data indicate that Blimp1 supports N202-1A proliferation under adherent conditions and resistance to anoikis. It is conceivable that these two mechanisms may co-exist during tumorigenesis, leading to increased tumor growth and ability to give rise to metastasis.

miR-23b as a new regulator of Blimp1 in breast cancer invasion. Once it has been demonstrated that Blimp1 overexpression is crucial for driving invasion in breast epithelial cells, the next step is looking for more selective mechanisms that can block its expression. It was therefore decided that we evaluate the possible interactions of miR-23b in this context, as it has previously been demonstrated to be downmodulated in invasive acini⁴, and that Blimp1 was predicted to be one of its putative targets (TargetScan v. 6.2).

MCF10A.B2 control and p130Cas overexpressing cells were either transiently transfected with a miR-23b precursor (pre-miR-23b) or negative controls (pre-control) and then either treated with AP1510 to drive the activation of ErbB2 or left untreated. miR-23b and Blimp1 expression were assessed 48 hours post transfection (Fig. 5A–C). The results shown in Fig. 5B and C indicate that miR-23b overexpression leads to a 50% reduction in Blimp1 expression in invasive Cas/ErbB2 conditions. Furthermore, the transfection of a specific miR-23b inhibitor (anti-miR-23b) increases Blimp1 expression both in Mock and Cas cells whether treated with the ErbB2 homodimerizer or not (Fig. 5D,E). This suggests that miR-23b acts as a regulator of Blimp1 in normal, transformed and invasive breast epithelial cells.

In order to determine whether this regulation is a consequence of the direct binding of miR-23b on PRDM1 3'UTR, we used a reporter vector containing part of the 3'UTR of PRDM1, from nucleotide 538 to 2419³¹, to perform luciferase reporter assays in HEK293T cells transfected with either pre-miR-23b or pre-control sequences. As shown in Fig. 5F, luciferase expression, which is driven by the 3'UTR of Blimp1, significantly decreased upon pre-miR-23b overexpression. Point mutations were inserted in the first miR-23b seed from nucleotide 907 to 914, as indicated in Fig. 5G, and luciferase expression was evaluated in the presence of miR-23b overexpression (Fig. 5F) as a means of evaluating miR-23b direct binding on Blimp1 3'UTR sequences. Taken together, these data indicate that miR-23b directly binds and regulates Blimp1 expression.

miR-23b impairs p130Cas/ErbB2 invasion by negatively regulating Blimp1 expression. The role of miR-23b in breast cancer invasion is still the subject of some controversy since both tumor suppressor and oncogenic activities have been reported as occurring in invasive breast cancer cells^{32,33}. It has been described that

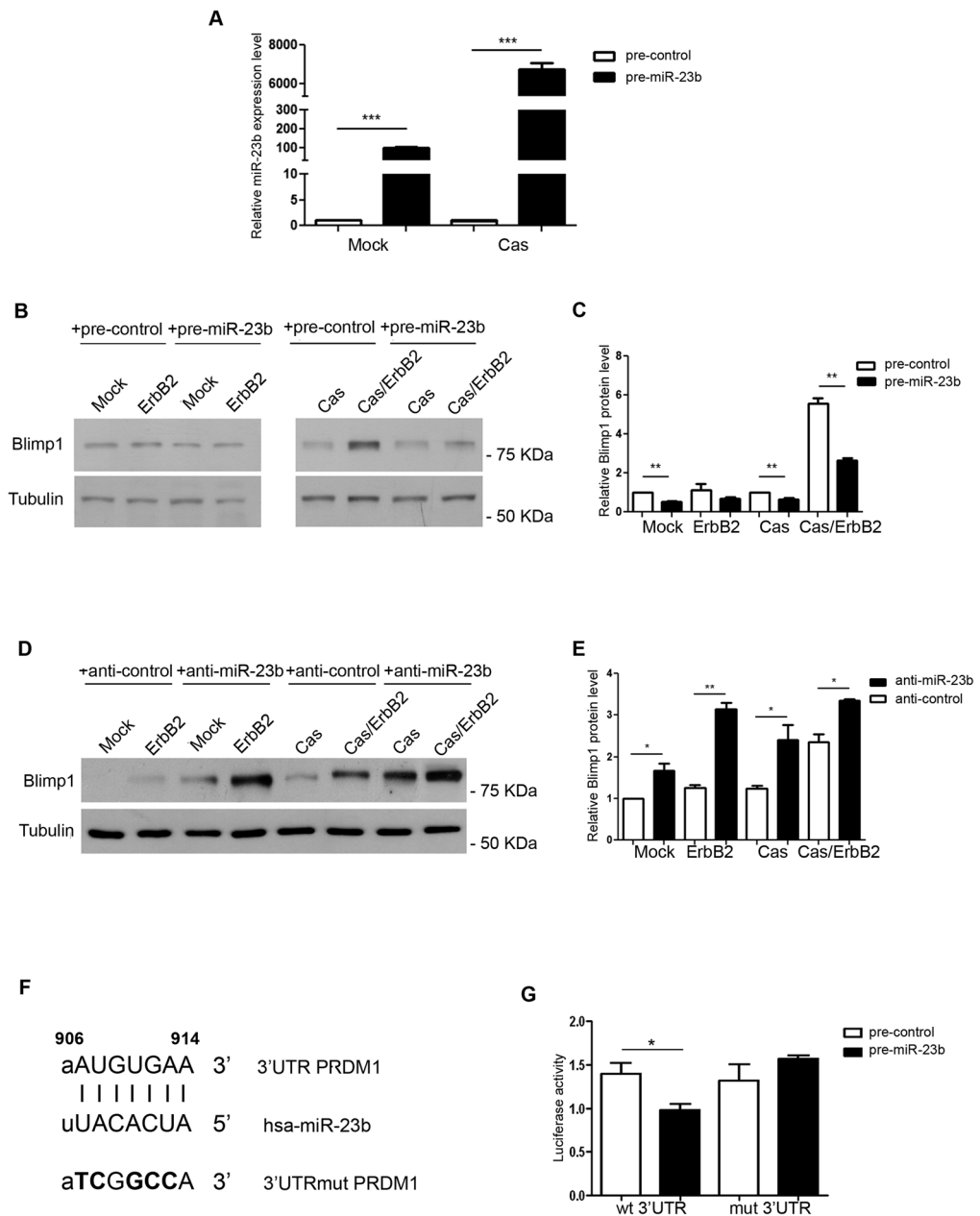


Figure 5. miR-23b directly binds to Blimp1 and regulates its expression. **(A)** miR-23b levels were evaluated using qRT-PCR in MCF10A.B2 Mock and Cas cells 48 hours after transfection with either the miR-23b precursor (pre-miR-23b) or negative controls (pre-control). Results were calculated as fold changes (mean \pm s.e.m.) relative to controls, normalized to U44 ($***p < 0.001$). **(B)** Total cell extracts from Mock and Cas cells, that had been treated with 1 μ M AP1510 or left untreated, 48 hours after transfection with either the miR-23b precursor (pre-miR-23b) or negative controls (pre-control) were probed for Blimp1 in a western blot analysis. Tubulin was used as the loading control. Blimp1 protein modulation was calculated relative to Mock level and normalized to tubulin as the loading control. **(C)** Densitometric analysis of protein levels in at least three independent experiments is shown (mean \pm s.e.m.). Statistical analysis was performed using the Student's t-test ($**p < 0.01$). **(D)** Total cell extracts from Mock and Cas cells, that had either been treated with 1 μ M AP1510 or left untreated, 24 hours after transfection with either the miR-23b inhibitor (anti-miR-23b) or negative controls (anti-control) were probed for Blimp1 in a western blot analysis. Tubulin was used as the loading control. Blimp1 protein modulation was calculated relative to Mock level and normalized to tubulin as the loading control. **(E)** Densitometric analyses of protein levels in at least three independent experiments are shown (mean \pm s.e.m.). Statistical analyses were performed using the Student's t-test ($*p < 0.05$, $**p < 0.01$). **(F)** Seed matches and mutated binding sites (3'UTRmut PRDM1) of miR-23b in the 3'UTR of PRDM1. Black bars indicate the seed matches, while bold letters indicate mutation sites. **(G)** Luciferase assays in HEK293 cells cotransfected with either wild-type or mutant PRDM1 3'UTR reporter constructs, together with miR-23b precursors (pre-miR-23b) and negative controls (pre-control).

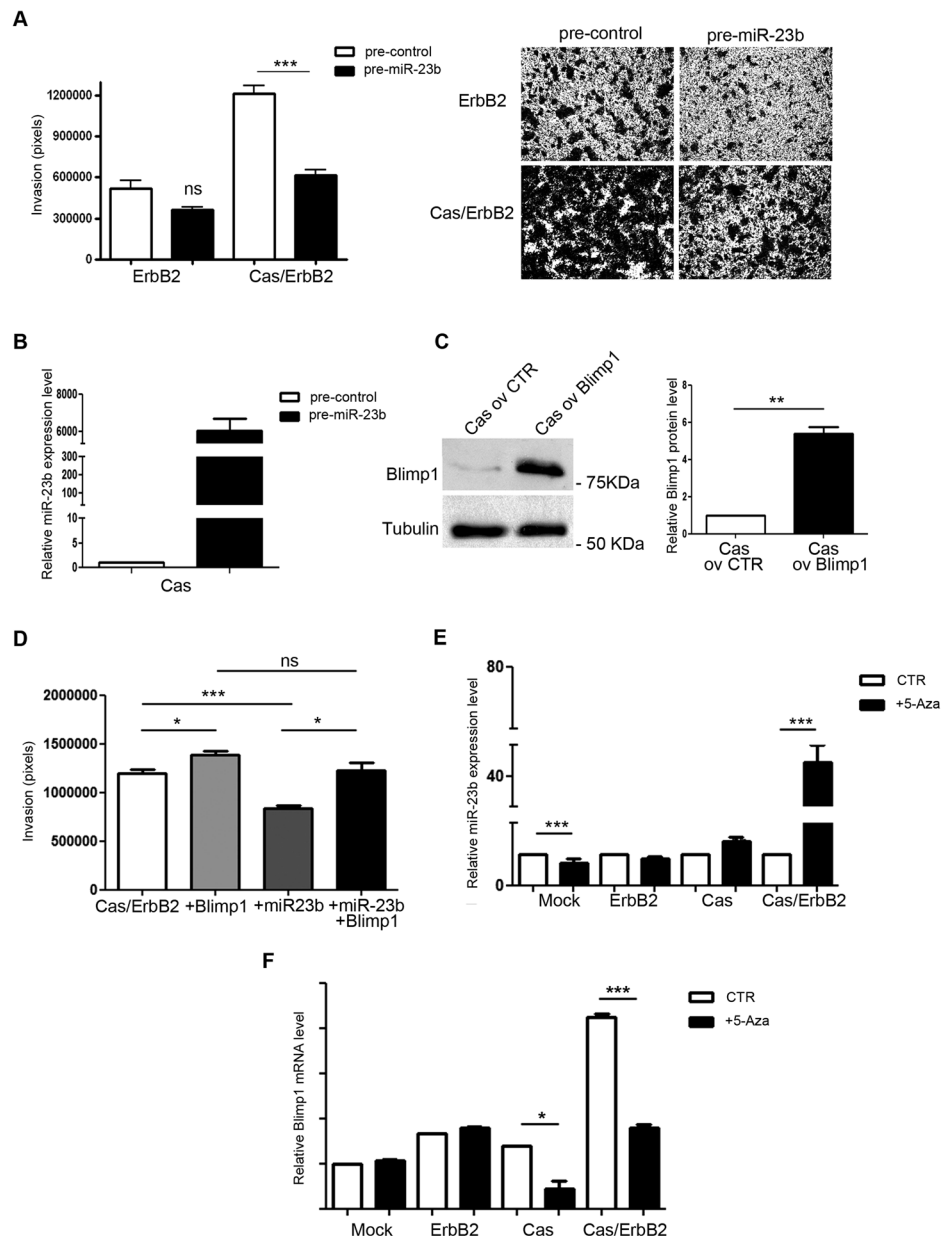


Figure 6. Blimp1 is a new negative target of miR-23b that impairs cell invasion. **(A)** MCF10A.B2 Mock and Cas cells 24 hours after transfection with either the miR-23b precursor (pre-miR-23b) or negative controls (pre-control) were subjected to transwell invasion assays for 48 hours in the presence of 1 μ M AP1510. Cell invasion quantification was performed across three different experiments. Results are presented as mean \pm s.e.m. of the area covered by invaded cells. Representative images of invaded cells after 48 hours, fixed and stained with Crystal violet are reported (** p < 0.001). Magnification 5X. **(B)** qRT-PCR of miR-23b in MCF10A.B2 Cas cells showing the levels of miR-23b expression 48 hours after pre-miR-23b transfection (pre-miR-23b) as compared to control (pre-control) transfected cells. Results were calculated as fold changes (mean \pm s.e.m.) relative to controls, normalized to U44 **(C)** MCF10A.B2 Cas cells overexpressing Blimp1 protein lacking its 3'UTR were probed for Blimp1 in a western blot analysis. Tubulin was used as the loading control. Densitometric analyses of protein levels in at least three independent experiments are shown (mean \pm s.e.m.). Statistical analyses were performed using the Student's t-test (** p < 0.01). **(D)** MCF10A.B2 Cas/ErbB2 cells were subjected to transwell invasion assays for 48 hours. Cas/ErbB2 cells were either transduced to overexpress Blimp1 protein (+Blimp1), transfected with the precursor miR-23b for 24 hours (+miR-23b) or transduced to overexpress Blimp1 protein and transfected with the precursor of miR-23b contemporary (+Blimp1, +miR-23b). Statistical analyses were performed at least on three independent experiments using the Student's t-test (* p < 0.05, *** p < 0.001). **(E)** qRT-PCR of miR-23b after treatment of MCF10A.B2 Mock, ErbB2, Cas, Cas/ErbB2 cells with 10 μ M 5-Aza or DMSO for 48 hours. Results were calculated as fold changes (mean \pm s.e.m.) relative to controls, normalized to U44 (** p < 0.001). **(F)** qRT-PCR of Blimp1 after treatment of MCF10A.B2 Mock, ErbB2, Cas, Cas/ErbB2 cells with 10 μ M 5-Aza or DMSO for 48 hours. Results were calculated as fold changes (mean \pm s.e.m.) relative to controls, normalized to 18S (* p < 0.05, *** p < 0.001).

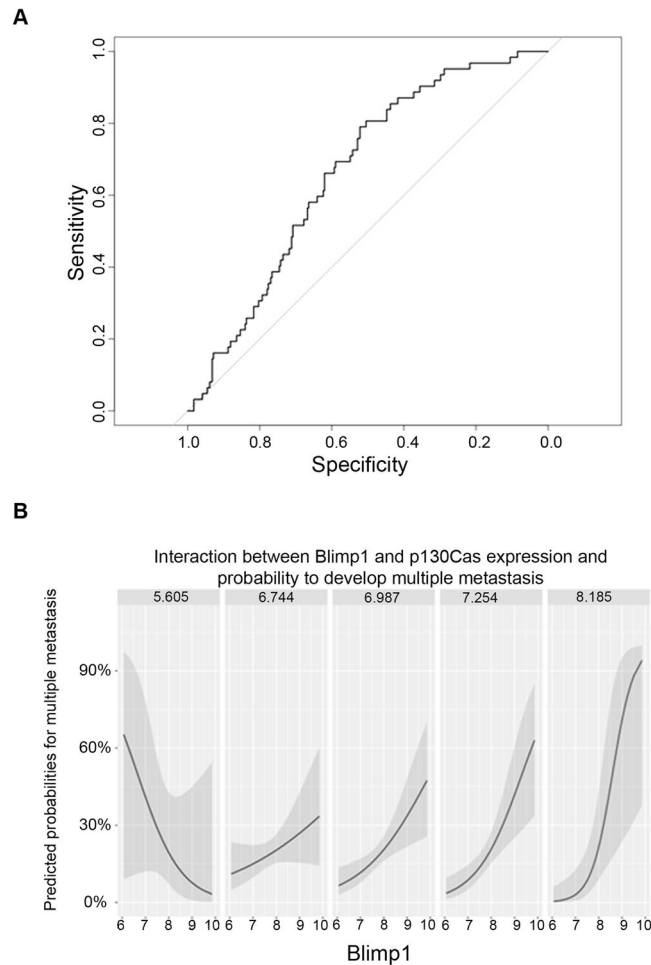


Figure 7. The interaction between Blimp1 and p130Cas levels positively correlates with the risk of developing multiple metastases. **(A)** ROC curve representing the prediction results of the logistic regression that discriminates between patients with single or multiple metastases using PRDM1 and BCAR1 expression levels and their interaction as predictors. **(B)** Effects plots of the regression. A separate plot of the fit is depicted for different levels of BCAR1, from left to right respectively: minimum, 1st quartile, median, 3rd quartile and maximum. In presence of higher expression of BCAR1, the effect of PRDM1 levels on the predicted probabilities becomes positive and progressively larger.

miR-23b is downmodulated in invasive acini, leading us to speculate that miR-23b may play a tumor suppressor role in the p130Cas/ErbB2 breast cancer model. Interestingly, the ectopic expression of miR-23b in Cas/ErbB2 MCF10A.B2 cells led to significantly lower migratory and invasive capacity than shown in the controls (Fig. 6A).

To ascertain whether the anti-migratory effect exerted by miR-23b was due to Blimp1 expression downmodulation, pre-miR-23b was transiently transfected in Cas overexpressing cells (Fig. 6B) that had previously been transfected with lentiviral vectors for the overexpression of Blimp1 lacking its 3'UTR or with empty vectors (Fig. 6C). Invasion was assessed by performing Transwell invasion assays (Fig. 6D). Interestingly, Blimp1 overexpression in Cas/ErbB2 cells leads to increased migratory and invasive capacities, while miR-23b overexpression-driven decreased cell invasion is rescued upon concomitant Blimp1 overexpression. These data suggest that miR-23b is an important regulator of Cas/ErbB2 breast cancer invasion and that it does so via the regulation of Blimp1 expression levels.

Moreover, the possible mechanisms that cause miR-23b downmodulation in p130Cas/ErbB2 invasive cells were evaluated. Recent evidence indicates that the miR-23b regulatory region in the genome contains a number of CpG islands that are distributed at a high density upstream of the transcription start site which could be affected by methylation and lead to the silencing of transcription³⁴. Therefore, we tested the effects of a compound that inhibits CpG islands methylation (5'-Aza) on miR-23b expression in Mock and Cas cells, activated or not for ErbB2. Importantly, inhibition of DNA methylation resulted in the up-regulation of miR-23b expression together with a reduction of its target Blimp1 mRNA in p130Cas/ErbB2 cells (Fig. 6E and F). Taken together, these data suggest that epigenetic regulation might be a possible mechanism of miR-23b downmodulation in p130Cas/ErbB2 cancer cells.

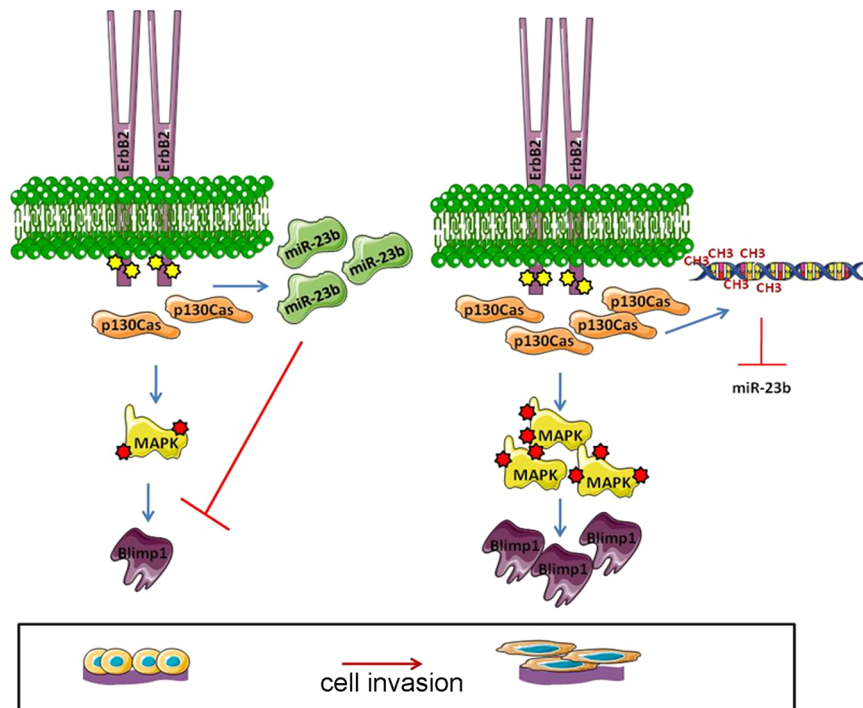


Figure 8. Graphical summary of the molecular mechanism leading to p130Cas/ErbB2/Blimp1 cell invasion. (A) In MCF10A.B2, the activation of ErbB2, in the absence of p130Cas overexpression, is not sufficient to increase Erk1/2 MAPKs activation and lower miR-23b expression to a threshold level that allows Blimp1 expression to occur (*left panel*). By contrast, ErbB2 activation and concomitant p130Cas overexpression strongly enhance Erk1/2 MAPKs activation and miR-23b promoter methylation, resulting in increased Blimp1 expression and, in turn, cell invasion (*right panel*).

Blimp1/PRDM1 expression levels correlate with the presence of multiple metastases. The *in vitro* and *in vivo* data presented above point out Blimp1 as a mediator of breast cancer progression. Therefore, Blimp1 expression levels in human breast tumors were evaluated as a means of further understanding their involvement in metastases formation.

To investigate the relationship between Blimp1 and p130Cas expression levels and their effect on the metastatic process, we fitted a logistic model to discriminate between patients with multiple distant or lymph nodal metastases ($n = 295$) and those with a single metastasis ($n = 62$), using Blimp1 and p130Cas expression levels and their interaction as predictors³⁵. We obtained an AUC of 0.66 (Fig. 7A) but more importantly a significant p-value for the interaction term, which indicates a higher risk of developing multiple metastases for patients with high expression of p130Cas and Blimp1 at the same time (Fig. 7B).

Blimp1 expression levels also change with different grading (Supplementary Figure 9) and staging of tumors (data not shown) (Kruskal-Wallis test p-values < 0.05). On the whole cohort we were not able to detect a significant effect on survival, however on the subset of patients with at least a metastasis, PRDM1 and BCAR expression levels are predictive of the overall survival, with worse prognoses for patients with higher expression (data not shown, PRDM p-value 0.02, 95% IC of HR 1.037–1.499, multivariate Cox regression). These results indicate that Blimp1 expression positively correlates with a higher probability of developing multiple metastasis in patients with high p130Cas, supporting the major role played by p130Cas in Blimp1-mediated invasion.

Discussion

We herein describe the role of the transcriptional repressor Blimp1 in p130Cas/ErbB2 breast cancer invasion in *in vitro* and *in vivo* models for the first time. In particular, we demonstrate that Blimp1 is highly expressed during p130Cas/ErbB2 dependent invasion in MCF10A.B2 cells and that the modulation of its expression is sufficient to severely impair tumor invasiveness *in vitro* and lung metastasis formation *in vivo*.

Specifically, a 3D model of MCF10A.B2 cells was used to demonstrate that high levels of Blimp1 expression specifically occur in invasive acini in which p130Cas is overexpressed and ErbB2 is activated.

Although the ability of the transcriptional repressor Blimp1 to influence cell migration has already been explored in the immune system, where its conditional knock-out in CD8⁺ T cells impairs the mobilization of virus-specific CD8⁺ T cells to the site of infection³⁶, the amount of data available on the role of Blimp1 in non-hematopoietic cells is still limited. Indeed, it has been shown that the downmodulation of Blimp1 in solid tumors leads to impaired cell migration both in non-small cell lung cancer and in ER α positive breast cancer cell lines, where Blimp1 represses the BMP5 protein^{16,18}.

This paper also shows proof that MAPK inhibition results in Blimp1 expression downmodulation and in the reduction of both multiacinar structures and invasive protrusions in p130Cas/ErbB2 cells. The involvement of

Erk1/2 MAPK activation signaling in p130Cas/ErbB2 invasion in the 3D cell model had already been described by our group⁸, however, this investigation provides further insight, as Blimp1 is described as a downstream effector of Erk1/2 activation.

The mechanisms via which MAPKs regulate the expression of Blimp1 have also been described; Erk1/2 activation in B cells inhibits the PAX5 transcription factor which acts as a negative regulator of Blimp1 expression, thus leading to its enhanced expression³⁷. However, preliminary data suggest that Pax5 is not involved in MAPK-dependent Blimp1 expression in our work, indicating that additional mechanisms, which will require further investigation, may well account for the modulation of Blimp1 expression in solid tumors.

Our data also indicate that Blimp1 overexpression is sufficient to provide p130Cas overexpressing MCF10.B2 mammary cells with invasive features, whereas its overexpression in ErbB2 only activated cells does not promote invasion. These data indicate that Blimp1 requires p130Cas expression to trigger invasion, whereas the activation of ErbB2 is dispensable for invasion in the absence of p130Cas. It is worth noting that *in silico* analyses of breast cancer patients support these data by pointing out that high levels of p130Cas and Blimp1 correlate with multiple metastasis. Our data also indicate that Blimp1 expression modulation results in an alteration in FAK activation and expression. The well-established role of FAK and p130Cas in cell migration and invasion^{23, 38, 39}, coupled with the fact that our findings identify FAK as an effector of Blimp1-dependent invasion lead to our speculation that Blimp1 overexpression is sufficient to induce invasion in p130Cas overexpressing mammary cells by leading to high FAK activation and expression, the consequent activation of p130Cas-dependent pathways, which, in turn, result in focal adhesion reorganization. However, Blimp1 overexpression in ErbB2 without the presence of high p130Cas levels does not provide a proper substrate for FAK-induced invasion. Intriguingly, *in silico* analyses that searched for Blimp1 binding sites on FAK promoters showed that PRDM1/Blimp1 binding sites are present in the proximity of FAK promoters, which further supports the relevance of Blimp1/FAK/p130Cas in cell invasion. These observations suggest that Blimp1 can act as a transcription factor that regulates FAK expression and shed additional light onto FAK transcriptional regulation.

On the other hand, our data also show that Blimp1 expression can be directly modulated by miR-23b. In particular, we herein describe, for the first time, that miR-23b is a direct Blimp1 negative modulator in solid tumors. In this context, we also demonstrate that miR-23b is a tumor suppressor miRNA in p130Cas/ErbB2 cells and that Blimp1 expression downmodulation is critical for miR-23b-dependent cell invasion impairment. Several reports have highlighted that cancer cell invasion and migration is also regulated by microRNAs (miRNAs); an important class of signaling modulators that are often deregulated in human cancers⁴⁰. miR-23b is a highly conserved miRNA that belongs to the miR-23b-27b-24-1 cluster (9q22.32), which is found intronically in the aminopeptidase O gene¹⁹. miR-23b is generally described as mediating tumor suppression in human cancers, but it also affects tumor formation and progression, according to tissue and cell contexts. In particular, miR-23b is found to be downmodulated in a number of human cancers including breast, bladder, prostate and pancreatic cancers²⁰. It has been described that miR-23b directly regulates target genes involved in cell migration, such as Zeb1, Src and PAK2^{20, 33, 40}. Moreover, miR-23b has recently been reported to target Blimp1 in B cells following histone deacetylases inhibition in antibody and autoantibody responses⁴¹.

Interestingly, we also demonstrate that miR-23b downmodulation is regulated by the methylation process in p130Cas/ErbB2 cells, which is in line with recently reported results in cervical cancer where several CpG islands were found to be part of the miR-23b regulatory region³⁴. This work describes, for the first time, that p130Cas and ErbB2 are able to influence epigenetic programs, such as methylation. On the basis of our data, we can speculate that increased DNA methylases expression or activation might occur in p130Cas/ErbB2 cells leading to miR-23b methylation. However, further research will be required to identify the specific mechanism through which miR-23b is regulated by methylation and the specific chromatin remodeling modifiers that are selectively induced upon p130Cas/ErbB2 cooperation. In conclusion, Blimp1 has been identified as a crucial regulator of p130Cas/ErbB2-mediated invasiveness *in vitro* and *in vivo* and has thus provided new insight into Blimp1 expression regulation and its mechanism of action. We have described two mechanisms by which p130Cas and ErbB2 synergism is able to induce Blimp1 expression; MAPK pathway activation and miR-23b downmodulation (See Fig. 8). Moreover, we have demonstrated, for the first time, that the Blimp1 protein is a prometastatic target of the tumor suppressor miR-23b in invasive breast cancer. Therefore this study can pave the way for the development of a miRNA-based therapeutic tool that can be used to treat p130Cas/ErbB2 aggressive tumors.

Methods

Cell lines and Cell culture. MCF10A.B2 cells were kindly provided by Dr Muthuswamy⁶ and maintained as described in ref. 4. MCF10A.B2 Mock and MCF10A.B2 Cas were generated as described in Cabodi *et al.*, 2011⁵. MCF10A.B2 without activation of ErbB2 was referred in the text as Mock, MCF10A.B2 with activation of ErbB2 as ErbB2, MCF10A.B2 overexpressing p130Cas without activation of ErbB2 as Cas, MCF10A.B2 overexpressing p130Cas with activation of ErbB2 as Cas/ErbB2. HEK293T were cultured in DMEM-10% FBS (Thermo Fisher Scientific), and N202-1A cells in DMEM-20% FBS (Thermo Fisher Scientific). All used cell lines were authenticated in the last 6 months by BMR Genomics (Padova, Italy), using the CELL ID System (Promega, Madison, WI).

MCF10.B2 and N202-1A cell populations were used for all the experiments described.

Three-Dimensional Culture. Three-dimensional morphogenic assays were performed according to instructions found below; http://muthuswamylib.cshl.edu/ml_protocols.html.

For the inhibition of PI3K/Akt, Erk1/2 MAPK pathway acini were treated with 10 μ M LY294002 (Calbiochem) and 25 μ M PD98059 (Sigma) either with or without 1 μ M AP1510 homodimerizer (A/A Homodimerizer, Clontech) at day 10. No off-target effects were reported after treating MCF10.B2 cells with 25–50 μ M PD98059^{8, 42–44}.

Transient Transfections of pre-miRs and anti-miRs. For transient transfection experiments, 0.8×10^6 MCF10A.B2 Mock and MCF10A.B2 Cas cells were seeded in a 6 well plate and the day after, transfected with either 75 nM pre-miR or 100 nM anti-miR using the Lipofectamine 2000™ reagent (Thermo Fisher Scientific), according to manufacturer's instructions. 1 μM AP1510, or ethanol for the control, was added to the medium. Cells were tested for overexpression/downmodulation 24 and 48 hrs later.

Luciferase assays. Cells (1.5×10^5) were cotransfected with 25 ng of the pSIC.PRDM1.3'UTR.538-2419 reporter construct which contained part of the 3'UTR of PRDM1 from nucleotide 538 to 2419³¹, and either 75 nM of pre-miR-23b-3p or 100 nM anti-miR using Lipofectamine2000 (Thermo Fisher Scientific). Lysates were collected 24–48 h after transfection and Firefly and Renilla luciferase activities were measured using a Dual Luciferase Reporter System (Promega). Where indicated, Blimp1 3'UTR was mutagenized at the first miR-23b recognition site (nucleotides 907–914) using the QuikChange Lightning Site-Directed Mutagenesis Kit (Stratagene), according to manufacturer's instructions.

Antibodies and reagents. Erk1/2 (T202/Y204), Akt (S473), Fak (397Tyr) phosphor-antibodies and Erk1/2, Akt, Blimp-1/PRDI-BF1 and cleaved caspase-3 antibodies were from Cell Signaling. Vinculin antibody was produced in our laboratory. Fak polyclonal antibodies were from Abcam. GAPDH antibodies from Millipore, p130Cas antibodies were from BD Biosciences. Matrigel and collagen bovine I were from Corning. Peroxidase-conjugated secondary antibodies were from GE Healthcare. Pre-miR™ microRNA Precursor Molecules for Negative Control #1, Hsa-miR-23b (PM10711), anti-miR™ miRNA Inhibitor Negative Control #1, anti-miR™ miRNA Inhibitor Hsa-miR-23b-3p (AM10711) (Ambion) and TaqMan® MicroRNA Assays for Hsa-miR-23b (ID 000399), U44 snRNA (ID 001094) were from Applied Biosystems.

Treatment of cell lines with 5'-Aza-2-deoxycytidine (5-Aza). MCF10A.B2 Mock and Cas cells were seeded in 6-well plates (4×10^5 cells/well). After 24 h, 10 μM 5-Aza (Sigma) dissolved in DMSO were added to fresh culture medium. 1 μM AP1510 was added an hour and a half later, where required. The cultures were incubated at 37 °C in 5% CO₂ for 48 h. Control cells were treated with DMSO.

Cell viability and survival. Cell Titer Blue assay was performed following manufacturer's recommendations. Briefly, Cell Titer Blue was mixed to the culture medium at a concentration of 20% (v/v). At each time point, N202-1A cells cultured in 48-well plates were washed with PBS to remove the medium, then 500 μl of the Cell Titer Blue/cell culture medium mixture was added to each sample. After 1 hour, 100 μl were removed from the plates and the absorbance was measured in a 96-well plate using GloMax-Multidetection System (Promega, Italy). Cell survival was evaluated by annexin V staining followed by FACS analysis.

Protein and RNA extraction, Immunoblotting and qRT-PCRs. Proteins, RNA extraction, immunoblotting were performed as previously described in ref. 4. qRT-PCRs for miR-23b detection were performed using TaqMan® MicroRNA Assays (Applied Biosystems) on 10 ng total RNA, according to manufacturer's instructions. For mRNA detection, 1 μg of DNase-treated RNA (DNA-free™ kit, Ambion) was retrotranscribed using RETROscript™ reagents (Ambion) and qRT-PCRs performed using gene-specific primers, on a 7900HT Fast Real Time PCR System. Quantitative normalization was performed on the expression of U44snRNA. For PRDM1 qRT-PCRs, the isolated total RNAs were reverse transcribed using a High Capacity cDNA Reverse Transcription kit (Applied Biosystems). The cDNA was diluted 1:5 in RNAase free water. qRT-PCR was performed on cDNA using the 7900HT Fast Real-Time PCR System (Applied Biosystems) with TaqMan Universal PCR Master Mix (Applied Biosystems). Primers used:

PRDM1 RIGHT: ACGTGTGGGTACGACCTTG, PRDM1 LEFT: CTGCCAATCCCTGAAACCT, MUT3'UTR PRDM1RIGHT:TTAAACATGGCATT'TTTTCTTCTGGCCGATTCTGATAATACAATGGA, MUT3'UTRPRDM1LEFT:CGGCCACATGACTTTTGCATCCATTGTATTATCAGAAATCGGCCAGAAGAA AAAAAATGCCATGTTTTAA).

Conditions were: 50 °C (2 min), 95 °C (2 min), followed by 45 cycles of 90 °C (15 s) and 60 °C (30 s). A total volume of 20 μl was used. Quantitative normalization was performed on the expression of endogenous control 18S (Thermo Fisher Scientific). The relative expression levels between samples were calculated using the comparative delta CT (threshold cycle number) method ($2^{-\Delta\Delta CT}$) using a control sample as reference point⁴⁵.

Immunofluorescence. Cells (2×10^5) were seeded into a 24-well plate (BD Falcon) and were either treated with ethanol (vehicle) or 10 μM AP1510 the next day. After 48 hours, cells were rinsed with ice-cold PBS and fixed with 4% paraformaldehyde for 10 min at RT, followed by permeabilization with 0.25% Triton X-100. Cells were stained with the vinculin (1:1000) antibody for 1 hour at RT, then washed with PBS and incubated with Alexa 568-labeled anti-mouse secondary antibody (Red) (1:500) (Thermo Fisher Scientific) at RT for 30 minutes together with TRITC-conjugated Phalloidin (Green) (P2141, Sigma). After 4, 6-diamino-2-phenylindole (DAPI, Thermo Fisher Scientific) staining, slides were mounted using Pro-long Gold Antifade Reagent (Thermo Fisher Scientific). Images were captured on a HCX PL APO CS 63 × 1.5 OIL Leica TCS-SP5 II confocal microscope and analyzed using LASAF software (Leica).

Lentiviral constructs. For PRDM1 overexpression, human PRDM1 cDNA (Source Bioscience) was cloned into the pLVX lentiviral vector and viral particle production was performed as previously described⁵. The PRDM1 shRNA library was purchased from GE Healthcare Dharmacon Inc. (TRC-Hs1.0 human clone ID: TRCN0000013612, TRC-Mm1.0 mouse clone ID: TRCN0000084714). For p130Cas expression, human p130Cas cDNA was cloned into the pCCL lentiviral vector and viral particle production was performed as described above.

Transwell invasion assay. Transwell invasion assay were performed as described in ref. 4. Briefly, 24-transwell chambers (Corning Costar, Cambridge, MA) were coated with 50 microliters of 1:1 mix matrigel plus collagen. MCF10A.B2 Mock and Cas cells (10^5) in 100 μ l of serum-free medium were seeded into the upper chamber. DMEM-F12 (100 μ l) with 5% horse serum plus AP1510 or ethanol for control, was added into the lower chamber as chemotactic stimulus. After 48 hrs, the migrated cells on the lower side of the membrane were fixed in 2.5% glutaraldehyde, stained with 0.1% crystal violet and photographed using an Olympus IX70 microscope. Invasion was evaluated by measuring the area occupied by migrated cells using the ImageJ software (<http://rsb-web.nih.gov/ij/>). For N202-1A cells, DMEM (500 μ l) with 20% FBS, or with water for the control, was added to the lower chamber as a chemotactic stimulus and invasion was evaluated, as above, after 72 hours.

In vivo assays. The use of animals was in compliance with the Guide for the Care and Use of Laboratory Animals published by the U.S. National Institutes of Health and approved by the Animal Care and Use Committee of the University of Turin and by the Italian Health Minister (authorization #1009/2016-PR). N202-1A control, Blimp1 silenced and Blimp1 overexpressing cells (10^5) were injected intravenously into the tail veins of NOD scid gamma (NSG) mice. The lungs were harvested, paraffin embedded, sectioned and stained with hematoxylin and eosin after 5 weeks. Slides were analyzed and photographed using an Olympus IX70 microscope and metastases were counted on H&E sections. N202-1A control, Blimp1 silenced and Blimp1 overexpressing cells (10^5) were also injected into the fat pad of NSG mice. After 3 weeks tumors were recovered and tumor weight was evaluated.

Bioinformatics analysis. Binding sites for Blimp1 were searched using the PRDM1 ChIP-seq on HeLa-S3 cells of the UCSC Track “Transcription Factor ChIP-seq Uniform Peaks from ENCODE/Analysis” on the promoter (1500 bp upstream and 500 downstream of TSS) of FAK on the human genome (release hg19), then inside the resulting peak we identified a subsequence with a high log-likelihood for the Jaspar PWM MA0508.1. Log-likelihoods⁴⁶ were computed using an ad-hoc C program and the background nucleotide frequencies were defined on human intergenic sequences.

For the *in silico* analyses of Blimp1 expression in breast cancer we used the METABRIC cohort of primary breast tumor samples, which comprises Illumina HT-12 expression data and several clinical parameters. Already normalized expression values in this cohort were downloaded from the European Genome-phenome Archive (EGAS00000000122:EGAD00010000434, original microarray data obtained in Curtis *et al.*³⁵ was then re-processed and normalized by ref. 47), and a subset of 357 samples with at least a single metastasis (considering both distal and lymph nodes metastases) were further analyzed. All analyses were performed with R (A language and environment for statistical computing. R Foundation for Statistical Computing, Vienna, Austria. URL <https://www.R-project.org/>), we used glm to fit the logistic model⁴⁸, the pROC package to plot the corresponding ROC curve and its AUC⁴⁹, sjPlot and effects packages to obtain the plots representing how BLIMP1 and BCAR1 expression levels interact with respect to the risk of developing multiple metastases (Lüdecke D. “sjPlot: Data Visualization for Statistics in Social Science”, (2017)).

Statistical analysis. The results are representative of at least three independent experiments performed in triplicate and are expressed as means \pm s.e.m. Statistical analysis of the data was performed using a Student’s t-test.

References

- Santa-Maria, C. A., Nye, L., Mutonga, M. B., Jain, S. & Gradishar, W. J. Management of Metastatic HER2-Positive Management of Metastatic HER2-Positive Breast Cancer: Where Are We and Where Do We Go From Here? Breast Cancer: Where Are We and Where Do We Go From Here? *Oncology (Williston Park)* **30**, 148–155 (2016).
- van de Vijver, M. J. *et al.* Neu-protein overexpression in breast cancer. Association with comedo-type ductal carcinoma *in situ* and limited prognostic value in stage II breast cancer. *N Engl J Med* **319**, 1239–1245, doi:10.1056/NEJM198811103191902 (1988).
- Moasser, M. M. The oncogene HER2: its signaling and transforming functions and its role in human cancer pathogenesis. *Oncogene* **26**, 6469–6487, doi:10.1038/sj.onc.1210477 (2007).
- Pincini, A. *et al.* Identification of p130Cas/ErbB2-dependent invasive signatures in transformed mammary epithelial cells. *Cell Cycle* **12**, 2409–2422, doi:10.4161/cc.25415 (2013).
- Cabodi, S. *et al.* p130Cas is an essential transducer element in ErbB2 transformation. *FASEB J* **24**, 3796–3808, doi:10.1096/fj.10-157347 (2010).
- Muthuswamy, S. K., Li, D., Lelievre, S., Bissell, M. J. & Brugge, J. S. ErbB2, but not ErbB1, reinitiates proliferation and induces luminal repopulation in epithelial acini. *Nat Cell Biol* **3**, 785–792, doi:10.1038/ncb0901-785 (2001).
- Cabodi, S. *et al.* p130Cas as a new regulator of mammary epithelial cell proliferation, survival, and HER2-neu oncogene-dependent breast tumorigenesis. *Cancer Res* **66**, 4672–4680, doi:10.1158/0008-5472.CAN-05-2909 (2006).
- Tornillo, G. *et al.* p130Cas promotes invasiveness of three-dimensional ErbB2-transformed mammary acinar structures by enhanced activation of mTOR/p70S6K and Rac1. *Eur J Cell Biol* **90**, 237–248, doi:10.1016/j.ejcb.2010.09.002 (2011).
- Nutt, S. L., Fairfax, K. A. & Kallies, A. BLIMP1 guides the fate of effector B and T cells. *Nat Rev Immunol* **7**, 923–927, doi:10.1038/nri2204 (2007).
- John, S. A. & Garrett-Sinha, L. A. Blimp1: a conserved transcriptional repressor critical for differentiation of many tissues. *Exp Cell Res* **315**, 1077–1084, doi:10.1016/j.yexcr.2008.11.015 (2009).
- Huang, T. F. *et al.* BLMP-1/Blimp-1 regulates the spatiotemporal cell migration pattern in *C. elegans*. *PLoS Genet* **10**, e1004428, doi:10.1371/journal.pgen.1004428 (2014).
- Welsh, R. M. Blimp hovers over T cell immunity. *Immunity* **31**, 178–180, doi:10.1016/j.immuni.2009.08.005 (2009).
- Wilm, T. P. & Solnica-Krezel, L. Essential roles of a zebrafish prdm1/blimp1 homolog in embryo patterning and organogenesis. *Development* **132**, 393–404, doi:10.1242/dev.01572 (2005).
- Boi, M., Zucca, E., Inghirami, G. & Bertoni, F. PRDM1/BLIMP1: a tumor suppressor gene in B and T cell lymphomas. *Leuk Lymphoma* **56**, 1223–1228, doi:10.3109/10428194.2014.953155 (2015).
- Karube, K. *et al.* Identification of FOXO3 and PRDM1 as tumor-suppressor gene candidates in NK-cell neoplasms by genomic and functional analyses. *Blood* **118**, 3195–3204, doi:10.1182/blood-2011-04-346890 (2011).
- Romagnoli, M. *et al.* Epithelial-to-mesenchymal transition induced by TGF-beta1 is mediated by Blimp-1-dependent repression of BMP-5. *Cancer Res* **72**, 6268–6278, doi:10.1158/0008-5472.CAN-12-2270 (2012).

17. Wang, X. *et al.* RelB NF-kappaB represses estrogen receptor alpha expression via induction of the zinc finger protein Blimp1. *Mol Cell Biol* **29**, 3832–3844, doi:10.1128/MCB.00032-09 (2009).
18. Yu, Z., Sato, S., Trackman, P. C., Kirsch, K. H. & Sonenshein, G. E. Blimp1 activation by AP-1 in human lung cancer cells promotes a migratory phenotype and is inhibited by the lysyl oxidase propeptide. *PLoS One* **7**, e33287, doi:10.1371/journal.pone.0033287 (2012).
19. Sikand, K., Slane, S. D. & Shukla, G. C. Intrinsic expression of host genes and intronic miRNAs in prostate carcinoma cells. *Cancer Cell Int* **9**, 21, doi:10.1186/1475-2867-9-21 (2009).
20. Donadelli, M., Dando, I., Fiorini, C. & Palmieri, M. Regulation of miR-23b expression and its dual role on ROS production and tumour development. *Cancer Lett* **349**, 107–113, doi:10.1016/j.canlet.2014.04.012 (2014).
21. Defilippi, P., Di Stefano, P. & Cabodi, S. p130Cas: a versatile scaffold in signaling networks. *Trends Cell Biol* **16**, 257–263, doi:10.1016/j.tcb.2006.03.003 (2006).
22. Singh, M. K. *et al.* A novel Cas family member, HEPL, regulates FAK and cell spreading. *Mol Biol Cell* **19**, 1627–1636, doi:10.1091/mbc.E07-09-0953 (2008).
23. Sulzmaier, F. J., Jean, C. & Schlaepfer, D. D. FAK in cancer: mechanistic findings and clinical applications. *Nat Rev Cancer* **14**, 598–610, doi:10.1038/nrc3792 (2014).
24. Tikhmyanova, N., Little, J. L. & Golemis, E. A. CAS proteins in normal and pathological cell growth control. *Cell Mol Life Sci* **67**, 1025–1048, doi:10.1007/s00018-009-0213-1 (2010).
25. Barrett, A., Pellet-Many, C., Zachary, I. C., Evans, I. M. & Frankel, P. p130Cas: a key signalling node in health and disease. *Cell Signal* **25**, 766–777, doi:10.1016/j.cellsig.2012.12.019 (2013).
26. Sieg, D. J., Hauck, C. R. & Schlaepfer, D. D. Required role of focal adhesion kinase (FAK) for integrin-stimulated cell migration. *J Cell Sci* **112** (Pt 16), 2677–2691 (1999).
27. Wang, Y. & McNiven, M. A. Invasive matrix degradation at focal adhesions occurs via protease recruitment by a FAK-p130Cas complex. *J Cell Biol* **196**, 375–385, doi:10.1083/jcb.201105153 (2012).
28. Webb, D. J. *et al.* FAK-Src signalling through paxillin, ERK and MLCK regulates adhesion disassembly. *Nat Cell Biol* **6**, 154–161, doi:10.1038/ncb1094 (2004).
29. An integrated encyclopedia of DNA elements in the human genome. *Nature* **489**, 57–74, doi:10.1038/nature11247 (2012).
30. Kent, W. J. *et al.* The human genome browser at UCSC. *Genome Res* **12**, 996–1006, doi:10.1101/gr.229102. Article published online before print in May 2002 (2002).
31. Nie, K. *et al.* MicroRNA-mediated down-regulation of PRDM1/Blimp-1 in Hodgkin/Reed-Sternberg cells: a potential pathogenetic lesion in Hodgkin lymphomas. *Am J Pathol* **173**, 242–252, doi:10.2353/ajpath.2008.080009 (2008).
32. Jin, L. *et al.* Prooncogenic factors miR-23b and miR-27b are regulated by Her2/Neu, EGF, and TNF-alpha in breast cancer. *Cancer Res* **73**, 2884–2896, doi:10.1158/0008-5472.CAN-12-2162 (2013).
33. Pellegrino, L. *et al.* miR-23b regulates cytoskeletal remodeling, motility and metastasis by directly targeting multiple transcripts. *Nucleic Acids Res* **41**, 5400–5412, doi:10.1093/nar/gkt245 (2013).
34. Campos-Viguri, G. E. *et al.* miR-23b as a potential tumor suppressor and its regulation by DNA methylation in cervical cancer. *Infect Agent Cancer* **10**, 42, doi:10.1186/s13027-015-0037-6 (2015).
35. Curtis, C. *et al.* The genomic and transcriptomic architecture of 2,000 breast tumours reveals novel subgroups. *Nature* **486**, 346–352, doi:10.1038/nature10983 (2012).
36. Kallies, A., Xin, A., Belz, G. T. & Nutt, S. L. Blimp-1 transcription factor is required for the differentiation of effector CD8(+) T cells and memory responses. *Immunity* **31**, 283–295 (2009).
37. Yasuda, T. *et al.* B cell receptor-ERK1/2 signal cancels PAX5-dependent repression of BLIMP1 through PAX5 phosphorylation: a mechanism of antigen-triggering plasma cell differentiation. *J Immunol* **188**, 6127–6134, doi:10.4049/jimmunol.1103039 (2012).
38. Cabodi, S., del P Camacho-Leal, M., Di Stefano, P. & Defilippi, P. Integrin signalling adaptors: not only figurants in the cancer story. *Nat Rev Cancer* **10**, 858–870, doi:10.1038/nrc2967 (2010).
39. Mitra, S. K., Hanson, D. A. & Schlaepfer, D. D. Focal adhesion kinase: in command and control of cell motility. *Nat Rev Mol Cell Biol* **6**, 56–68, doi:10.1038/nrm1549 (2005).
40. Zhang, H. *et al.* Genome-wide functional screening of miR-23b as a pleiotropic modulator suppressing cancer metastasis. *Nat Commun* **2**, 554, doi:10.1038/ncomms1555 (2011).
41. White, C. A. *et al.* Histone deacetylase inhibitors upregulate B cell microRNAs that silence AID and Blimp-1 expression for epigenetic modulation of antibody and autoantibody responses. *J Immunol* **193**, 5933–5950, doi:10.4049/jimmunol.1401702 (2014).
42. Qie, S., Chu, C., Li, W., Wang, C. & Sang, N. ErbB2 activation upregulates glutaminase 1 expression which promotes breast cancer cell proliferation. *J Cell Biochem* **115**, 498–509, doi:10.1002/jcb.24684 (2014).
43. Seton-Rogers, S. E. *et al.* Cooperation of the ErbB2 receptor and transforming growth factor beta in induction of migration and invasion in mammary epithelial cells. *Proc Natl Acad Sci USA* **101**, 1257–1262, doi:10.1073/pnas.0308090100 (2004).
44. Xue, B., Krishnamurthy, K., Allred, D. C. & Muthuswamy, S. K. Loss of Par3 promotes breast cancer metastasis by compromising cell-cell cohesion. *Nat Cell Biol* **15**, 189–200, doi:10.1038/ncb2663 (2013).
45. Bookout, A. L. & Mangelsdorf, D. J. Quantitative real-time PCR protocol for analysis of nuclear receptor signaling pathways. *Nucl Recept Signal* **1**, e012, doi:10.1621/nrs.01012 (2003).
46. Wasserman, W. W. & Sandelin, A. Applied bioinformatics for the identification of regulatory elements. *Nat Rev Genet* **5**, 276–287 (2004).
47. Dvinge, H. *et al.* The shaping and functional consequences of the microRNA landscape in breast cancer. *Nature* **497**, 378–382 (2013).
48. Friedman, J., Hastie, T. & Tibshirani, R. Regularization Paths for Generalized Linear Models via Coordinate Descent. *J Stat Softw* **33**, 1–22 (2010).
49. Robin, X. *et al.* pROC: an open-source package for R and S+ to analyze and compare ROC curves. *BMC Bioinformatics* **12**, 77 (2011).

Acknowledgements

This work has been supported by AIRC (Associazione Italiana Ricerca Cancro), to SC (IG11346 and IG15970) and PD (IG15399); MIUR (FIRB giovani 2008 RBF08F2FS to SC and FO), MIUR (Ministero Università Ricerca, PRIN 2010/2011) to PD and Compagnia San Paolo, Turin; Progetto d'Ateneo, University of Turin 2011 to PD, Ricerca Sanitaria Finalizzata GR-2009-1543842 to SC, AIRC (Associazione Italiana Ricerca Cancro) to DT (IG 2013-10104), Fondazione Cassa di Risparmio Torino CRT to DT (2014.1085). MPCL is supported by an Umberto Veronesi Fellowship. We are grateful to Marta Gai for her help with confocal microscopy and to Giusy Tornillo for critical reading of the manuscript.

Author Contributions

M.S. performed the experiments, analyzed the data and wrote the manuscript. M.P.C.L. performed *in vivo* experiments. F.O. contributed to miRNA experiments and discussion. E.G. performed bioinformatic analysis. A.C. generated the Blimp1 overexpressing construct. P.P. took part in discussions. W.T. generated the pSIC.

PRDM1.3'UTR.538-2419 reporter construct. E.T. took part in discussions. P.D. took part in discussions. D.T. contributed to miRNA experiments and discussions. S.C. designed and supervised the experiments and wrote the manuscript. All authors read and approved the final manuscript.

Additional Information

Supplementary information accompanies this paper at doi:[10.1038/s41598-017-01332-z](https://doi.org/10.1038/s41598-017-01332-z)

Competing Interests: The authors declare that they have no competing interests.

Publisher's note: Springer Nature remains neutral with regard to jurisdictional claims in published maps and institutional affiliations.



Open Access This article is licensed under a Creative Commons Attribution 4.0 International License, which permits use, sharing, adaptation, distribution and reproduction in any medium or format, as long as you give appropriate credit to the original author(s) and the source, provide a link to the Creative Commons license, and indicate if changes were made. The images or other third party material in this article are included in the article's Creative Commons license, unless indicated otherwise in a credit line to the material. If material is not included in the article's Creative Commons license and your intended use is not permitted by statutory regulation or exceeds the permitted use, you will need to obtain permission directly from the copyright holder. To view a copy of this license, visit <http://creativecommons.org/licenses/by/4.0/>.

© The Author(s) 2017

p130Cas scaffold protein regulates ErbB2 stability by altering breast cancer cell sensitivity to autophagy

Brigitte Bisaro¹, Marianna Sciortino¹, Shana Colombo¹, Maria Pilar Camacho Leal¹, Andrea Costamagna¹, Isabella Castellano², Filippo Montemurro³, Valentina Rossi³, Giorgio Valabrega^{4,2}, Emilia Turco¹, Paola Defilippi¹, Sara Cabodi¹

¹Department of Biotechnology and Health Sciences, University of Torino, Torino, Italy

²Department of Medical Sciences, University of Torino, Torino, Italy

³Investigative Clinical Oncology (INCO), Fondazione del Piemonte per l'Oncologia (FPO)-Candiolo Cancer Center (IRCCs), Torino, Italy

⁴Department of Oncology, University of Torino, Torino, Italy

Correspondence to: Sara Cabodi, e-mail: sara.cabodi@unito.it

Keywords: p130Cas, ErbB2, autophagy, breast cancer resistance

Received: June 16, 2015

Accepted: November 25, 2015

Published: December 21, 2015

ABSTRACT

Overexpression of the ErbB2/HER2 receptor tyrosine kinase occurs in up to 20% of human breast cancers and correlates with aggressive disease. Several efficacious targeted therapies, including antibodies and kinase inhibitors, have been developed but the occurring of resistance to these agents is often observed. New therapeutic agents targeting the endocytic recycling and intracellular trafficking of membrane in tumor cells overexpressing ErbB2 are actually in clinical development. Nevertheless the mechanisms underlying ErbB2 downregulation are still obscure. We have previously demonstrated that the overexpression of the p130Cas adaptor protein in ErbB2 positive breast cancer, promotes tumor aggressiveness and progression. Here we demonstrate that lowering p130Cas expression in breast cancer cells is sufficient to induce ErbB2 degradation by autophagy. Conversely, p130Cas overexpression protects ErbB2 from degradation by autophagy. Furthermore, this autophagy-dependent preferential degradation of ErbB2 in absence of p130Cas is due to an increased ErbB2 ubiquitination. Indeed, the overexpression of p130Cas impairs ErbB2 ubiquitination by inhibiting the binding of Cbl and CHIP E3 ligases to ErbB2. Finally, our results indicate that p130Cas-dependent ErbB2 protection from degradation by autophagy may alter the sensitivity to the humanized monoclonal antibody trastuzumab. Consistently, in human ErbB2 positive breast cancers that develop resistance to trastuzumab, p130Cas expression is significantly increased suggesting that elevated levels of p130Cas can be involved in trastuzumab resistance.

INTRODUCTION

Molecular and clinical studies indicate that ErbB2 has important implications in tumor etiology and progression. Overexpression of ErbB2 (Her2/Neu), is involved in the pathogenesis of nearly 20–30% of invasive breast cancers and is associated with an aggressive phenotype. Although ErbB2 overexpression identifies patients who are likely to respond to therapy with trastuzumab, not all patients benefit from treatment. Approximately 15% of patients relapse after therapy due to de novo or acquired resistance [1–3]. Therefore, intense investigations are necessary to understand the factors that contribute to the resistance

and to identify therapeutic strategies to overcome the resistance. Several mechanisms have been proposed for the acquirement of resistance including the poor internalization of ErbB2 resulting in a long half-life at the plasma membrane [4–7]. Although it has been shown that Hsp90 inhibition can induce ErbB2 ubiquitination followed by its downregulation [8, 9], the mechanisms underlying ErbB2 downregulation are still obscure.

p130Cas is a signaling molecule involved in the linkage of actin cytoskeleton to the extracellular matrix during cell migration, cell invasion and cell transformation. p130Cas protein has been described as a major player in the cross-talk between EGF Receptor and integrins

[10]. Due to its modular structure, p130Cas has been shown to play a crucial role in signaling originating from many amplified or mutated oncogenes, by undergoing hyperphosphorylation and association with multiple signaling partners required for transformation [11–13].

The overexpression of p130Cas in the mammary gland leads to hyperplasia and delayed involution but does not promote tumorigenesis [14]. Double transgenic mice originated by crossing MMTV-p130Cas and MMTV-NeuT mice, which express the oncogenic form of the rat *neu* gene, homologous to human ErbB2, showed an accelerated onset of mammary tumor formation. Moreover, the analysis of human breast samples revealed that tumors overexpressing both p130Cas and ErbB2 are characterized by an elevated proliferation index [14]. Our previous data demonstrated that p130Cas is an essential transducer element in ErbB2 transformation and progression showing that p130Cas is necessary for ErbB2-dependent foci formation, anchorage-independent growth, *in vivo* tumor growth and metastatization [15]. Moreover, we have reported that p130Cas over-expression promotes ErbB2-dependent invasion in three-dimensional (3D) cultures of human mammary epithelial cells and we have identified the gene expression changes underlying this invasive behavior [16, 17].

Moreover, p130Cas has been proposed as a crucial modulator of both anti-estrogen and adriamycin resistance [18, 19].

Here we demonstrate that in breast cancer cells overexpressing ErbB2, p130Cas protects ErbB2 from autophagy-mediated degradation by interfering with its ubiquitination. Moreover, changes on the receptor ubiquitination caused by modulation of p130Cas expression leads to expression of different types of autophagic markers, suggesting a link between ErbB2 degradation and autophagy in a p130Cas-dependent manner. Here we show for the first time that high levels of p130Cas expression might be crucial to promote resistance to trastuzumab treatment by protecting ErbB2 from degradation.

RESULTS

Modulation of p130Cas expression interferes with ErbB2 protein stability

To investigate the relevance of the modulation of p130Cas expression in the control of ErbB2 stability we used, as an experimental model, ErbB2 positive BT474 breast cancer cells. We infected cells with lentiviruses expressing either p130Cas shRNAs or scramble control shRNA sequences, and lentiviruses overexpressing p130Cas with related control vectors. Within 48 hours, p130Cas expression was effectively silenced by about 80% compared to cells infected with scramble sequences, while p130Cas overexpression resulted in about 30–40% increase of protein expression compared to control infected

cells (Figure 1A). Interestingly, when we evaluated ErbB2 expression in these cell lysates, we found that p130Cas expression modulation results in changes of ErbB2 expression levels. Indeed, lowering p130Cas expression in BT474 cells (Figure 1A) is sufficient to cause ErbB2 downregulation. The same results were obtained by performing experiments in ErbB2 positive breast cancer cell line SKBR3, further supporting the expression correlation between ErbB2 and p130Cas (Supplementary Figure 1A). To exclude that the ErbB2 downregulation is an off-target effect of sh-p130Cas sequence, we tested four different sequences and we confirmed that lowering p130Cas expression results in ErbB2 downregulation (Supplementary Figure 1B). Consistently, overexpression of p130Cas leads to an increase of ErbB2 expression (Figure 1A). These changes in ErbB2 expression upon modulation of p130Cas expression, were not dependent on alterations of HER2 gene transcription as shown in Figure 1B, (right panel) but rather to its availability on the cell membrane as demonstrated by FACS analysis (Figure 1C). In addition, the alterations of ErbB2 expression upon modulation of p130Cas expression were highly specific, since no expression changes were observed for Hsp90 and ER alpha (Figure 1D).

Therefore, these data indicate that modulation of p130Cas expression in breast cancer cells is sufficient to strongly affect ErbB2 expression.

p130Cas silencing drives proteasome independent-ErbB2 degradation

Little attention has been paid to the role of ErbB2 degradation in cancers, although when compromised, it may lead to increased ErbB2 levels and activity. Several studies have shown that endocytic downregulation of ErbB2 is impaired in cancer cells although there is poor understanding of how this is achieved [4, 20]. It was recently demonstrated that treatment of ErbB2 positive SKBR3 and BT474 breast cancer cell lines with proteasome inhibitor causes a 50% downregulation of ErbB2 protein expression ([21] and Supplementary Figure 2), indicating that ErbB2 degradation is proteasome independent. In addition, p130Cas has been recently described to regulate cell sensitivity to proteasome inhibition [22].

To understand whether ErbB2 altered protein levels, as a consequence of modulation of p130Cas expression, implicate proteasome activity, we treated p130Cas silenced, p130Cas overexpressing and relative BT474 control cells for 16 hours with the proteasome inhibitor MG132. As shown in Figure 2, proteasome inhibition induces ErbB2 degradation in control cells, as previously demonstrated. However, we observed a significant increased degradation of ErbB2 in p130Cas silenced cells compared to control cells following treatment with 2 μ M of MG132 for 16 hours, while overexpression of p130Cas minimizes the degradation of ErbB2 upon proteasome

inhibition. Interestingly, these data indicate that lowering p130Cas expression can lead to further degradation of ErbB2, while the overexpression of p130Cas protects ErbB2 from degradation. Moreover, treatment of p130Cas silenced and relative BT474 control cells with cycloheximide with or without MG132, indicates that ErbB2 degradation is prompted in p130Cas-silenced conditions (Supplementary Figure 3).

It was previously demonstrated that ErbB2 degradation upon proteasome inhibition leads to the formation of cytosolic aggregates directed to lysosomal degradation [23]. Consistently, the treatment of control (Ctr) cells with MG132 induced a reduction of ErbB2 level and an increased amount of the autophagic markers LC3-II (Figure 2 left and right panels), indicating that

the induction of autophagy correlates with decreased ErbB2 protein levels. Noteworthy, the downregulation of p130Cas is sufficient to lower ErbB2 expression and to enhance the conversion of LC3-I to its lipidated form LC3-II respect to the control and to the p130Cas overexpressing cells, suggesting that p130Cas-dependent ErbB2 degradation is due to an increased activation of the autophagic process. These experiments were also performed in SKBR3 cell lines showing the same results (Supplementary Figure 4A and 4B).

Most interestingly, high levels of p130Cas expression that protect ErbB2 from degradation correlate with low expression of the autophagy marker LC3-II independently of proteasome inhibition. These data indicate that in ErbB2 positive cells silenced for p130Cas and treated

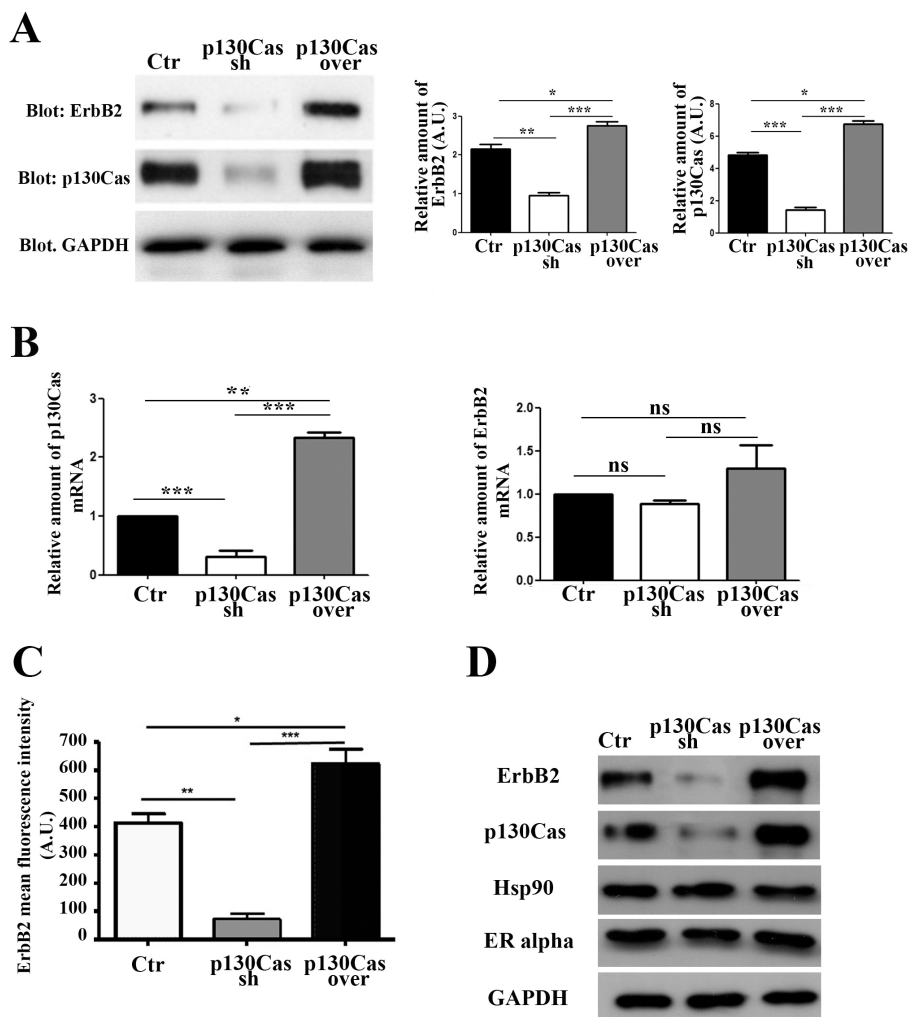


Figure 1: Modulation of p130Cas expression specifically affects ErbB2 expression. (A) Left panel: Total cell lysates of BT474 cells infected with lentiviral vectors to silence (Cas sh) or overexpress p130Cas (Cas over) were blotted with p130Cas and ErbB2 antibodies. GAPDH was used as loading control. Right panel: Histograms show ErbB2 and p130Cas levels, normalized to GAPDH. Bars represent the means \pm SEM of three independent experiments ($*p < 0.05$; $**p < 0.01$; $***p < 0.001$). (B) qRT-PCR analysis of p130Cas mRNA (left panel) and ErbB2 mRNAs (right panel) expression from cells as in (A). Quantification of results from three independent experiments is shown (ns: not significant; $**p < 0.01$; $***p < 0.001$). (C) Histograms show the expression of cell membrane ErbB2 evaluated by FACS analysis on control, p130Cas silenced and p130Cas overexpressing BT474 cells. Bars represent the means \pm SEM of three independent experiments ($*p < 0.05$; $**p < 0.01$; $***p < 0.001$). (D) Total cell lysates obtained from cells as in (A) were probed with antibodies to ErbB2, p130Cas, Hsp90 and ER alpha and normalized with GAPDH.

with MG132, p130Cas inhibition leads to a stronger activation of the autophagic flux leading to increased ErbB2 degradation whereas p130Cas overexpression is sufficient to impair autophagy thereby preventing ErbB2 degradation.

p130Cas expression level alters sensitivity of breast cancer cells to autophagy

To demonstrate that the p130Cas expression can interfere with the autophagic degradation of ErbB2, Ctr, p130Cas silenced and overexpressing BT474 cells were starved and cultured for 6 hours in presence of HBSS (Hank's balanced salt solution) to induce autophagy alone or in combination with Chloroquine, a drug that arrests the latter step of autophagy, resulting in the failure of the autophagy process [24]. Cell lysates from control, p130Cas silenced and overexpressing cells were collected and western blot analysis performed. The results shown in Figure 3A (left and right panels) confirm that in untreated cells, silencing of p130Cas is sufficient to induce ErbB2 downregulation by autophagy as demonstrated by LC3-II upregulation. In addition, the induction of autophagy by HBSS treatment leads to approximately 50% reduction of ErbB2 in Ctr cells compared to untreated cells demonstrating that autophagy is implicated in the degradation of ErbB2. The effectiveness of HBSS treatment to trigger the autophagic flux is confirmed by the presence of the lipidated form of LC3. Most interestingly, in p130Cas overexpressing cells the HBSS treatment does

not significantly affect ErbB2 expression levels indicating that the overexpression of p130Cas renders ErbB2 less sensitive to autophagy degradation. Moreover, the concomitant treatment of HBSS and Chloroquine results in the re-establishment of ErbB2 expression in p130Cas silenced cells upon autophagy inhibition (Figure 3A) and the concomitant accumulation of LC3-II expression, confirming that absence of p130Cas favors ErbB2 degradation through autophagy.

Accordingly, as shown in Figure 3B (left and right panels), the treatment with Chloroquine (100 μ M) was sufficient to restore ErbB2 levels in both control and p130Cas silenced cells, while in p130Cas overexpressing cells did not result in a significant change in the amount of ErbB2 expression. Therefore, these results indicate that blocking the autophagic flux, as demonstrated by the increased expression of the lipidated form of LC3, rescues ErbB2 expression in both control and p130Cas silenced cells.

p130Cas-dependent ErbB2 degradation by autophagy is regulated by mTOR activity

It is known that class I and class III of phosphatidylinositol 3-kinase (PI3K) can regulate autophagy in different ways. In cancer cells the growth factor receptor-induced activation of class I PI3K/AKT/mTOR axis, inhibits autophagy. Conversely, class III PI3K activity is required for the sequestration of cytoplasmic material that characterizes the autophagy process [25, 26].

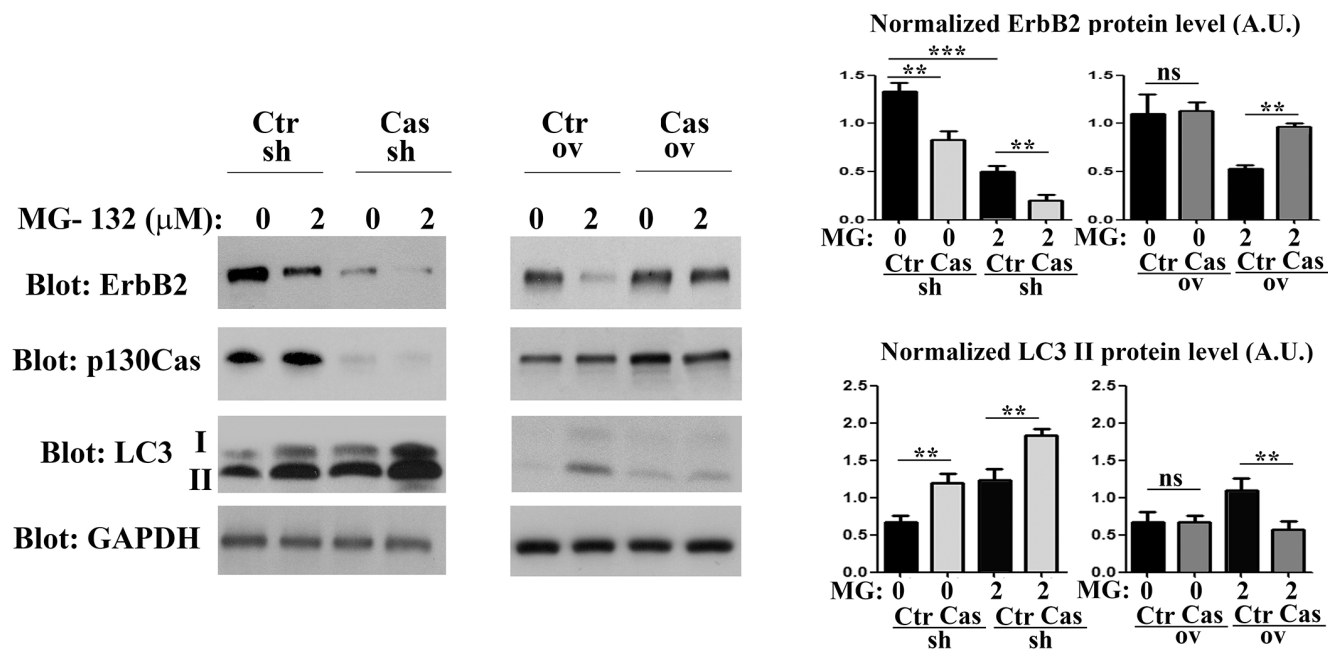


Figure 2: p130Cas expression prevents proteasome-independent ErbB2 degradation. Left panel: BT474 silenced for or overexpressing p130Cas and relative controls were treated for 16 hours with MG132 (2 μ M). Protein extracts were then blotted with antibodies against ErbB2, p130Cas and LC3. GAPDH was used as loading control. Right panel: Histograms show ErbB2 and LC3-II levels, normalized to GAPDH. Bars represent the means \pm SEM of five independent experiments (ns: not significant; ** p < 0.01; *** p < 0.001).

In addition, we have previously demonstrated that p130Cas overexpression in ErbB2 transformed cells leads to the activation of mTOR [17]. Therefore, to identify which autophagy signaling pathways were specifically involved in p130Cas-mediated ErbB2 degradation, we treated control, p130Cas silenced and overexpressing BT474 cells for 16 hours with the mTOR activator MHY1485 (2 μ M) to block autophagy [27] and with mTOR inhibitor rapamycin (100 nM) to induce autophagy.

The results in Figure 4 indicate that treatment with Rapamycin in p130Cas silenced cells increased ErbB2 degradation. As expected, LC3-II expression was present following p130Cas silencing in control cells and was strongly upregulated in cells treated with Rapamycin. Conversely, experiments performed by treating cells with

the mTOR activator, indicate that the resulting inhibition of autophagy is sufficient to reverse ErbB2 levels in p130Cas silenced BT474 cells, further confirming the key role of p130Cas in affecting signaling leading to autophagy that is instrumental for ErbB2 degradation. Importantly, p130Cas overexpressing cells were less prone to undergo autophagic degradation induced by Rapamycin. The inhibition of autophagy in cells treated with the mTOR activator is supported by low levels of LC3 expression and increased p62/sequestosome-1 protein expression. The same results were obtained by using the inhibitor of class III PI3K wortmannin, known to inhibit autophagy (data not shown) [25]. These data show that ErbB2 degradation by autophagy depends on p130Cas expression levels, with low levels of p130Cas sensitizing

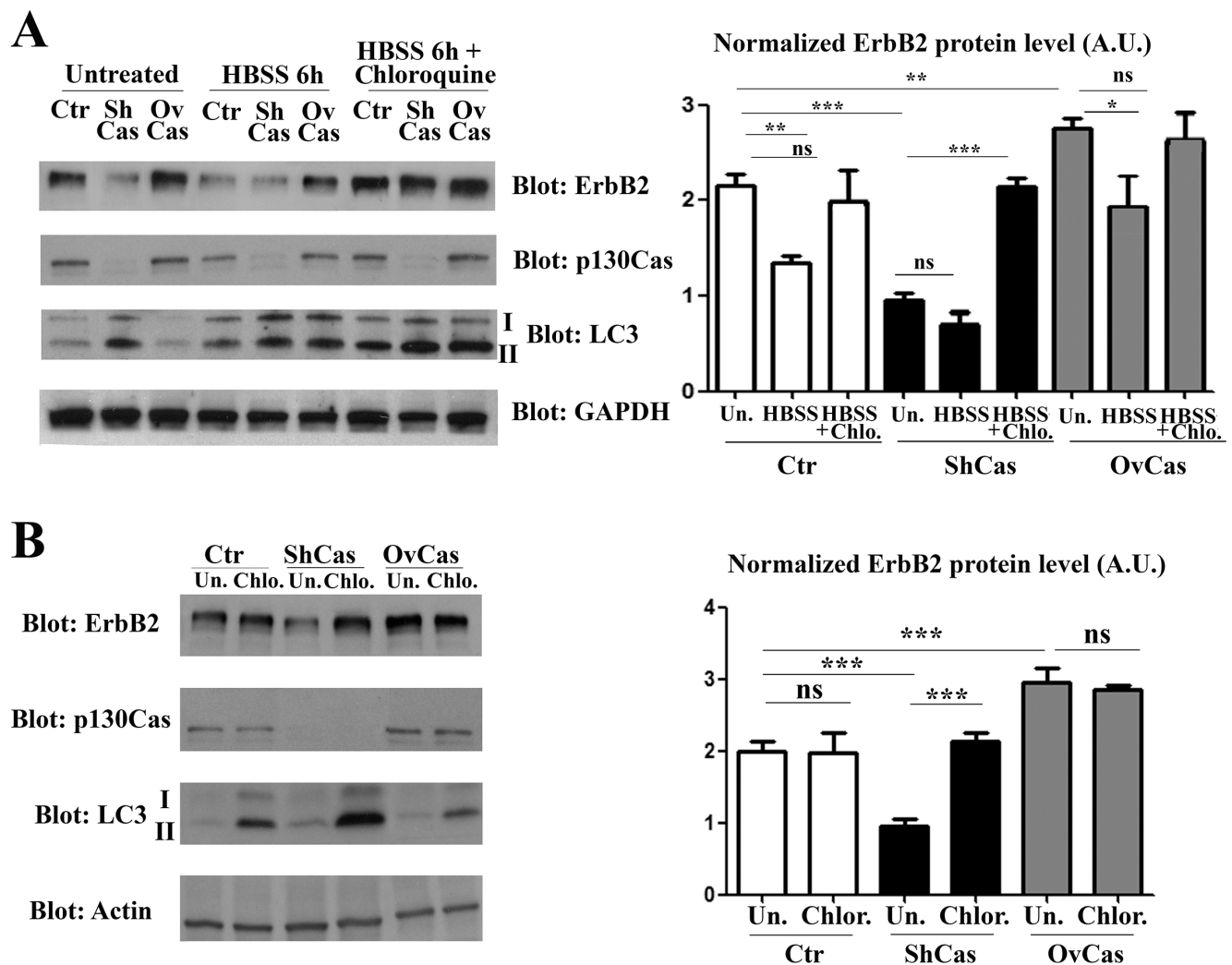


Figure 3: p130Cas protects ErbB2 from autophagy-dependent degradation. (A) Left panel: Extracts from p130Cas silenced, overexpressing and control (Ctr) BT474 cells cultured for 6 hours in HBSS in absence or presence of chloroquine (100 μ M) were blotted with antibodies to ErbB2, p130Cas, LC3 and GAPDH as loading control. Right panel: Histograms show ErbB2 levels, normalized to GAPDH. Bars represent the means \pm SEM of five independent experiments (ns: not significant; ** p < 0.01; *** p < 0.001). (B) Left panel: BT474 cells as in (A) were treated with 100 μ M chloroquine for 6 hours. Cell lysates were blotted with antibodies against ErbB2, p130Cas, LC3 and Actin as loading control. Right panel: Histograms show ErbB2 levels, normalized to Actin. Bars represent the means \pm SEM of four independent experiments (ns: not significant; *** p < 0.001).

ErbB2 to autophagy degradation and high p130Cas levels protecting it from degradation.

p130Cas protection of ErbB2 from ubiquitination

It has been recently demonstrated that ubiquitin can be a crucial element to target protein aggregates to selective autophagy [28]. Therefore, we speculated that p130Cas can modify ErbB2 sensitivity to autophagy degradation by affecting its ubiquitination status. Therefore, ErbB2 was immunoprecipitated from p130Cas silenced or overexpressing BT474 cells and the immunoprecipitates were probed with anti-ubiquitin antibodies. As shown in Figure 5A, greater amounts of ubiquitinated ErbB2 were observed upon p130Cas silencing compared to control cells. In addition, higher levels of p130Cas were associated with lower ubiquitination of ErbB2. Western blotting analysis on the same cell extracts were performed to verify changes in ErbB2 level after modulation of p130Cas (Figure 5B).

These results indicate that the presence or absence of p130Cas can affect the ubiquitination of ErbB2. Since CHIP and Cbl E3 ligases have been reported to associate with ErbB2 and to mediate its ubiquitination [29–31] and we have previously demonstrated that p130Cas immunoprecipitates with ErbB2 ([15] and Supplementary Figure 5), we tested whether the observed differences of

ErbB2 ubiquitination in presence or absence of p130Cas can be due to an impaired accessibility of ErbB2 by its E3 ligases. To this end, ErbB2 immunoprecipitates from BT474 cells in which p130Cas was silenced or overexpressed were probed with Cbl and CHIP antibodies. The results show that both CHIP and Cbl association to ErbB2 is highly increased in p130Cas silenced cells (Figure 5C), indicating that the binding of p130Cas to ErbB2 is sufficient to interfere with its polyubiquitination by reducing the binding of E3 enzymes, pointing out an uncovered chaperone function for p130Cas.

p130Cas sustains ErbB2 stability and resistance to trastuzumab

Since activation of ErbB2 downstream signaling and increased ErbB2 stability are hallmarks of resistance to trastuzumab treatment [32], we hypothesized that p130Cas can be a mediator of trastuzumab resistance. To examine whether p130Cas levels of expression is involved in trastuzumab resistance, experiments were performed in ErbB2 overexpressing BT474 and SKBR3 made resistant to trastuzumab [33]. Sensitive and resistant cells were first compared for levels of p130Cas mRNA and protein levels by performing quantitative real-time PCR and western blot analysis. The results indicate that transcription of p130Cas mRNA and its expression is upregulated

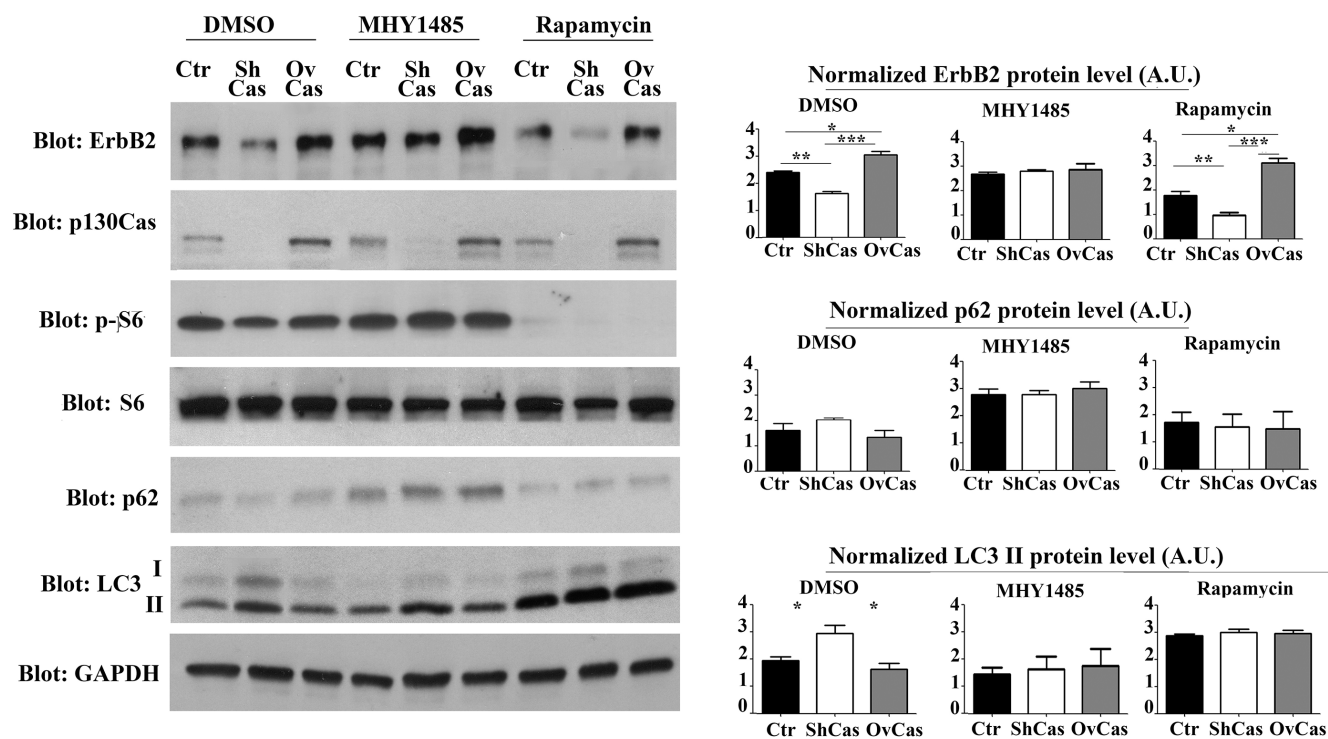


Figure 4: Inhibition of autophagy is sufficient to rescue p130Cas-dependent ErbB2 expression. Left panel: BT474 silenced for p130Cas, overexpressing p130Cas and control cells were treated for 16 hours with mTOR activator MHY1485 (2 μ M), with mTOR inhibitor Rapamycin (100 mM) and DMSO as control. Protein extracts were then blotted with antibodies against ErbB2, p130Cas, phospho-S6, S6, p62, LC3 and GAPDH as loading control. Right panel: Histograms show ErbB2, p62 and LC3 II levels, normalized to GAPDH. Bars represent the means \pm SEM of five independent experiments (* p < 0.05; ** p < 0.01; *** p < 0.001).

in resistant SKBR3R and BT474R cells compared to wt cells suggesting a functional role of p130Cas in the acquired resistance to trastuzumab (Figure 6A and 6B). To assess whether the increased stability of ErbB2 following p130Cas-dependent inhibition of autophagy is a possible mechanism to induce resistance to trastuzumab, p130Cas overexpressing BT474 cells and relative controls were treated for 24 hours with rapamycin (100 nM) and trastuzumab (10 μ M) alone and/or in combination. As shown in Figure 6C, the treatment of cells with rapamycin and trastuzumab does not affect significantly the expression of ErbB2, whereas the combination of treatments results in downregulation of ErbB2, confirming what previously observed in preclinical studies using mTOR inhibitor and trastuzumab alone or in combination [34, 35]. Notably, the overexpression of p130Cas, as expected, is sufficient to induce the expression of ErbB2 and to prevent its downregulation in the combined treatment observed in control cells. These results indicate that the overexpression of p130Cas can be one important factor that contributes to trastuzumab resistance.

To further assess the involvement of p130Cas in clinical resistance to trastuzumab, we evaluated the correlation between p130Cas expression and failure to trastuzumab-based therapy in ErbB2 positive breast cancer patients. Therefore, we assessed the expression of p130Cas in ErbB2 positive primary tumors of 11 patients and in the relapsing trastuzumab resistant counterparts. As

shown in Table 1, 8 out of 11 tumors showed an increase in p130Cas expression at the time of progression. Moreover, 3 out of 11 tumors were already 2+/3+ for p130Cas at first diagnosis of breast cancer and they retained this high p130Cas positivity after trastuzumab treatment (Figure 6D). These data suggest that high levels of p130Cas may promote acquired resistance to trastuzumab therapy in ErbB2 positive breast cancer.

Overall our results indicate that the modulation of p130Cas expression correlates with alterations of ErbB2 expression, and in particular we demonstrated that p130Cas protects ErbB2 from autophagy degradation. This protection from degradation points out p130Cas as a crucial player in ErbB2 resistance to targeted therapy.

DISCUSSION

Here we demonstrate for the first time that the adaptor protein p130Cas can act as a protecting agent against ErbB2 degradation. Consistently, we show that lowering p130Cas expression is sufficient to get ErbB2 degraded while p130Cas overexpression increased ErbB2 stability at the cell membrane. Our data also show that p130Cas-dependent ErbB2 degradation occurs preferentially by autophagy rather than by proteasome. Interestingly, we have demonstrated that the presence of p130Cas can impair the binding of the ErbB2 with its E3 ligases CHIP and Cbl, resulting in a defective ubiquitination.

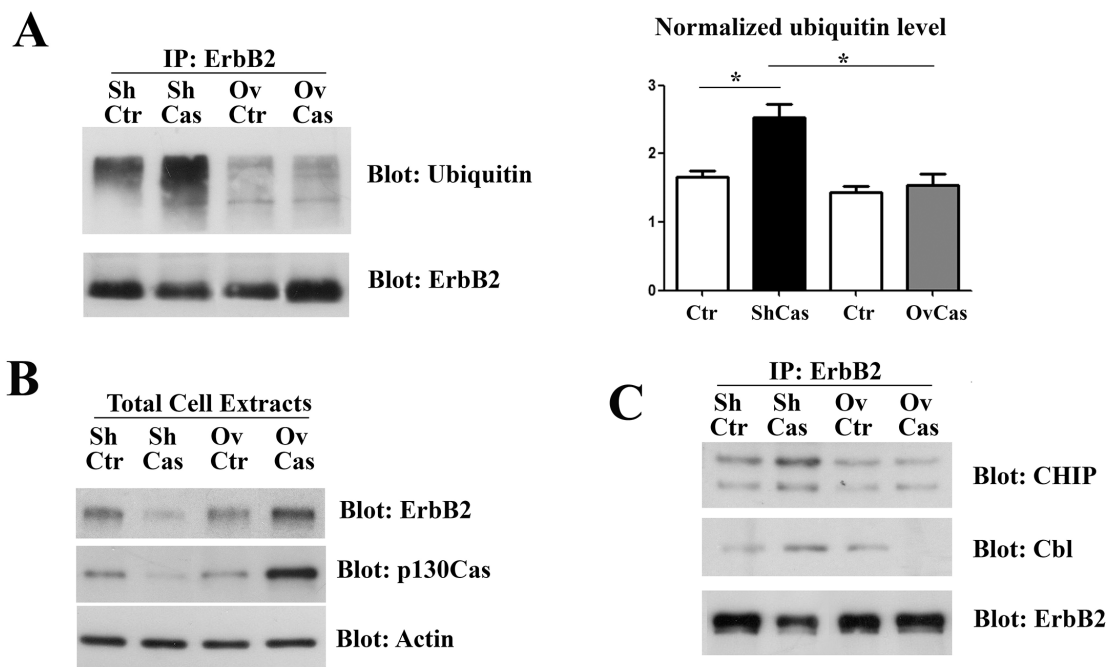


Figure 5: p130Cas expression influences ErbB2 ubiquitination. (A) Left panel: Cell extracts from control (Ctr), p130Cas silenced and p130Cas overexpressing BT474 cells were immunoprecipitated with ErbB2 antibodies, followed by immunoblotting against Ubiquitin and ErbB2 antibodies. Right panel: Histograms show the levels of ubiquitin, normalized to ErbB2. Bars represent the means \pm SEM of three independent experiments (* $p < 0.05$; ** $p < 0.01$; *** $p < 0.001$). (B) Cell extracts as in A were probed with antibodies to p130Cas, ErbB2 and normalized with Vinculin. (C) Cell extracts from control (Ctr), p130Cas silenced and p130Cas overexpressing BT474 cells were immunoprecipitated with ErbB2 antibodies and blotted with Cbl, CHIP and ErbB2 antibodies.

We have previously extensively shown that p130Cas supports and amplifies ErbB2 downstream signaling pathways both *in vivo* and *in vitro* promoting tumorigenesis and progression [14–17]. Here we describe for the first time one possible mechanism through which p130Cas can affect ErbB2 tumorigenesis. Our present data indicate that p130Cas by binding to ErbB2, stabilizes the receptor preventing its ubiquitinylation and subsequent degradation by selective autophagy. Indeed p130Cas by binding to ErbB2 does not allow the association with CHIP and Cbl E3 ligases, possibly due to steric hindrance. Conversely, low levels of p130Cas allows the binding of CHIP and Cbl E3 ligases to ErbB2 promoting its degradation by autophagy.

It was previously inferred that ErbB2 receptor is resistant to down-regulation by endocytosis, probably because of its association to Hsp90 chaperone that might prevent due to steric hindrance the binding of E3 ligase to ErbB2 resulting in impaired ubiquitinylation and degradation [23]. Indeed Hsp90 inhibitors, such as geldamycin, induces a rapid ubiquitin-dependent

degradation of the receptor [8, 9, 20, 36]. We can speculate that p130Cas mirrors in ErbB2 positive breast cancer the function of Hsp90, protecting ErbB2 from degradation but at the same time, assembling a signaling platform that sustains and reinforces breast cancer growth, migration and invasion.

Our data also points out that lowering p130Cas is sufficient to induce ErbB2 degradation that preferentially occurs by autophagy rather than by proteasome.

Interestingly, it has been speculated that the docking of proteins to be degraded to the ubiquitin-proteasome system (UPS) or to the autophagy—lysosomal pathway depends on the differential attachment of ubiquitin moieties. The association with K48-linked polyUb chains will represent the recognition signal for proteasome degradation, whereas the K63-linked chains may preferentially target substrates to degradation by autophagy [23, 28, 37, 38].

In parallel, it has been recently proposed in SKBR3 breast cancer cells that ErbB2 degradation is proteasome independent and that the conjugation of K63-linked

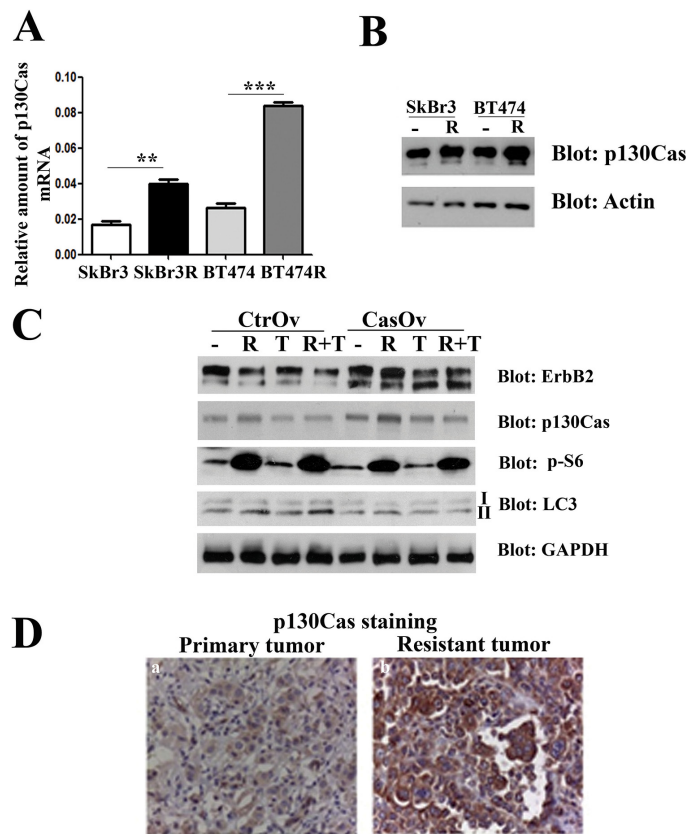


Figure 6: p130Cas overexpression promotes resistance to trastuzumab. (A) Quantification of p130Cas mRNA by qRT PCR in wild type SKBR3 (SKBr3), in trastuzumab resistant SKBR3 (SKBr3R), in BT474 wild type (BT474) and in trastuzumab resistant BT474 cells (BT474R). The 18S housekeeping gene was used as an internal control for data normalization. (B) Cell extracts from trastuzumab sensitive and resistant SKBR3 and BT474 cells were probed with p130Cas antibodies and normalized with Actin. (C) Cell extracts from p130Cas overexpressing BT474 cells and relative control cells untreated or treated with 100 nM Rapamycin (R), 10 μ M/ml trastuzumab (T) alone or in combination (R + T) were blotted with antibodies against ErbB2, p130Cas, phospho-S6, LC3 and GAPDH as loading control. (D) Representative images of p130Cas expression in primary tumor at the time of diagnosis (left panel) and in relapsing trastuzumab resistant tumor (right panel) of patient n°2 (see Table 1).

Table 1: Grade of p130Cas expression in primary and relapsing breast cancer patients before and after trastuzumab treatment

Case N°	Stage	Histology	Mol. Subtype	Surgery at diagnosis	p130Cas (IHC before trastuzumab)	p130Cas (IHC) after trastuzumab
1	III	CDI	HER2-Enriched	Yes	2+	3+
2	III	CDI	HER2-Enriched	Yes	1+	3+
3	III	CLI	HER2-Enriched	Yes	1+	3+
4	III	CDI	HER2-Enriched	Yes	3+	3+
5	III	CDI	HER2-Enriched	Yes	2+	3+
6	III	CDI	Luminal-HER2	Yes	1+	3+
7	III	CDI	Luminal-HER2	Yes	2+	3+
8	IV	CDI	Luminal-HER2	Not	3+	3+
9	I	CLI	HER2-Enriched	Yes	1+	2+
10	III	CDI	HER2-Enriched	Yes	2+	3+
11	III	CDI	HER2-Enriched	Yes	2+	2+

CDI: Ductal Infiltrating Carcinoma; CLI: Lobular Infiltrating Carcinoma; IHC: immunohistochemistry.

polyubiquitin chains to ErbB2 might be relevant to target its degradation by the autophagy-lysosomal system [21, 23]. On the basis of these data we can speculate that in the absence of p130Cas the observed ErbB2 degradation by autophagy might be dependent by an increased amount of K63 linkages that in turn are recognized by the autophagy receptors and finally degraded. Further investigations are needed to verify this hypothesis and to identify the molecular players involved in p130Cas-dependent ErbB2 degradation and/or stability.

Nevertheless, the translational importance of the levels of p130Cas expression in the regulation of ErbB2 stability is evident. Indeed, the p130Cas silencing in a therapeutic setting will contribute to ErbB2 degradation and thereby to limitations of its oncogenic properties, whereas the overexpression of p130Cas by protecting ErbB2 from autophagy can be implicated in resistance to trastuzumab treatment. Our data indeed indicate that high levels of p130Cas expression inversely correlate with ErbB2 sensitivity to trastuzumab and the induction of autophagy is not sufficient to promote its degradation. The mechanism through which p130Cas mediates resistance to trastuzumab might rely on the increased ErbB2 stability to the cell membrane. However, it has been reported that increased autophagosome formation in trastuzumab resistant cells preserves breast cancer cell survival [39]. These opposite data can be reconciled by the fact that overexpression of p130Cas drives resistance to trastuzumab by increasing ErbB2 stability and by blocking the receptor ubiquitination and thus its degradation, regardless of activation of downstream autophagy flux.

Our and others previous and current results indicate that high levels of p130Cas are hallmarks of breast cancer progression, invasion, metastatization and resistance

[11, 13, 40]. However, the mechanisms through which p130Cas expression is upregulated in breast cancer still remain an open question.

In conclusion, we provided evidence that p130Cas overexpression prevents ErbB2 degradation by autophagy. The resulting increased stabilization of ErbB2 by p130Cas might be the crucial event driving breast cancer progression and resistance, strengthening the relevance of p130Cas as an unfavorable prognostic marker and a putative therapeutic target to overcome resistance to trastuzumab based treatment in ErbB2 positive breast cancers.

MATERIALS AND METHODS

Antibodies

p130Cas mAbs have been previously described [41]. ErbB2 NCL-L-Cb11 mAbs were purchased from Novocastra (Leica Microsystems Srl, Germany). An additional mAb directed to the cytoplasmic domain of ErbB2 were prepared in our laboratory, by immunizing mice with a recombinant protein encompassing amino acids 1031–1160 of rat ErbB2 cDNA sequence. mAbs to Vinculin were from Millipore (Billerica, MA, USA). Antibodies to c-Src, p-Tyr PY99, Actin, Cbl and CHIP were from Santa Cruz Biotechnologies (Palo Alto, CA, USA). pTyr416 c-Src and Beclin-1 antibodies were from Cell Signaling (Beverly, MA, USA). Mono- and polyubiquitylated conjugates antibody was from Enzo Life Sciences (Farmingdale, NY). LC3 polyclonal antibody was from Thermo Scientific Pierce Antibodies (Rockford, Illinois). Secondary antibodies conjugated with peroxidase were from Sigma-Aldrich (St. Louis, MO, USA).

Cell lines

SKBR3 cells were cultured in McCoy's 5A–15% FBS and BT474 cell lines were cultured in DMEM-F12 with 10% FBS. SKBR3 and BT474 resistant cells were respectively cultured in RPMI-1640 10% FBS and DMEM 10% FBS. SKBR3 and BT474 made resistant to trastuzumab were generated by Dr. Valabrega as described in [33].

Proteasome and autophagy experiments

For proteasome inhibition experiments, MG132 (CAS-133407-82-6, Calbiochem, Darmstadt, Germany) was directly added into medium at a concentration of 0.5, 2 and 6 μ M for 16 hours. Cycloheximide was used at 100 mg/ml and purchased from Sigma (Sigma-Aldrich, St. Louis, MO, USA). For autophagy induction cells were cultured in Hank's balanced salt solution (HBSS, Invitrogen Life Technologies, Carlsbad, CA, USA) for 2, 4 and 6 hours. For autophagy pharmacological inhibition, cells were treated with the PI3-kinase inhibitor, wortmannin (Enzo Life Sciences, Farmingdale, NY) at 100 nM and with chloroquine (Sigma-Aldrich, St. Louis, MO, USA), an inhibitor of autophagosome formation at 100 μ M for 16 hours. For mTOR inhibition cells were treated with rapamycin (Cell Signaling Technology, Beverly, MA) at 100 nM for 16 hours. For resistance experiments, cells were treated for 20 hours with trastuzumab (10 microg/ml) or Rapamycin (100 nM) or with combination of both.

Lentivirus generation

A pLKO.1 lentiviral vector carrying a shRNA directed to human p130Cas (p130Cas shRNA) was selected in the pLKO.1 target gene shRNA set (clone ID TRCN0000115985), purchased from Open Biosystem (Huntsville, AL, USA, <http://www.thermoscientificbio.com>). pLKO.1 scramble shRNA vector (Addgene, Cambridge, MA, USA, <http://www.addgene.com>) was used as negative control. Lentiviral particles were generated and concentrated by ultracentrifugation (50,000 g, 2 hours). BT474 and SKBR3 cells were infected with the lentiviral p130Cas-shRNA (sh-p130Cas) and scramble-shRNA (Ctr). Puromycin (Sigma) (0.5 mg/ml) was added 24 hours after infection with PLKO.1 vectors as described in [42]. For p130Cas expression, human p130Cas cDNA, mouse p130Cas cDNA were cloned into pCCL lentiviral vector, and viral particles production was performed as described in [42].

Immunoblotting and immunoprecipitation analysis

Cells were extracted with RIPA buffer (1% Triton X-100, 0.1% SDS, 1% sodium deoxycholate, 150 mM NaCl, 50 mM Tris-HCl pH 7, 0.4 mM Na₃VO₄, inhibitor

mix). Cell lysates were centrifuged at 13,000 g for 10 minutes and the supernatants were collected and assayed for protein concentration with the Bio-Rad protein assay method (Biorad, Hercules, CA, USA). Proteins were run on SDS-PAGE under reducing conditions. Following SDS-PAGE, proteins were transferred to nitrocellulose, incubated with specific antibodies and then detected with peroxidase conjugated secondary antibodies and chemoluminescent ECL reagent. When appropriate, the nitrocellulose membranes were stripped according to manufacturers' recommendations and re-probed. Densitometric analysis was performed using the GS 250 Molecular Imager (Biorad).

For immunoprecipitation assay, 1 mg of cell extracts were immunoprecipitated with ErbB2 antibody and then probed for specific antibodies.

For ubiquitination experiments, 10 mg of cell extracts were immunoprecipitated with ErbB2 antibody. After blotting, the membrane were pre-incubated with denaturing buffer (6 M guanidine-HCl, 20 mM Tris-HCl pH 7.5, 5 mM b-mercapto-ethanol, 1 mM PMSF) for 30' at 4°C and washed in PBS buffer. Then the membrane was blocked with 5% BSA in TBS buffer for 6 hours at room temperature and incubated overnight at 4°C with the anti-ubiquitin antibody.

RNA isolation and qRT-PCR for mRNA detection

Total RNA was isolated from cells using TRIzol™ Reagent (Invitrogen Life Technologies, Carlsbad, CA, USA). 1 μ g of DNase-treated RNA (RQ1 RNase-Free DNase kit, Promega, Madison, WI, USA) was retrotranscribed with High Capacity cDNA Reverse Transcription Kit (Invitrogen Life Technologies, Carlsbad, CA, USA). Quantitative PCR was performed on an Applied Biosystems, 7900HT Fast Real-Time PCR System (standard settings) using the Universal Probe Library system (Roche Italia, Monza, Italy) and Platinum™ Quantitative PCR SuperMix-UDG (Invitrogen Life Technologies, Carlsbad, CA, USA). Results were analyzed with the 2^{- $\Delta\Delta$ Ct} method using the 18 S rRNA predeveloped TaqMan assay (Invitrogen Life Technologies, Carlsbad, CA, USA) as an internal control. The median expression across samples was used as calibrator.

In vitro cell assays

For proliferation assay, MTT (4,5 dimethyl-2-yl 2,5-diphenyl tetrazolium bromide) from Sigma Chemical Co. (St. Louis, MO, USA) was performed on SKBR3 and BT474 upon treatment with freshly added trastuzumab (Herceptin) (2 μ g/ml) for 4 days. For FACS analysis cells were stained with ErbB2 mAb and with Alexa 488 secondary antibody (Invitrogen Life Technologies, Carlsbad, CA, USA). Alexa 488 emission was detected in the green channel (525 nm) following excitation by a 488 nm laser on a FACS Calibur cytometer (Becton, Dickinson and Company, Franklin Lakes, NJ, USA).

Immunohistochemistry procedures

Human investigations were performed with informed consent and were preceded by local institutional review board approval.

Samples were routinely fixed in 10% formaldehyde buffer (pH 7.4) for 24 hrs, paraffin-embedded, and processed for immunohistochemical analysis. Slides were incubated with anti-p130Cas (Labvision Thermo Scientific) (1 microg/mL) for 1 hr at room temperature, after antigen retrieval (citrate buffer, at 98°C for 40 min). Staining was detected with EnVision System-HRP Labelled Polymer anti-mouse (DakoCytomation) and developed with the LiquidDAB Substrate Pack (BioGenex, San Ramon, CA, USA). Nuclei were counterstained with Mayer hemalum. Images were taken using a Leica DM 2000 microscope.

Statistical analysis

The results are representative of at least three independent experiments performed in triplicate and are expressed as the means \pm s.e.m. Statistical analysis of the data was performed using a Student's *t*-test.

ACKNOWLEDGMENTS AND FUNDING

This work was supported by AIRC (Associazione Italiana Ricerca Cancro) to SC (IG11346 and IG15970) and PD (IG15399); MIUR (FIRB giovani 2008 RBFR08F2FS to SC), MIUR (Ministero Università Ricerca, PRIN 2010/2011) to PD and Compagnia San Paolo, Torino; Progetto d'Ateneo, Università di Torino 2011 to PD and Ricerca Sanitaria Finalizzata GR-2009-1543842 to GV and SC. MPC is supported by an Umberto Veronesi Fellowship. B.B. was supported by an AIRC fellowship.

CONFLICTS OF INTEREST

The authors declare no conflicts of interest.

REFERENCES

1. Baselga J. Treatment of HER2-overexpressing breast cancer. *Ann Oncol.* 2010; 21:36–40.
2. Emde A, Kostler WJ, Yarden Y. Therapeutic strategies and mechanisms of tumorigenesis of HER2-overexpressing breast cancer. *Crit Rev Oncol Hematol.* 2012; 84:e49–57.
3. Valabrega G, Montemurro F, Aglietta M. Trastuzumab: mechanism of action, resistance and future perspectives in HER2-overexpressing breast cancer. *Ann Oncol.* 2007; 18:977–984.
4. Mohd Sharial MS, Crown J, Hennessy BT. Overcoming resistance and restoring sensitivity to HER2-targeted therapies in breast cancer. *Ann Oncol.* 2012; 23:3007–3016.
5. Muthuswamy SK. Trastuzumab resistance: all roads lead to SRC. *Nat Med.* 2011; 17:416–418.
6. Pohlmann PR, Mayer IA and Mernaugh R. Resistance to Trastuzumab in Breast Cancer. *Clin Cancer Res.* 2009; 15:7479–7491.
7. Valabrega G, Montemurro F, Sarotto I, Petrelli A, Rubini P, Tacchetti C, Aglietta M, Comoglio PM, Giordano S. TGFalpha expression impairs Trastuzumab-induced HER2 downregulation. *Oncogene.* 2005; 24:3002–3010.
8. Lerdrup M, Hommelgaard AM, Grandal M, van Deurs B. Geldanamycin stimulates internalization of ErbB2 in a proteasome-dependent way. *J Cell Sci.* 2006; 119:85–95.
9. Raja SM, Clubb RJ, Bhattacharyya M, Dimri M, Cheng H, Pan W, Ortega-Cava C, Lakku-Reddi A, Naramura M, Band V, Band H. A combination of Trastuzumab and 17-AAG induces enhanced ubiquitinylation and lysosomal pathway-dependent ErbB2 degradation and cytotoxicity in ErbB2-overexpressing breast cancer cells. *Cancer Biol Ther.* 2008; 7:1630–1640.
10. Defilippi P, Di Stefano P, Cabodi S. p130Cas: a versatile scaffold in signaling networks. *Trends Cell Biol.* 2006; 16:257–263.
11. Cabodi S, del Pilar Camacho-Leal M, Di Stefano P, Defilippi P. Integrin signalling adaptors: not only figurants in the cancer story. *Nat Rev Cancer.* 2010; 10:858–870.
12. Nikonova AS, Gaponova AV, Kudinov AE, Golemis EA. CAS proteins in health and disease: an update. *IUBMB Life.* 2014; 66:387–395.
13. Tornillo G, Defilippi P, Cabodi S. Cas proteins: dodgy scaffolding in breast cancer. *Breast Cancer Res.* 2014; 16:443.
14. Cabodi S, Tinnirello A, Di Stefano P, Bisaro B, Ambrosino E, Castellano I, Sapino A, Arisio R, Cavallo F, Forni G, Glukhova M, Silengo L, Altruda F, et al. p130Cas as a new regulator of mammary epithelial cell proliferation, survival, and HER2-neu oncogene-dependent breast tumorigenesis. *Cancer Res.* 2006; 66:4672–4680.
15. Cabodi S, Tinnirello A, Bisaro B, Tornillo G, del Pilar Camacho-Leal M, Forni G, Cojoca R, Iezzi M, Amici A, Montani M, Eva A, Di Stefano P, Muthuswamy SK, et al. p130Cas is an essential transducer element in ErbB2 transformation. *FASEB J.* 2010; 24:3796–3808.
16. Pincini A, Tornillo G, Orso F, Sciortino M, Bisaro B, Leal Mdel P, Lembo A, Brizzi MF, Turco E, De Pitta C, Provero P, Medico E, Defilippi P, et al. Identification of p130Cas/ErbB2-dependent invasive signatures in transformed mammary epithelial cells. *Cell Cycle.* 2013; 12:2409–2422.
17. Tornillo G, Bisaro B, Camacho-Leal Mdel P, Galie M, Provero P, Di Stefano P, Turco E, Defilippi P, Cabodi S. p130Cas promotes invasiveness of three-dimensional ErbB2-transformed mammary acinar structures by enhanced activation of mTOR/p70S6K and Rac1. *Eur J Cell Biol.* 2011; 90:237–248.

18. Brinkman A, van der Flier S, Kok EM, Dorssers LC. BCAR1, a human homologue of the adapter protein p130Cas, and antiestrogen resistance in breast cancer cells. *J Natl Cancer Inst.* 2000; 92:112–120.
19. Ta HQ, Thomas KS, Schrecengost RS, Bouton AH. A novel association between p130Cas and resistance to the chemotherapeutic drug adriamycin in human breast cancer cells. *Cancer Res.* 2008; 68:8796–8804.
20. Bertelsen V, Stang E. The Mysterious Ways of ErbB2/HER2 Trafficking. *Membranes (Basel).* 2014; 4:424–446.
21. Marx C, Yau C, Banwait S, Zhou Y, Scott GK, Hann B, Park JW, Benz CC. Proteasome-regulated ERBB2 and estrogen receptor pathways in breast cancer. *Mol Pharmacol.* 2007; 71:1525–1534.
22. Zhao M, Vuori K. The docking protein p130Cas regulates cell sensitivity to proteasome inhibition. *BMC Biol.* 2011; 9:73.
23. Marx C, Held JM, Gibson BW, Benz CC. ErbB2 trafficking and degradation associated with K48 and K63 polyubiquitination. *Cancer Res.* 2010; 70:3709–3717.
24. Kimura T, Takabatake Y, Takahashi A, Isaka Y. Chloroquine in cancer therapy: a double-edged sword of autophagy. *Cancer Res.* 2013; 73:3–7.
25. Kondo Y, Kanzawa T, Sawaya R, Kondo S. The role of autophagy in cancer development and response to therapy. *Nat Rev Cancer.* 2005; 5:726–734.
26. Mizushima N, Yoshimori T, Levine B. Methods in mammalian autophagy research. *Cell.* 2010; 140:313–326.
27. Choi YJ, Park YJ, Park JY, Jeong HO, Kim DH, Ha YM, Kim JM, Song YM, Heo HS, Yu BP, Chun P, Moon HR, Chung HY. Inhibitory effect of mTOR activator MHY1485 on autophagy: suppression of lysosomal fusion. *PLoS One.* 2012; 7:e43418.
28. Kirkin V, McEwan DG, Novak I, Dikic I. A role for ubiquitin in selective autophagy. *Mol Cell.* 2009; 34:259–269.
29. Klapper LN, Waterman H, Sela M, Yarden Y. Tumor-inhibitory antibodies to HER-2/ErbB-2 may act by recruiting c-Cbl and enhancing ubiquitination of HER-2. *Cancer Res.* 2000; 60:3384–3388.
30. Xu W, Marcu M, Yuan X, Mimnaugh E, Patterson C, Neckers L. Chaperone-dependent E3 ubiquitin ligase CHIP mediates a degradative pathway for c-ErbB2/Neu. *Proc Natl Acad Sci U S A.* 2002; 99:12847–12852.
31. Zhou P, Fernandes N, Dodge IL, Reddi AL, Rao N, Safran H, DiPetrillo TA, Wazer DE, Band V, Band H. ErbB2 degradation mediated by the co-chaperone protein CHIP. *J Biol Chem.* 2003; 278:13829–13837.
32. Bailey TA, Luan H, Clubb RJ, Naramura M, Band V, Raja SM, Band H. Mechanisms of Trastuzumab resistance in ErbB2-driven breast cancer and newer opportunities to overcome therapy resistance. *J Carcinog.* 2011; 10:28.
33. Valabrega G, Capellero S, Cavalloni G, Zaccarello G, Petrelli A, Migliardi G, Milani A, Peraldo-Neia C, Gammaitoni L, Sapino A, Pecchioni C, Moggio A, Giordano S, et al. HER2-positive breast cancer cells resistant to trastuzumab and lapatinib lose reliance upon HER2 and are sensitive to the multitargeted kinase inhibitor sorafenib. *Breast Cancer Res Treat.* 2011; 130:29–40.
34. Miller TW, Forbes JT, Shah C, Wyatt SK, Manning HC, Olivares MG, Sanchez V, Dugger TC, de Matos Granja N, Narasanna A, Cook RS, Kennedy JP, Lindsley CW, et al. Inhibition of mammalian target of rapamycin is required for optimal antitumor effect of HER2 inhibitors against HER2-overexpressing cancer cells. *Clin Cancer Res.* 2009; 15:7266–7276.
35. Zhu Y, Zhang X, Liu Y, Zhang S, Liu J, Ma Y, Zhang J. Antitumor effect of the mTOR inhibitor everolimus in combination with trastuzumab on human breast cancer stem cells *in vitro* and *in vivo*. *Tumour Biol.* 2012; 33:1349–1362.
36. Pedersen NM, Madshus IH, Haslekas C, Stang E. Geldanamycin-induced down-regulation of ErbB2 from the plasma membrane is clathrin dependent but proteasomal activity independent. *Mol Cancer Res.* 2008; 6:491–500.
37. Olzmann JA, Chin LS. Parkin-mediated K63-linked polyubiquitination: a signal for targeting misfolded proteins to the aggresome-autophagy pathway. *Autophagy.* 2008; 4:85–87.
38. Shaid S, Brandts CH, Serve H, Dikic I. Ubiquitination and selective autophagy. *Cell Death Differ.* 2013; 20:21–30.
39. Vazquez-Martin A, Oliveras-Ferraro C, Menendez JA. Autophagy facilitates the development of breast cancer resistance to the anti-HER2 monoclonal antibody trastuzumab. *PLoS One.* 2009; 4:e6251.
40. Tikhmyanova N, Golemis EA. NEDD9 and BCAR1 negatively regulate E-cadherin membrane localization, and promote E-cadherin degradation. *PLoS One.* 2011; 6:e22102.
41. Cabodi S, Moro L, Baj G, Smeriglio M, Di Stefano P, Gippone S, Surico N, Silengo L, Turco E, Tarone G, Defilippi P. p130Cas interacts with estrogen receptor alpha and modulates non-genomic estrogen signaling in breast cancer cells. *J Cell Sci.* 2004; 117:1603–1611.
42. Bisaro B, Montani M, Konstantinidou G, Marchini C, Pietrella L, Iezzi M, Galie M, Orso F, Camporeale A, Colombo SM, Di Stefano P, Tornillo G, Camacho-Leal MP, et al. p130Cas/Cyclooxygenase-2 axis in the control of mesenchymal plasticity of breast cancer cells. *Breast Cancer Res.* 2012; 14:R137.